Polish Academy of Sciences

Institute of Fundamental Technological Research

Archives of Mechanics

Archiwum Mechaniki Stosowanej

volume 49 issue 4

Polish Scientific Publishers PWN

Warszawa 1997

ARCHIVES OF MECHANICS IS DEVOTED TO
Theory of elasticity and plasticity • Theory of nonclassical continua • Physics of continuous media • Mechanics of discrete media • Nonlinear mechanics • Rheology • Fluid gas-mechanics • Rarefied gas • Thermodynamics

---

Printed in Poland, Editorial Office: Świętokrzyska 21,
00-049 Warszawa (Poland)

e-mail: publikac@ippt.gov.pl

Arkuszy wydawniczych 13,75. Arkuszy drukarskich 12.
Papier offset. kl. III 70 g. B1. Odddano do składania w lipcu 1997 r.
Druk ukończono w sierpniu 1997 r.
Skład i łamanie: "MAT-TEX"
Druk i oprawa: Drukarnia Braci Grodzickich, Żabieniec ul. Przelotowa 7

Arch. Mech., 49, 4, pp. 615–633, Warszawa 1997

Dynamics of turbulent helium II, limits of the Vinen model

T. LIPNIACKI (WARSZAWA)

THE DYNAMICS of superfluid helium is considered within the framework of the Vinen model. According to Vinen equation, counterflow (the relative velocity of the two helium components) gives rise to quantum turbulence. The mutual friction force, exerted on the vortex tangle by the normal component, couples it with the superfluid component. The system of 3 ordinary equations is numerically solved to calculate the characteristic entrainment time in which the counterflow ceases. For the typical velocities of order 1 cm/s, the entrainment time is found to be much smaller than the vorticity diffusion time for the length scale of 1 cm. It suggests that in the typical spin-up experiments the quantum turbulence plays a key role coupling the two components. Unfortunately the Vinen model applied to spin-up turned out to be inconsistent; the vortex line density calculated from the superfluid component vorticity was found to be much larger than that predicted by the Vinen equation.

1. Introduction

THE LANDAU'S two-fluid theory [1] has proved to be indispensable for understanding of the peculiar flow properties of ^{4}He below the λ-point. In the two-fluid theory He II (superfluid ^{4}He) is a sum of the Bose condensate (superfluid component) and the gas of thermal excitation (normal component). Densities of superfluid and normal components ϱ_s, ϱ_n respectively, are temperature-dependent and satisfy

$$\varrho = \varrho_n + \varrho_s \,, \tag{1.1}$$

where ϱ denotes the total mass density of the liquid.

The theory was later improved by ONSAGER [2] and FEYNMAN [3] who found that Landau's assumption of rotationless flow of the superfluid component was violated on one-dimensional singularities called now quantum vortices. The circulation of the superfluid velocity about these lines remains constant, $\kappa = h/m_{\mathrm{He}} = 9.97 \cdot 10^{-4}\,\mathrm{cm}^2/\mathrm{s}$, where h is Planck's constant, and m_{He} is the mass of helium atom. The interaction between the vortices and the elementary excitation couples the normal and superfluid components. Within the limits of that de facto three-fluid theory, two main models were proposed:

1) the VINEN model [4] which describes helium in the state of a superfluid turbulence, when the quantum vortices form an irregular tangle, and

2) the Hall – Vinen – Bekarevich – Khalatnikov [5] (HVBK) model concerning the case when moving vortices form a regular pattern of parallel orientation (superfluid laminar flow).

When the magnitude of relative velocity $V_{ns} = |V_n - V_s|$ gets sufficiently large, superfluid laminar flow develops into superfluid turbulent flow. It significantly restricts the usage of the HVBK model.

The easiest way of generating a sizable V_{ns} is to seal one end of the channel and place a heater there. The normal fluid produced by the heater flows out of the channel with an average velocity V_n proportional to the heat input to the channel. The normal fluid moving away from the heater is replaced by a superfluid flowing in the opposite direction, the superfluid velocity V_s being determined by the condition of zero mass transport $\varrho_s V_s + \varrho_n V_n = 0$.

Because there is a variety of observations on superfluid turbulence caused by heat flows in a counterflow channel, the Vinen model has been usually connected with the problems of the heat transport. In fact not only the heat transfer may cause the counterflow.

For example the viscous forces in a rotating cylinder or a moving channel may give rise to the difference in the components velocities. The calculations show that even the relative velocity of order 1 cm/s may cause the quantum turbulence strong enough to influence the dynamics of the two components.

To study this problem in more detail, we recall basic facts of the Vinen model according to the approach developed by SCHWARZ [6, 7]. We use the modified vortex-line-length density L_m

$$L_m = (I_{||} - c_L I_l) L, \tag{1.2}$$

where L is the total line-length density (i.e. the length of vortices per unit of volume). $(I_{||} - c_L I_l)$ is a coefficient describing vortex tangle anisotropy and is equal to 2/3 for isotropic tangle. The modified density was introduced by Schwarz as a quantity which can be directly measured in thermal-counterflow experiments.

The time evolution of the modified vortex-line-length density is governed by Vinen-type equation

$$\frac{dL_m}{dt} = \alpha I_{lm} \left(V_{ns} L_m^{3/2} - \frac{\beta}{c_{Lm}} L_m^2 \right), \tag{1.3}$$

where I_{lm}, c_{Lm} are temperature-dependent dimensionless coefficients, α is the friction coefficient, and β is defined by

$$\beta = \frac{\kappa}{4\pi} \ln \left(\frac{c}{a_0 < s'' >} \right) \approx \kappa, \tag{1.4}$$

where κ is the quantum of circulation, c is a constant of order one, $< s'' >$ is the average curvature of the vortices in the tangle and $a_0 \simeq 1.3 \cdot 10^{-8}$ cm is the effective core radius of a quantized vortex. Although β has the logarithmic dependence on the tangle density since $< s'' >$ increases as the tangle density increases, it can usually be treated as a constant. For the typical tangle densities we can replace everywhere β by κ. The values of the dimensionless parameters used

in that paper, based on numerical simulations by SCHWARZ [6] (from GEURST and BEELEN [8]), are presented in the Table 1. The thermal excitation (phonons and rotons) exerts the force on the quantized vortices of a vortex tangle, what gives rise to the friction force between the two components. The density of that force is F_{ns}

$$F_{ns} = \varrho_s \kappa \alpha L_m V_{ns} \,. \tag{1.5}$$

Table 1. Values of dimensionless parameters [8] and kinematic viscosity ν_n [cm^2/s].

Temp.	1.07	1.26	1.62	2.01	2.15
ϱ_n/ϱ	0.013	0.039	0.174	0.576	0.886
α	0.010	0.030	0.100	0.300	1.00
$I_{\parallel} - c_L I_l$	0.70	0.72	0.71	0.77	0.85
I_{lm}	0.51	0.52	0.54	0.52	0.39
c_{Lm}	0.031	0.062	0.11	0.19	0.26
c_I	0.061	0.12	0.20	0.36	0.67
ν_n	$1.5 \cdot 10^{-2}$	$3.0 \cdot 10^{-3}$	$5.1 \cdot 10^{-4}$	$1.8 \cdot 10^{-4}$	$1.7 \cdot 10^{-4}$

In incompressible approximation $\operatorname{div} V_n = \operatorname{div} V_s = 0$, the dynamical equations are [9]

$$\begin{aligned} \varrho_n \left(\frac{\partial V_n}{\partial t} + V_n \nabla V_n \right) + \nabla p_n &= \nu_n \Delta^2 V_n - F_{ns} \,, \\ \varrho_s \left(\frac{\partial V_s}{\partial t} + V_s \nabla V_s \right) + \nabla \mu &= F_{ns} \,, \end{aligned} \tag{1.6}$$

where

$$p_n = \frac{p}{\varrho_n} - \frac{\varrho_n \mu}{\varrho_s} \tag{1.7}$$

and p, ν_n, μ are pressure, kinematic viscosity of the normal component and chemical potential, correspondingly.

We illustrate the applications of Vinen model solving 3 simple problems.

2. Thermal-counterflow

The switched on heater power gives rise to a counterflow of the prescribed velocity V_{ns} (the inertia forces are neglected). According to Eq. (1.3), the counterflow makes the vortex line-length density to start growing from the initial value L_0 to the asymptotic one L_f

$$L_f = \left(\frac{c_{Lm}}{\kappa} \right)^2 V_{ns}^2 . \tag{2.1}$$

Then at the given time, the heater power is switched off ($V_{ns} = 0$) and the vortex line-length density sharply decreases. The solution $L_m(t)$ to equation (1.3) is shown in the Fig. 1. The characteristic tangle production time T_{prod} in which the vortex line-density reaches half of its asymptotic value is

$$T_{\text{prod}} = \int_{L_0}^{L_f/2} \frac{dl}{\alpha I_{lm}\left(V_{ns}L_m^{3/2} - \dfrac{\kappa}{c_{Lm}}L_m^2\right)} \simeq \frac{2}{\alpha I_{lm} V_{ns} L_0^{1/2}}. \tag{2.2}$$

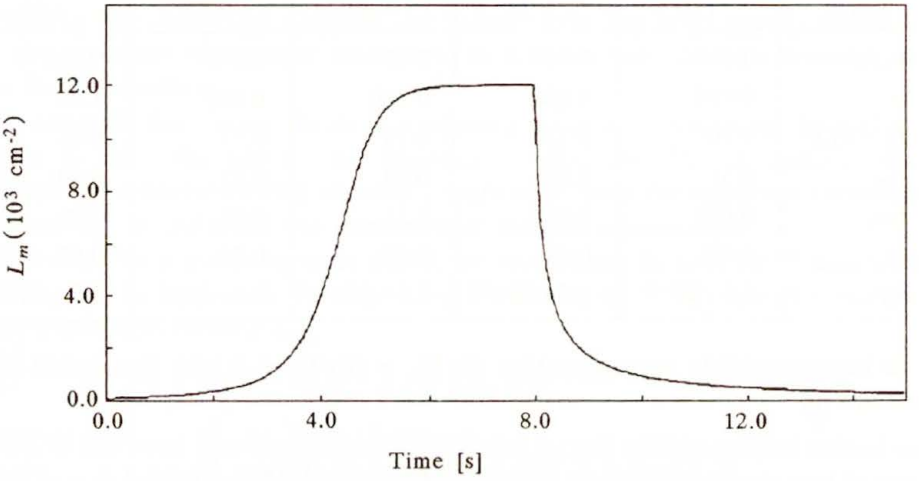

FIG. 1. Rise and decrease of vortex tangle density. At the time $t = 0$ heater power is switched on causing the thermal-counterflow of value 1 cm/s, then at the time $t = 8$ s heater power is switched off and the vortex line-length density sharply decreases. Temp. = 1.62° K.

The tangle production time is inversely proportional to the root of the initial vortex line-density, which can be small if the helium was left in peace for a long time, but even after very long time some remnant vortices are present. The minimum line-density observed value was $10\,\text{cm}^{-2}$, while the typical value for the superfluid turbulence is $10^3 \sim 10^7$ [cm^{-2}].

3. Entrainment Problem (1)

Here we restrict ourselves to the case in which the component velocities and the line-length density are only time-dependent. Let us assume that in the initial state the normal component is moving with the uniform velocity V_0, while the superfluid component remains at rest. The initial line-length density L_0 is assumed to be small when compared to the asymptotic value L_f for the steady

counterflow $V_{ns} = V_0$. The system is described by the set of 3 ordinary equations

$$\begin{aligned} \frac{dV_n}{dt} &= -\frac{\varrho_s \kappa \alpha L_m (V_n - V_s)}{\varrho_n}, \\ \frac{dV_s}{dt} &= \kappa \alpha L_m (V_n - V_s), \\ \frac{dL_m}{dt} &= \alpha I_{lm} \left(|V_n - V_s| L_m^{3/2} - \frac{\kappa}{c_{Lm}} L_m^2 \right). \end{aligned} \tag{3.1}$$

To rewrite the equations in the dimensionless form we introduce new variables

$$v_n = \frac{V_n}{V_0}, \qquad v_s = \frac{V_s}{V_0}, \qquad l = \frac{L_m}{L_f}, \tag{3.2}$$

where L_f is the asymptotic value for the steady counterflow $V_{ns} = V_0$ given in Eq. (2.1).

Then we have

$$\begin{aligned} \frac{dv_n}{dt} &= -\frac{1}{T_{ns}} \frac{l(v_n - v_s)\varrho_s}{\varrho_n}, \\ \frac{dv_s}{dt} &= \frac{1}{T_{ns}} L_m (v_n - v_s), \\ \frac{dl}{dt} &= \frac{1}{T_l} l^{3/2} \left(|v_n - v_s| - l^{1/2} \right), \end{aligned} \tag{3.3}$$

where T_{ns}, T_l are the characteristic times defined as follows:

$$\begin{aligned} T_{ns} &= \kappa \alpha^{-1} c_{Lm}^{-2} V_0^{-2}, \\ T_l &= \kappa \alpha^{-1} c_{Lm}^{-1} V_0^{-2} I_{lm}. \end{aligned} \tag{3.4}$$

T_l is the characteristic time scale of line density changes (when the density is of order L_f) and should not be confused with T_{prod} which is the time scale for the line-length density growth from a small initial value.

Introducing the new time $\tau = t/T_l$ we obtain

$$\begin{aligned} \frac{dv_n}{d\tau} &= -c_I \frac{l(v_n - v_s)\varrho_s}{\varrho_n}, \\ \frac{dv_s}{d\tau} &= c_I l (v_n - v_s), \\ \frac{dl}{d\tau} &= l^{3/2} \left(|v_n - v_s| - l^{1/2} \right), \end{aligned} \tag{3.5}$$

where

$$c_I = \frac{T_l}{T_{ns}} = \frac{c_{Lm}}{I_{lm}} \tag{3.6}$$

is the dimensionless temperature-dependent parameter.

The problem can be further reduced to the set of two equations

$$\begin{aligned} \frac{dv_{ns}}{d\tau} &= Clv_{ns}\,, \\ \frac{dl}{d\tau} &= l^{3/2}\left(|v_{ns}| - l^{1/2}\right), \end{aligned} \tag{3.7}$$

with $v_{ns} = v_n - v_s$ and $C = c_I(\varrho_n + \varrho_s)/\varrho_n$. Multiplying Eq. $(3.7)_1$ by v_{ns} one can see that v_{ns}^2 is not growing, so v_{ns} may not change the sign. It is enough to consider the case $v_{ns} \geq 0$ since the case $v_{ns} \leq 0$ is identical. The points ($l = 0$, v_{ns} – arbitrary) are invariant points to the set of Eq. (3.7). Although the case $l = 0$ is unphysical since some remnant vortices are always present, it may be still interesting to see if the manifold $l = 0$ is stable. Since $dl/d\tau > 0$ for $0 < l < v_{ns}^2$ all the points ($l = 0$, $v_{ns} > 0$) are unstable. The point ($l = 0$, $v_{ns} = 0$) is stable, moreover all trajectories starting from points ($l \neq 0$) tend to it. To prove the last fact it is enough to solve the following equations resulting from Eq. (3.7)

$$\frac{dl}{dv_{ns}} = K\left(\frac{l}{v_{ns}} - l^{1/2}\right), \tag{3.8}$$

with $K = 1/C$. Its solution is

$$l = (v_{ns})^K \left(\frac{K(v_{ns})^{(1-K/2)}}{K-2} + C_0\right)^2. \tag{3.9}$$

Now from Eq. $(3.7)_1$ we see that for positive l, v_{ns} tends to zero, and from Eq. (3.9) that l tends to zero with v_{ns} tending to zero. The last solution can be put into Eq. $(3.7)_1$ and then the equation is integrated.

The solutions to Eqs. (3.5) for 3 various temperatures and $V_0 = 1\,\mathrm{cm/s}$, $L_0 = 100\,\mathrm{cm}^{-2}$ are presented in Figs. 2–4. One can see that due to the initial relative velocity, the vortex line-length density grows up. Then the friction force (F_{ns}) makes the relative velocity decrease and may not sustain the vortex tangle, so the vortex line density decreases. The characteristic time T_{ent} in which the relative velocity V_{ns} is reduced e times from its initial value to V_0/e, decreases with increasing temperature. It is also worth to notice that since

$$T_{ns} \sim V_0^{-2}, \qquad T_l \sim V_0^{-2}, \tag{3.10}$$

hence

$$T_{\mathrm{ent}} \sim V_0^{-2}. \tag{3.11}$$

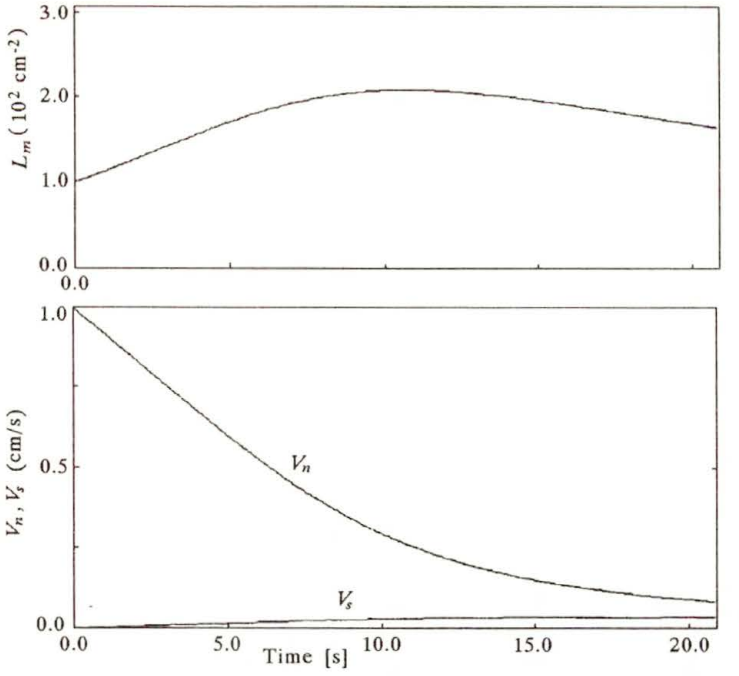

FIG. 2. Numerical solutions for the entrainment problem equations with the initial values $V_0 = 1\,\text{cm/s}$, $L_0 = 100\,\text{cm}^{-2}$. Temp. = 1.26° K.

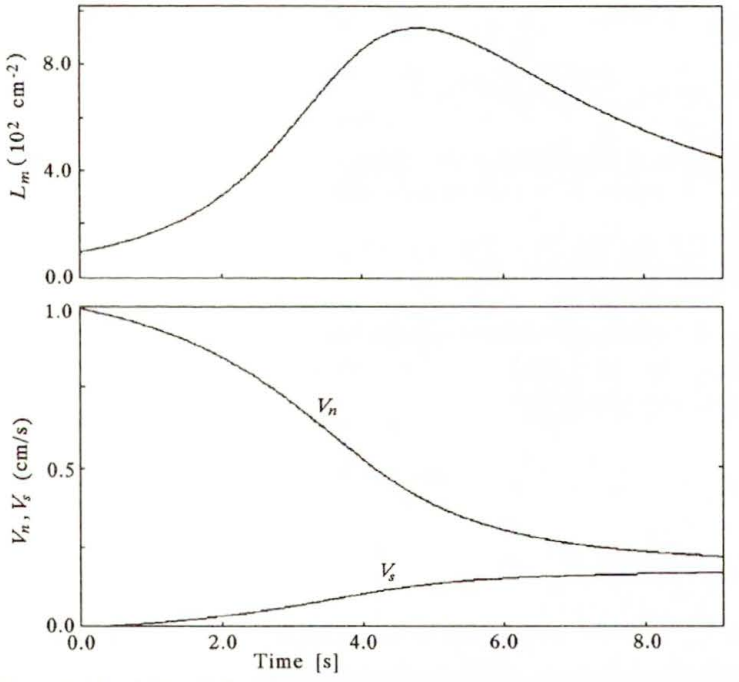

FIG. 3. Numerical solutions for the entrainment problem equations with the initial values $V_0 = 1\,\text{cm/s}$, $L_0 = 100\,\text{cm}^{-2}$. Temp. = 1.62° K.

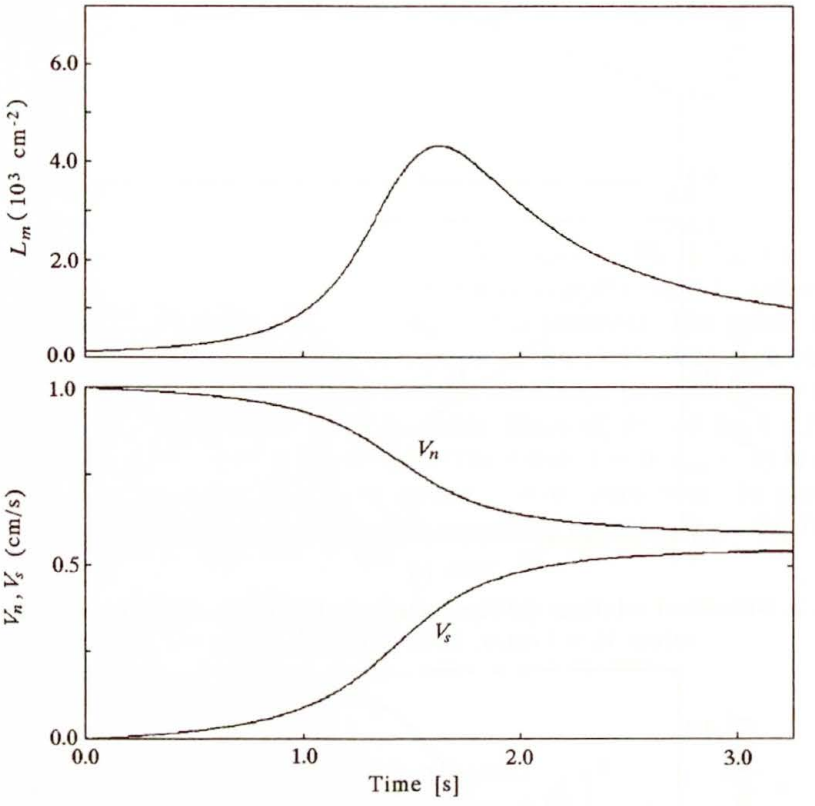

FIG. 4. Numerical solutions for the entrainment problem equations with the initial values $V_0 = 1\,\mathrm{cm/s}$, $L_0 = 100\,\mathrm{cm}^{-2}$. Temp. = 2.01° K.

4. Entrainment problem (2)

Another interesting problem arises when the normal component velocity V_s is fixed in time (for example by strong viscous forces). Then the problem reduces to the set of two equations

$$\begin{aligned} \frac{dv_s}{d\tau} &= c_I l(1 - v_s), \\ \frac{dl}{d\tau} &= l^{3/2}\left(|1 - v_s| - l^{1/2}\right). \end{aligned} \tag{4.1}$$

Putting $v_{ns} = 1 - v_s$ we get the same equations as (3.7) but with $C = c_I$. Now, for the same temperature the entrainment time ($\widetilde{T_{\mathrm{ent}}}$) is longer. The difference between $\widetilde{T_{\mathrm{ent}}}$ and T_{ent} is especially great for low temperatures when $\varrho_s \gg \varrho_n$. The solution to Eqs. (4.1) is given in Fig. 5, while Table 2 presents times $\widetilde{T_{\mathrm{ent}}}$ and T_{ent}, and gives values of L_f for the thermal-counterflow problem.

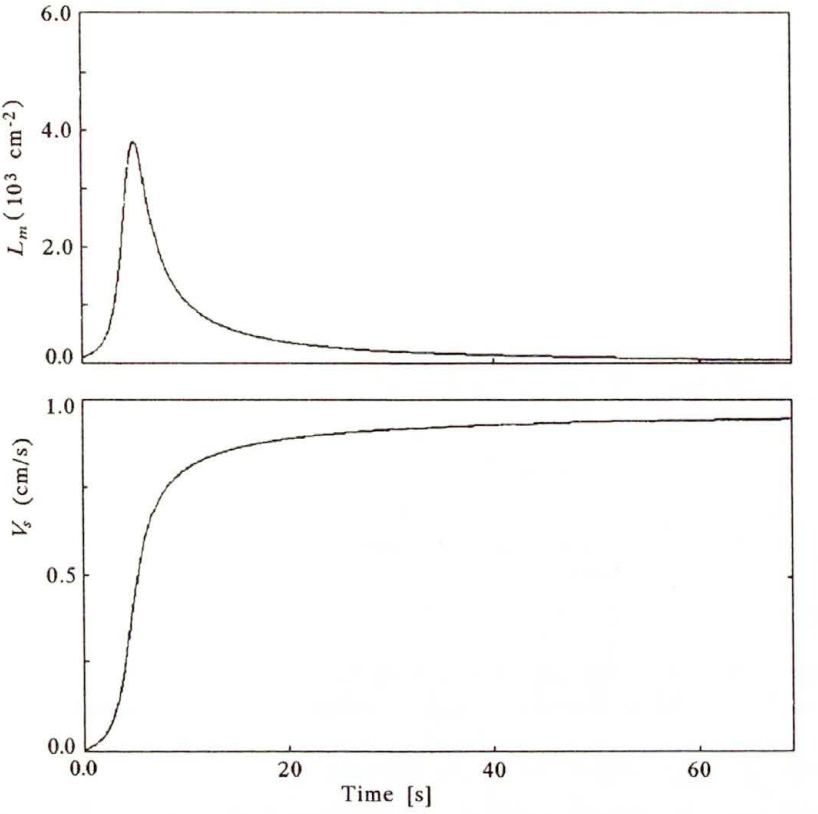

FIG. 5. Numerical solutions for the entrainment problem (2) equations with the initial values $V_0 = 1\,\mathrm{cm/s}$, $L_0 = 100\,\mathrm{cm}^{-2}$. Temp $= 1.62°$ K.

When considering the hydrodynamics of superfluid helium it is important to compare the entrainment times $\widetilde{T_{\mathrm{ent}}}$ and T_{ent} with the characteristic vorticity diffusion time scale

$$T_d = \frac{R_0^2}{\nu_n}, \tag{4.2}$$

where $\nu_n = \eta_n/\varrho_n$ is the viscosity of the normal component and R_0 is the characteristic length. In Table 2 the entrainment and the diffusion characteristic time scales are compared for various temperatures. When the characteristic relative velocity $V_{ns} = 1\,\mathrm{cm/s}$ and the characteristic size of a helium container $R_0 = 1\,\mathrm{cm}$, the diffusion time is much longer than the entrainment time, especially in a higher temperature. Whereas in very low temperatures, when the normal component is less abundant but more viscous, the two time scales are comparable.

For higher velocities and larger containers the T_d/T_{ent} ratio is even greater. It means that in the larger scale motions, helium II will behave almost like a classical fluid with the overall viscosity $\nu = \eta_n/\varrho$. In the finer scale however,

Table 2. Characteristic times [s] ($\widetilde{T_{\rm ent}}$ **and** $T_{\rm ent}$ **– numerical results for** $L_0 = 100\,{\rm cm}^{-2}$**) and the asymptotic line density** [${\rm cm}^{-2}$]. **All values are given for** V_0, $V_{ns} = 1\,{\rm cm/s}$, $\omega = 1/{\rm s}$, $R_0 = 1\,{\rm cm}$, **while appropriate scaling is given in last column.**

Temp.	1.07	1.26	1.62	2.01	2.15	scaling
$T_{\rm ent}$	11.5	8.0	4.3	1.60	0.63	$\sim V^{-2}$
$\widetilde{T_{\rm ent}}$	310	35	6.3	1.70	0.63	$\sim V^{-2}$
T_l	6.4	1.04	0.17	0.034	0.010	$\sim V^{-2}$
T_{ns}	104	8.8	0.84	0.092	0.015	$\sim V^{-2}$
$T_{\rm prod}$	39	12.8	3.7	1.28	0.51	$\sim V^{-1}$
T_d	67	330	1960	5550	5880	$\sim R^2$
$\widetilde{T_d}$	5150	8540	11260	9640	6640	$\sim R^2$
q	0.64	37.8	530	4340	11530	$\sim R^4\omega^2$
L_f	$9.5 \cdot 10^2$	$3.7 \cdot 10^3$	$1.2 \cdot 10^4$	$3.6 \cdot 10^4$	$6.8 \cdot 10^4$	$\sim V^2$

when the diffusion time is shorter and the smaller velocity may not sustain the quantum turbulence, the two components may move separately.

To see the problem in more detail we analyse the spin-up process focusing on the intermediate scale $V \sim 1\,{\rm cm/s}$, $R \sim 1\,{\rm cm}$. In the finer scale the Vinen (and any other continuum model) cannot be applied, just because few vortices are expected, and the spacing between the vortices is comparable with the length scale.

5. Analysis of the spin-up in an infinitely long cylinder

We consider here the problem of a spin-up in an infinitely long circular cylinder being impulsively subjected to spinning about its axis of rotation. The case of a finite cylinder is much more complicated because usually the spin-up process is dominated by a secondary flow which transports the vorticity from the boundaries to the center of the cylinder. The secondary flow arises because the fluid at the cylinder ends rotates with the velocity of the wall, and therefore is subject to centrifugal forces which drive it outwards.

In an infinitely long cylinder, the velocity is purely azimuthal and the spin-up of a classical fluid is described by linear equation

$$\frac{\partial V}{\partial t} = \nu \frac{\partial^2 V}{\partial r^2} + \frac{\partial}{\partial r}\left(\frac{V}{r}\right), \tag{5.1}$$

where ν is the kinematic viscosity.

In our case of two fluids, the component velocities $V_n(r,t)$, $V_s(r,t)$ and line length-density $L_m(r,t)$ satisfy the set of 3 differential equations

$$
\begin{aligned}
\frac{dV_n}{dt} &= \nu_n \Delta V_n - \frac{\varrho_s \kappa \alpha L_m (V_n - V_s)}{\varrho_n}, \\
\frac{dV_s}{dt} &= \kappa \alpha L_m (V_n - V_s), \\
\frac{dL_m}{dt} &= \alpha I_{lm} \left(|V_n - V_s| L_m^{3/2} - \frac{\kappa}{c_{Lm}} L_m^2 \right),
\end{aligned}
\tag{5.2}
$$

where

$$
\Delta V_n = \frac{\partial^2 V_n}{\partial r^2} + \frac{\partial}{\partial r}\left(\frac{V_n}{r}\right),
\tag{5.3}
$$

and $\nu_n = \eta_n/\varrho_n$ is the kinematic viscosity of the normal component. Let us assume that at time $t = 0$ the cylinder of radius R_0 starts to spin about its axis of symmetry with the constant angular velocity ω. The corresponding initial and boundary conditions are

$$
\begin{aligned}
V_n(r,0) = 0, \quad V_n(R_0,t) &= \omega \quad \text{for} \quad r < R_0\,, \quad t > 0, \\
V_s(r,0) &= 0 \quad \text{for} \quad r \le R_0\,, \\
L_m(r,0) &= L_0 \quad \text{for} \quad r \le R_0\,.
\end{aligned}
\tag{5.4}
$$

Again, to rewrite the equations in the dimensionless form we introduce the new variables

$$
v_n = \frac{V_n}{V_0}, \qquad v_s = \frac{V_s}{V_0}, \qquad l = \frac{L_m}{L_f},
\tag{5.5}
$$

where $V_0 = \omega R_0$ and L_f is the asymptotic value for the steady counterflow $V_{ns} = V_0$

$$
L_f = \left(\frac{c_{Lm}}{\kappa}\right)^2 (\omega R_0)^2.
\tag{5.6}
$$

Then we have

$$
\begin{aligned}
\frac{dv_n}{dt} &= \nu_n \Delta v_n - \frac{1}{T_{ns}} \frac{l(v_n - v_s)\varrho_s}{\varrho_n}, \\
\frac{dv_s}{dt} &= \frac{1}{T_{ns}} l (v_n - v_s), \\
\frac{dl}{dt} &= \frac{1}{T_l} l^{3/2} \left(|v_n - v_s| - l^{1/2} \right),
\end{aligned}
\tag{5.7}
$$

where T_{ns}, T_l are the characteristic times defined as earlier (3.4). Now, let $\xi = r/R_0$.

Introducing the new time variable $\tau = t/T_d$, where

$$T_d = \frac{R_0^2}{\nu_n} \tag{5.8}$$

is the characteristic diffusion time scale, we obtain

$$\begin{aligned} \frac{dv_n}{d\tau} &= \Delta_\xi v_n - q\frac{l(v_n - v_s)\varrho_s}{\varrho_n}, \\ \frac{dv_s}{d\tau} &= ql(v_n - v_s), \\ \frac{dl}{d\tau} &= \frac{q}{c_I} l^{3/2}\left(|v_n - v_s| - l^{1/2}\right), \end{aligned} \tag{5.9}$$

where

$$\begin{aligned} \Delta_\xi v_n &= \frac{\partial^2 v_n}{\partial \xi^2} + \frac{\partial}{\partial \xi}\left(\frac{v_n}{\xi}\right), \\ q &= \frac{T_d}{T_{ns}} = \frac{\alpha c_{Lm}^2 R_0^4 \omega^2}{\kappa \nu_n}, \end{aligned} \tag{5.10}$$

and

$$c_I = \frac{T_l}{T_{ns}} = \frac{c_{Lm}}{I_{lm}} \tag{5.11}$$

is defined as before.

We should notice that while c_I depends on temperature only, parameter q depends on the "experimental conditions" i.e. on the angular velocity and the radius of the cylinder.

When $q \gg 1$ i.e. when there is a strong coupling between the components, the fluid behaves like a classical one satisfying Eq. (5.1) with the overall viscosity $\nu = \eta_n/\varrho$. The velocity profile for the classical fluid with the viscosity equal to the overall helium viscosity at $T = 1.62°$ K are reproduced as a reference in Fig. 6.

The numerical solutions to the set of Eqs. (5.9) obtained for $R_0 = 1$ cm, $\omega = 1/\mathrm{s}$ for 3 various temperatures are presented in Figs. 7 – 10.

Figures 7 – 9 a, b show the velocity profiles of the normal and superfluid components for various temperatures. The line-length density profiles are given in Fig. 10. Figures 7 – 9 c show the scaled angular momentum m_n, m_s of the two components as a function of time.

$$m_s = \frac{M_s}{M_{s_f}}, \qquad m_n = \frac{M_n}{M_{n_f}}, \tag{5.12}$$

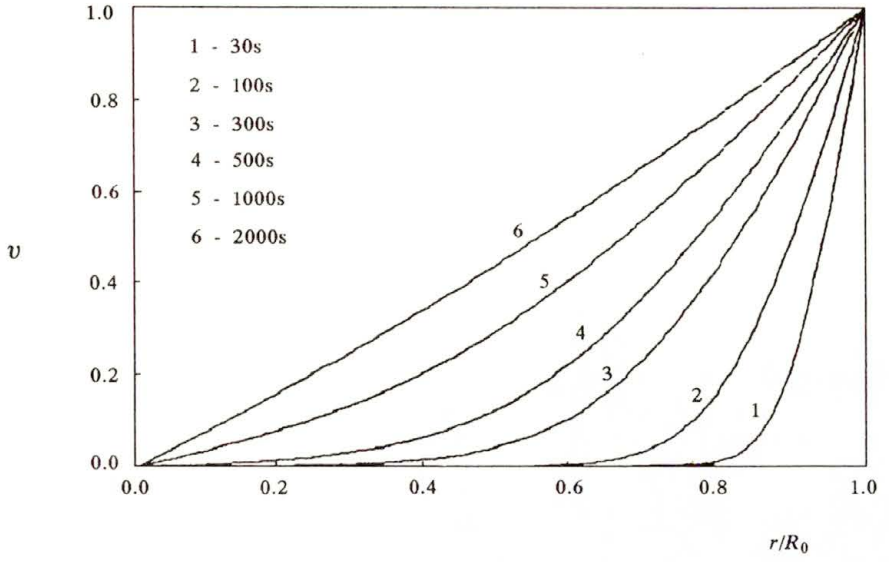

FIG. 6. Evolution of velocity profiles. Classical fluid with viscosity equal to overall viscosity of helium II at 1.62° K.

where the index f means the assymptotic value. Figures 7 – 9 d compare the time evolutions of the total angular momentum for the superfluid and the classical fluid having the same overall viscosity. One can see that for higher temperatures, the total angular momentum of the fluid grows almost as fast as in the classical case.

Table 3. Values of spin-up time T_{spin} for helium II and for classical fluid $\widetilde{T_{\mathrm{spin}}}$ with the same overall viscosity. T_n and T_s are spin-up times for normal and superfluid components, respectively.

Temp.	1.26	1.62	2.01
T_{spin}	450 s	590 s	510 s
$\widetilde{T_{\mathrm{spin}}}$	820 s	830 s	480 s
T_s	840 s	910 s	720 s
T_n	340 s	510 s	880 s

Let us define the spin-up time as a time in which the angular momentum of the fluid reaches 2/3 of its final value. Table 3 compares the spin-up time of the two component fluid with the spin-up time of the classical fluid with the same overall viscosity. The spin-up times of normal and superfluid components are also given for better reference.

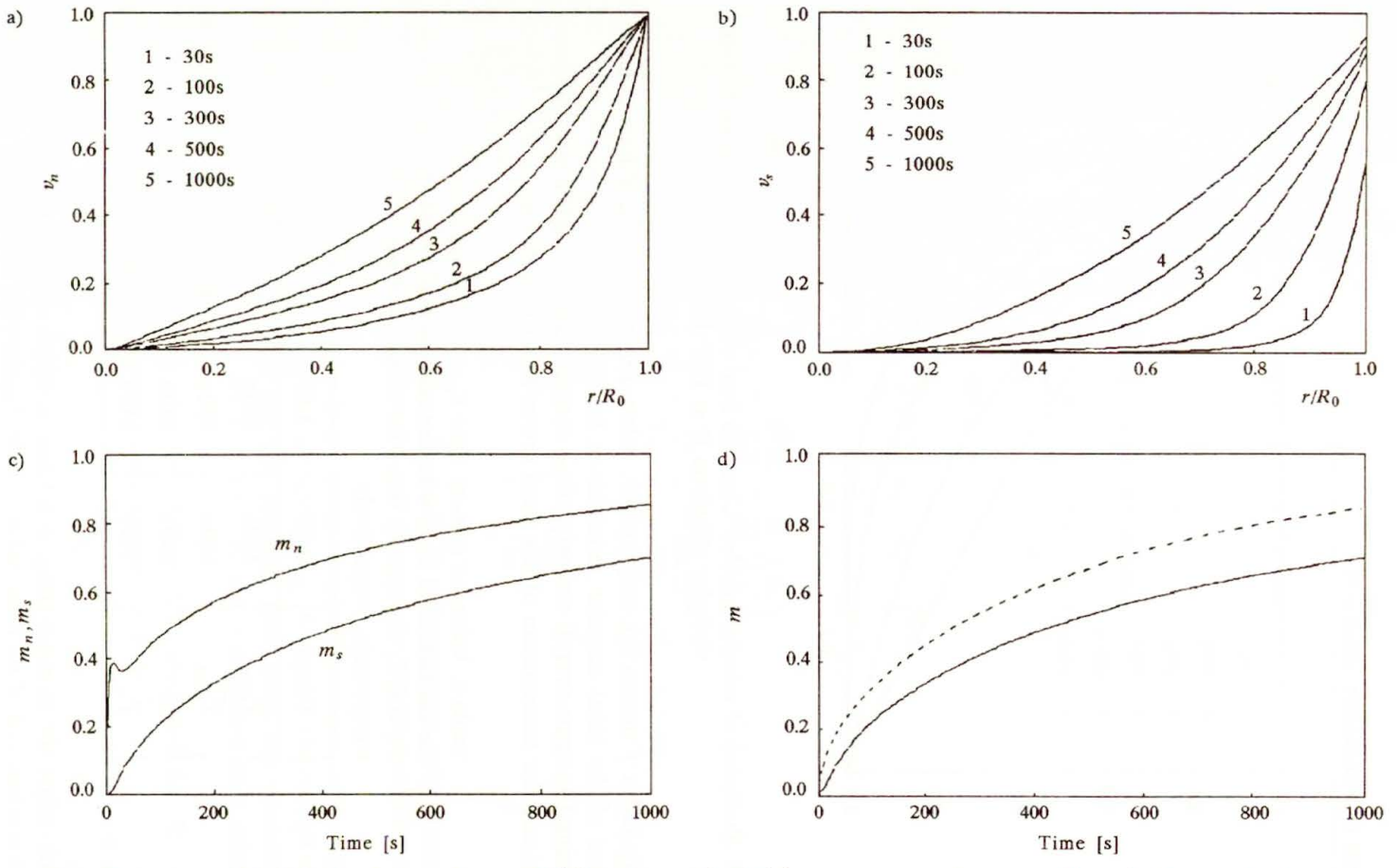

FIG. 7. Temp. = 1.26° K. Evolution of normal (a) and superfluid (b) component velocity profiles. c) Time evolution of scaled angular momentum, upper curve – normal component, lower curve – superfluid component. d) Time evolution of total angular momentum, dotted curve – classical fluid with the same overall viscosity.

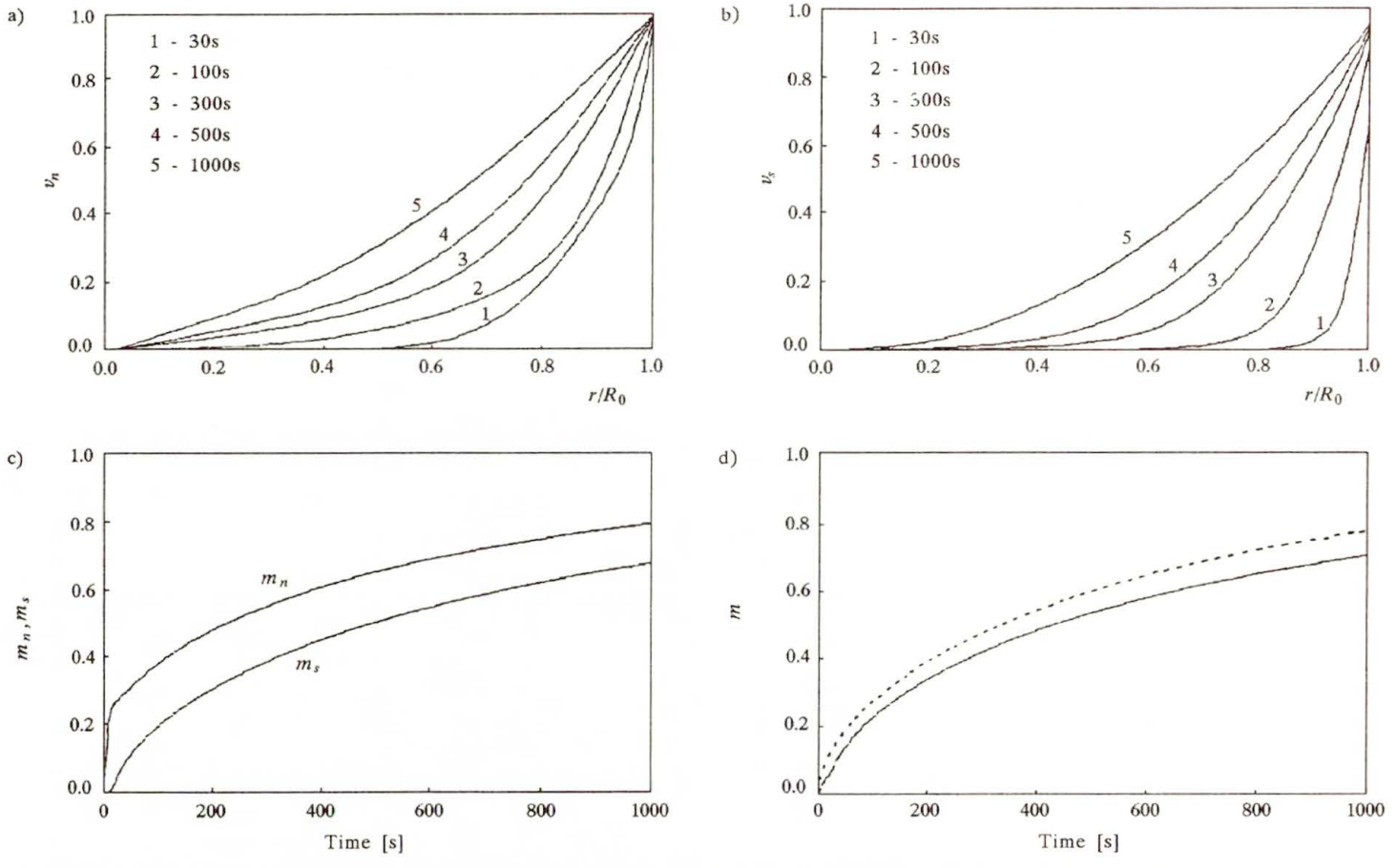

FIG. 8. Temp. = 1.62° K. Evolution of normal (a) and superfluid (b) component velocity profiles. c) Time evolution of scaled angular momentum, upper curve – normal component, lower curve – superfluid component. d) Time evolution of total angular momentum, dotted curve – classical fluid with the same overall viscosity.

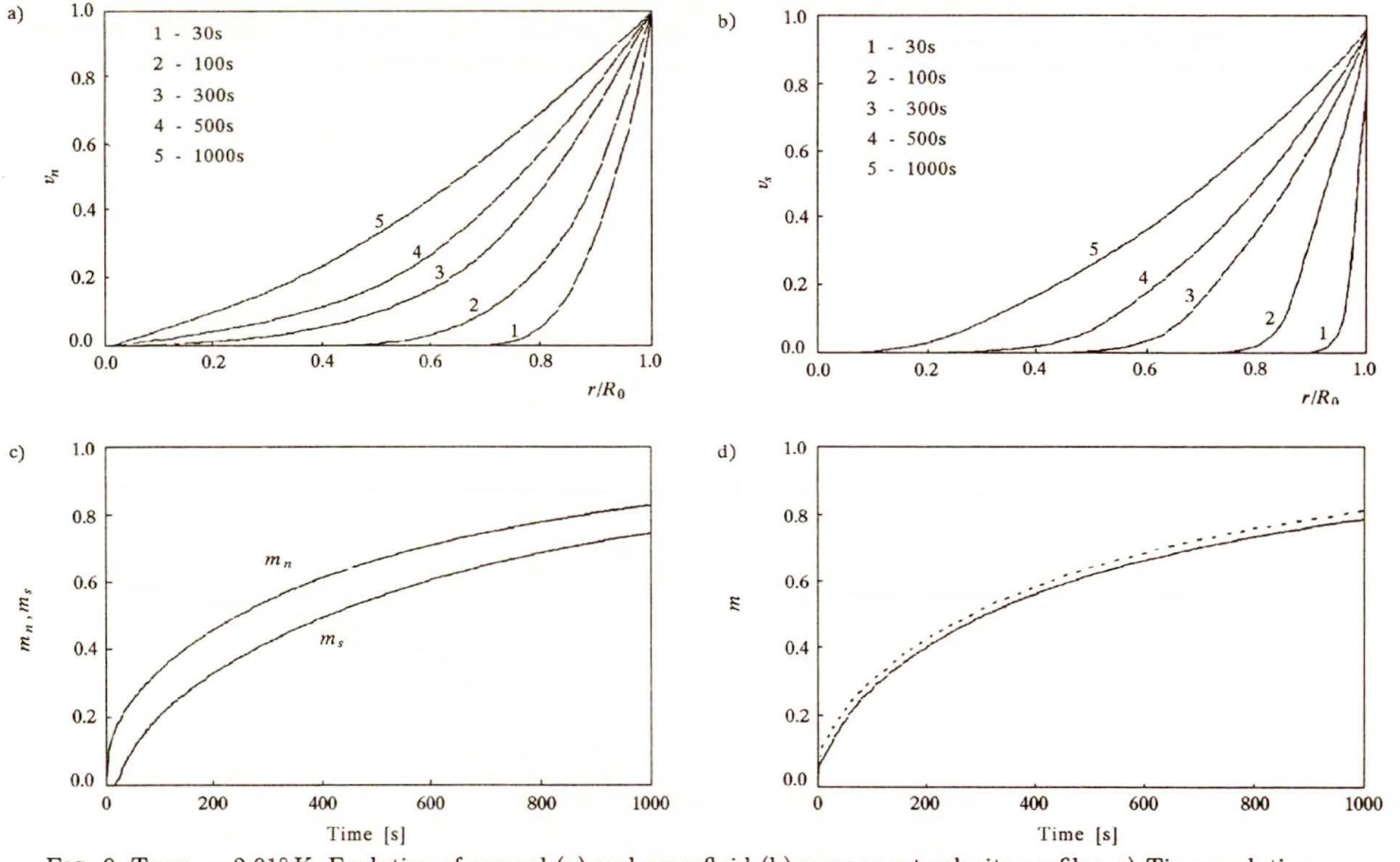

FIG. 9. Temp. = 2.01° K. Evolution of normal (a) and superfluid (b) component velocity profiles. c) Time evolution of scaled angular momentum, upper curve – normal component, lower curve – superfluid component. d) Time evolution of total angular momentum, dotted curve – classical fluid with the same overall viscosity.

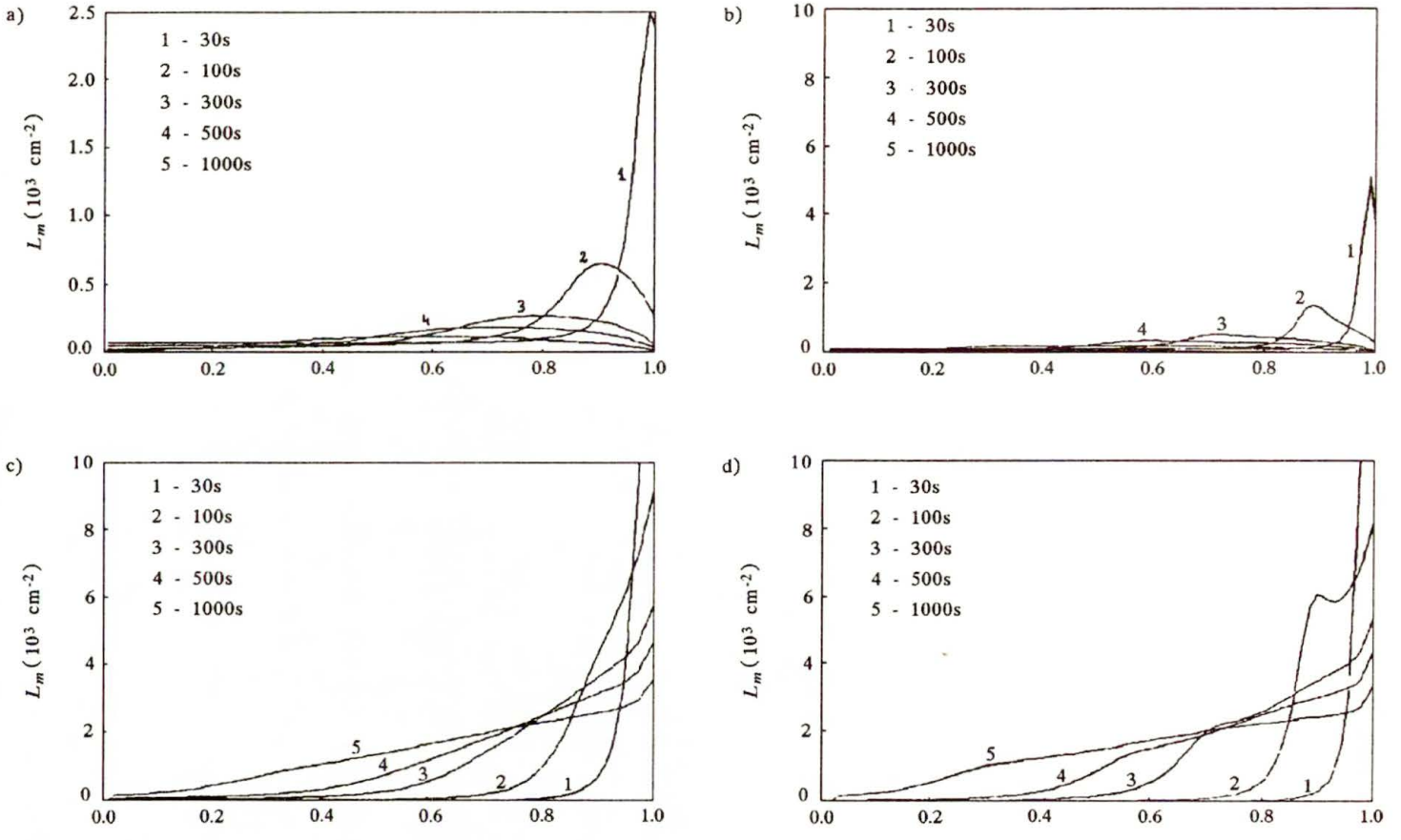

FIG. 10. Evolution of turbulent line-length density L_m, a) Temp. = 1.62 b) Temp. = 2.01 and parallel vortex line-length density $L_{\|}$, c) Temp = 1.62, d) Temp. = 2.01.

6. Conclusions

The presented mechanism of the spin-up process, based on the Vinen model, can be summed up as follows. When the cylinder starts moving, it drags the normal viscous component of helium II. Then according to Vinen equation (1.3), relative velocity of the two components gives rise to quantum turbulence. The mutual friction force caused by the turbulence couples the components, and the superfluid starts spinning. After a sufficiently long time both components will rotate as a rigid body (with the same velocities) and the turbulent vortex line-length density will decrease (according to Vinen equation) to zero. This cannot be of course satisfied, because the spinning superfluid component has to contain vortices. Their minimum length density $L_{||}$ (in the case when they are parallel) is

$$L_{||} = \frac{\omega}{\kappa}. \tag{6.1}$$

In the considered case the final value of $L_{||}$ is $2000/\mathrm{cm}^2$. Moreover one can see in Fig. 10 that the turbulent line-length density is much smaller than the "parallel vortex" line-length density calculated from superfluid velocity profiles. On the one hand, the large density of parallel vortices is due to the fact that mutual friction force makes the superfluid velocity profiles very steep. On the other hand, the Vinen equation (1.3) does not explain how such number of vortices may arise.

It can be clearly seen now that the Vinen model (in the present shape) cannot describe the turbulent flow which arises in the spinning cylinder. However, the first 3 examples show that the spin-up process is dominated by quickly arising turbulence. It points that the more accurate model should be rather based on the Vinen model than on the HVBH one (the analysis of spin-up in the HBVK model may be found in [10]).

The modified model should be related to the following facts:

1. The parallel vortices cannot decay unless the net superfluid vorticity change. Hence the second term in Vinen Equation has to be modified. The production of turbulent vortices due to the counterflow (first term in Vinen Equation) may be also influenced be an array of parallel vortices.

2. When the superfluid is dragged by normal component and starts spinning, the "turbulent vortices" have to change into locally parallel vortices. This means the negative source of turbulent vortices.

3. The Magnus force acting on the vortex tangle with a net vorticity makes that the vortex tangle moves across the counterflow; in the considered case inward the cylinder.

Pinning is the other important fenomena which may significantly influence the spin-up process. Quantum vortices pinned to the vessel boundaries may transfer the angular momentum directly from the cylinder to the superfluid component

(see [11]). This may be especially important in low temperatures when the normal component is less abundant.

Coming back to the entrainment and spin-up problem, we recall that the entrainment time scale $T_{\text{ent}} \sim V_0^{-2}$, where V_0 is characteristic counterflow velocity. This means that in experiments with larger velocities, the dynamics of helium II should be closer to the dynamics of classical fluid with the same overall viscosity.

Acknowledgments

Author is grateful to Prof. Z. PERADZYŃSKI for helpful discussion.

References

1. L. LANDAU, J. Phys., **5**, 71, 1941.
2. L. ONSAGER, Nouovo Cimento, **6**, 249, 1949.
3. R.P. FEYNMAN, [in:] Progress in Low Temperature Physics, Vol. I, p. 17, C.J. GORTER [Ed.] North-Holland, Amsterdam 1955.
4. W.F. VINEN, Proc. R. Soc. London, **A 240**, 114, (**240**, 128), (**242**, 493) 1957.
5. I.L. BEKAREVICH and I.M. KHALATNIKOV, Sov. Phys. JETP, **13**, 643, 1961.
6. K.W. SCHWARZ, Phys. Rev., **B 38**, 2398, 1988.
7. K.W. SCHWARZ and J.R. ROZEN, Phys. Rev., **B 44**, 7563, 1991.
8. J.A. GEURST and H. VAN BEELEN, Physica, **B 205**, 209, 1995.
9. S.K. NEMIROWSKII and D.W. SCHMIDT, [in:] Reflections on Some Problems Concerning the Role of Superfluid Turbulence, Max-Planck-Institut für Strömungsforschung, Bericht 8/1990.
10. Z. PERADZYŃSKI, S. FILIPKOWSKI and W. FISZDON, Eur. J. Mech., B/Fluids, **9**, 3, 259, 1990.
11. P.W. ADAMS, M. CIEPLAK and W.I. GLABERSON, Phys. Rev., **B 32**, 1, 171, 1985.

POLISH ACADEMY OF SCIENCES
INSTITUTE OF FUNDAMENTAL TECHNOLOGICAL RESEARCH
e-mail: tlipnia@ippt.gov.pl

Received November 8, 1996.

Arch. Mech., 49, 4, pp. 635–645, Warszawa 1997

Application of the Fourier cosine series to the approximation of solutions to initial non-Dirichlet boundary-value problems

Z. TUREK (WARSZAWA)

THE PAPER deals with an application of the Fourier cosine series to the determination of an approximate solution to some one-dimensional initial boundary-value problems. With the new approach one can approximate solutions of many equations of engineering and physics, without solving the eigenvalue problems. It has been found out that the new method can successfully be used for linear partial differential equations with non-Dirichlet boundary conditions. The heat equation and the wave equation with constant coefficients have been solved using the method described. The solutions have been compared to those obtained by means of the method of seperation of variables. The numerical results show that the new solutions approximate well the classical solutions. For the heat equation, even the boundary conditions at the initial instant of time are satisfied. This does not occur, however, in the case of the wave equation, since the initial displacement of the rod does not satisfy prescribed boundary conditions.

1. Introduction

THERE ARE some useful methods of solving linear initial boundary-value problems of partial differential equations. One of them is the method of seperation of variables, called the Fourier method [1]. It consists first in finding solutions of the corresponding eigenvalue problem for functions of spatial variables and next, in solving the set of decoupled ordinary differential equations for functions of time variable only. Finally the solution to the boundary-value problem is represented by an infinite series of these functions.

In [5] presenting the solution of the heat conduction equation it has been shown, that the solution to the problem can be represented, with an arbitrary accuracy, by the Fourier cosine series whose spatial components do not satisfy the boundary conditions given. In [6] the approach was applied to many other differential equations, both ordinary and partial. Many initial and boundary-value problems of linear and nonlinear ordinary differential equations were solved. Many cases with variable parameters were treated with this method as well.

In the present paper we prove that the Fourier cosine series is the "weak" solution to the heat conduction problem and to the wave equation, which is the solution to the so-called Integro-Differential-Boundary Equations (IDBE) [5] derived for the corresponding equation. The Fourier coefficients are calculated from the corresponding Infinite Set of Ordinary Differential Equations (ISODE)

using the Runge–Kutta method. The way how to get the IDBE and ISODE is shown in Secs. 3 and 4 of the paper, as well as in [5, 6].

In this paper, using the Fourier cosine series we solve two initial boundary-value problems with non-Dirichlet boundary conditions without solving the eigenvalue problems. The new approach has been applied to the equation describing the heat conduction subject to non-Dirichlet boundary conditions, and for the wave equation describing the vibrations of a rod also subject to non-Dirichlet boundary conditions. Solving the corresponding ISODE truncated at $N_a = 10$ for the heat equation and at $N_a = 15$ for the wave equation, a satisfactory approximation of the solutions obtained by means of the method of seperation of variables (called classical solutions), truncated at $N_c = 5$ for the heat equation and at $N_c = 10$ for the wave equation, have been achieved. Analysis of the boundary conditions has shown that for the heat conduction equation with prescribed initial condition, the boundary conditions at $t = 0$ are satisfied with an error decreasing as the number of components of the Fourier cosine series N_a increases. Analysing the boundary conditions of the wave equation for a given initial displacement of the rod, we have derived formulas for the boundary conditions at $t = 0$. They are expressed as convergent series of the Fourier cosine coefficients $c_k(0)$ but they do not tend to zero, which means that the new method of solution does not satisfy the prescribed boundary conditions at $t = 0$. The classical solution to the wave equation (derived by the method of separation of variables) is a generalized solution [2] and does not satisfy the prescribed boundary conditions either, since the initial condition u_0 for the problem does not satisfy the boundary conditions given [2].

2. Description of the method

Let us consider two second-order linear partial differential equations of the form:

$$\begin{aligned} &\frac{\partial U}{\partial t} - P\frac{\partial^2 U}{\partial x^2} - R\frac{\partial U}{\partial x} - QU = 0 \quad \text{for} \quad (x,t) \in (0,L) \times (0,t_e), \\ &\frac{\partial^2 U}{\partial t^2} - P\frac{\partial^2 U}{\partial x^2} - R\frac{\partial U}{\partial x} - QU = 0 \quad \text{for} \quad (x,t) \in (0,L) \times (0,t_e), \end{aligned} \tag{2.1}$$

with the boundary conditions

$$\begin{aligned} &\alpha U + \beta\frac{\partial U}{\partial x} = 0 \qquad \text{for} \quad x = 0, \\ &\gamma U + \delta\frac{\partial U}{\partial x} = 0 \qquad \text{for} \quad x = L \end{aligned} \tag{2.2}$$

for $t \in [0, t_e)$, and the initial conditions

$$U(x,0) = u_0(x), \qquad \frac{\partial U}{\partial t}(x,0) = v_0(x), \qquad \text{for} \quad x \in [0,L]. \tag{2.3}$$

P, Q, R in (2.1) are constants or functions of t only, α, β, γ and δ in (2.2) are constants and u_0 and v_0 in (2.3) are given functions of $x \in [0, L]$.

We assume that

$$\beta\delta \neq 0. \tag{2.4}$$

Let ϕ_n with $n = 0, 1, 2, \ldots$, denote functions of one space variable which form an orthogonal set on $\mathcal{L}^2[0, L]$ and let $\phi_n'' = -\mu_n^2 \phi_n$ for each n, where the double prime denotes the second derivative. Upon multiplying (2.1) by ϕ_n and integrating over the interval $(0, L)$, we see that

$$\begin{aligned} \frac{d^i}{dt^i}\int_0^L U(x,t)\phi_n(x)\,dx - P\int_0^L \frac{\partial^2 U}{\partial x^2}(x,t)\phi_n(x)\,dx - R\int_0^L \frac{\partial U}{\partial x}(x,t)\phi_n(x)\,dx \\ - Q\int_0^L U(x,t)\phi_n(x)\,dx = 0, \end{aligned} \tag{2.5}$$

where $i = 1$ corresponds to Eq. $(2.1)_1$ and $i = 2$ corresponds to Eq. $(2.1)_2$. Putting the following

$$\int_0^L \frac{\partial U}{\partial x}(x,t)\phi_n(x)\,dx = \phi_n(x)U(x,t)\Big|_0^L - \int_0^L U(x,t)\phi_n'(x)\,dx,$$

$$\begin{aligned} \int_0^L \frac{\partial^2 U}{\partial x^2}(x,t)\phi_n(x)\,dx = \phi_n(x)\frac{\partial U}{\partial x}(x,t)\Big|_0^L - \phi_n'(x)U(x,t)\Big|_0^L \\ -\mu_n^2\int_0^L U(x,t)\phi_n(x)\,dx \end{aligned}$$

into (2.5), we obtain the Integro-Differential-Boundary Equations [5] for the problems

$$\begin{aligned} \frac{d^i}{dt^i}\int_0^L U(x,t)\phi_n(x)\,dx + (P\mu_n^2 - Q)\int_0^L U(x,t)\phi_n(x)\,dx \\ + R\int_0^L U(x,t)\phi_n'(x)\,dx = F_n, \end{aligned}$$

$$\begin{aligned} F_n := U(0,t)\left(P\phi_n'(0) + \left(P\frac{\alpha}{\beta} - R\right)\phi_n(0)\right) \\ - U(L,t)\left(P\phi_n'(L) + \left(P\frac{\gamma}{\delta} - R\right)\phi_n(L)\right), \qquad n = 0, 1, 2, \ldots . \end{aligned} \tag{2.6}$$

On the right-hand side of F_n boundary conditions (2.2) have been taken into account. The functions F_n do not describe the case with Dirichlet boundary conditions. They are valid only for $\beta\delta \neq 0$ (non-Dirichlet boundary conditions).

3. "Weak" solutions to some boundary value problems

Let us consider the IDBE (2.6) with $R = 0$

$$\frac{d^i}{dt^i}\int_0^L U(x,t)\phi_n(x)dx + (P\mu_n^2 - Q)\int_0^L U(x,t)\phi_n(x)\,dx = F_n\,,$$

$$F_n = U(0,t)\left(\phi_n'(0) + \frac{\alpha}{\beta}\phi_n(0)\right)P \tag{3.1}$$

$$- U(L,t)\left(\phi_n'(L) + \frac{\gamma}{\delta}\phi_n(L)\right)P, \qquad n = 0,1,2,\ldots,$$

and introduce

DEFINITION. *A function*

$$u(\cdot,\cdot) : [0,L]\times[0,t_e) \to \mathcal{R}$$

is a "weak" solution to the boundary-value problem $(2.1)_1$, (2.2) *or* $(2.1)_2$, (2.2) *(for* $R = 0$*) with initial conditions* $(2.3)_1$ *or* (2.3), *respectively, if it satisfies the IDBE* (3.1), *that is the function* u *is a solution to*

$$\frac{d^i}{dt^i}\int_0^L u(x,t)\phi_n(x)\,dx + (P\,\mu_n^2 - Q)\int_0^L u(x,t)\phi_n(x)\,dx = F_n\,,$$

$$F_n = u(0,t)\left(\phi_n'(0) + \frac{\alpha}{\beta}\phi_n(0)\right)P \tag{3.2}$$

$$- u(L,t)\left(\phi_n'(L) + \frac{\gamma}{\delta}\phi_n(L)\right)P, \qquad n = 0,1,2,\ldots,$$

with $i = 1$ *for the heat equation and* $i = 2$ *for the wave equation.*

This definition differs from the definition known from the literature [3]; that is why we put it in quotes and name it "weak".

Now we shall prove the following

PROPOSITION. The "weak" solution to the boundary-value problem $(2.1)_1$, (2.2) or $(2.1)_2$, (2.2) (for $R = 0$) with initial conditions $(2.3)_1$ or (2.3), respectively, can be represented by the Fourier cosine series

$$u(x,t) \sim \frac{c_0(t)}{2} + \sum_{n=1}^{\infty} c_n(t)\cos\left(\frac{n\pi}{L}x\right), \tag{3.3}$$

whose coefficients satisfy an Infinite Set of Ordinary Differential Equations (ISODE):

$$
\begin{aligned}
&\frac{d^i}{dt^i}c_n + (P\mu_n^2 - Q)c_n = \frac{2}{L}F_n\,,\\
&F_n = \left(u(0,t)\frac{\alpha}{\beta} - u(L,t)\frac{\gamma}{\delta}(-1)^n\right)P,\\
&c_n(0) = \frac{2}{L}\int_0^L u_0(x)\cos\left(\frac{n\pi}{L}x\right)dx \qquad \text{for} \quad i = 1,2,\\
&\dot{c}_n(0) = \frac{2}{L}\int_0^L v_0(x)\cos\left(\frac{n\pi}{L}x\right)dx \qquad \text{for} \quad i = 2 \ \text{ only},\\
&n = 0,1,2,\dots\,,
\end{aligned}
\tag{3.4}
$$

where $\mu_n = n\pi/L$.

P r o o f. Let $u(x,t)$ represented by (3.3) be the solution to (3.2). For this representation, $\phi_n \equiv \cos(n\pi x/L)$ for $n = 0,1,2,...$, constitute the orthogonal bases in $\mathcal{L}^2[0,L]$, with $\mu_n = n\pi/L$ and the Fourier cosine series coefficients of the solution (3.3) can be calculated from

$$
c_n(t) = \frac{2}{L}\int_0^L u(x,t)\cos\left(\frac{n\pi}{L}x\right)dx, \qquad n = 0,1,2,\dots\,. \tag{3.5}
$$

If we now multiply $(3.2)_1$ by $2/L$ then we simply come to ISODEs $(3.4)_{1,2}$ for coefficients c_n. The initial conditions $(3.4)_{3,4}$ for the ISODEs follow from (3.5).

4. Main results

We shall consider two initial boundary value problems with non-Dirichlet boundary conditions:

- the heat conduction problem

$$
\frac{\partial U}{\partial t} - \frac{\partial^2 U}{\partial x^2} = 0 \qquad \text{for} \quad (x,t) \in (0,L)\times(0,t_e) \tag{4.1}
$$

with boundary conditions

$$
\begin{aligned}
&\frac{\partial U}{\partial x} - \mathrm{Bi}\,U = 0 \qquad \text{for} \quad x = 0,\\
&\frac{\partial U}{\partial x} + \mathrm{Bi}\,U = 0 \qquad \text{for} \quad x = L
\end{aligned}
\tag{4.2}
$$

for $t \in [0,t_e)$, where Bi is the Biot number,

and the initial condition

$$U(x,0) = u_0(x), \qquad \text{for} \quad x \in [0,L], \tag{4.3}$$

and

- the problem of vibration of a rod

$$\frac{\partial^2 U}{\partial t^2} - \frac{\partial^2 U}{\partial x^2} = 0 \qquad \text{for} \quad (x,t) \in (0,L) \times (0,t_e) \tag{4.4}$$

with the boundary conditions

$$\begin{aligned} \frac{\partial U}{\partial x} &= 0 \qquad \text{for} \quad x = 0, \\ \frac{\partial U}{\partial x} + gU &= 0 \qquad \text{for} \quad x = L \end{aligned} \tag{4.5}$$

for $t \in [0,t_e)$, where g is constant,
and the initial conditions

$$U(x,0) = u_0(x), \qquad \frac{\partial U}{\partial t}(x,0) = v_0(x), \qquad \text{for} \quad x \in [0,L]. \tag{4.6}$$

4.1. The heat conduction problem

The corresponding ISODE for the problem is the following one:

$$\begin{aligned} &\dot{c}_k + \mu_k^2 c_k + \frac{2\mathrm{Bi}}{L}\left(\frac{c_0(t)}{2}[1+(-1)^k] + \sum_{n=1}^{\infty} c_n(t)[1+(-1)^k(-1)^n]\right) = 0, \\ &c_k(0) = \frac{2}{L}\int_0^L u_0(x)\cos\left(\frac{k\pi}{L}x\right)dx, \qquad k = 0,1,2,\ldots . \end{aligned} \tag{4.7}$$

The calculations were carried out for $u_0(x) = 1+\sin[2\pi(x-L/4)/L]$, $L = 1$ with the Biot number $\mathrm{Bi} = 0.185$. The solution

$$U_a(x,t) \approx c_0(t)/2 + \sum_{k=1}^{N_a} c_k(t)\cos(k\pi x/L) \tag{4.8}$$

for $N_a = 10$ and its spatial derivatives for $N_a = 30$ evaluated for some time instants for every section of the layer, are presented in Figs. 1 and 2, respectively. The new results have been compared to the corresponding results of the classical solution

$$U_c(x,t) = \sum_{k=1}^{\infty} a_k \exp(-\omega_k^2 t)\psi_k(x), \tag{4.9}$$

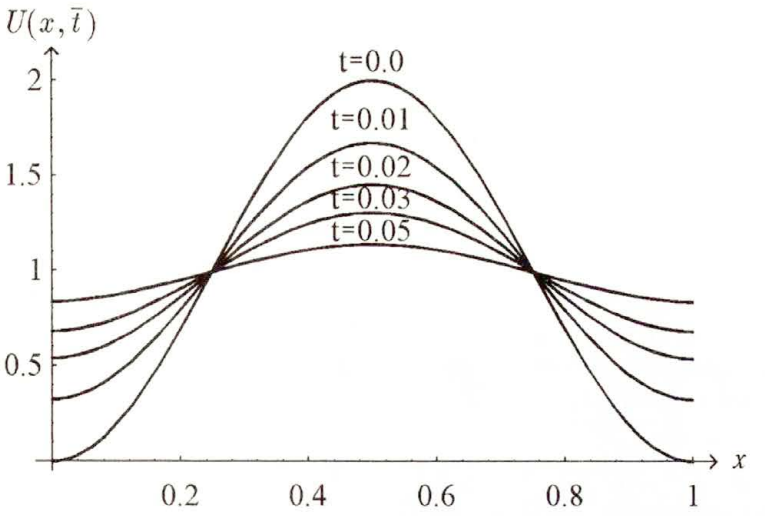

FIG. 1. Solution of the heat equation for some values of $\bar{t}$, for new solution (4.8) and for classical solution (4.9) (they cannot be distinguished).

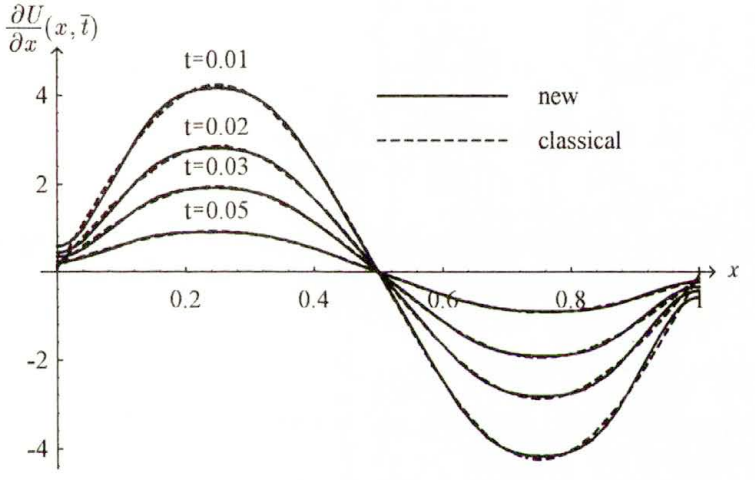

FIG. 2. Spatial derivative of the solution of the heat equation for some values of $\bar{t}$.

where $N_c = 5$ components of the series (4.9) were taken, and

$$\psi_k(x) = \omega_k \cos(\omega_k x) + \mathrm{Bi} \sin(\omega_k x)$$

are the eigenfunctions of the problem (4.1) – (4.3), with eigenvalues calculated from the equation

$$\mathrm{ctg}(\omega L) = \frac{\omega^2 - \mathrm{Bi}^2}{2\omega\,\mathrm{Bi}},$$

and

$$a_k = \int_0^L u_0(x)\psi_k(x)\,dx / \|\psi_k(x)\|^2.$$

From the figures presented one can see that the new solution and the classical solution cannot be distinguished even at the boundaries. This shows how the new solution converges well to the classical one. The spatial derivative of the new solution calculated for $N_a = 30$ does not approximate so well the spatial derivative of the classical solution as it happens in the case of the solutions themselves. This is true especially at the boundaries. The error is the largest for $t = 0$. One can show, however, that the error at $t = 0$ tends to 0 as the number N_a increases (see Fig. 3).

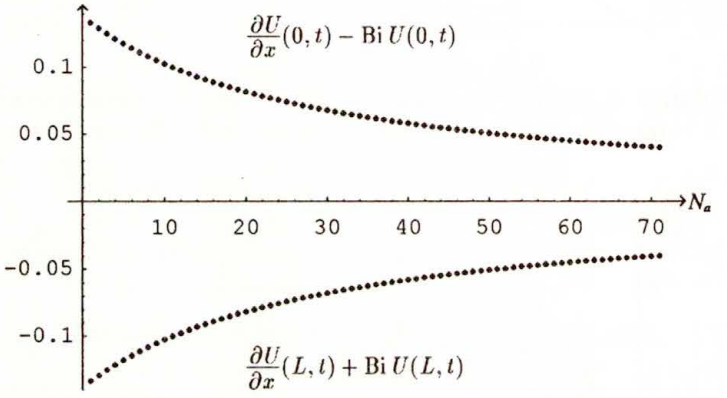

FIG. 3. Boundary conditions for the heat conduction at $t = 0$ according to the new approach.

4.2. Vibrations of a rod

For the vibrations of a rod we solved the following ISODE

$$\ddot{c}_k + \mu_k^2 c_k + (-1)^k \frac{2g}{L}\left(\frac{c_0(t)}{2} + \sum_{n=1}^{\infty} c_n(t)(-1)^n\right) = 0,$$

$$c_k(0) = \frac{2}{L}\int_0^L u_0(x)\cos\left(\frac{k\pi}{L}x\right)dx, \tag{4.10}$$

$$\dot{c}_k(0) = \frac{2}{L}\int_0^L v_0(x)\cos\left(\frac{k\pi}{L}x\right)dx, \qquad k = 0,1,2,\ldots .$$

The calculations were carried out for $u_0(x) \equiv a(x - L)$, $v_0(x) \equiv 0$, $g = 2$,

$a = -0.01$. The solution

$$U_a(x,t) \approx c_0(t)/2 + \sum_{k=1}^{N_a=15} c_k(t)\cos(k\pi x/L) \tag{4.11}$$

for some time instants for every cross-section of the rod is presented in Fig. 4, but the solution for chosen cross-sections of the rod in the given time period are shown in Fig. 5. The new results have been compared with the classical solutions

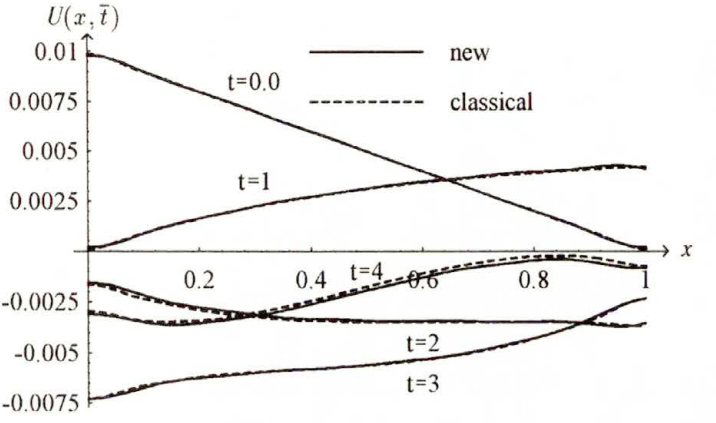

FIG. 4. Solution of the wave equation for some values of $\bar{t}$.

of the problem (4.4) – (4.6),

$$U_c(x,t) = \sum_{k=1}^{\infty}[a_k\cos(\omega_k t) + b_k\sin(\omega_k t)]\cos(\omega_k x), \tag{4.12}$$

with $N_c = 10$ components of the series (4.12) taken, and with eigenvalues calculated from the equation

$$\omega\tan(\omega L) = g$$

and

$$a_k = \int_0^L u_0(x)\cos(\omega_k x)\,dx/\|\cos(\omega_k x)\|^2,$$

$$b_k = \frac{1}{\omega_k}\int_0^L v_0(x)\cos(\omega_k x)\,dx/\|\cos(\omega_k x)\|^2 = 0.$$

From Figs. 4 and 5 one can see that the new solution approximates well the classical solution, although the curves are quite complicated.

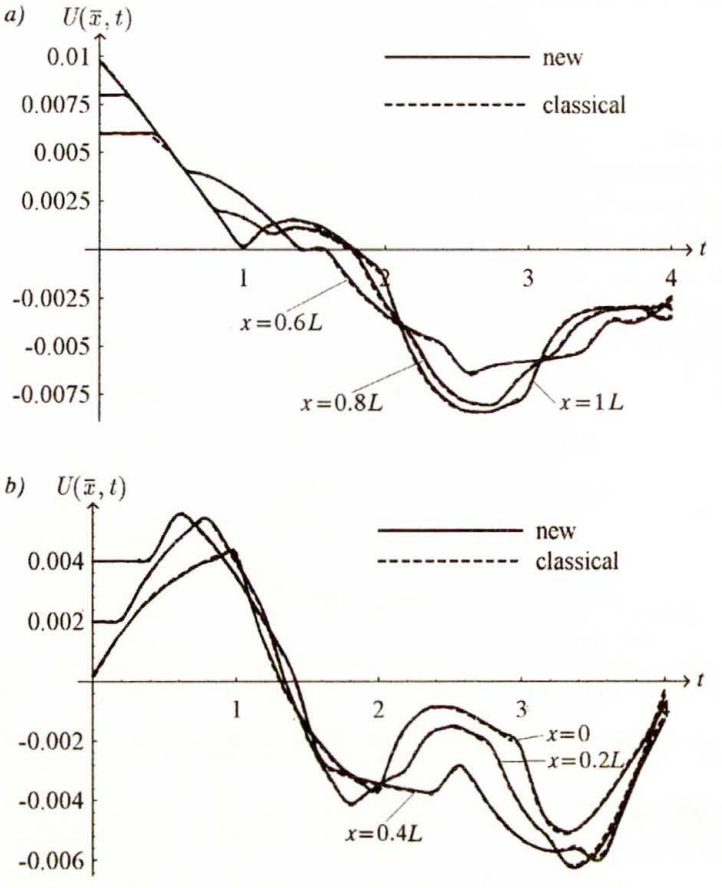

FIG. 5. Solution of the wave equation for some values of $\bar{x}$.

From the boundary conditions of the problem considered, using Theorem 6 from [6], one can derive the following formulas for the boundary conditions at $t = 0$:

$$
\begin{aligned}
a + \sum_{k=1}^{\infty} \bar{c}_k(0) &= 0 \qquad \text{for} \quad x = 0, \\
a - g\frac{aL}{2} + \sum_{k=1}^{\infty} \left[\bar{c}_k(0) + g\, c_k(0)\right](-1)^k &= 0 \qquad \text{for} \quad x = L,
\end{aligned}
\tag{4.13}
$$

where

$$
\bar{c}_k(0) := \frac{16a}{\pi^2} \sum_{j=1}^{\infty} \frac{1}{(2k)^2 - (2j-1)^2}, \qquad k = 1, 2,
$$

and

$$c_k(0) = -\frac{4aL}{(2k-1)^2\pi^2}, \qquad k = 1, 2, \ldots .$$

The left-hand sides of (4.13) are covergent series but they do not equal 0. Their value is a for both $x = 0$ and $x = L$. Therefore the boundary conditions for this initial condition are not satisfied in the new approach. The conditions are not satisfied in the classical approach as well, as the classical solution (4.12), for this initial condition u_0 is in a generalized form [2].

5. Remarks

The results obtained in the paper have revealed that the new method can succesfully be used for the solution to other boundary value problems with non-Dirichlet boundary conditions. The experience gained also shows that the new approach can be used for other boundary conditions (e.g. Dirichlet conditions) [6] and for other BVPs that cannot be solved by the method of seperation of variables (e.g. boundary value problems with mixed derivatives).

Acknowledgment

The author thanks Prof. A. CIARKOWSKI for valuable comments which resulted in improving the final version of the paper.

References

1. R.V. CHURCHILL and J.W. BROWN, *Fourier series and boundary value problems*, McGraw-Hill Book Company, New York 1978.
2. S. KALISKI [Ed.] *Vibrations and waves* [in Polish], PWN, Warszawa 1966.
3. H. MARCINKOWSKA, *Introduction to the theory of partial differential equations* [in Polish], PWN, Warszawa 1986.
4. A.N. TICHONOV and A.A. SAMARSKI, *Equations of mathematical physics* [in Polish], PWN, Warszawa 1963.
5. Z. TUREK, *A new method of finding approximate solutions of the heat conduction equation*, Engng. Trans., **44**, 2, pp. 295–301, 1996.
6. Z. TUREK, *Application of the Fourier cosine series for the solution of differential equations* [in Polish], ZTUREK Research-Scientific Institute, Warszawa 1996.

ZTUREK RESEARCH–SCIENTIFIC INSTITUTE
02-352 Warszawa, Szczęśliwicka 2/26.
e-mail: zturek@ippt.gov.pl

Received April 4, 1996; new version October 8, 1996.

Arch. Mech., 49, 4, pp. 647–663, Warszawa 1997

Rigorous bounds on the asymptotic expansions of effective transport coefficients of two-phase media

S. TOKARZEWSKI, A. GAŁKA (WARSZAWA)
and G. STARUSHENKO (DNEPROPETROVSK)

THE FUNDAMENTAL inequalities for two-point Padé approximants corresponding to two asymptotic expansions of the effective transport coefficients $\lambda_e(x)/\lambda_1$, $x = \lambda_2/\lambda_1 - 1$ have been derived, where λ_1 and λ_2 denote the transport moduli of the composite components. The inequalities achieved constitute the new bounds on the values of $\lambda_e(x)/\lambda_1$ – the best with respect to the given number of coefficients of the asymptotic expansions of $\lambda_e(x)/\lambda_1$ at $x = 0$ and $x = \infty$. For the particular cases, our two-point Padé bounds reduce to the classical estimations of $\lambda_e(x)/\lambda_1$ available in literature [7, 9, 17, 24].

1. Introduction

PREDICTION of the macroscopic behaviour of a composite from the known physical and geometrical properties of the components is one of the basic problems of mechanics of inhomogeneous media. Most of the papers which have appeared in recent years dealt with the estimations of the effective transport coefficients $\lambda_e(x)$, $x = \lambda_2/\lambda_1 - 1$ such as thermal and electrical conductivities, magnetic permeability, diffusion coefficient, filtration coefficients and many others. Here λ_1 and λ_2 denote the moduli of the components of an investigated composite, cf. [6, 7, 9, 17, 23, 24].

WIENER [34] derived optimal bounds on $\lambda_e(x)$ with prescribed volume fractions. These bounds are known as the arithmetic and harmonic mean bounds. For isotropic materials HASHIN and SHTRIKMAN [17] improved Wiener's bounds using variational principles. BERGMAN [4, 5, 6] introduced a method for obtaining bounds on $\lambda_e(x)$, which does not rely on variational principles. Instead it exploits the properties of the effective parameters being analytic functions of the components moduli. The method of Bergman was studied in more detail and applied to several physical problems by MILTON [23, 24]. A rigorous justification of Bergman's approach was given by GOLDEN and PAPANICOLAOU [14]. Recently special continued fraction techniques for evaluation of the bounds on $\lambda_e(x)$ have been used by BERGMAN [7] for three-dimensional, and CLARK and MILTON [9] – for two-dimensional systems. Both MILTON [24] and BERGMAN [7] have incorporated into the bounds the power expansion of $\lambda_e(x)$ at $x = 0$ and the discrete values of $\lambda_e(x)$ given by $\lambda_e(x_1)$, $\lambda_e(x_2)$, ..., $\lambda_e(x_K)$ only.

The present paper incorporates into bounds on $\lambda_e(x)$ two formal power expansions of $\lambda_e(x)$ available at $x = 0$ and $x = \infty$. That incorporation problem has

been studied recently in the contexts of the estimation of Stieltjes functions [11, 25, 27, 28] and the bounds on the effective conductivity of regular composites [26, 29–32]. However, the estimations derived in [11, 28, 29] are valid for $x > 0$ only. Consequently they are not the best possible bounds on $\lambda_e(x)$.

The main aim of this paper is to establish new bounds on real-valued moduli $\lambda_e(x)$ of two-phase media, the best with respect to the available coefficients of the power expansions of $\lambda_e(x)$ at $x = 0$ and $x = \infty$.

This paper is organized as follows: In Sec. 2 we introduce the basic definitions, notations and assumptions dealing with a Stieltjes function $xf_1(x)$ and two-point Padé approximants of the types $2PAs$ and $\overline{2PAs}$ constructed for $xf_1(x)$. In Sec. 3 we recall the relevant results for one-point Padé approximants. In Sec. 4 we propose special continued fraction representations for $2PAs$ and $\overline{2PAs}$. The fundamental inequalities for $2PAs$ and $\overline{2PAs}$ to $xf_1(x)$ have been derived in Sec. 5 and 6. In Sec. 7 the effective conductivity of a square array of cylinders has been investigated in terms of low order $2PAs$ and $\overline{2PAs}$ bounds. The results achieved are summarized in Sec. 8.

2. Preliminaries

Let us consider the effective conductivity $\Lambda_e(x)$ of a two-phase medium for the case, where the conductivity coefficients λ_1 and λ_2 of both components are real, $x = (\lambda_2/\lambda_1) - 1$. The bulk conductivity $\Lambda_e(x)$ is defined by the linear relationship between the volume-averaged gradient temperature $<\overrightarrow{\nabla T}>$ and the volume-averaged heat flux $<\vec{q}>$

$$<\vec{q}> = \Lambda_e(x) <\overrightarrow{\nabla T}> . \tag{2.1}$$

For the sake of simplicity, the averaging is performed over the unit cell of a periodic composite, where T denotes the temperature. In general, Λ_e is a second-rank symmetric tensor, even when λ_1 and λ_2 are both scalars. Our study will be focused upon one of the diagonal values of Λ_e denoted by λ_e. The remaining diagonals can be studied analogously.

The analytic properties of the bulk conductivity coefficient $\lambda_e(\lambda_1, \lambda_2)$ were examined by BERGMAN in [4]. He noticed that $\lambda_e(\lambda_1, \lambda_2)/\lambda_1 = \lambda_e(1, \lambda_2/\lambda_1)$ is an analytical function in the complex plane except on the negative part of the real axis. GOLDEN and PAPANICOLAOU [14] rigorously proved that $\lambda_e(x)$, $x = h - 1$, $h = \lambda_2/\lambda_1$ has a Stieltjes-integral representation of the type:

$$\frac{\lambda_e(x)}{\lambda_1} - 1 = xf_1(x) = x \int_0^1 \frac{d\gamma_1(u)}{1 + xu}, \qquad -1 < x < \infty. \tag{2.2}$$

For composites consisting of non-touching inclusions of modulus λ_2 embedded in a matrix material of modulus λ_1, the function $xf_1(x)$ obeys the following physical

restriction, cf. [4–7],

$$\lim_{x\to -1_+} x f_1(x) \geq -1. \tag{2.3}$$

The spectrum $\gamma_1(u)$ appearing in (2.2) is a real, bounded and non-decreasing function defined on $0 \leq u \leq 1$. Consider the power expansion of $xf_1(x)$ at $x = 0$, cf. (2.2),

$$x f_1(x) = \sum_{n=1}^{\infty} c_n^{(1)} x^n. \tag{2.4}$$

Here the coefficients

$$c_n^{(1)} = (-1)^{n+1} \int_0^1 u^{n-1}\, d\gamma_1(u) \tag{2.5}$$

are real and finite. Note that on account of (2.2), the power series (2.4) has a radius of convergence at least equal 1. The power series expansion of $xf_1(x)$ at $x = \infty$ takes the form, cf. (2.2),

$$x f_1(x) = \sum_{n=0}^{\infty} C_n^{(1)} s^n, \qquad s = 1/x, \tag{2.6}$$

where the moments

$$C_n^{(1)} = (-1)^n \int_0^1 u^{-1-n}\, d\gamma_1(u), \qquad n = 0, 1, 2, \ldots \tag{2.7}$$

are assumed to be finite for any fixed n. Two-point Padé approximants of the type $[k/M]$ and $\overline{[k/M]}$ to series (2.4) and (2.6) are given by the following rational functions

$$[k/M] = \frac{a_{1k}x + a_{2k}x^2 + \cdots + a_{Mk}x^M}{1 + b_{1k}x + b_{2k}x^2 + \cdots + b_{Mk}x^M}, \tag{2.8}$$

$$\overline{[k/M]} = \frac{\bar{a}_{1k}x + \cdots + \bar{a}_{(M+\delta_{0k})k}x^{(M+\delta_{0k})}}{1 + \bar{b}_{1k}x + \cdots + \bar{b}_{Mk}x^M}, \qquad \delta_{0k} = \begin{cases} 1, & \text{if } k = 0, \\ 0, & \text{if } k > 0. \end{cases} \tag{2.9}$$

Consider the power expansions of (2.8) and (2.9) at $x = 0$:

$$[k/M] = \sum_{n=1}^{\infty} c_{nk} x^n, \qquad \overline{[k/M]} = \sum_{n=1}^{\infty} \bar{c}_{nk} x^n, \tag{2.10}$$

and at $x = \infty$

$$[k/M] = \sum_{n=0}^{\infty} C_{nk} s^n, \qquad \overline{[k/M]} = \sum_{n=0}^{\infty} \overline{C}_{nk} s^n, \qquad s = 1/x. \tag{2.11}$$

Now we are in a position to introduce the definitions of two-point Padé approximants of the types $2PAs$ and $\overline{2PAs}$ to $xf_1(x)$:

DEFINITION 1. *The rational function* $[k/M]$ *given by* (2.8) *is a* $2PAs$ *(two-point Padé approximant) to* $xf_1(x)$, *if*

$$c_{nk} = c_n^{(1)} \qquad \text{for} \quad n = 1, 2, ..., p, \quad p = 2M - k \tag{2.12}$$

and

$$C_{nk} = C_n^{(1)} \qquad \text{for} \quad n = 0, 1, ..., k-2, \quad C_{(k-1)k} = C_{k-1}^{(1)}. \tag{2.13}$$

Note that for $k = 0$ *and* $k = 2M$, *the rational functions* $[k/M]$ *stand for one-point Padé approximants* ($1PAs$), cf. [1, 2]. □

DEFINITION 2. *The rational function* $\overline{[k/M]}$ *given by* (2.9) *is a* $\overline{2PAs}$ *to* $xf_1(x)$, *if*

$$\overline{c}_{nk} = c_n^{(1)} \qquad \text{for} \quad n = 1, 2, ..., p, \quad p = 2M - k, \tag{2.14}$$

and

$$\begin{aligned} \overline{C}_{nk} &= C_n^{(1)} \qquad \text{for} \quad n = 0, 1, ..., k-2, \\ \overline{[k/M]} &= -1 \qquad \text{for} \quad x = -1. \end{aligned} \tag{2.15}$$ □

Throughout this paper the parameter p $(0 \leq p \leq 2M)$ will denote a number of the available coefficients of the power series (2.4), while k $(0 \leq k \leq 2M)$ – a number of relations given by (2.13) if we deal with $[k/M]$, or by (2.15) if we study $\overline{[k/M]}$. The parameters p, k and M are interrelated by $p + k = 2M$.

3. One-point Padé approximants

We start our discussion by recalling some results for one-point Padé approximants $[0/M]$ to $xf_1(x)$, indispensable for our further investigations. Those results may be summarized as follows:

1. $[0/M]$ has the continued fraction representation of the type S [1–3]

$$[0/M] = \frac{xe_1}{1} + \frac{xe_2}{1} + \ldots + \frac{xe_{2M-1}}{1} + \frac{xe_{2M}}{1}. \tag{3.1}$$

2. The coefficients of the continued fraction (3.1) are positive

$$e_n > 0, \qquad n = 1, 2, ..., 2M. \tag{3.2}$$

3. For $x > -1$ the Padé approximants $[0/M]$ to power series (2.4) converge to the Stieltjes function (2.2), cf. [1, Th. 16.2]

$$\lim_{M\to\infty} [0/M] = xf_1(x). \tag{3.3}$$

4. If $xf_j(x)$ is a Stieltjes function

$$xf_j(x) = x \int_0^1 \frac{d\gamma_j(u)}{1+xu}, \tag{3.4}$$

then the function $xf_{j+1}(x)$ is also a Stieltjes function

$$xf_{j+1}(x) = x \int_0^1 \frac{d\gamma_{j+1}(u)}{1+xu}, \tag{3.5}$$

provided that

$$f_j(x) = \frac{f_j(0)}{1+xf_{j+1}(x)}, \tag{3.6}$$

cf. [1, Lemma 15.3] and [1, p. 235]. If the expansion of $xf_j(x)$ at $x = \infty$ is given by

$$xf_j(x) = \sum_{n=0}^{\infty} C_n^{(j)} (1/x)^n, \qquad C_0^{(j)} > 0, \tag{3.7}$$

then on account of (3.6), the expansion of $xf_{j+1}(x)$, also at $x = \infty$, takes the form

$$xf_{j+1}(x) = C^{(j+1)}x + \sum_{n=0}^{\infty} C_n^{(j+2)} (1/x)^n, \qquad C^{(j+1)} = \frac{f_j(0)}{C_0^{(j)}} > 0. \tag{3.8}$$

Consequently we have the following relations

$$xf_{j+1}(x) = C^{(j+1)}x + xf_{j+2}(x), \tag{3.9}$$

where

$$f_{j+2}(x) = \int_0^1 \frac{d\gamma_{j+2}(u)}{1+xu} \tag{3.10}$$

is a Stieltjes function. The relations (3.7) – (3.10) permit us to formulate the following remark:

REMARK 1. If $xf_j(x)$ is a Stieltjes function

$$xf_j(x) = x\int_0^1 \frac{d\gamma_j(u)}{1+xu} = \sum_{n=0}^{\infty} C_n^{(j)} s^n, \qquad s = 1/x, \tag{3.11}$$

then $xf_{j+2}(x)$ is also a Stieltjes function

$$xf_{j+2}(x) = x\int_0^1 \frac{d\gamma_{j+2}(u)}{1+xu}, \tag{3.12}$$

provided that

$$f_j(x) = \frac{f_j(0)}{1 + C^{(j+1)}x + xf_{j+2}(x)}, \qquad C^{(j+1)} = \frac{f_j(0)}{C_0^{(j)}}. \tag{3.13}$$ □

Note that by inserting $x = 1/s$ into (3.4) we obtain the identity

$$xf_j(x) = s^{-1}\int_0^1 \frac{d\gamma_j(u)}{s+u} = \varphi_j(s) = \int_1^{\infty} \frac{d\beta_j(\tau)}{1+s\tau}, \tag{3.14}$$

where

$$d\beta_j(\tau) = -\frac{1}{\tau} d\gamma_j(1/\tau) \geq 0. \tag{3.15}$$

REMARK 2. If $xf_j(x)$ is a Stieltjes function with respect to a variable x, then $\varphi_j(s) = xf_j(x)$ is a Stieltjes function with respect to s, provided $x = 1/s$, cf. (3.14) – (3.15). □

The fractional transformations (3.6) and (3.13) and the identity (3.14) will be used for the construction of a special continued fraction representations for Padé approximants $[k/M]$ and $\overline{[k/M]}$, cf. (2.8) – (2.15).

4. Continued fractions for $2PAs$ and $\overline{2PAs}$

Let us apply the fractional transformation (3.13) to $xf_1(x)$ k times. Thus we obtain a T-continued fraction to $xf_1(x)$, cf. [15, 20],

$$xf_1(x) = \frac{xG_1}{1+xG_2} + \frac{xG_3}{1+xG_4} + \ldots + \frac{xG_{2k-1}}{1+xG_{2k}+xf_{2k+1}(x)}. \tag{4.1}$$

Here the parameters G_n are uniquely determined by the initial k coefficients of a power series (2.4) and (2.6). On account of Remark 2, for $s = 1/x$ we have $xf_{2k+1}(x) = \varphi_{2k+1}(s)$, where $xf_{2k+1}(x)$ and $\varphi_{2k+1}(s)$ are Stieltjes functions. By employing the transformation (3.6) $(p-k)$ times to the function $xf_{2k+1}(x)$, if $p > k$ and $(k-p)$ times to $\varphi_{2k+1}(s)$, if $k > p$ we arrive at

$$xf_{2k+1}(x) = \begin{cases} \dfrac{xg_{2k+1}}{1} + \dfrac{xg_{2k+2}}{1} + \ldots + \dfrac{xg_{p+k}}{1 + xf_{p+k+1}(x)}, & p \geq k, \\ \dfrac{d_{2p+1}}{1} + \dfrac{d_{2p+2}}{x} + \dfrac{d_{2p+3}}{1} + \ldots + \dfrac{d_{p+k}}{x + xt_{p+k+1}(x)}, & k \geq p. \end{cases} \tag{4.2}$$

Note that functions $f_{p+k+1}(x)$ and $t_{p+k+1}(x)$ appearing in (4.2) are also Stieltjes functions of the type (2.2). The substitution of (4.2) into (4.1) yields the continued fraction representations for Padé approximants $[k/M]$, $[2M-p/M]$

$$\begin{aligned} [k/M] &= \frac{xG_1}{1+xG_2} + \cdots + \frac{xG_{2k-1}}{1+xG_{2k}} + \frac{xg_{2k+1}}{1} + \ldots + \frac{xg_{2M}}{1}, \\ [2M-p/M] &= \frac{xG_1}{1+xG_2} + \cdots + \frac{xG_{2p-1}}{1+xG_{2p}} + \frac{d_{2p+1}}{1} + \frac{d_{2p+2}}{x} \\ &\qquad + \frac{d_{2p+3}}{1} + \ldots + \frac{d_{2M}}{x}, \end{aligned} \tag{4.3}$$

and $\overline{[k/M]}$, $\overline{[2M-p/M]}$

$$\begin{aligned} \overline{[k/M]} &= \frac{xG_1}{1+xG_2} + \cdots + \frac{xG_{2k-1}}{1+xG_{2k}} + \frac{xg_{2k+1}}{1} \\ &\qquad + \ldots + \frac{xg_{2M}}{1} + \frac{xV_{2M+1}}{1}, \\ \overline{[2M-p/M]} &= \frac{xG_1}{1+xG_2} + \cdots + \frac{xG_{2p-1}}{1+xG_{2p}} + \frac{d_{2p+1}}{1} + \frac{d_{2p+2}}{x} \\ &\qquad + \ldots + \frac{d_{2M}}{x} + \frac{xT_{2M+1}}{1}. \end{aligned} \tag{4.4}$$

On account of Def. 2, V_{2M+1} and T_{2M+1} satisfy the relations

$$\begin{aligned} &\frac{xG_1}{1+xG_2} + \cdots + \frac{xG_{2k-1}}{1+xG_{2k}} + \frac{xg_{2k+1}}{1} + \ldots + \frac{xg_{2M}}{1} \\ &\qquad + \frac{xV_{2M+1}}{1} = -1, \qquad \text{if} \quad x = -1, \\ &\frac{xG_1}{1+xG_2} + \cdots + \frac{xG_{2p-1}}{1+xG_{2p}} + \frac{d_{2p+1}}{1} + \frac{d_{2p+2}}{x} + \ldots + \frac{d_{2M}}{x} \\ &\qquad + \frac{xT_{2M+1}}{1} = -1, \qquad \text{if} \quad x = -1. \end{aligned} \tag{4.5}$$

For $k > 0$ the parameters p, k, M are interrelated by

$$p + k = 2M, \qquad 0 < k < 2M, \qquad 0 < p < 2M. \tag{4.6}$$

The coefficients G_n $(n = 1, 2, ..., 2k)$, g_{2k+j} $(j = 1, 2, ..., p - k)$, V_{2M+1}, d_{2k+j} $(j = 1, 2, ..., k - p)$ and T_{2M+1} appearing in (4.3) – (4.4) are positive, i.e.,

$$\begin{aligned} &G_n > 0, && n = 1, 2, ..., 2k; \\ &g_{2k+j} > 0, && j = 1, 2, ..., p - k \geq 0; && V_{2M+1} > 0, \\ &G_n > 0, && n = 1, 2, ..., 2p; \\ &d_{2k+j} > 0, && j = 1, 2, ..., k - p \geq 0; && T_{2M+1} > 0. \end{aligned} \tag{4.7}$$

Now we are in a position to study the convergence of $[k/M]$ (k fixed) and $[2M - p/M]$ (p fixed) to $xf_1(x)$, when M goes to infinity. Due to nonzero radius of convergence of the power expansion (4.2) we infer, cf. [2, Th. 16.2],

$$\begin{aligned} &\lim_{M\to\infty} \frac{xg_{2k+1}}{1} + \frac{xg_{2k+2}}{1} + ... + \frac{xg_{2M}}{1} = xf_{2k+1}(x), \quad -1 < x < \infty, \\ &\lim_{M\to\infty} \frac{d_{2p+1}}{1} + \frac{d_{2p+2}}{x} + \frac{d_{2p+3}}{1} + ... + \frac{d_{2M}}{x} = xf_{2k+1}(x), \quad -1 < x < \infty. \end{aligned} \tag{4.8}$$

Consequently the relation (4.1) yields

$$\lim_{M\to\infty} [k/M] = \lim_{M\to\infty} [2M - p/M] = xf_1(x), \qquad -1 < x < \infty. \tag{4.9}$$

From (4.3) and (4.4), it follows: $\overline{[k/M]} = [k/M]$, if $V_{2M+1} = 0$; $\overline{[k/M]} = [k - 1/M - 1]$, if $V_{2M+1} = \infty$; $\overline{[2M - p/M]} = [2M - p/M]$, if $T_{2M+1} = 0$; $\overline{[2M - p/M]} = [2M - p - 1/M - 1]_{2M-p-1}$, if $T_{2M+1} = \infty$. For $x \in (0, \infty)$ $\overline{[k/M]}$ and $\overline{[2M - p/M]}$ are monotonic functions of the parameters $V_{2M+1} \geq 0$ and $T_{2M+1} \geq 0$, respectively. Hence for fixed $x \in (0, \infty)$, $\overline{[k/M]}$ takes values within $[k/M]$ and $[k - 1/M - 1]$, while $\overline{[2M - p/M]}$ within $[2M - p/M]$ and $[2M - p - 1/M - 1]$. On account of that and due to (4.9) we obtain

$$\lim_{M\to\infty} \overline{[k/M]} = \lim_{M\to\infty} \overline{[2M - p/M]} = xf_1(x), \qquad 0 < x < \infty. \tag{4.10}$$

The Padé approximants $\overline{[k/M]}$ and $\overline{[2M - p/M]}$ are analytical functions for $-1 < x < \infty$ (their poles lie on the real axis at $-\infty < x \leq -1$ only). Hence the convergence relations given by (4.10) holds for $-1 < x \leq 0$ as well. Consequently we can write

$$\lim_{M\to\infty} \overline{[k/M]} = \lim_{M\to\infty} \overline{[2M - p/M]} = xf_1(x), \qquad -1 < x < \infty. \tag{4.11}$$

REMARK 3. For fixed k $(k = 0, ..., 2M)$ the approximants $[k/M]$ and $\overline{[k/M]}$, while for fixed p $(p = 0, ..., 2M)$ the approximants $[2M - p/M]$ and $\overline{[2M - p/M]}$

converge to the Stieltjes function $xf_1(x)$ for $-1 < x < \infty$, as M goes to infinity, cf. (4.9), (4.10) and (4.11). □

In the next section the properties of the convergence of $[k/M]$, $\overline{[k/M]}$, $[2M - p/M]$, and $\overline{[2M - p/M]}_{2M-p}$ will be investigated. To this end the continued fractions (4.3) and (4.4), the restrictions (2.3) and (4.7), and the convergence relations (4.9) – (4.11) will be used.

5. Two-point Padé bounds on $xf_1(x)$

For simultaneous representation of the sequences $[k/M]$, $[M + r/M]$, $[2M - p/M]$ $\{\overline{[k/M]}, \overline{[M + r/M]}, \overline{[2M - p/M]}\}$ it is convenient to introduce the notation $[I_M/M]$ $\{\overline{[I_M/M]}\}$, where $I_M = k$, $M + r$, $2M - p$. Now we are prepared to formulate the fundamental theorem establishing $2PAs$ and $\overline{2PAs}$ bounds on $xf_1(x) = \lambda_e(x)/\lambda_1 - 1$, cf. (2.2):

THEOREM 1. *For $I_M = k$, $M + r$, $2M - p$ ($0 \le I_M \le 2M$, $M \ge |r|$) the Padé approximants $[I_M/M]$ and $\overline{[I_M/M]}$ (cf. Defs. 1 and 2)) to the power expansions of $xf_1(x)$ at $x = 0$ and $x = \infty$ (cf. (2.4) and (2.6)) obey the following inequalities, where $xf_1(x)$ stands for the limit of $[I_M/M]$ and $\overline{[I_M/M]}$, as M tends to infinity:*

(i) *If $-1 < x < 0$ then*

$$[I_M/M] - [I_{M+1}/M + 1] > 0, \tag{5.1}$$

$$\overline{[I_M/M]} - \overline{[I_{M+1}/M + 1]} < 0, \tag{5.2}$$

$$[I_M/M] > xf_1(x) > \overline{[I_M/M]}. \tag{5.3}$$

(ii) *If $0 < x < \infty$ then*

$$(-1)^{I_M+1}[I_{M+1}/M + 1] - (-1)^{I_M}[I_M/M] > 0, \tag{5.4}$$

$$(-1)^{I_M+1}\overline{[I_{M+1}/M + 1]} - (-1)^{I_M}\overline{[I_M/M]} < 0, \tag{5.5}$$

$$(-1)^{I_M}[I_M/M] < (-1)^{I_M}xf_1(x) < (-1)^{I_M}\overline{[I_M/M]}. \tag{5.6}$$

The inequalities (5.1) – (5.2) and (5.4) – (5.5) have a consequence that the bounds $[I_M/M]$ $\{\overline{[I_M/M]}\}$ are the best with respect to the given coefficients p of the power series (2.4) and terms k of the power expansion (2.6), and that the use of additional input data (higher p and k) improves the bounds on $xf_1(x)$.

P r o o f. As an example, the inequality (5.2), $I_M = 2M - p$ will be proved only. The remaining inequalities one can prove in a similar manner. Let us start from the continued fractions (4.3)

$$\begin{aligned} \overline{[2M - p/M]} &= \cfrac{xG_1}{1 + xG_2 + \ldots + \cfrac{xT_{2M+1}}{1}}, \\ \overline{[2M + 2 - p/M + 1]} &= \cfrac{xG_1}{1 + xG_2 + \ldots + \cfrac{d_{2M+1}}{1} + \cfrac{d_{2M+2}}{x} + \cfrac{xT_{2M+3}}{1}}. \end{aligned} \tag{5.7}$$

Of interest is the difference $\delta(x)$ given by (see (5.7))

$$\delta(x) = \frac{d_{2M+1}}{1} + \frac{d_{2M+2}}{x} + \frac{xT_{2M+3}}{1} - \frac{xT_{2M+1}}{1} = x\left(\frac{d_{2M+1}(1+T_{2M+3})}{x(1+T_{2M+3})+d_{2M+2}} - T_{2M+1}\right). \tag{5.8}$$

On the basis of (4.5) and (4.7) we have

$$\begin{aligned} &\frac{d_{2M+1}(1+T_{2M+3})}{x(1+T_{2M+3})+d_{2M+2}} - T_{2M+1} = 0, \qquad \text{if} \quad x = -1, \\ &\frac{d_{2M+1}(1+T_{2M+3})}{x(1+T_{2M+3})+d_{2M+2}} - T_{2M+1} < 0, \qquad \text{if} \quad -1 < x < \infty. \end{aligned} \tag{5.9}$$

The relations (5.9), the restrictions (4.7) and the recurrence formula for the continued fractions (5.7) lead immediately to the inequality (5.2), $I_M = 2M - p$. The remaining inequalities, namely (5.1), (5.2), $I_M = k$, $M + r/M$, (5.4) and (5.5), can be proved analogously. The relations (5.3) and (5.6) are direct consequence of (4.9), (4.11), (5.1) – (5.2) and (5.4) – (5.5).

Now we are prepared to prove that, with respect to a given number of coefficients of power series (2.4) and (2.6), the $2PAs$ and $\overline{2PAs}$ provide the best estimations for $xf_1(x)$. Assume that $[k_1/M_1]$ $\{[k_2/M_2]\}$ is determined by p_1 $\{p_2\}$ coefficients of (2.4) and k_1 $\{k_2\}$ coefficients of (2.6), where $p_1 + k_1 = 2M_1$, $p_2 + k_2 = 2M_2$, $p_1 \leq p_2$ and $k_1 \leq k_2$. Of interest is the following scheme of transition of $[k_1/M_1]$ to $[k_2/M_2]$:

$$[k_1/M_1] \to [k_1/M'] = [2M' - p_2/M'] \to [2M' - p_2/M_2] = [k_2/M_2],$$

where $M_1 \leq M' \leq M_2$. By applying the inequalities (5.1) – (5.3) and (5.4) – (5.6) successively to the above transition scheme, we arrive at

$$|xf_1(x) - [k_1/M_1]| \geq |xf_1(x) - [k_2/M_2]|. \tag{5.10}$$

Analogously we obtain

$$|xf_1(x) - \overline{[k_1/M_1]}| \geq |xf_1(x) - \overline{[k_2/M_2]}|. \tag{5.11}$$

From (5.10) – (5.11), it follows that for $p_2 \geq p_1$ and $k_2 \geq k_1$ the estimations $[k_2/M_2]$, $\overline{[k_2/M_2]}$ of $xf_1(x)$ are better than $[k_1/M_1]$, $\overline{[k_1/M_1]}$. □

For a better understanding of Th. 1 it is convenient to arrange Padé approximants $[k/M]$ and $\overline{[k/M]}$ in the following triangular array

$$
\begin{array}{ccccccc}
 & & & & 0/3 & \dots \\
 & & & 0/2 & 1/3 & \dots \\
 & & 0/1 & 1/2 & 2/3 & \dots \\
 & 0/0 & 1/1 & 2/2 & 3/3 & \dots \\
 & & 2/1 & 3/2 & 4/3 & \dots \\
 & & & 4/2 & 5/3 & \dots \\
 & & & & 6/3 & \dots
\end{array} \tag{5.12}
$$

called $2PAs$-table if $k/M = [k/M]$, or $\overline{2PAs}$-table, if $k/M = \overline{[k/M]}$. The sequence M/M is named the main row. Besides M/M one finds the sequences $M + r/M$, k/M and $2M - p/M$ constituting the r-th rows, the diagonals going up and the diagonals going down. Note that the sequences $0/M$ and $1/M$ represent the classical Milton's estimations of $xf_1(x)$, cf. [24], while $0/1$ are the well known Hashin – Shtrikman bounds on $xf_1(x)$, cf. [17]. The remaining bounds appearing in (5.12) are new.

6. General power expansions of $xf_1(x)$

The most general input data for evaluation of the $2PAs$ and $\overline{2PAs}$ to $xf_1(x)$ are given by:

$$
\begin{aligned}
xf_1(x) &= \sum_{n=1}^{\infty} c_n^{(1)} x^n, \\
xf_1(x) &= \sum_{n=0}^{\infty} C_{n\nu}^{(1)} s_\nu^n, \qquad s_\nu = 1/(x - \nu).
\end{aligned} \tag{6.1}
$$

Here ν is an arbitrary, non-negative number. Since $(6.1)_1$ coincides with (2.4), of interest is the expansion $(6.1)_2$ only. From (2.6) and $(6.1)_2$ we have

$$
\begin{aligned}
xf_1(x) &= \sum_{n=0}^{\infty} C_n^{(1)} s^n = \sum_{n=0}^{\infty} C_{n\nu}^{(1)} s_\nu^n, \\
s &= \frac{1}{x}, \qquad s_\nu = \frac{1}{x - \nu}, \qquad s_\nu = \frac{s}{1 - s\nu}.
\end{aligned} \tag{6.2}
$$

Equality (6.2) provides the following recurrence formulae interrelating the coefficients $C_n^{(1)}$ and $C_{k\nu}^{(1)}$:

$$
C_0^{(1)} = C_{0\nu}^{(1)}, \qquad C_1^{(1)} = C_{1\nu}^{(1)}, \tag{6.3}
$$

$$C_n^{(1)} = \sum_{k=1}^{n} \nu^{n-k} A_n^k C_{k\nu}^{(1)}, \qquad n = 2, 3, \ldots, \tag{6.4}$$

where

$$A_n^k = \begin{cases} 1, & \text{if } k = 1, \\ A_{n-1}^{k-1} + A_{n-1}^k, & \text{if } k = 2, 3, \ldots, n-1, \\ 1, & \text{if } k = n. \end{cases} \tag{6.5}$$

From (6.3) – (6.5) it follows:

REMARK 4. Any power expansions of $xf_1(x)$ at $x = 0$ and $x = \infty$ given by (6.1), ($\nu > 0$) can always be reduced to the standard ones (6.1), ($\nu = 0$), cf. (2.4) and (2.6). It means that $2PAs$ and $\overline{2PAs}$ to power series (6.1), ($\nu \geq 0$) do not depend on ν.

7. Physical example

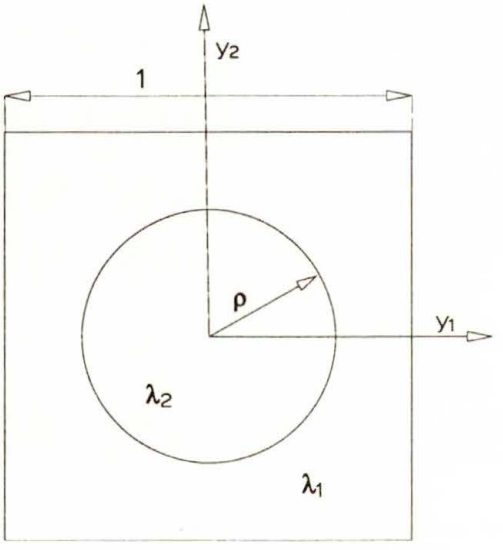

FIG. 1. Unit cell for a square array of cylinders.

In this section we evaluate low order Padé bounds $[k/M]$ and $\overline{[k/M]}$ on the effective conductivity $\lambda_e(x)/\lambda_1$ of a composite material consisting of equally-sized cylinders embedded in an infinite matrix, cf. Fig. 1. To this end we set: $\phi = \pi\varrho^2$ – volume fraction of inclusions, ϱ – the radius of cylinders, λ_1, λ_2 conductivity of the matrix and inclusions, $x = (\lambda_2/\lambda_1) - 1$ – normalized physical properties

of the composite components. Two coefficients of the expansion of $\lambda_e(x)/\lambda_1$ at $x = 0$ are reported in [4],

$$xf_1(x) = \frac{\lambda_e(x)}{\lambda_1} - 1 = c_1^{(1)}x + c_2^{(1)}x^2 + O(x^3),$$
$$c_1^{(1)} = \phi = \pi\varrho^2, \qquad c_2^{(1)} = \xi = -0.5\phi(1-\phi), \tag{7.1}$$

while at $x = \infty$ in [22]

$$xf_1(x) = \frac{\lambda_e(x)}{\lambda_1} - 1 = C_0^{(1)} + C_1^{(1)}\frac{1}{x} + O\left(\frac{1}{x}\right)^2,$$
$$C_0^{(1)} = A = [\pi(w-1) - 1], \tag{7.2}$$
$$C_1^{(1)} = B = -2\pi w(w-1)\ln(w), \qquad w = \sqrt{\pi/(\pi - 4\phi)}.$$

Low order $2PAs$ and $\overline{2PAs}$ bounds corresponding to (7.1) and (7.2) are given by:

$$[0/0] = 1, \qquad \overline{[0/0]} = x,$$
$$[0/1] = \frac{\phi x}{1 + 0.5(1-\phi)x}, \qquad \overline{[0/1]} = \frac{\phi x + 0.5\phi x^2}{1 + x - 0.5\phi x},$$
$$[1/1] = \frac{\phi x}{1 + (\phi/A)x}, \qquad \overline{[1/1]} = \frac{\phi x}{1 + (1-\phi)x},$$
$$[2/1] = -\frac{(A^2/B)x}{1 - (A/B)x}, \qquad \overline{[2/1]} = \frac{Ax}{1 + A + x}, \tag{7.3}$$
$$[2/2] = \frac{G_1 x + G_1 G_4 x^2}{1 + (G_2 + G_3 + G_4)x + G_2 G_4 x^2},$$
$$\overline{[2/2]} = \frac{G_1 x + G_1(G_4 + V_5)x^2}{1 + (G_2 + G_3 + G_4 + V_5)x + G_2(G_4 + V_5)x^2},$$

where

$$G_1 = \phi, \qquad G_2 = \frac{\phi}{A}, \qquad G_3 = -\frac{\phi}{A} - \frac{\xi}{\phi}, \tag{7.4}$$

$$G_4 = \frac{\phi^2 + A\xi}{A^2 + \phi B}\frac{A}{\phi}, \qquad V_5 = 1 - G_4 - \frac{G_3}{1 - G_1 - G_2}. \tag{7.5}$$

For $\phi = 0.7853$ $2PAs$ and $\overline{2PAs}$ given by (7.3) are depicted in Figs. 2 and 3. It follows that for $x > 0$ the upper Padé estimation $1 + \overline{[2/2]}$ of $\lambda_e(x)/\lambda_1$ provides the significant improvement over the upper Hashin–Shtrikman bound $1 + \overline{[0/1]}$. Moreover, for $x \to \infty$ the Padé bound $1 + \overline{[2/2]}$ takes finite values, while the Hashin–Shtrikman bound $1 + \overline{[0/1]}$ goes to infinity. We have to add that in our previous papers the only $2PAs$ bounds on $xf_1(x)$ have been investigated [28, 29]. The two-point Padé bounds of the type $\overline{2PAs}$, used in this paper, are new.

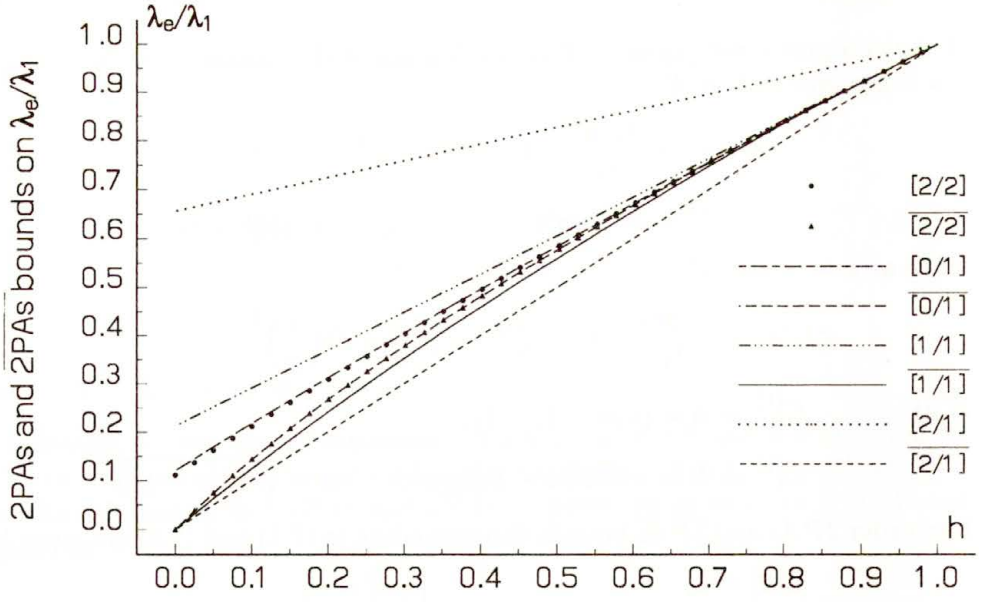

FIG. 2. Low order $2PAs$ and $\overline{2PAs}$ bounds on the effective conductivity $\lambda_e(x)/\lambda_1$ of a square array of densely spaced cylinders – a comparison with Hashin–Sthrikman estimations $1 + [0/1]$ and $1 + \overline{[0/1]}$; $\phi = 0.7853$, $h < 1$.

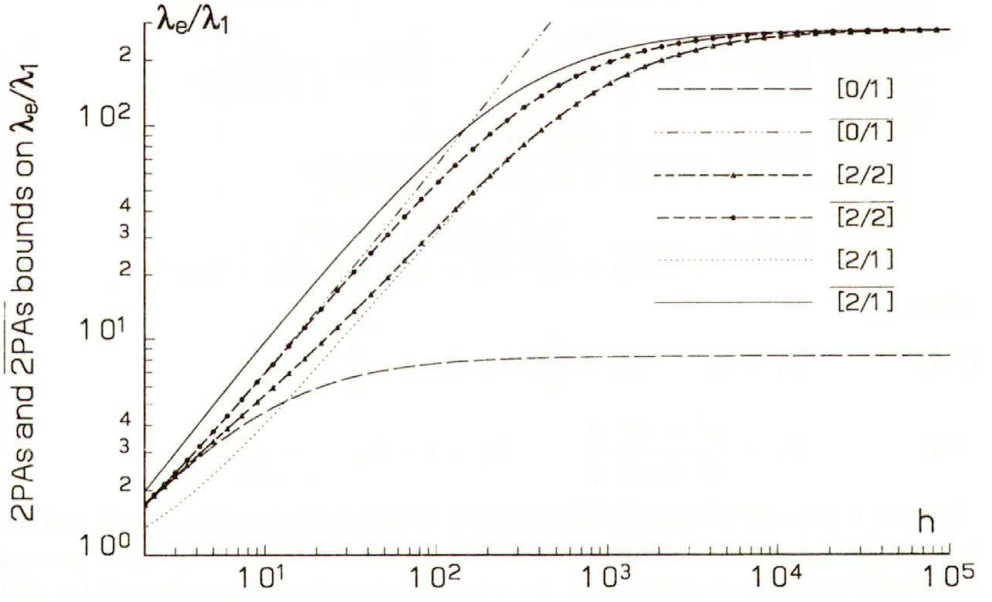

FIG. 3. Low order $2PAs$ and $\overline{2PAs}$ bounds on the effective conductivity $\lambda_e(x)/\lambda_1$ of a square array of densely spaced cylinders – a comparison with Hashin–Sthrikman estimations $1 + [0/1]$ and $1 + \overline{[0/1]}$; $\phi = 0.7853$, $h > 1$.

8. Conclusions

The main result of this paper, formulated as Th. 1 establishes, in terms of two-point Padé approximants $2PAs$ and $\overline{2PAs}$, the new bounds on the real-valued moduli $\lambda_e(x)/\lambda_1$ of two-phase media. The bounds achieved are the best possible with respect to the given number of coefficients of the power expansions of $\lambda_e(x)/\lambda_1$ at $x = 0$ and $x = \infty$. Moreover, for $x > 0$ they provide a significant improvement over the corresponding ones reported in the literature, cf. [24].

If the orientation of the principal axis of a composite does not depend on the properties of components, $2PAs$ and $\overline{2PAs}$ can be used for estimation of the principal values of a second-rank tensors, i.e. for bounding the anisotropic transport coefficients.

For a power expansion of $\lambda_e(x)/\lambda_1$ available at $x = 0$ only, $2PAs$ and $\overline{2PAs}$ to $\lambda_e(x)/\lambda_1$ reduce to the classical bounds on $\lambda_e(x)/\lambda_1$ originally derived by MILTON in [24].

The $2PAs$ and $\overline{2PAs}$ bounds on $\lambda_e(x)/\lambda_1$ can be improved by incorporating the additional information about the composite such as the Keller identity for two-dimensional system or the Schulgasser inequality for three-dimensional ones, cf. [7] and [9]. The Keller's and Schulgasser's restrictions and their influence on the Padé bounds on $\lambda_e(x)/\lambda_1$ will be investigated in a separate paper.

Acknowledgment

The authors were supported by the State Committee for Scientific Research through the Grant No. 7 T07A 016 12 and through the fund for Polish-Ukrainian cooperation No. 4222/DZ/95.

References

1. G.A. BAKER, *Essentials of Padé approximants*, Acad. Press, London 1975.
2. G.A. BAKER, P.GRAVES-MORRIS, *Padé approximants. Part I. Basic theory*, [in:] Encyclopedia of Mathematics and its Applications, G.C. ROTA [Ed.], **13**, Addison-Wesley Publ. Co., London 1981.
3. G.A. BAKER and P. GRAVES-MORRIS, *Padé approximants. Part II. Extensions and applications*, [in:] Encyclopedia of Mathematics and its Applications, G.C. ROTA [Ed.], **14**, Addison-Wesley Publ. Co., London 1981.
4. D.J. BERGMAN, *The dielectric constant of a composite material – A problem in classical physics*, Phys. Report., **C 43**, 377–407, 1978.
5. D.J. BERGMAN, *Bounds for the complex dielectric constants of two-component composite material*, Phys. Rev., **B 23**, 6, 3058–3065, 1981.
6. D.J. BERGMAN, *Rigorous bounds for the complex dielectric constants of a two-component composite material*, Ann. Phys., **138**, 78–114, 1982.
7. D.J. BERGMAN, *Hierarchies of Stieltjes functions and their application to the calculation of bounds for the dielectric constant of a two-components composite medium*, SIAM J. Appl. Math., **53**, 915–930, 1993.

8. O.P. BRUNO, *The effective conductivity of an infinitely interchangeable mixture*, Comm. Pure Appl. Math., **43**, 769–807, 1990.
9. K.E. CLARK and G.W. MILTON, *Optimal bounds correlating electric, magnetic and thermal properties of two-phase, two-dimensional composites*, Proc. Roy. Soc. London, **A 448**, 161–190, 1995.
10. A. BULTHEEL, *Laurent series and their Padé approximants*, Birkhäuser-Verlag, Basel 1987.
11. A. BULTHEEL, P. GONZÁLES-VERA and R. ORIVE, *Quadrature on the half-line and two-point Padé approximants to Stieltjes functions. Part I. Algebraic aspects*, J. Comp. Appl. Math., **65**, 57–72, 1995.
12. L. CASASÚS and P. GONZÁLEZ–VERA, *Two-point Padé type approximants for Stieltjes functions*, [in:] Proc. Polinômes Ortogonaux et Applications, C. BREZINSKI, A. DRAUX, A.P. MAGNUS, P. MORONI and A. RONVEAUX [Eds.], Bar-le-Duc, 1984, Lecture Notes in Math., **1171**, 408–418, Springer, Berlin 1985.
13. J. GILEWICZ, *Approximants de Padé*, Springer-Verlag, Berlin 1978.
14. K. GOLDEN and G. PAPANICOLAOU, *Bounds for effective parameters of heterogeneous media by analytic continuation*, Comm. Math. Phys., **90**, 473–491, 1983.
15. P. GONZÁLEZ-VERA and O. NJÅSTAD, *Convergence of two-point Padé approximants to series of Stieltjes*, J. Comp. Appl. Math., **32**, 97–105, 1990.
16. W.B. GRAGG, *Truncation error bounds for T-fractions*, [in:] Approximation Theory III, E.W. CHENEY [Ed.], 455–460, Academic Press, New York 1980.
17. Z. HASHIN and S. SHTRIKMAN, *A variational approach to the theory of the effective magnetic permeability of multiphase materials*, J. Appl. Phys. Sol., **33**, 3125–3131, 1962.
18. W.B. JONES, O. NJÅSTAD and W.J. THRON, *Two-point Padé expansions for a family of analytic functions*, J. Comp. Appl. Math., **9**, 105–123, 1983.
19. W.B. JONES and W.J. THRON, *A posterior bound for truncation error of continued fraction*, SIAM J. Num. Anal., **8**, 693–705, 1970.
20. W.B. JONES and W.J. THRON, *Continued fraction analytic theory and its applications*, [in:] Encyclopedia of Mathematics and its Applications, G.-C. ROTA [Ed.], **11**, Addison-Wesley Publ. Co., London 1980.
21. R.C. MCPHEDRAN and G.W. MILTON, *Bounds and exact theories for the transport properties of inhomogeneous media*, Appl. Phys., **A 26**, 207–220, 1981.
22. R.C. MCPHEDRAN, L. POLADIAN and G.W. MILTON, *Asymptotic studies of closely spaced highly conducting cylinders*, Proc. R. Soc. London, **A 415**, 185–196, 1988.
23. G.W. MILTON, *Bounds on the complex permittivity of a two-component composite material*, J. Appl. Phys., **52**, 5286–5293, 1981.
24. G.W. MILTON, *Bounds on the transport and optical properties of two-component material*, J. Appl. Phys., **52**, 5294–5304, 1981.
25. S. TOKARZEWSKI, *The inequalities for two-point Padé approximants to the expansions of Stieltjes functions in real domain*, J. Comp. Appl. Math., **67**, 59–72, 1996.
26. S. TOKARZEWSKI, *Inequalities for the effective transport coefficients*, Arch. Mech., **46**, 611–623, 1994.
27. S. TOKARZEWSKI, *N-point Padé approximants to real-valued Stieltjes series with nonzero radii of convergence*, J. Comp. Appl. Math. [in press].
28. S. TOKARZEWSKI, J. BŁAWZDZIEWICZ and I.V. ANDRIANOV, *Two-point Padé approximants for formal Stieltjes series*, Num. Algorithms, **8**, 313–328, 1994.
29. S. TOKARZEWSKI, J. BŁAWZDZIEWICZ and I.V. ANDRIANOV, *Effective conductivity of densely packed highly conducting cylinders*, Appl. Phys., **A 59**, 601–604, 1994.

30. S. TOKARZEWSKI, A. GAŁKA and I.V. ANDRIANOV, *Bounds on the effective transport coefficients of two-phase media from the discrete theoretical and experimental data*, Comp. Assis. Mech. and Engng. Sc., **4**, 229–241, 1997.

31. S. TOKARZEWSKI and J.J. TELEGA, *Two-point Padé approximants to Stieltjes series representation of bulk moduli of regular composites*, Comp. Assis. Mech. and Engng. Sc., **3**, 121–132, 1996.

32. S. TOKARZEWSKI and J.J. TELEGA, *A contribution to the bounds on real effective moduli of two-phase composite materials*, Math. Models and Meth. in Appl. Sci. [in press].

33. H.S. WALL, *Analytic theory of continued fractions*, Van Nostrand, New York 1948.

34. O. WIENER, *Abhandlungen der mathematisch-physischen Klasse der Königlichen Sächsischen Gesellschaft der Wissenschaften*, Abh. Sächs. Akad. Wiss. Leipzig Math.-Naturwiss. Kl., **32**, 509, 1912.

POLISH ACADEMY OF SCIENCES
INSTITUTE OF FUNDAMENTAL TECHNOLOGICAL RESEARCH

e-mail: stokarz@ippt.gov.pl

e-mail: agalka@ippt.gov.pl

and

DEPARTMENT OF MATHEMATICS,
UKRAINIAN STATE CHEMICAL TECHNOLOGICAL UNIVERSITY DNEPROPETROVSK, UKRAINE.

Received November 27, 1996.

Arch. Mech., 49, 4, pp. 665–675, Warszawa 1997

Decay and continuous dependence estimates for harmonic vibrations of micropolar elastic cylinders

M. ARON (PLYMOUTH) and S. CHIRITA (IASI)

A PRINCIPLE OF SAINT-VENANT-TYPE is established for a right cylinder composed of an anisotropic, linear, homogeneous micropolar elastic solid and subjected to harmonic loading on one of its ends. The amplitude of the harmonic vibrations of this cylinder is also shown to depend continuously on the prescribed data.

1. Introduction

FOR CYLINDRICAL DOMAINS, the Saint-Venant principle in linear micropolar elastostatics was established by BERGLUND [1] and CHIRITA and ARON [2] (see also [3]). By adapting certain ideas originally due to TOUPIN [4], these authors have shown that certain global measures of the displacements which depend upon the distance from the loaded end of the cylinder, decay exponentially with that distance.

More recently, certain aspects of the dynamical version of the Saint-Venant principle have been investigated within the framework of the theory of linear elasticity. In particular, FLAVIN and KNOPS [5], FLAVIN, KNOPS and PAYNE [6] and KNOPS [7] have considered the Saint-Venant principle for the harmonic vibrations of linearly elastic cylinders subjected to harmonic type loadings on one of their ends.

In this paper we deal with the Saint-Venant principle for the harmonic vibrations of right cylinders composed of an anisotropic, linear, homogeneous micropolar elastic solid. Following [5–7] we show that when one end of the cylinder is subjected to prescribed harmonic tractions, and provided that the prescribed frequency of vibrations is strictly less than a certain critical frequency, the energy $E(z)$ stored in a part of the cylinder that lies above a cross-section which is at the distance z from the loaded end, decays faster than a certain exponentially decreasing function of z. The critical frequency depends upon the characteristics of the material and upon the geometry of the body. Additionally, we establish here an estimate for the total energy of the considered cylinder which implies that the amplitude of vibrations depends continuously on the prescribed data and which, when coupled with the Saint-Venant-type estimate mentioned above, provides us with a more explicit description of the way in which $E(z)$ decays as a function of z. Other continuous dependence results in micropolar elasticity

have been obtained previously by ARON [8] who considered the case of physically nonlinear micropolar elastostatics.

2. Preliminaries

Consider a body B composed of a homogeneous anisotropic micropolar linear elastic material ([1]). The motion of a particle which belongs to such a body is described by the displacement vector field $\mathbf{u}$ and the microrotation vector field $\boldsymbol{\varphi}$. In what follows we will be employing a six-dimensional vector field $\mathbf{U}$ defined by

$$\mathbf{U} \equiv (\mathbf{u}, j\boldsymbol{\varphi}), \qquad j = \text{const}, \qquad j > 0, \tag{2.1}$$

where j is the square root of the smallest eigenvalue of the microinertia tensor $\mathbf{j}$. The microinertia tensor is assumed to be symmetric and positive definite [9]. As usual, the inner product in the six-dimensional vector space is defined by

$$\mathbf{U}\cdot\mathbf{V} \equiv u_i v_i + j^2 \varphi_i \psi_i\,, \qquad i = 1,2,3, \tag{2.2}$$

where u_i, v_i, φ_i, ψ_i are the components of the vectors $\mathbf{u}$, $\mathbf{v}$, $\boldsymbol{\varphi}$, $\boldsymbol{\psi}$, respectively, with respect to a Cartesian system of coordinates $Ox_1x_2x_3$ and where the summation convention over repeated indices has been adopted. In view of (2.2), the magnitude of the vector field $\mathbf{V} \equiv (\mathbf{v}, j\boldsymbol{\psi})$ is given by

$$|\mathbf{V}| \equiv (\mathbf{V}\cdot\mathbf{V})^{1/2} = (v_i v_i + j^2 \psi_i \psi_i)^{1/2}. \tag{2.3}$$

The theory of micropolar elasticity employs two strain tensors, e_{rs} and κ_{rs}, which are defined by

$$e_{rs}(\mathbf{U}) \equiv u_{s,r} + \varepsilon_{srk}\varphi_k\,, \qquad \kappa_{rs}(\mathbf{U}) \equiv \varphi_{s,r}\,, \qquad r,s = 1,2,3, \tag{2.4}$$

where ε_{srk} denotes the well-known alternating symbol and a comma followed by r stands for the partial differentiation with respect to x_r. These are related to the stress tensor t_{kl} and couple stress tensor m_{kl} by the equations

$$\begin{aligned} t_{kl}(\mathbf{U}) &= a_{klrs}\, e_{rs}(\mathbf{U}) + b_{klrs}\, \kappa_{rs}(\mathbf{U}), \\ m_{kl}(\mathbf{U}) &= b_{rskl}\, e_{rs}(\mathbf{U}) + c_{klrs}\, \kappa_{rs}(\mathbf{U}), \\ & \qquad k,l,r,s = 1,2,3, \end{aligned} \tag{2.5}$$

where a_{klrs} etc. are material constants which satisfy

$$a_{klrs} = a_{rskl}\,, \qquad c_{klrs} = c_{rskl}\,. \tag{2.6}$$

([1]) The theory of linear micropolar elasticity was introduced by ERINGEN in [9].

Accordingly, the strain energy density corresponding to $\mathbf{U}$ is given by

$$W(\mathbf{U}) \equiv \frac{1}{2}a_{klrs}e_{kl}(\mathbf{U})e_{rs}(\mathbf{U}) + b_{klrs}e_{kl}(\mathbf{U})\kappa_{rs}(\mathbf{U}) + \frac{1}{2}c_{klrs}\kappa_{kl}(\mathbf{U})\kappa_{rs}(\mathbf{U}) \tag{2.7}$$

and in what follows we shall assume that this quadratic form is positive definite.

Following IESAN [3] we label the nine independent index combinations (rs) or (kl) by capital Greek letters Γ, Δ, etc. so that the constitutive equations can be written as

$$\begin{aligned} t_\Gamma(\mathbf{U}) &= a_{\Gamma\Delta}e_\Delta(\mathbf{U}) + b_{\Gamma\Delta}\kappa_\Delta(\mathbf{U}), \\ m_\Gamma(\mathbf{U}) &= b_{\Delta\Gamma}e_\Delta(\mathbf{U}) + c_{\Gamma\Delta}\kappa_\Delta(\mathbf{U}), \\ &\Gamma, \Delta = 1, 2, ..., 9. \end{aligned} \tag{2.8}$$

Introducing the further notations

$$\begin{aligned} &T_\Gamma \equiv t_\Gamma, \qquad T_{9+\Gamma} \equiv j^{-1}m_\Gamma, \qquad E_\Gamma \equiv e_\Gamma, \\ &E_{9+\Gamma} \equiv j\kappa_\Gamma, \qquad A_{\Gamma\Delta} \equiv a_{\Gamma\Delta}, \qquad A_{\Gamma(9+\Delta)} \equiv j^{-1}b_{\Gamma\Delta}, \\ &A_{(9+\Gamma)\Delta} \equiv j^{-1}b_{\Delta\Gamma}, \qquad A_{(9+\Gamma)(9+\Delta)} \equiv j^{-2}c_{\Gamma\Delta} \end{aligned} \tag{2.9}$$

we can rewrite the constitutive equations (2.8) in the form

$$T_K(\mathbf{U}) = A_{KL}\,E_L(\mathbf{U}), \qquad K, L = 1, 2, ..., 18. \tag{2.10}$$

We define now the tensor

$$\mathbf{T}(\mathbf{U}) \equiv [t_{rs}(\mathbf{U}),\ j^{-1}m_{rs}(\mathbf{U})] \tag{2.11}$$

whose magnitude is

$$|\mathbf{T}(\mathbf{U})| \equiv [t_{rs}(\mathbf{U})t_{rs}(\mathbf{U}) + j^{-2}m_{rs}(\mathbf{U})m_{rs}(\mathbf{U})]^{1/2}, \tag{2.12}$$

and, using the notations (2.9), we write the strain-energy density function (2.7) as

$$W(\mathbf{U}) = \frac{1}{2}A_{KL}E_K(\mathbf{U})E_L(\mathbf{U}), \qquad K, L = 1, 2, ..., 18, \tag{2.13}$$

where A_{KL} are the components of a symmetric and positive definite tensor. According to GURTIN [10, p. 197], IESAN [3, p. 97] and MEHRABADI, COWIN and HORGAN [11], if μ_M denotes the largest characteristic value of A_{KL}, we have

$$|\mathbf{T}(\mathbf{U})|^2 = T_K(\mathbf{U})T_K(\mathbf{U}) = A_{KL}A_{KS}E_L(\mathbf{U})E_S(\mathbf{U}) \leq 2\mu_M W(\mathbf{U}). \tag{2.14}$$

Denoting by $s_i(\mathbf{U})$ and $q_i(\mathbf{U})$ the components of the stress and couple stress vectors acting on the surface ∂B of B, respectively, we have

$$s_i(\mathbf{U}) = t_{ri}(\mathbf{U})n_r, \qquad q_i(\mathbf{U}) = m_{ri}(\mathbf{U})n_r, \tag{2.15}$$

where n_r are the components of the outwardly directed unit vector normal to ∂B.

In the absence of body forces and couples, the equations of motion are written as

$$
\begin{aligned}
[t_{si}(\mathbf{U})]_{,s} &= \varrho\, \ddot{u}_i\,, \\
[m_{si}(\mathbf{U})]_{,s} + \varepsilon_{irs}\, t_{rs}(\mathbf{U}) &= \varrho j_{is}\, \ddot{\varphi}_s\,, \qquad \varrho = \text{const}, \quad \varrho > 0,
\end{aligned} \tag{2.16}
$$

where j_{is} are the components of $\mathbf{j}$ and ϱ is the mass-density of the body, and these have to be supplemented by appropriate boundary and initial conditions. As usual, in (2.16), a superposed dot denotes the partial derivative with respect to the time t.

3. An energy decay estimate for the case of harmonic vibrations

In this section B will be assumed to occupy a right cylinder of length L whose cross-section is bounded by one or more piecewise smooth curves. The Cartesian system of coordinates is chosen so that the origin belongs to one of the ends and thus the ends of the cylinder lie in the planes $x_3 = 0$ and $x_3 = L$. An arbitrary cross-section of the cylinder at the distance z from $x_3 = 0$ will be referred to as S_z whereas the part of the cylinder which lies above S_z will be denoted by B_z. Clearly, our notation implies that $B_0 = B$.

We further assume here that

$$
\begin{aligned}
u_i(\mathbf{x}, t) &= 0, \qquad \varphi_i(\mathbf{x}, t) = 0, \\
\mathbf{x} &\equiv (x_1, x_2, x_3) \in \partial B \backslash S_0\,, \qquad t \in (0, \infty)
\end{aligned} \tag{3.1}
$$

and that

$$
\begin{aligned}
s_i(\mathbf{U}) &= t_i(\mathbf{x}) \sin(\omega t), \\
q_i(\mathbf{U}) &= p_i(\mathbf{x}) \sin(\omega t), \qquad \mathbf{x} \in S_0\,, \quad t \in (0, \infty),
\end{aligned} \tag{3.2}
$$

where t_i and p_i are given functions on S_0 and $\omega > 0$ is a given constant.

Seeking solutions (to the problem given by (2.5), (2.16), (3.1) and (3.2)) of the form

$$
u_i(\mathbf{x}, t) = v_i(\mathbf{x}) \sin(\omega t), \qquad \varphi_i(\mathbf{x}, t) = \psi_i(\mathbf{x}) \sin(\omega t) \tag{3.3}
$$

we find that the functions v_i and ψ_i must satisfy

$$
[t_{si}(\mathbf{V})]_{,s} + \varrho\omega^2 v_i = 0, \tag{3.4}
$$

$$
[m_{si}(\mathbf{V})]_{,s} + \varepsilon_{irs}\, t_{rs}(\mathbf{V}) + \varrho\omega^2 j_{is}\psi_s = 0, \qquad \mathbf{V} \equiv (v_i, j\psi_i), \tag{3.4}
$$

$$
v_i(\mathbf{x}) = \psi_i(\mathbf{x}) = 0, \qquad \mathbf{x} \in \partial B \backslash S_0\,, \tag{3.5}
$$

and

$$s_i(\mathbf{V}) = t_i(\mathbf{x}), \qquad q_i(\mathbf{V}) = p_i(\mathbf{x}), \qquad \mathbf{x} \in S_0\,, \tag{3.6}$$

and, according to the theory developed by FICHERA [12], under our assumptions there exists a unique solution $\mathbf{V}$ to the problem (3.4) – (3.6). For the remainder of this section we will be discussing the decay properties of the amplitude function $\mathbf{V}$ of the harmonic vibrations $\mathbf{U}$.

We begin by introducing an auxiliary function given by

$$I(z) \equiv -\int_{S_z} [t_{3r}(\mathbf{V})v_r + m_{3r}(\mathbf{V})\psi_r]\, dA, \qquad z \in [0, L] \tag{3.7}$$

and note that, in view of the Cauchy – Schwarz inequality and the arithmetic-geometric mean inequality, we have the estimate

$$I(z) \leq \frac{1}{2}\alpha \int_{S_z} \left[t_{3r}(\mathbf{V})\, t_{3r}(\mathbf{V}) + j^{-2} m_{3r}(\mathbf{V})\, m_{3r}(\mathbf{V})\right] dA + \frac{1}{2\alpha}\int_{S_z} (v_r v_r + j^2 \psi_r \psi_r)\, dA, \qquad z \in [0, L], \tag{3.8}$$

where α is an arbitrary positive constant. On combining (3.8) and (2.14), and on taking into account the meaning of the constant j, we infer that

$$I(z) \leq \mu_M \alpha \int_{S_z} W(\mathbf{V})\, dA + \frac{1}{2\alpha\varrho}\int_{S_z} \varrho(v_r v_r + j_{rs}\psi_r\psi_s)\, dA, \qquad z \in [0, L]. \tag{3.9}$$

Using (3.5) and the Divergence Theorem we also find, from (3.7), that

$$\begin{aligned} I(L) - I(z) &= -\int_{\partial B_z} [t_{sr}(\mathbf{V})n_s v_r + m_{sr}(\mathbf{V})n_s\psi_r]\, d\Sigma \\ &= -\int_{B_z} [(t_{sr}v_r)_{,s} + (m_{sr}\psi_r)_{,s}]\, dV, \qquad z \in [0, L]. \end{aligned} \tag{3.10}$$

Since, by assumption, we have $I(L) = 0$, it follows, from (3.10), (3.4) and (2.4) – (2.6), that

$$I(z) = \int_{B_z} \left[2W(\mathbf{V}) - \varrho\omega^2(v_r v_r + j_{rs}\psi_r\psi_s)\right] dV, \qquad z \in [0, L]. \tag{3.11}$$

We now consider (analogously with equation (2.17) in FLAVIN and KNOPS [5])

$$\omega_m^2(h, L) \equiv \inf \int_R 2W(\mathbf{U})\, dV \Big/ \int_R \varrho(u_r u_r + j_{rs}\varphi_r\varphi_s)\, dV; \tag{3.12}$$

a) within the class of all right cylinders R which share the end $x_3 = L$ and whose lengths belong to the interval $[h, L]$ (where h is an arbitrary fixed number strictly less than L), and

b) within the class of smooth vector fields $\mathbf{U}$ which are such that $u_r = 0$, $\varphi_r = 0$, $r = 1, 2, 3$, on both $x_3 = L$ and the lateral boundaries of these cylinders.

$\omega_m/2\pi$ therefore, represents the minimum fundamental frequency of vibration of cylinders described in (a) whose lateral surfaces and ends $x_3 = L$ are clamped and whose other ends are free. Equations (3.11) and (3.12) lead to

$$I(z) \geq \left(1 - \frac{\omega^2}{\omega_m^2}\right) \int_{B_z} 2W(\mathbf{V})\, dV, \qquad z \in [0, L-h], \tag{3.13}$$

which, when combined with (3.9), gives

$$\left(1 - \frac{\omega^2}{\omega_m^2}\right) \int_{B_z} 2W(\mathbf{V})\, dV \leq \frac{\mu_M \alpha}{2} \int_{S_z} 2W(\mathbf{V})\, dA + \frac{1}{2\alpha\varrho} \int_{S_z} \varrho(v_r v_r + j_{rs}\psi_r\psi_s)\, dA, \qquad z \in [0, L-h]. \tag{3.14}$$

Following TOUPIN [4], we integrate in (3.14) from z to $z+h$, $z \in [0, L-h]$, and on making use of the notations

$$E(z) \equiv \int_{B_z} 2W(\mathbf{V})\, dV, \qquad Q(z,h) \equiv \frac{1}{h} \int_z^{z+h} E(\zeta)\, d\zeta, \tag{3.15}$$

we obtain

$$\left(1 - \frac{\omega^2}{\omega_m^2}\right) Q(z,h) \leq \frac{\alpha\mu_M}{2h} \int_{B(z,h)} 2W(\mathbf{V})\, dV + \frac{1}{2\alpha\varrho h} \int_{B(z,h)} \varrho(v_r v_r + j_{rs}\psi_r\psi_s)\, dV, \tag{3.16}$$

where $B(z,h)$ stands for the cylindrical slice $B_z \backslash B_{z+h}$.

Denoting by $\omega_0(h)/2\pi$ the lowest frequency of vibrations of the slice $B(z,h)$ (whose lateral surface is clamped and whose ends are free) we have, analogously with (3.12),

$$\int_{B(z,h)} 2W(\mathbf{V})\, dV \geq \varrho\omega_0^2(h) \int_{B(z,h)} (v_r v_r + j_{rs}\psi_r\psi_s)\, dV. \tag{3.17}$$

Now (3.17), together with (3.16), leads to

$$\left(1-\frac{\omega^2}{\omega_m^2}\right)Q(z,h)\leq\frac{1}{2h}\left[\mu_M\alpha+\frac{1}{\alpha\varrho\omega_0^2(h)}\right]\int\limits_{B(z,h)}2W(\mathbf{V})\,dV, \tag{3.18}$$

$$z\in[0,L-h].$$

Since

$$\frac{dQ}{dz}(z,h)=\frac{1}{h}\left[E(z+h)-E(z)\right]=-\frac{1}{h}\int\limits_{B(z,h)}2W(\mathbf{V})\,dV \tag{3.19}$$

and

$$\frac{1}{2}\left[\mu_M\alpha+\frac{1}{\alpha\varrho\omega_0^2(h)}\right]\geq\frac{1}{\omega_0(h)}(\mu_M/\varrho)^{1/2}, \tag{3.20}$$

we obtain from (3.18) the following first-order differential inequality

$$\frac{1}{\omega_0(h)}(\mu_M/\varrho)^{1/2}\frac{dQ}{dz}(z,h)+\left(1-\frac{\omega^2}{\omega_m^2}\right)Q(z,h)\leq 0,\qquad z\in[0,L-h], \tag{3.21}$$

which, by integration, leads to the estimate

$$Q(z,h)\leq Q(0,h)\exp\left[-z\left(1-\frac{\omega^2}{\omega_m^2}\right)\omega_0(h)(\mu_M/\varrho)^{-1/2}\right], \tag{3.22}$$

$$z\in[0,L-h].$$

Since $E(z)$ is a non-increasing function of z we have, for all $\zeta\in[z,z+h]$,

$$E(z)\geq E(\zeta)\geq E(z+h) \tag{3.23}$$

which, on account of $(3.15)_2$, gives

$$E(z)\geq Q(z,h)\geq E(z+h),\qquad z\in[0,L-h]. \tag{3.24}$$

Equation (3.24) implies

$$Q(0,h)\leq E(0) \tag{3.25}$$

and thus, on account of $(3.24)_2$ and (3.22), we have

$$E(z+h)\leq E(0)\exp\left[-z\left(1-\frac{\omega^2}{\omega_m^2}\right)\omega_0(h)(\mu_M/\varrho)^{-1/2}\right],\quad z\in[0,L-h], \tag{3.26}$$

which can be re-written as

$$E(z) \leq E(0) \exp\left[-(z-h)\left(1-\frac{\omega^2}{\omega_m^2}\right)\omega_0(h)(\mu_M/\varrho)^{-1/2}\right], \quad z \in [h, L]. \tag{3.27}$$

Inequality (3.27) shows that, in the strain-energy measure, the amplitude $\mathbf{V}$ decays exponentially as a function of $z \in [h, L]$, provided that $\omega < \omega_m$. As such, (3.27) is a Saint-Venant type inequality as originally envisaged by TOUPIN [4]. In the following section we will be obtaining an estimate for $E(0)$ which, in addition to providing us with an explicit estimate for $E(z)$ in terms of the data, implies the continuous dependence on data of solutions to the boundary value problem (3.4) – (3.6).

4. The estimate for $E(0)$

Since, by (3.13), we have (see $(3.15)_1$)

$$E(0) \leq \frac{\omega_m^2}{\omega_m^2 - \omega^2} I(0), \qquad \omega < \omega_m, \tag{4.1}$$

we will be estimating in what follows the quantity $I(0)$ which, in view of (3.6), can be written as

$$I(0) = -\int_{S_0} (t_r v_r + p_r \psi_r)\, dA. \tag{4.2}$$

To this end, we note that the Cauchy – Schwarz inequality implies

$$I(0) \leq \left[\int_{S_0} \left(t_r t_r + j^{-2} p_r p_r\right) dA\right]^{1/2} \cdot D(\mathbf{V})^{1/2}, \tag{4.3}$$

where we have employed the notation

$$D(\mathbf{V}) \equiv \int_{S_0} \left(v_r v_r + j^2 \psi_r \psi_r\right) dA. \tag{4.4}$$

Next, we use an appropriate re-scaling of the well-known trace theorem [12, p. 353] which reads

$$\int_{\partial B} w_r w_r\, ds \leq A_1 \int_B w_r w_r\, dV + A_2 \int_B w_{r,s} w_{r,s}\, dV, \tag{4.5}$$

where A_1 and A_2 are positive constants which depend upon B and ∂B and where w_r are functions of class $C^1(B \cup \partial B)$. Accordingly, from (4.4) and (4.5), we infer

$$D(\mathbf{V}) \leq A_1 \int_B \left(v_r v_r + j^2 \psi_r \psi_r\right) dV + A_2 \int_B \left(v_{r,s} v_{r,s} + j^2 \psi_{r,s} \psi_{r,s}\right) dV \tag{4.6}$$

which, in view of the significance of the constant j, leads to (see $(2.4)_2$)

$$D(\mathbf{V}) \leq A_1 \int_B (v_r v_r + j_{rs} \psi_r \psi_s)\, dV + A_2 \int_B \left[v_{r,s} v_{r,s} + j^2 \kappa_{rs}(\mathbf{V}) \kappa_{rs}(\mathbf{V})\right] dV. \tag{4.7}$$

Since $\mathbf{v} = \mathbf{0}$ on $\partial B \backslash S_0$ we have the first Korn inequality

$$\int_B v_{r,s} v_{r,s}\, dV \leq \frac{1}{4} A_3 \int_B (v_{r,s} + v_{s,r})(v_{r,s} + v_{s,r})\, dV, \qquad A_3 = A_3(B) = \text{const}, \quad A_3 > 0, \tag{4.8}$$

which, when combined with [8]

$$\frac{1}{4}(v_{r,s} + v_{s,r})(v_{r,s} + v_{s,r}) \leq e_{rs}(\mathbf{V})\, e_{rs}(\mathbf{V}) \tag{4.9}$$

and (4.7), gives

$$D(\mathbf{V}) \leq A_1 \int_B (v_r v_r + j_{rs} \psi_r \psi_s)\, dV + A_4 \int_B \left[e_{rs}(\mathbf{V}) e_{rs}(\mathbf{V}) + j^2 \kappa_{rs}(\mathbf{V})\, \kappa_{rs}(\mathbf{V})\right] dV, \tag{4.10}$$

where

$$A_4 \equiv A_2 \max(1, A_3).$$

The assumption that W is positive definite implies that there exists a positive constant μ_m[2] so that

$$2W(\mathbf{U}) \geq \mu_m \left[e_{rs}(\mathbf{U})\, e_{rs}(\mathbf{U}) + j^2 \kappa_{rs}(\mathbf{U})\, \kappa_{rs}(\mathbf{U})\right] \tag{4.11}$$

[2] μ_m is the lowest characteristic value of A_{KL}. See [10, p. 197].

and, by denoting with $\omega_v/2\pi$ the fundamental frequency of the cylinder B whose entire surface, apart from its end plane S_0, is clamped we also have, as before,

$$\int_B 2W(\mathbf{U})\,dV \geq \varrho\omega_v^2 \int_B (u_r u_r + j_{rs}\varphi_r\varphi_s)\,dV, \tag{4.12}$$

for any smooth vector field $\mathbf{U}$. Thus, from (4.3), (4.10), (4.11) and (4.12) we find (see $(3.15)_1$)

$$I(0) \leq \left(\frac{A_1}{\varrho\omega_v^2} + \frac{A_4}{\mu_m}\right)^{1/2} E(0)^{1/2} \left[\int_{S_0} \left(t_r t_r + j^{-2} p_r p_r\right) dA\right]^{1/2}, \tag{4.13}$$

which, together with (4.1), gives

$$E(0) \leq \frac{\omega_m^4}{(\omega_m^2 - \omega^2)^2} \left(\frac{A_1}{\varrho\omega_v^2} + \frac{A_4}{\mu_m}\right) \int_{S_0} \left(t_r t_r + j^{-2} p_r p_r\right) dA. \tag{4.14}$$

Inequality (4.14) expresses the fact that in the strain-energy measure, the solution to the boundary value problem (3.4) – (3.6) depends continuously on the data fot $\omega < \omega_m$. Continuous dependence estimates for stresses, strains and displacements can be obtained by combining (4.14) with (2.14), (4.11) and (4.12), respectively. Finally, we note that on combining (4.14) with (3.27) we can obtain an explicit decay estimate for $E(z)$ in terms of the data prescribed on the boundary of the cylinder.

Acknowledgment

This work has been completed in Autumn 1996 when the second author visited the School of Mathematics and Statistics of the University of Plymouth. The second author gratefully acknowledges the hospitality and support extended to him by the School.

References

1. K. BERGLUND, *Generalization of Saint-Venant's principle to micropolar continua*, Arch. Rational Mech. Anal., **64**, 317–326, 1977.
2. S. CHIRITA and M. ARON, *On Saint-Venant's principle in micropolar elasticity*, Int. J. Engng. Sci., **32**, 1893–1901, 1994.
3. D. IESAN, *Saint-Venant's problem*, [in:] Lecture Notes in Mathematics, A. DOLD and B. ECKMANN [Eds.], Vol. 1279, Springer-Verlag, Berlin-Heidelberg-New York 1987.
4. R.A. TOUPIN, *Saint-Venant's principle*, Arch. Rational Mech. Anal., **18**, 83–96, 1965.
5. J.N. FLAVIN and R.J. KNOPS, *Some spatial decay estimates in continuous dynamics*, J. Elasticity, **17**, 249–264, 1987.

6. J.N. FLAVIN, R.J. KNOPS and L.E. PAYNE, *Energy bounds in dynamical problems for a semi-infinite elastic beam*, [in:] Elasticity: Mathematical Methods and Applications. The Ian N. Sneddon 70th Birthday Volume, pp. 101–112, G. EASON and R.W. OGDEN [Eds.], Ellis Horwood, Chichester 1990.
7. R.J. KNOPS, *Spatial decay estimates in the vibrating anisotropic elastic beam*, [in:] Waves and Stability in Continuous Media, pp. 192–203, S. RIONERO [Ed.], World Scientific, Singapore 1991.
8. M. ARON, *Continuous dependence results and a priori estimates in nonlinear micropolar elasticity*, Acta Mech., **37**, 131–136, 1980.
9. A.C. ERINGEN, *Theory of micropolar elasticity*, [in:] Fracture, H. LEIBOVITZ [Ed.], Vol. 2, Academic Press, New York 1968.
10. M.E. GURTIN, *The linear theory of elasticity*, [in:] Handbuch der Physik, pp. 1–295, C. TRUESDELL [Ed.], Vol. VI a/2, Springer-Verlag, Berlin-Heidelberg-New York 1972.
11. M.M. MEHRABADI, S.C. COWIN and C.O. HORGAN, *Strain energy density bounds for linear anisotropic elastic materials*, J. Elasticity, **30**, 191–196, 1993.
12. G. FICHERA, *Existence theorems in elasticity*, [in:] Handbuch der Physik, pp. 347–389, C. TRUESDELL [Ed.], Vol. VI a/2, Springer-Verlag, Berlin-Heidelberg-New York 1972.

SCHOOL OF MATHEMATICS AND STATISTICS
UNIVERSITY OF PLYMOUTH, PLYMOUTH, ENGLAND

and

MATHEMATICAL SEMINARIUM
UNIVERSITY OF IASI, IASI, ROMANIA.

Received December 6, 1996.

Arch. Mech., 49, 4, pp. 677–695, Warszawa 1997

Remarks on Il'iushin's postulate

CH. TSAKMAKIS (KARLSRUHE)

IN ITS ORIGINAL VERSION (strong form), the postulate of Il'iushin states that the integral of the stress power of an elastic-plastic material must be non-negative for any closed strain path. As a consequence, it has been shown that the so-called simple endochronic theory of plasticity violates this postulate of "material stability". The characteristic feature of this theory is that yield surfaces and related loading conditions are not involved in the governing constitutive equations. In the present paper it is shown, with reference to a well-established class of plasticity laws, that the strong form of Il'iushin's postulate may be violated as well, if the constitutive theory is constructed on the basis of a yield surface and related loading conditions. The question arises if such strain-stress relations preserve some weaker stability conditions in the sense of Il'iushin. It turns out that they satisfy a weaker form of Il'iushin's postulate, in which the integral of the stress power is required to be non-negative only for special, so-called small cycles of deformation, as defined by Lucchesi and Silhavy. From a physical point of view on a phenomenological level, it seems that there is no experimental evidence to exclude from a general theory of plasticity such material behaviour which complies with the weak form of Il'iushin's postulate. Moreover, if the validity of the weak form of Il'iushin's postulate is assumed, then it is shown that the simple endochronic theory of plasticity is no longer in conflict with this version of the postulate.

1. Introduction

WHEN FORMULATING the framework for constitutive relations, it is convenient to introduce some constitutive inequalities limiting the types of the mechanical behaviour to be modeled. Such inequalities represent in some sense "material stability" conditions (see i.e. DRUCKER [8, 9], PALMER, MAIER and DRUCKER [24], HILL [13, 14], WANG and TRUESDELL [30, Ch. III.7–III.9], MARTIN [21, Sec. 2.4, 2.5], OGDEN [22, Sec. 6.2.8], LUBLINER [19, Sec. 3.2], HAVNER [12, Sec. 3.6] and the references cited therein). In the context of a pure mechanical theory concerning elastic-plastic material properties, a material stability condition frequently assumed is the postulate of Il'iushin. In its original form (strong form), this postulate is referred to small deformations and states that the integral of the stress power of a material element must be non-negative in any closed strain path (see IL'IUSHIN [16]). As a consequence (see SANDLER [26] as well as RIVLIN [25]), the linear isotropic version of the so-called simple endochronic theory of plasticity (see VALANIS [28]) violates this postulate. This fact was a reason for the simple endochronic theory of plasticity to be discredited.

The purpose of the present paper is to motivate the introduction of a weaker formulation of the postulate of Il'iushin and then to discuss the simple en-

dochronic theory with respect to this weaker formulation of the postulate. Specifically, in Sec. 2 we will consider a class of plasticity laws which is defined in terms of a yield function and the related loading conditions. These plasticity laws exhibit kinematic hardening only, the well-known hardening rule of ARMSTRONG and FREDERICK [1] included as a particular case. Also, the linear isotropic version of the simple endochronic theory of plasticity is contained as a limiting case. Section 3 deals with an elementary proof of the fact that well-established plasticity laws, included in the class defined in Sec. 2, with kinematic hardening of the Armstrong–Frederick type, may violate the postulate of Il'iushin, if the material parameters do not have appropriate values. There arises then the question if these plasticity laws satisfy some kind of material stability in a weaker form.

Indeed, it is proved in Sec. 4, that the material behaviour predicted by these plasticity laws is in agreement with a weaker form of Il'iushin's postulate, in which the integral of the stress power is required to be non-negative only for special, so-called small strain cycles, as defined by LUCCHESI and SILHAVY [20]. Finally, it is shown in Sec. 5 that if the weak form of Il'iushin's postulate is assumed to apply in a general theory of plasticity, then the simple endochronic theory is no longer in conflict with this postulate.

In the following, we use bold-face and calligraphic letters for second-order and fourth-order tensors, respectively. In particular, $\mathbf{1}$ represents the identity second-order tensor and $\mathbf{A}^T$ denotes the transpose of $\mathbf{A}$. We write $\operatorname{tr}\mathbf{A}$ for the trace of $\mathbf{A}$, $\mathbf{A}^D = \mathbf{A} - \frac{1}{3}(\operatorname{tr}\mathbf{A})\mathbf{1}$ for the deviator of $\mathbf{A}$, as well as $\mathbf{A}\cdot\mathbf{B} = \operatorname{tr}(\mathbf{A}\mathbf{B}^T)$ for the inner product of $\mathbf{A}$ and $\mathbf{B}$. We denote by $\mathcal{E}$ the fourth-order tensor, which has components

$$\frac{1}{2}(\delta_{ij}\delta_{mn} + \delta_{in}\delta_{mj})\,\mathbf{e}_i \otimes \mathbf{e}_m \otimes \mathbf{e}_j \otimes \mathbf{e}_n$$

relative to the orthonormal basis $\{\mathbf{e}_i\}$, $i = 1, 2, 3$, where the symbol $\otimes$ denotes the tensor product, and δ_{ij} is the Kronecker delta. Further, if $\mathcal{K}$ and $\mathbf{A}$ are fourth-order and second-order tensors, respectively, represented by $\mathcal{K} = \mathcal{K}_{ijkl}\mathbf{e}_i \otimes \mathbf{e}_j \otimes \mathbf{e}_k \otimes \mathbf{e}_l$ and $\mathbf{A} = A_{ij}\mathbf{e}_i \otimes \mathbf{e}_j$, then $\mathcal{K}[\mathbf{A}] := \mathcal{K}_{ijmn}A_{mn}\mathbf{e}_i \otimes \mathbf{e}_j$. For a real a, $|a|$ is the absolute value of a, while $(\,)^{\cdot}$ denotes the material time derivative of $(\,)$, the variable time being represented by t. If nothing is said to the contrary, the material parameters used will take values on the real interval $[0, \infty)$. The deformations considered are small isothermal deformations. Since the following is not affected by a space dependence, an explicit reference to space will be dropped. All components of tensor variables are related to a Cartesian coordinate system.

2. Plasticity laws with kinematic hardening

Consider the class of plasticity models with kinematic hardening summarized in Table 1.

Table 1. A class of plasticity models with kinematic hardening.

(2.1) $\mathbf{E} = \mathbf{E}_{\mathrm{e}} + \mathbf{E}_{\mathrm{p}}$,

(2.2) $\mathbf{T} = 2\mu\mathbf{E}_{\mathrm{e}} + \lambda(\operatorname{tr}\mathbf{E}_{\mathrm{e}})\mathbf{1}$,

(2.3) μ, λ – Elasticity constants ($\mu > 0$, $2\mu + 3\lambda > 0$),

(2.4) F – yield function,

(2.5) $\mathsf{F}(t) = \bar{\mathsf{F}}(\mathbf{T}(t), \boldsymbol{\xi}(t)) := \sqrt{\frac{3}{2}(\mathbf{T} - \boldsymbol{\xi})^D \cdot (\mathbf{T} - \boldsymbol{\xi})^D + \alpha(\operatorname{tr}[\mathbf{T} - \boldsymbol{\xi}])^2} - k$,

(2.6) $k = \text{const}, \quad 0 \leq \alpha \leq \frac{1}{2}$,

(2.7) yield condition $\iff$ $\mathsf{F} = 0$,

(2.8) $\dot{\mathbf{E}}_{\mathrm{p}} := \begin{cases} \Lambda \dfrac{\partial \bar{\mathsf{F}}}{\partial \mathbf{T}} & \text{in plastic loading,} \\ \mathbf{0} & \text{otherwise,} \end{cases}$

(2.9) plastic loading $\iff$ $\mathsf{F} = 0$ & $(\dot{\mathsf{F}})_{s=\text{const}} > 0$,

(2.10) $\dot{s} = \sqrt{\dot{\mathbf{E}}_{\mathrm{p}} \cdot \mathcal{P}[\dot{\mathbf{E}}_{\mathrm{p}}]}$,

(2.11) $\mathcal{P} = p_1\mathcal{E} + p_2\mathbf{1} \otimes \mathbf{1}$,

(2.12) p_1, p_2 – const $(p_1 \geq 0, \quad p_1 + 3p_2 \geq 0)$,

(2.13) $\dot{z} = g\dot{s}$,

(2.14) g – constitutive function,

(2.15) $\boldsymbol{\xi} := \sum_{j=1}^{N} \mathbf{Z}_j + \sum_{r=1}^{n} \frac{1}{3} M_r \mathbf{1}$,

(2.16) $\frac{d\mathbf{Z}_j}{dz} = c_j \frac{d\mathbf{E}_{\mathrm{p}}}{dz} - b_j \mathbf{Z}_j$,

(2.17) c_j, $b_j > 0$ if $1 \leq j < N$, $c_N > 0$, $b_N \geq 0$,

(2.18) $\frac{dM_r}{dz} = c_r^* \frac{d(\operatorname{tr}\mathbf{E}_{\mathrm{p}})}{dz} - b_r^* M_r$,

(2.19) c_r^*, $b_r^* > 0$ if $1 \leq r < n$, $c_n^* > 0$, $b_n^* \geq 0$.

In these formulas, $\mathbf{E}_{\mathrm{e}}$ and $\mathbf{E}_{\mathrm{p}}$ denote the elastic and plastic parts in the additive decomposition of the linearized Green strain tensor $\mathbf{E}$, $\mathbf{T}$ is the Cauchy stress tensor and $\boldsymbol{\xi}$ represents the variable describing kinematic hardening (back stress). The scalar factor Λ is to be determined from the so-called consistency equation $\dot{\mathsf{F}} = 0$. The characteristic features of these plasticity laws are the yield function (2.5), (2.6) and the evolution equations (2.10) – (2.19) for the back stress. The yield function (2.5) is related to the general definition for yield functions, given

by SHRIVASTAVA, MROZ and DUBEY [27]. A yield function of the form (2.5), (2.6) as well as the hardening rule (2.10) – (2.19) with $p_2 = 0$, $p_1 = 1$ and g as positive continuous monotonic and bounded function of s were proposed by KORZEN [17, Ch.5] as a generalization of the hardening rule introduced by CHABOCHE, DANG VAN and CORDIER [5]. However, it should be mentioned that relations of the form (2.10) – (2.19) indicate the typical structure of constitutive equations according to the simple endochronic theory of plasticity and were introduced by VALANIS [28] at first. Note in passing that g can be chosen to be a constitutive function of additional variables, for which then appropriate evolution equations are needed. Such examples are given e.g. in HAUPT, KAMLAH and TSAKMAKIS [11]. Aslo, it is perhaps of interest to remark that, for $\boldsymbol{\xi} = \mathbf{0}$, (2.5) reduces to a yield function proposed earlier by Burzynski (see Życzkowski [31, Sec. 11], where the original work of Burzynski is cited).

There are two particular cases in the class of plasticity laws (2.1) – (2.19), which will now be discussed briefly.

2.1. Plasticity laws with kinematic hardening of the Armstrong–Frederick type

On setting $\alpha = 0$, Eq. (2.5) reduces to a v. Mises yield function with kinematic hardening. Hence, by (2.8), $\mathbf{E}_\mathrm{p}$ becomes deviatoric. Further, we set $p_1 = 2/3$, $p_2 = 0$ and $g \equiv 1$. Then,

$$\dot{s} = \dot{z} = \sqrt{\frac{2}{3}\dot{\mathbf{E}}_\mathrm{p} \cdot \dot{\mathbf{E}}_\mathrm{p}}\,, \tag{2.20}$$

i.e., $\dot{s}$ reduces to the well-known plastic arc length formula. In addition, we assume homogeneous initial conditions, such that $M_r \equiv 0$ for every r. Finally, if we set $N = 1$ and $c_1 = c$, $b_1 = b$, Eqs. (2.15) – (2.19) yield the well-known hardening rule of ARMSTRONG and FREDERICK [1] (see also CHABOCHE [6]):

$$\dot{\boldsymbol{\xi}} = c\dot{\mathbf{E}}_\mathrm{p} - b\dot{s}\boldsymbol{\xi}\,. \tag{2.21}$$

This hardening rule together with the relations (2.1) – (2.9) and $\alpha = 0$ form a well established plasticity model, which will be discussed in Sec. 3 for one-dimensional loading histories. The one-dimensional relations needed for this discussion read as follows. Using the definitions $(\mathbf{T})_{11} = \sigma$, $(\mathbf{E})_{11} = \varepsilon$, $(\mathbf{E}_\mathrm{e})_{11} = \varepsilon_\mathrm{e}$, $(\mathbf{E}_\mathrm{p})_{11} = \varepsilon_\mathrm{p}$, $\dot{s} = |\dot{\varepsilon}_\mathrm{p}|$, $\frac{3}{2}(\boldsymbol{\xi})_{11} = \xi$, $E = \dfrac{\mu(3\lambda + 2\mu)}{\lambda + \mu}$ (E – elasticity modulus), we get:

$$\varepsilon = \varepsilon_\mathrm{e} + \varepsilon_\mathrm{p}\,, \tag{2.22}$$

$$\sigma = E\varepsilon_\mathrm{e}\,, \tag{2.23}$$

$$\left.\begin{aligned} &|\sigma - \xi| = k\,, && (2.24)\\ &\dot{\sigma} = \dot{\xi}\,, && (2.25)\\ &\dot{\xi} = \frac{3}{2}c\dot{\varepsilon}_\mathrm{p} - b|\dot{\varepsilon}_\mathrm{p}|\xi\,, && (2.26) \end{aligned}\right\} \quad \text{for plastic loading.}$$

Thus,

$$\frac{d\varepsilon_{\mathrm{p}}}{d\varepsilon} = \frac{E}{E + \dfrac{3c}{2} \pm b\xi}, \tag{2.27}$$

where + denotes compressive loading and − tensile loading.

2.2. The case $k = 0$

Let $k = 0$ in Eq. (2.5). Then, from (2.5) − (2.7),

$$\mathbf{T} \equiv \boldsymbol{\xi}, \tag{2.28}$$

i.e., a pure elastic range is no longer present. Roughly speaking, the yield surface shrinks to a point in the stress space. However, according to (2.1), (2.2), the decomposition of the total strain into elastic and plastic parts still remains valid. Note that $k = 0$ always implies plastic loading. Further, (2.8) is meaningless now, for a unique normal on the yield surface no longer exists. But such an equation is no longer needed. In other words, the plastic strain $\mathbf{E}_{\mathrm{p}}$ is now postulated to depend upon the previous loading history by means of an implicitly defined functional. This functional is represented through the constitutive relations for the kinematic hardening. To be more specific, if we are given a loading history, then the decomposition for the strain (2.1), the elasticity law (2.2), the identity (2.28) and the kinematic hardening rule form a system of four equations for the determination of the four unknown $\boldsymbol{\xi}$, $\mathbf{E}_{\mathrm{e}}$, $\mathbf{E}_{\mathrm{p}}$ and $\mathbf{T}$ or $\mathbf{E}$.

Next, we note that if $\mu, \lambda \to \infty$, then $\mathbf{E}_{\mathrm{e}} \to \mathbf{0}$ in order for the stress to remain finite. This means that the assumption $\mu, \lambda \to \infty$ implies

$$\mathbf{E}_{\mathrm{p}} \to \mathbf{E}. \tag{2.29}$$

Now, let us integrate Eqs. (2.15) − (2.19) for homogeneous initial conditions and assume g to be a function of the arc length s. Then, by (2.28), (2.29),

$$\mathbf{T} = \int_0^z \Psi(z - \bar{z}) \left(\frac{d}{d\bar{z}} \mathbf{E}(\bar{z}) \right) d\bar{z} + \mathbf{1} \int_0^z \chi(z - \bar{z}) \left(\frac{d}{d\bar{z}} \operatorname{tr} \mathbf{E}(\bar{z}) \right) d\bar{z}, \tag{2.30}$$

$$\Psi(z) = \sum_{j=1}^{N} c_j e^{-b_j z}, \tag{2.31}$$

$$\chi(z) = \sum_{r=1}^{n} c_r^* e^{-b_r^* z}, \tag{2.32}$$

$$\dot{z} = g(s)\dot{s}, \tag{2.33}$$

$$\dot{s} = \sqrt{\dot{\mathbf{E}} \cdot \mathcal{P}[\dot{\mathbf{E}}]}. \tag{2.34}$$

Equations (2.30) – (2.34) represent the linear isotropic version of the so-called simple endochronic theory of plasticity. This constitutive model was postulated by VALANIS [28] (for a brief review of the simple endochronic theory of plasticity see also VALANIS and LEE [29]) in order to describe plastic material properties without using a yield surface as well as loading conditions. It must be emphasized that Valanis introduced this theory by replacing the natural time t in the linear viscoelasticity by the arc length z defined through (2.33), (2.34). In the present paper, it is shown that the simple endochronic theory of plasticity can be interpreted as a limiting case of the class of plasticity laws represented in Table 1 ([1]). In particular, this was the reason for defining the arc lengths s and z as in (2.10) – (2.14), which is typical for the endochronic theory of plasticity.

3. The postulate of Il'iushin for arbitrary strain cycles

For a fixed material particle, let us consider a strain cycle, which begins at time t_0 and ends at time t_e. Such strain cycles are denoted by $C[t_0, t_e]$. Il'iushin's postulate (strong form) requires the work to be non-negative in any strain cycle:

$$I(t_0, t_e) = \int_{t_0}^{t_e} \mathbf{T}(t) \cdot \dot{\mathbf{E}}(t)\, dt \geq 0 \qquad \text{for every} \qquad C[t_0, t_e]. \tag{3.1}$$

Evidently, a strain cycle does not generally imply a cycle for other process variables, if irreversible deformations are involved. To emphasize this fact, ŻYCZKOWSKI [31, p. 119] introduced the term quasi-cycle. However, in dealing with Il'iushin's postulate, it is customary (see e.g. LUBLINER [19, p. 122]) to denote closed trajectories in strain space simply as strain cycles, a notion which is adopted in the present paper as well.

We now proceed to examine compatibility of the plasticity laws given in Sec. 2.1 with the inequality (3.1). Especially, we will show that these plasticity laws can contradict inequality (3.1) for some special strain cycles, and thus in general. To this end, it suffices to consider one-dimensional strain-controlled processes involving tension and compression loading. The constitutive relations governing the material response are given by (2.22) – (2.27). Specifically, we consider strain cycles of the form $A'C'A'$ (see Fig. 1) to which the (ε, σ)-paths of the kind $ABCDE$ correspond. In the following, we denote by $(\,)^P$ the value of $(\,)$ at the point P.

Plastic flow first occurs during compression at point B and during tension at point D. We may parameterize the (ε, σ)-path e.g. by using the time t as a parameter. We denote by t_A, t_B, t_C, t_D, t_E, $(t_A < t_B < t_C < t_D < t_E)$, the times belonging to the (ε, σ)-points A, B, C, D, E, respectively. Thus, plastic

([1]) Actually, we deal only with the linear isotropic version of the simple endochronic theory here, but it is not difficult to extend the above discussion to the non-isotropic case.

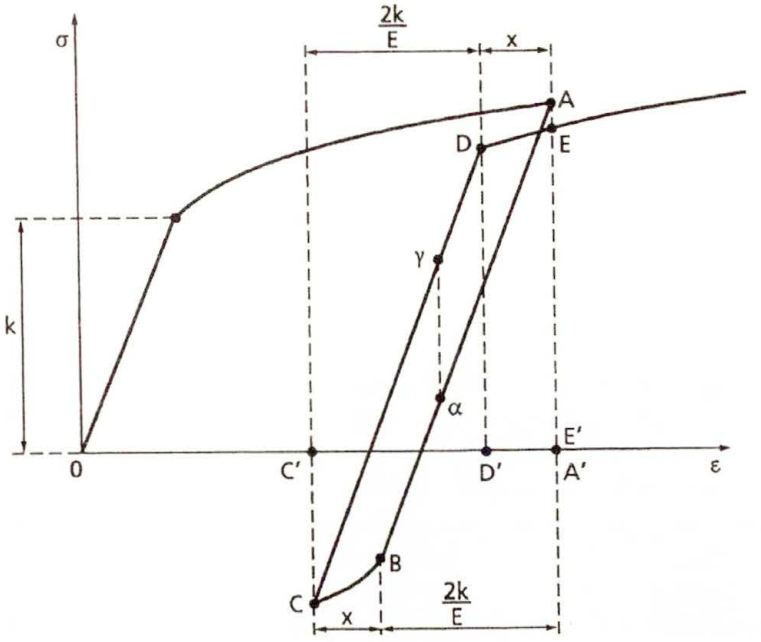

FIG. 1. Uniaxial strain cycle. To the cycle $A'C'A'$ in the strain axis corresponds the (ε, σ)-path $ABCDE$.

deformations are only involved during the time intervals $[t_B, t_C]$ and $[t_D, t_E]$, while pure elastic deformations take place during the time intervals $[t_A, t_B]$ and $[t_C, t_D]$. Since kinematic hardening is only incorporated, the strain differences between E and D, and between B and C, are equal:

$$\varepsilon^E - \varepsilon^D = \varepsilon^B - \varepsilon^C =: x\,. \tag{3.2}$$

The strain differences between A and B, and between D and C, satisfy the relations (see Fig. 1)

$$\varepsilon^A - \varepsilon^B = \varepsilon^D - \varepsilon^C = \frac{2k}{E}\,. \tag{3.3}$$

The work of the stress power for the time interval $[t_A, t_E]$ is

$$I_{AE} = \int_{t_A}^{t_E} \sigma(t)\,\dot{\varepsilon}\,(t)\,dt\,, \tag{3.4}$$

or, by (2.22), (2.23),

$$I_{AE} = E \int_{t_A}^{t_E} \varepsilon(t)\,\dot{\varepsilon}\,(t)\,dt - E \int_{t_A}^{t_E} \varepsilon_{\mathrm{p}}(t)\,\dot{\varepsilon}\,(t)\,dt\,. \tag{3.5}$$

Recalling that $\varepsilon^A = \varepsilon^E$, the last equation reduces to

$$I_{AE} = -E \int_{t_A}^{t_E} \varepsilon_{\mathrm{p}}(t)\, \dot{\varepsilon}(t)\, dt\,, \tag{3.6}$$

or

$$I_{AE} = 2k\left(\varepsilon_{\mathrm{p}}^A - \varepsilon_{\mathrm{p}}^C\right) - E\left(\int_{t_B}^{t_C} \varepsilon_{\mathrm{p}}(t)\, \dot{\varepsilon}(t)\, dt + \int_{t_D}^{t_E} \varepsilon_{\mathrm{p}}(t)\, \dot{\varepsilon}(t)\, dt\right), \tag{3.7}$$

in view of the fact that $\varepsilon_{\mathrm{p}}(t) = \varepsilon_{\mathrm{p}}^A = \text{const}$ for $t \in [t_A, t_B]$ and $\varepsilon_{\mathrm{p}}(t) = \varepsilon_{\mathrm{p}}^C = \text{const}$ for $t \in [t_C, t_D]$. Now fix t_A (and therefore ε^A, ε^B too) and change the integration variable from t to ε. This is possible, since the strain ε is a monotonic function of t for $t \in [t_B, t_C]$ and $t \in [t_D, t_E]$, respectively. Further, suppose that the values of ε_{p} and ξ are known at t_A, and therefore at t_B too. Then, for $t \in [t_B, t_C]$, the solutions of Eqs. (2.22) – (2.26), with $\sigma - \xi = -k$ and $\dot{\varepsilon}_{\mathrm{p}} < 0$, define ε_{p} and ξ as functions of the strain $\bar{\varepsilon}_{\mathrm{p}}(\varepsilon)$ and $\bar{\xi}(\varepsilon)$, respectively. Hence the values of ε_{p} and ξ at t_C, and therefore at t_D as well, are determined as a function of x, respectively, where x is defined by (3.2). We may use these values as initial conditions in (2.22) – (2.26), with $\sigma - \xi = k$ and $\dot{\varepsilon}_{\mathrm{p}} > 0$, to obtain ε_{p} and ξ for $t \in [t_D, t_E]$ as functions of the strain $\bar{\bar{\varepsilon}}_{\mathrm{p}}(\varepsilon; x)$ and $\bar{\bar{\xi}}(\varepsilon; x)$, respectively:

$$(\varepsilon_{\mathrm{p}}(t), \xi(t)) = \begin{cases} (\bar{\varepsilon}_{\mathrm{p}}(\varepsilon), \bar{\xi}(\varepsilon)) & \text{if} \quad t \in [t_B, t_C], \\ (\bar{\bar{\varepsilon}}_{\mathrm{p}}(\varepsilon; x), \bar{\bar{\xi}}(\varepsilon; x)) & \text{if} \quad t \in [t_D, t_E]. \end{cases} \tag{3.8}$$

Clearly,

$$\varepsilon_{\mathrm{p}}^A = \varepsilon_{\mathrm{p}}^B = \bar{\varepsilon}_{\mathrm{p}}(\varepsilon^B) = \bar{\bar{\varepsilon}}_{\mathrm{p}}(\varepsilon^A; 0), \tag{3.9}$$

$$\xi^A = \xi^B = \bar{\xi}(\varepsilon^B) = \bar{\bar{\xi}}(\varepsilon^A; 0). \tag{3.10}$$

Then, (3.7) can be written as

$$I_{AE}(x) = \varphi_1(x) - \varphi_2(x) - \varphi_3(x) \tag{3.11}$$

with

$$\varphi_1(x) = 2k\left(\varepsilon_{\mathrm{p}}^A - \bar{\varepsilon}_{\mathrm{p}}(\varepsilon^B - x)\right), \tag{3.12}$$

$$\varphi_2(x) = E \int_{\varepsilon^B}^{\varepsilon^B - x} \bar{\varepsilon}_{\mathrm{p}}(\varepsilon)\, d\varepsilon\,, \tag{3.13}$$

$$\varphi_3(x) = E \int_{\varepsilon^A - x}^{\varepsilon^A} \bar{\bar{\varepsilon}}_{\mathrm{p}}(\varepsilon; x)\, d\varepsilon\,. \tag{3.14}$$

For our purpose it is convenient to expand $I_{AE}(x)$ into a Taylor's series about $x = 0$:

$$I_{AE}(x) = [\varphi_1(x) - \varphi_2(x) - \varphi_3(x)]_{x=0} + x\left[\frac{d}{dx}(\varphi_1(x) - \varphi_2(x) - \varphi_3(x))\right]_{x=0} + \frac{1}{2}x^2\left[\frac{d^2}{dx^2}(\varphi_1(x) - \varphi_2(x) - \varphi_3(x))\right]_{x=0} + O(x^3) \tag{3.15}$$

with O denoting the usual order symbol. The derivatives of the functions in (3.12) – (3.14) are given by

$$\frac{d\varphi_1(x)}{dx} = 2k\left[\frac{d\bar{\varepsilon}_p(\varepsilon)}{d\varepsilon}\right]_{\varepsilon=\varepsilon^B-x}, \tag{3.16}$$

$$\frac{d^2\varphi_1(x)}{dx^2} = -2k\left[\frac{d^2\bar{\varepsilon}_p(\varepsilon)}{d\varepsilon^2}\right]_{\varepsilon=\varepsilon^B-x}, \tag{3.17}$$

$$\frac{d\varphi_2(x)}{dx} = -E\bar{\varepsilon}_p(\varepsilon^B - x), \tag{3.18}$$

$$\frac{d^2\varphi_2(x)}{dx^2} = E\left[\frac{d\bar{\varepsilon}_p(\varepsilon)}{d\varepsilon}\right]_{\varepsilon=\varepsilon^B-x}, \tag{3.19}$$

$$\frac{d\varphi_3(x)}{dx} = E\bar{\bar{\varepsilon}}_p(\varepsilon^A - x; x) + E\int_{\varepsilon^A-x}^{\varepsilon^A}\frac{\partial\bar{\bar{\varepsilon}}_p(\varepsilon; x)}{\partial x}d\varepsilon, \tag{3.20}$$

$$\frac{d^2\varphi_3(x)}{dx^2} = E\left[2\frac{\partial\bar{\bar{\varepsilon}}_p(\varepsilon; x)}{\partial x} - \frac{\partial\bar{\bar{\varepsilon}}_p(\varepsilon; x)}{\partial\varepsilon}\right]_{\varepsilon=\varepsilon^A-x} + E\int_{\varepsilon^A-x}^{\varepsilon^A}\frac{\partial^2\bar{\bar{\varepsilon}}_p(\varepsilon; x)}{\partial x^2}d\varepsilon. \tag{3.21}$$

Before proceeding to calculate the values of these functions for $x = 0$, it is first necessary to establish some results concerning the derivatives of the functions in (3.8). From (2.27) and (3.10) we obtain

$$\left[\frac{d\bar{\varepsilon}_p(\varepsilon)}{d\varepsilon}\right]_{\varepsilon=\varepsilon^B} = \left[\frac{E}{E+\frac{3c}{2}+b\bar{\xi}(\varepsilon)}\right]_{\varepsilon=\varepsilon^B} = \frac{E}{E+\frac{3c}{2}+b\xi^B}, \tag{3.22}$$

$$\left[\frac{\partial\bar{\bar{\varepsilon}}_p(\varepsilon; x)}{\partial\varepsilon}\right]_{\varepsilon=\varepsilon^A,\ x=0} = \left[\frac{E}{E+\frac{3c}{2}-b\bar{\bar{\xi}}(\varepsilon; x)}\right]_{\varepsilon=\varepsilon^A,\ x=0} = \frac{E}{E+\frac{3c}{2}-b\xi^B}. \tag{3.23}$$

Also, if $\varepsilon^D \leq \varepsilon \leq \varepsilon^E = \varepsilon^A$, we may diffenrentiate the identity

$$\bar{\bar{\varepsilon}}_{\mathrm{p}}(\varepsilon; x) = \bar{\varepsilon}_{\mathrm{p}}(\varepsilon^B - x) + \int_{\varepsilon^A - x}^{\varepsilon} \frac{\partial \bar{\bar{\varepsilon}}_{\mathrm{p}}(u; x)}{\partial u} du \tag{3.24}$$

with respect to x to obtain

$$\frac{\partial \bar{\bar{\varepsilon}}_{\mathrm{p}}(\varepsilon; x)}{\partial x} = -\left[\frac{d\bar{\varepsilon}_{\mathrm{p}}(u)}{du}\right]_{u=\varepsilon^B - x} + \left[\frac{\partial \bar{\bar{\varepsilon}}_{\mathrm{p}}(u; x)}{\partial u}\right]_{u=\varepsilon^A - x} + \int_{\varepsilon^A - x}^{\varepsilon} \frac{\partial^2 \bar{\bar{\varepsilon}}_{\mathrm{p}}(u; x)}{\partial u \partial x} du\,. \tag{3.25}$$

This implies

$$\left[\frac{\partial \bar{\bar{\varepsilon}}_{\mathrm{p}}(\varepsilon; x)}{\partial x}\right]_{\varepsilon=\varepsilon^A,\ x=0} = -\left[\frac{d\bar{\varepsilon}_{\mathrm{p}}(\varepsilon)}{d\varepsilon}\right]_{\varepsilon=\varepsilon^B} + \left[\frac{\partial \bar{\bar{\varepsilon}}_{\mathrm{p}}(\varepsilon; x)}{\partial \varepsilon}\right]_{\varepsilon=\varepsilon^A,\ x=0}, \tag{3.26}$$

the variable u in the two first terms on the right-hand side of (3.25) being replaced with ε. Using (3.12) – (3.14), (3.16) – (3.21), as well as (3.8), (3.9) and (3.26), it is now straightforward to deduce that

$$\varphi_1(0) = 0\,, \tag{3.27}$$

$$\left[\frac{d\varphi_1(x)}{dx}\right]_{x=0} = 2k\left[\frac{d\bar{\varepsilon}_{\mathrm{p}}(\varepsilon)}{d\varepsilon}\right]_{\varepsilon=\varepsilon^B}, \tag{3.28}$$

$$\left[\frac{d^2\varphi_1(x)}{dx^2}\right]_{x=0} = -2k\left[\frac{d^2\bar{\varepsilon}_{\mathrm{p}}(\varepsilon)}{d\varepsilon^2}\right]_{\varepsilon=\varepsilon^B}, \tag{3.29}$$

$$\varphi_2(0) = 0\,, \tag{3.30}$$

$$\left[\frac{d\varphi_2(x)}{dx}\right]_{x=0} = -E\varepsilon_{\mathrm{p}}^A\,, \tag{3.31}$$

$$\left[\frac{d^2\varphi_2(x)}{dx^2}\right]_{x=0} = E\left[\frac{d\bar{\varepsilon}_{\mathrm{p}}(\varepsilon)}{d\varepsilon}\right]_{\varepsilon=\varepsilon^B}, \tag{3.32}$$

$$\varphi_3(0) = 0\,, \tag{3.33}$$

$$\left[\frac{d\varphi_3(x)}{dx}\right]_{x=0} = E\varepsilon_{\mathrm{p}}^A\,, \tag{3.34}$$

$$\left[\frac{d^2\varphi_3(x)}{dx^2}\right]_{x=0} = -2E\left[\frac{d\bar{\varepsilon}_{\mathrm{p}}(\varepsilon)}{d\varepsilon}\right]_{\varepsilon=\varepsilon^B} + E\left[\frac{\partial \bar{\bar{\varepsilon}}_{\mathrm{p}}(\varepsilon; x)}{\partial \varepsilon}\right]_{\varepsilon=\varepsilon^A,\ x=0} \tag{3.35}$$

Thus, by substituting (3.27) – (3.35) into (3.15) and rearranging the terms appropriately, $I_{AE}(x)$ takes the more specific form

$$I_{AE}(x) = 2k\left\{x\left[\frac{d\bar{\varepsilon}_{\mathrm{p}}(\varepsilon)}{d\varepsilon}\right]_{\varepsilon=\varepsilon^B} - \frac{1}{2}x^2\left[\frac{d^2\bar{\varepsilon}_{\mathrm{p}}(\varepsilon)}{d\varepsilon^2}\right]_{\varepsilon=\varepsilon^B}\right\} + \frac{E}{2}x^2\left\{\left[\frac{d\bar{\varepsilon}_{\mathrm{p}}(\varepsilon)}{d\varepsilon}\right]_{\varepsilon=\varepsilon^B} - \left[\frac{\partial\bar{\bar{\varepsilon}}_{\mathrm{p}}(\varepsilon;x)}{\partial\varepsilon}\right]_{\varepsilon=\varepsilon^A,\ x=0}\right\} + O(x^3). \tag{3.36}$$

Now, we are in a position to show that the sign of $I_{AE}(x)$ can become negative. To this end, suppose $\xi^B > 0$, so that, from (3.22), (3.23),

$$\left[\frac{d\bar{\varepsilon}_{\mathrm{p}}(\varepsilon)}{d\varepsilon}\right]_{\varepsilon=\varepsilon^B} - \left[\frac{\partial\bar{\bar{\varepsilon}}_{\mathrm{p}}(\varepsilon;x)}{\partial\varepsilon}\right]_{\varepsilon=\varepsilon^A,\ x=0} < 0\,. \tag{3.37}$$

Then, in view of (3.36), we recognize that there exist strain cycles with sufficiently small x, such that $I_{AE}(x)$ can be approximated by second-order terms in x. Further, by virtue of (3.37), $I_{AE}(x)$ can become negative if k is sufficiently small (but in general not infinitesimally small).

It must be noted that, as mentioned in the Introduction (Sec. 1), a negative work during strain cycles for the simple endochronic theory was calculated by SANDLER [26] and RIVLIN [25]. However, it was shown in Sec. 2.2 that constitutive models of the simple endochronic theory do not possess a finite elastic range, even not an elastic part of deformation. Roughly speaking, the qualitative difference between our work and the calculations of Sandler and Rivlin is that here we deal with plastic materials exhibiting finite elastic range.

4. The postulate of Il'iushin for small strain cycles

In the previous section, we have shown with reference to the well-established plasticity laws given in Sec. 2.1, that if the hardening parameters, and in particular the yield stress, are required to be only non-negative, a physically plausible assumption, then inequality (3.1) may be violated. It is then of interest to know if these plasticity laws satisfy some weaker forms of material stability([2]) than (3.1). In the following, we will show that indeed they satisfy a weaker form of the postulate of Il'iushin, in which the integral of the stress power is required to be non-negative only for special, so-called small strain cycles.

We observe from Fig. 1 that during the loading segment corresponding to the time interval $(t_B, t_C]$, the initial strain state (point A') always lies outside the elastic ranges surrounded by the yield surfaces in the strain axis (strain space).

([2]) The terms strong and weak forms of work postulate are introduced by MARTIN [21, Sec. 2.4] in relation to various inequalities imposing restrictions on constitutive relations.

For example, point A' is out of the line segment $C'D'$, which represents the one-dimensional elastic range assigned to the point C. Following LUCCHESI and SILHAVY [20] we denote strain cycles which always contain the initial strain state as small strain cycles. It can be seen that during a (simple closed) small strain cycle, generation of plastic deformation occurs only either due to compression or due to tension. For example, with regard to the small strain cycle corresponding to the strain-stress-path $\alpha BC\gamma$ (see Fig. 1), $\dot{\varepsilon}_{\mathrm{p}}(t) \neq 0$ is satisfied only in the time interval $[t_B, t_C]$. In this case, regardless of the value of k, we have ($t_A < t_B < t_C < t_\gamma$)

$$
\begin{aligned}
(4.1) \qquad I_{\alpha\gamma} &= \int_{t_\alpha}^{t_\gamma} \sigma(t)\,\dot{\varepsilon}(t)\,dt = -E\int_{t_\alpha}^{t_\gamma} \varepsilon_{\mathrm{p}}(t)\,\dot{\varepsilon}(t)\,dt \\
&= E\left(\varepsilon_{\mathrm{p}}^{\alpha}(\varepsilon^{\alpha}-\varepsilon^{B}) + \int_{\varepsilon^C}^{\varepsilon^B} \bar{\varepsilon}_{\mathrm{p}}(\varepsilon)\,d\varepsilon - \varepsilon_{\mathrm{p}}^{C}(\varepsilon^{\alpha}-\varepsilon^{C})\right) \\
&\geq E\left[\varepsilon^{\alpha}(\varepsilon^{\alpha}-\varepsilon^{B}) + \varepsilon_{\mathrm{p}}^{C}(\varepsilon^{B}-\varepsilon^{C}) - \varepsilon_{\mathrm{p}}^{C}(\varepsilon^{\alpha}-\varepsilon^{C})\right] \\
&= E(\varepsilon_{\mathrm{p}}^{\alpha}-\varepsilon_{\mathrm{p}}^{C})(\varepsilon^{\alpha}-\varepsilon^{B}) > 0\,.
\end{aligned}
$$

Hence, in the case of uniaxial loading, the plasticity laws given in Sec. 2.1 are stable in the sense of Il'iushin for all small cycles.

In order to extend this result to the three-dimensional case, it is convenient to introduce the notion of small strain cycles within a general framework for plastic constitutive relations. Suppose that the yield surface is represented in strain space by an equation of the form

$$
(4.2) \qquad \tilde{\mathrm{G}}(\mathbf{E}, \mathbf{E}_{\mathrm{p}}, \mathbf{q}) = 0\,,
$$

where $\mathbf{q}$ represents a set of plastic internal variables q_i, $1 \leq i \leq m$, which are scalar-valued or components of tensors. The internal variables q_i are supposed to change only when plastic flow occurs. We consider strain cycles which satisfy the following condition. During the cyclic process, the initial strain state is always included within or lies on the boundary of every yield surface corresponding to the process. In other words, the initial strain state always lies in the intersection of all the elastic ranges surrounded by the yield surfaces during the process. Generalizing the one-dimensional definition, we denote such strain cycles as small cycles, and write $C_s[t_0, t_{\mathrm{e}}]$ for a small cycle which begins at time t_0 and ends at time t_{e}. Then, a material is defined to satisfy the postulate of Il'iushin for small cycles (weak form of the postulate of Il'iushin), if

$$
(4.3) \qquad I(t_0, t_{\mathrm{e}}) = \int_{t_0}^{t_{\mathrm{e}}} \mathbf{T}(t)\cdot\dot{\mathbf{E}}(t)\,dt \geq 0 \qquad \text{for every} \qquad C_s[t_0, t_{\mathrm{e}}].
$$

In Appendix A, it is shown in a general context, that if the elasticity law is independent of the plastic deformations, then the weak form of Il'iushin's postulate (4.2) is equivalent to the two following conditions: i) the yield surface in stress space is convex, and ii) the plastic strain rate $\dot{\mathbf{E}}_p$ is directed along the outward normal to the yield surface in stress space (normality rule). Since the plasticity laws of Sec. 2.1 satisfy these convexity and normality conditions, it follows that they satisfy (4.3) as well. This proves, for the three-dimensional case, stability in the sense of the weak form of Il'iushin's postulate for the plasticity laws given in Sec. 2.1.

Until now we have introduced the stability condition (4.3) in relation to specific constitutive models. However, from a physical point of view on a phenomenological level, it seems that there is no experimental evidence to exclude from a general theory of plasticity such material response which is concordant with the stability condition (4.3). Thus, regarding inequality (3.1) as being too restrictive for the material response, we may assume the weaker inequality (4.3) as a general principle which is in agreement with the observed behaviour of various materials. Note that such an assumption is in harmony with the statement by PALMER, MAIER and DRUCKER [24, p. 468], that "the degree of stability to be required of a material or a structural element is a matter of matching the observed or calculated behaviour of a selected portion of the real world with a sufficiently simple model".

On the other hand, it can be seen (see e.g. Appendix A), that if the elasticity law is independent of the plastic deformations, then (4.3) is equivalent to the so-called principle of maximum plastic dissipation. The latter was also derived from considerations of crystal plasticity by BISHOP and HILL [2]. This motivates from a physical point of view on a microstructural level, the use of the stability condition (4.3) in a general theory on plasticity.

It must be emphasized that, in the framework of the assumptions made in the present paper, (4.3) is the isothermal version of a general dissipation postulate, which has been proposed by LUCCHESI and SILHAVY [20] as a non-isothermal generalization of Il'iushin's inequality (3.1). However, it is of interest to note that the condition that the cycles should be small was imposed by Lucchesi and Silhavy in order to make Il'iushin's postulate "derivable from some sufficient conditions (the normality rule)". This is rather a mathematical point of view, while the condition of small cycles is assumed in the present work in order to obtain a stability condition for material response which is not too restrictive when modeling the observed behaviour of various materials. This is rather a physical point of view.

5. Consequences for the case of vanishing elastic range

In order to give a general treatment for the case of vanishing elastic range it is necessary to introduce a distance between two elements in the considered vector

space of second-order tensors. Since we deal with normed vector spaces, we define the distance between two tensors to be the norm of their difference. Further, we denote by δ_G the supremum of the diameters of all the yield surfaces during the strain cycle (the diameter of a yield surface in a strain space representation is defined to be the supremum of the distances between two points on the yield surface). We assume that the yield surface is a closed hypersurface, at least in the space of deviatoric strain tensors. If the yield surface is a closed hypersurface in the space of strain tensors, then δ_G should be understood to be defined in the space of strain tensors. Otherwise, δ_G should be understood to be defined in the space of deviatoric strain tensors. In the latter case, plastic incompressibility is supposed to apply as well.

Next, suppose the yield surface to be given in a strain space representation as defined by (4.2) and consider the small strain cycle $ABCD$ displayed in Fig. 3 (see Appendix A). Let us denote by x the supremum of the distances between the strain points along BC and the initial yield surface $\bar{G}(\mathbf{E}, \mathbf{E}_p^B \mathbf{q}^B) = 0$ (the distance between a strain point and a surface is defined to be the infimum of all the distances between the strain point considered and arbitrary points on the surface). Since $ABCD$ is supposed to be a small cycle, the inequality

$$\delta_G \geq x \tag{5.1}$$

applies. The case of vanishing elastic range is equivalent to

$$\delta_G = 0. \tag{5.2}$$

Indeed, in view of the definition for δ_G, (5.2) implies that the yield surface shrinks to a point (it does not degenerate to some line segment).

Clearly, taking into account (5.1) and that $x \geq 0$, Eq. (5.2) implies

$$x = 0\,. \tag{5.3}$$

This result states that, in the case of vanishing elastic range, there are no small cycles, apart from the trivial cycle $E = E^A = E^B = E^C = E^D$. That is, concerning materials with vanishing elastic range, only trivial cycles satisfy the conditions for small cycles, and hence, (4.3) is satisfied trivially.

As a consequence, now we obtain compatibility between the simple endochronic theory of plasticity and the version (4.3) of Il'iushin's postulate. To see this, it is necessary to transform the yield condition (2.5) – (2.7),

$$\bar{F}(\mathbf{T}, \boldsymbol{\xi}) = \sqrt{\frac{3}{2}(\mathbf{T} - \boldsymbol{\xi})^D \cdot (\mathbf{T} - \boldsymbol{\xi})^D + \alpha(\mathrm{tr}\,(\mathbf{T} - \boldsymbol{\xi}))^2} - k = 0 \tag{5.4}$$

into a strain space formulation. We denote by $\boldsymbol{\Delta}_e$ the elastic strain with the property

$$\boldsymbol{\xi} = [\mathbf{T}]_{\mathbf{E}_e = \boldsymbol{\Delta}_e} = 2\mu \boldsymbol{\Delta}_e + \lambda(\mathrm{tr}\,\boldsymbol{\Delta}_e)\mathbf{1}\,. \tag{5.5}$$

Using this relation, as well as the elasticity law (2.2), and the decomposition of strain (2.1), we may rewrite (5.4) as

$$\bar{\mathrm{G}}(\mathbf{E},\boldsymbol{\Delta}) = \sqrt{\frac{3}{2}(\mathbf{E}-\boldsymbol{\Delta})^{D}\cdot(\mathbf{E}-\boldsymbol{\Delta})^{D} + \alpha\left(\frac{2\mu+3\lambda}{2\mu}\right)2(\mathrm{tr}\,(\mathbf{E}-\boldsymbol{\Delta}))^{2}} - \frac{k}{2\mu} = 0, \tag{5.6}$$

(see Fig.2), where

$$\boldsymbol{\Delta} = \boldsymbol{\Delta}_{\mathrm{e}} + \mathbf{E}_{\mathrm{p}}\,. \tag{5.7}$$

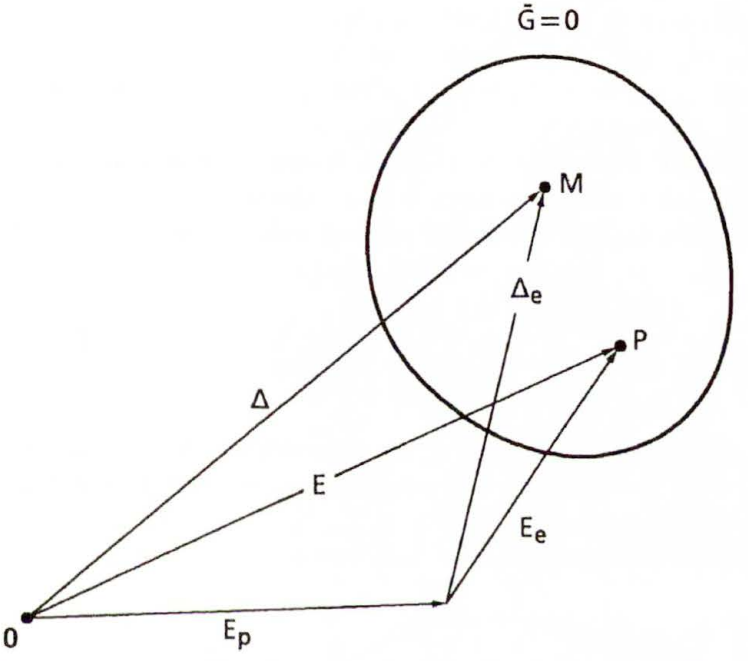

FIG. 2. Schematic representation of the yield surface in strain space: M denotes the "center" of the yield surface while P denotes an arbitrary strain state in the elastic range.

Equation (5.6) is a representation of the yield surface in strain space formulation. Evidently, if $k = 0$, then $\mathbf{E} = \boldsymbol{\Delta}$, and the yield surface shrinks to a point. Consequently, Il'iushin's postulate in the form (4.3) is satisfied trivially. Of course, this also applies to the case where, in addition,

$$\mu,\ \lambda \to \infty\,, \tag{5.8}$$

which in turn leads to the simple endochronic theory of plasticity, as shown in Sec. 2.2.

Appendix A

There are many investigations concerning integral inequalities like that obtained by Il'iushin's postulate as e.g. the works of IL'IUSHIN [16], PALMER, MAIER and DRUCKER [24], HILL [13, 14], HILL and RICE [15], MARTIN [21, Sec. 2.4, 2.5], DAFALIAS [7], PALGEN and DRUCKER [23], CASEY and TSENG [3], LUBLINER [19], CARROLL [4], LIN and NAGHDI [18], LUCCHESI and SILHAVY [20], HAVNER [12, Sec. 3.6], FOSDICK and VOLKMANN [10]. Apart from technical details, all these investigations utilize a common method for deriving consequences from the integral inequalities. This is now briefly described for the particular case that the elasticity law is independent of the plastic deformations, but otherwise a general theory with plastic internal variables $\mathbf{q}$ is assumed to apply.

Suppose that the stress tensor $\mathbf{T}$ satisfies an elasticity law of the form $\mathbf{T} = \widehat{\mathbf{T}}(\mathbf{E}_e)$, which possesses an inverse $\mathbf{E}_e = \widehat{\mathbf{E}}_e(\mathbf{T})$, so that $\mathbf{E} = \mathbf{E}_p + \widehat{\mathbf{E}}_e(\mathbf{T})$. We may use the last relation in Eq. (4.2) to obtain a representation of the yield surface in stress space: $\widetilde{F}(\mathbf{T}, \mathbf{E}_p, \mathbf{q}) = 0$. Further, it can be shown that a necessary and sufficient condition for the validity of (4.3), the latter being considered for pure elastic processes, is the existence of a scalar-valued function $\Psi = \widehat{\Psi}_e(\mathbf{E}_e) + \Psi_p = \bar{\Psi}_e(\mathbf{E}, \mathbf{E}_p) + \Psi_p$ such that the potential relation

$$\text{(A.1)} \qquad \mathbf{T} = \widehat{\mathbf{T}}(\mathbf{E}_e) = \frac{\partial \widehat{\Psi}_e(\mathbf{E}_e)}{\partial \mathbf{E}_e} = \frac{\partial \bar{\Psi}_e(\mathbf{E}, \mathbf{E}_p)}{\partial \mathbf{E}} = -\frac{\partial \bar{\Psi}_e(\mathbf{E}, \mathbf{E}_p)}{\partial \mathbf{E}_p}$$

holds. Ψ_p may depend on $\mathbf{E}_p$ and $\mathbf{q}$. We assume that (A.1) applies during plastic loading as well, and consider a small strain cycle $ABCD$ as in Fig. 3, which is parameterized by time t. We denote by t_A, t_B, t_C, t_D, $(t_A < t_B < t_C < t_D)$, the times related to the points A, B, C, D, respectively.

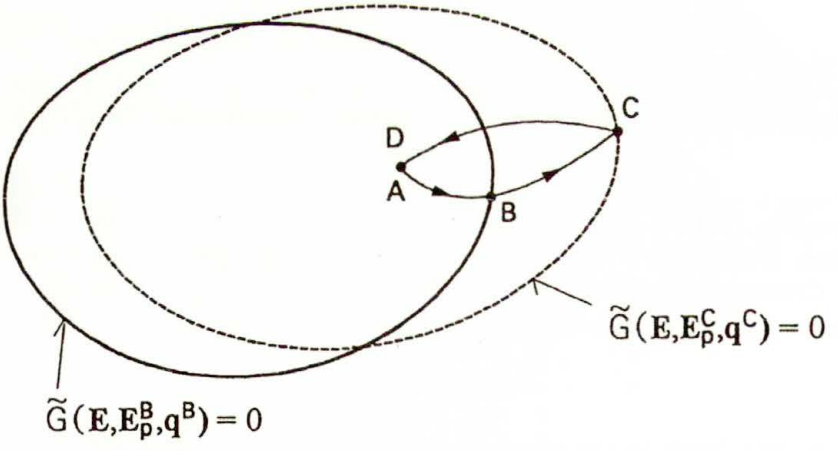

FIG. 3. During the small strain cycle $ABCD$ plastic flow occurs between B and C only.

The strain cycle begins and ends at $E = E^A = E^D$. Plastic flow occurs between B and C only. It follows from (4.3) that

$$\text{(A.2)} \qquad I(t_A, t_D) = \int_{t_A}^{t_D} \mathbf{T}(t)\cdot\dot{\mathbf{E}}(t)\,dt = \int_{t_A}^{t_D} \frac{\partial\bar{\Psi}_{\mathrm{e}}(\mathbf{E}(t), \mathbf{E}_{\mathrm{p}}(t))}{\partial\mathbf{E}(t)}\cdot\dot{\mathbf{E}}(t)\,dt$$

$$= \bar{\Psi}_{\mathrm{e}}(\mathbf{E}^A, \mathbf{E}_{\mathrm{p}}^C) - \bar{\Psi}_{\mathrm{e}}(\mathbf{E}^A, \mathbf{E}_{\mathrm{p}}^B) - \int_{t_B}^{t_C} \frac{\partial\bar{\Psi}_{\mathrm{e}}(\mathbf{E}(t), \mathbf{E}_{\mathrm{p}}(t))}{\partial\mathbf{E}(t)}\cdot\dot{\mathbf{E}}_{\mathrm{p}}(t)\,dt$$

$$= \int_{t_B}^{t_C}\left[\frac{\partial\bar{\Psi}_{\mathrm{e}}(\mathbf{E}^A, \mathbf{E}_{\mathrm{p}}(t))}{\partial\mathbf{E}_{\mathrm{p}}(t)} - \frac{\partial\bar{\Psi}_{\mathrm{e}}(\mathbf{E}(t), \mathbf{E}_{\mathrm{p}}(t))}{\partial\mathbf{E}(t)}\right]\cdot\dot{\mathbf{E}}_{\mathrm{p}}(t)\,dt \geq 0.$$

We may apply Taylor's theorem to establish the relation

$$\text{(A.3)} \qquad \lim_{t_C\to t_B}\frac{I(t_A, t_D)}{(t_C - t_B)} = \left[\frac{\partial\bar{\Psi}_{\mathrm{e}}(\mathbf{E}^A, \mathbf{E}_{\mathrm{p}}(t))}{\partial\mathbf{E}_{\mathrm{p}}(t)}\cdot\dot{\mathbf{E}}_{\mathrm{p}}(t) - \frac{\partial\bar{\Psi}_{\mathrm{e}}(\mathbf{E}(t), \mathbf{E}_{\mathrm{p}}(t))}{\partial\mathbf{E}(t)}\cdot\dot{\mathbf{E}}_{\mathrm{p}}(t)\right]_{t=t_B} \geq 0.$$

Thus, dropping t_B in (A.3), we obtain as a necessary condition for (4.3) the inequality

$$\text{(A.4)} \qquad -\frac{\partial\bar{\Psi}_{\mathrm{e}}(\mathbf{E}, \mathbf{E}_{\mathrm{p}})}{\partial\mathbf{E}_{\mathrm{p}}}\cdot\dot{\mathbf{E}}_{\mathrm{p}} \geq -\frac{\partial\bar{\Psi}_{\mathrm{e}}(\mathbf{E}^A, \mathbf{E}_{\mathrm{p}})}{\partial\mathbf{E}_{\mathrm{p}}}\cdot\dot{\mathbf{E}}_{\mathrm{p}}\,,$$

with $\mathbf{E}$ denoting a strain state on the yield surface $\bar{\mathrm{G}} = 0$, $\mathbf{E}_{\mathrm{p}}$ the corresponding plastic strain, and $\mathbf{E}^A$ a strain state on or inside the yield surface $\bar{\mathrm{G}} = 0$. Conversely, (A.4) constitutes a sufficient condition for (4.3). To see this, we take the integral of (A.4) along a strain cycle as shown in Fig. 3. For (A.4) to remain valid during this strain cycle, $\mathbf{E}^A$ must always lie in the intersection of all the elastic ranges during the strain cycle, which in turn implies that the strain cycle ABCD must be small. Then, following the steps similar to those used in (A.2), it is a straightforward matter to arrive at (4.3). Note that, with equation (A.1) in mind, we may introduce the definition

$$\text{(A.5)} \qquad \mathbf{T}^A = -\frac{\partial\bar{\Psi}_{\mathrm{e}}(\mathbf{E}^A, \mathbf{E}_{\mathrm{p}})}{\partial\mathbf{E}_{\mathrm{p}}}\,,$$

where $\mathbf{T}^A$ is a stress tensor on or inside the yield surface in stress space. Then, inequality (A.4) is equivalent to

$$\text{(A.6)} \qquad \mathbf{T}\cdot\dot{\mathbf{E}}_{\mathrm{p}} \geq \mathbf{T}^A\cdot\dot{\mathbf{E}}_{\mathrm{p}}\,,$$

where $\mathbf{T}$ is a stress tensor on the yield surface in stress space $\tilde{F} = 0$. Inequality (A.6) is known as the principle of maximum plastic dissipation and is equivalent to the following two conditions (for a proof of this fact see e.g. LUBLINER [19, Ch. 3.2.2]):

i) the yield surface $\tilde{F}(\mathbf{T}, \mathbf{E}_p, \mathbf{q}) = 0$ is convex, and

ii) $\dot{\mathbf{E}}_p$ is normal to $\tilde{F}(\mathbf{T}, \mathbf{E}_p, \mathbf{q}) = 0$ (normality rule).

Apart from notational differences, a large part of the analysis above follows closely that given by LUBLINER [19, Ch. 3.2]. Lubliner's analysis, however, deals with the strong form of Il'iushins's postulate and therefore (A.6) represents only a necessary condition for (4.3). Also, it must be mentioned that LUCCHESI and SILHAVY [20] have developed a finite plasticity theory which is based on the theory of materials with elastic range, and is formulated in a general mathematical framework. They discussed several interrelationships between inequalities of the work type, including the main results of the present Appendix.

References

1. P.J. ARMSTRONG and C.O. FREDERICK, *A mathematical representation of the multiaxial Bauschinger effect*, CEGB, Report RD/B/N 731, 1966.
2. J.F. BISHOP and R. HILL, *A theory of plastic distortion of a polycrystalline aggregate under combined stresses*, Philos. Mag., **42**, pp. 414–427, 1951.
3. J. CASEY and M. TSENG, *A constitutive restriction related to convexity of yield surfaces in plasticity*, J. Appl. Math. and Phys. (ZAMP), **35**, pp. 478–496, 1984.
4. M.M. CARROLL, *A rate-independent constitutive theory for finite inelastic deformation*, J. Appl. Mech., **54**, pp. 15–21, 1987.
5. J.L. CHABOCHE, K. DANG VAN and G. CORDIER, *Modelisation of the strain memory effect on the cyclic hardening of 316 stainless steel*, SMIRT-S, L11/3, Berlin 1979.
6. J.L. CHABOCHE, *Time-independent constitutive theories for cyclic plasticity*, Int. J. Plasticity, **2**, pp. 149–188, 1986.
7. Y.F. DAFALIAS, *Il'iushin's postulate and resulting thermodynamic conditions on elastoplastic coupling*, Int. J. Solids Struct., **13**, pp. 239–251, 1977.
8. D.C. DRUCKER, *A more fundamental approach to plastic stress-strain relations*, Proc. of the first U.S. National Congress of Applied Mechanics, ASME, pp. 487–491, 1951.
9. D.C. DRUCKER, *On the postulate of stability of materials in the mechanics of continua*, J. Mécanique, **3**, pp. 235–249, 1964.
10. R. FOSDICK and E. VOLKMANN, *Normality and convexity of the yield surface in nonlinear plasticity*, Quart. Appl. Math., **LI**, pp. 117–127, 1993.
11. P. HAUPT, M. KAMLAH and CH. TSAKMAKIS, *Continuous representation of hardening properties in cyclic plasticity*, Int. J. Plasticity, **8**, pp. 803–817, 1993.
12. K.S. HAVNER, *Finite plastic deformation of crystalline solids*, Cambridge University Press, 1992.
13. R. HILL, *On constitutive inequalities for simple materials – I*, J. Mech. Phys. Solids, **16**, pp. 229–242, 1968.
14. R. HILL, *On constitutive inequalities for simple materials – II*, J. Mech. Phys. Solids, **16**, pp. 315–322, 1968.

15. R. HILL and J.R. RICE, *Elastic potentials and the structure of inelastic constitutive laws*, SIAM J. Appl. Math., **25**, pp. 448–461, 1973.
16. A.A. IL'IUSHIN, *On the postulate of plasticity*, PMM, **25**, pp. 746–752, 1961.
17. M. KORZEN, *Beschreibung des inelastischen Materialverhaltens im Rahmen der Kontinuumsmechanik: Vorschlag einer Materialgleichung vom viskoelastisch-plastischen Typ*, Dissertation, Technische Hochschule Darmstadt, Institut für Mechanik, 1988.
18. H.C. LIN and P.M. NAGHDI, *Necessary and sufficient conditions for the validity of a work inequality in finite plasticity*, Quart. J. Mech. Appl. Math., **42**, pp. 13–21, 1989.
19. J. LUBLINER, *Plasticity theory*, Macmillan Publishing Company, New York 1990.
20. M. LUCCHESI and M. SILHAVY, *Il'iushin's conditions in non-isothermal plasticity*, Arch. Rational Mech. Anal., **113**, pp. 121–163, 1991.
21. J.B. MARTIN, *Plasticity: Fundamentals and general results*, The MIT Press, Cambridge, Massachusetts and London, England 1975.
22. R.W. OGDEN, *Non-linear elastic deformations*, Ellis Hordwood Limited Publishers, England 1984.
23. L. PALGEN and D.C. DRUCKER, *The structure of stress-strain relations in finite elastoplasticity*, Int. J. Solids Struct., **19**, pp. 519–531, 1983.
24. A.C. PALMER, G. MAIER and D.C. DRUCKER, *Normality relations and convexity of yield surfaces for unstable materials or structural elements*, Transactions of the ASME, J. Appl. Mech., **24**, pp. 464–470, 1967.
25. R.S. RIVLIN, *Some comments on the endochronic theory of plasticity*, Int. J. Solids Struct., **17**, pp. 231–248, 1981.
26. I.S. SANDLER, *On the uniqueness and stability of endochronic theories of material behavior*, Transactions of the ASME, J. Appl. Mech., **45**, pp. 263–266, 1978.
27. H.P. SHRIVASTAVA, Z. MROZ and R.N. DUBEY, *Yield criterion and the hardening rule for a plastic solid*, Z. Angew. Math. Mech., **53**, pp. 625–633, 1973.
28. K.C. VALANIS, *A theory of viscoplasticity without a yield surface. Part I. General theory*, Arch. Mech., **23**, pp. 517–533, 1971.
29. K.C. VALANIS and C.F. LEE, *Some recent developments in the endochronic theory with application to cyclic histories*, [in:] Nonlinear Constitutive Relations for High Temperature Applications, NASA Conference Publication, 2271, 1982.
30. C.-C. WANG and C. TRUESDELL, *Introduction to rational elasticity*, Noordhoff International Publishing Leyden, The Netherlands 1973.
31. M. ŻYCZKOWSKI, *Combined loadings in the theory of plasticity*, PWN-Polish Scientific Publishers, 1981.

FORSCHUNGSZENTRUM KARLSRUHE,
INSTITUT FÜR MATERIALFORSCHUNG II,
Postfach 3640, 76021 Karlsruhe, Germany.

Received May 20, 1996; new version December 30, 1996.

Arch. Mech., 49, 4, pp. 697–704, Warszawa 1997

A nonexistence theorem of small periodic traveling wave solutions to the generalized Boussinesq equation

Y. CHEN (FAYETTEVILLE)

THE GENERALIZED Boussinesq equation, $u_{tt} - u_{xx} + [f(u)]_{xx} + u_{xxxx} = 0$, and its periodic traveling wave solutions are considered. Using the transform $z = x - \omega t$, the equation is converted to a nonlinear ordinary differential equation with periodic boundary conditions. An equivalent relation between the ordinary differential equation and a Hammerstein-type integral equation is then established by using the Green's function method. This integral equation generates compact operators in $(C_{2T}, \|\cdot\|)$, a Banach space of real-valued continuous periodic functions with a given period $2T$. We prove that for small $T > 0$, there exists an $r > 0$ such that there is no nontrivial solution to the integral equation in the ball $B(0, r) \subseteq C_{2T}$. And hence, the generalized Boussinesq equation has no $2T$-periodic traveling wave solutions having amplitude less than r.

1. Introduction

IN THE 1870's, Boussinesq derived some model equations for the propagation of small amplitude long wave on the surface of water [1]. These equations possess special traveling wave solutions called solitary waves. Boussinesq's theory was the first to give a satisfactory and scientific explanation of the phenomenon of solitary waves discovered by Scott Russell in his experimental observation of shallow water propagation some thirty years earlier [2].

The original equation due to Boussinesq is not the only mathematical model for small amplitude planar long waves on the surface of shallow water. Different choices of the independent variables and the possibility of modifying lower order terms by the use of the leading order relationships can lead to a whole range of equations, all of which have the same formal validity [3]. All of these models possess one obvious characteristic, however, which is that they are perturbations of the linear wave equation that takes account of small effects of nonlinearity and dispersion.

In this paper, we consider a generalized Boussinesq equation of the form

$$u_{tt} - u_{xx} + [f(u)]_{xx} + u_{xxxx} = 0, \tag{1.1}$$

where $u = u(t, x)$ and $f(u)$ is a C^1 function in its argument.

We shall prove a nonexistence theorem of periodic traveling wave solutions to this equation following the idea of LIU and PAO [4], SOEWONO [5], and CHEN and HE [6]. Of course, this does not establish the nonexistence of periodic traveling wave solutions to the generalized Boussinesq equation. We merely prove that

for a given small $T > 0$, under certain conditions, $2T$-periodic traveling wave solutions with small amplitude to the generalized Boussinesq equation do not exist. There is no doubt about the existence of periodic traveling wave solutions to the generalized Boussinesq equation when $f(u) = u^n$ for some positive integer n. It is well known that the periodic cnoidal wave solutions exist and can be representable as infinite sums of solitons when $f(u) = u^n$ and $n = 1,\ 2$ [7, 8, 9].

The plan of this paper is as follows. In Sec. 2, the generalized Boussinesq equation is transformed to an ordinary differential equation with periodic boundary conditions. We then apply the Green's function method to derive a nonlinear integral equation equivalent to the ordinary differential equation. The nonexistence of small periodic solutions to the integral equation is proved in Sec. 3. Therefore, the nonexistence of small $2T$-periodic traveling wave solutions to the generalized Boussinesq equation is established.

2. Formulation of the problem

We start from the generalized Boussinesq equation of the form

$$u_{tt} - u_{xx} + [f(u)]_{xx} + u_{xxxx} = 0, \tag{2.1}$$

where the function f is C^1 in its argument. We are interested in the periodic traveling wave solutions of the form $u(x,t) = U(z) = U(x - \omega t)$, where $\omega > 0$ is the wave speed and $z = x - \omega t$ is the characteristic variable. Substitution of the $U(z)$ into Eq. (2.1) then leads to the fourth order nonlinear ordinary differential equation

$$U^{(4)}(z) = CU''(z) - [f(U(z))]'', \tag{2.2}$$

where $C = (1 - \omega^2)$. To obtain periodic solutions, we impose the following boundary conditions

$$U^{(n)}(0) = U^{(n)}(2T), \qquad n = 0, 1, 2, 3, \tag{2.3}$$

where T is a preassigned positive number. To eliminate nontrivial constant solutions to the ordinary differential equation (2.2), another condition is introduced

$$\int_0^{2T} U(z)\, dz = 0. \tag{2.4}$$

It is obvious that any solution $U(z)$ of the boundary value problem consisting of Eqs. (2.2) – (2.4) can be extended to a $2T$-periodic traveling wave solution to the original evolution equation (2.1).

Integrating both sides of Eq. (2.2) with respect to z twice and using Eqs. (2.3), (2.4) yield

$$U''(z) - CU(z) = E - f(U(z)), \tag{2.5}$$

$$U^{(n)}(0) = U^{(n)}(2T), \qquad n = 0, 1, \tag{2.6}$$

where

$$E = \int_0^{2T} f(U(z))\, dz/(2T).$$

Conversely, integrating both sides of Eq. (2.5) from 0 to $2T$ and using Eqs. (2.6) will give us Eq. (2.4), and direct differentiations of Eq.(2.5) will give us Eqs. (2.2), (2.3). Therefore, we have proved the following theorem.

THEOREM 1. *Suppose $C \neq 0$, a function $U(z)$ is a $2T$-periodic traveling wave solution to* Eq. (2.1) *satisfying the boundary conditions* Eqs. (2.3), (2.4) *if and only if it is a solution to the boundary value problem consisting of* Eqs. (2.5), (2.6).

From now on we only consider the two cases: 1. $C > 0$ and 2. $C < 0$ but $-C \neq (k\pi/T)^2$ with k being any integer. Treating the right-hand side of Eq. (2.5) as a forcing term and using the Green's function method [4, 10], the boundary value problem Eqs. (2.5), (2.6) can be converted to a nonlinear integral equation of the form

$$U(z) = \int_0^{2T} K_i(z, s) f(U(s))\, ds, \qquad \forall z \in [0, 2T], \tag{2.7}$$

where the kernels K_i, $i = 1, 2$, are defined as follows:

1. When $C > 0$, we denote $\lambda_1 = \sqrt{C}$, then

$$K_1(z, s) = \frac{\cosh \lambda_1 (T - |z - s|)}{2\lambda_1 \sinh \lambda_1 T} - \frac{1}{2\lambda_1^2 T}, \qquad \forall z, s \in [0, 2T]. \tag{2.8}$$

2. When $C < 0$ but $-C \neq (k\pi/T)^2$ with k being any integer, let $\lambda_2 = \sqrt{-C}$, then

$$K_2(z, s) = \frac{\cos \lambda_2 (T - |z - s|)}{2\lambda_2 \sin \lambda_2 T} - \frac{1}{2\lambda_2^2 T}, \qquad \forall z, s \in [0, 2T]. \tag{2.9}$$

LEMMA 1. The kernels K_1 and K_2 have the following properties:

$$K_i(0, s) = K_i(2T, s), \qquad \forall s \in [0, 2T], \quad i = 1, 2,$$

$$K_i(z, 2T - s) = K_i(2T - z, s), \qquad \forall z, s \in [0, 2T], \quad i = 1, 2,$$

$$\int_0^{2T} K_i(z, s) ds = 0, \qquad \forall z \in [0, 2T], \quad i = 1, 2.$$

P r o o f. Straightforward computations based on the definitions of the $K_1(z,s)$ and $K_2(z,s)$ given in Eqs. (2.8), (2.9).

□

THEOREM 2. *A function $U(z)$ is a solution of the boundary value problem consisting of* Eqs. (2.5), (2.6) *if and only if it is a solution of the integral equation* (2.7).

P r o o f. The "if" part can be proved by direct differentiations of Eq. (2.7) and the "only if" part is based on the Green's function method by treating the right-hand side of Eq. (2.5) as a nonhomogeneous term.

□

3. Nonexistence theorem

It is seen from the Theorem 1 and 2 that $U(z)$ is a solution to the integral equation (2.7) if and only if it is a solution to Eq. (2.1) satisfying the boundary conditions Eqs. (2.3), (2.4). Therefore, to show the nonexistence of small $2T$-periodic traveling wave solutions to Eq. (2.1) with the boundary conditions Eqs. (2.3), (2.4), it is sufficient to show that small solution to Eq. (2.7) does not exist.

To this end we define C_{2T} as a collection of real-valued continuous functions, $v(z)$, on $[0,2T]$ such that $v(0) = v(2T)$. Equip C_{2T} with the sup norm $\|\cdot\|$ as $\|v\| = \sup_{0\le z\le 2T} |v(z)|$, for each $v \in C_{2T}$, then $(C_{2T}, \|\cdot\|)$ becomes a Banach space and $\|v\|$ is the amplitude of v.

We now define the operators $\mathcal{A}_i$, $i = 1,2$, on C_{2T} as

$$\mathcal{A}_i v(z) = \int_0^{2T} K_i(z,s) f(v(s))\, ds, \qquad \forall v \in C_{2T}, \tag{3.1}$$

where the kernels K_i, $i = 1,2$, are defined in Eqs. (2.8), (2.9). Notice that the operator $\mathcal{A}_i$ depends on T and λ_i, $i = 1,2$.

We shall show that for any given small $T > 0$, there exists an $r > 0$ such that $\|\mathcal{A}_i v\| < \|v\|$ for any nontrivial function $v \in B(0,r) \subseteq C_{2T}$, $i = 1,2$. This implies that the equation $\mathcal{A}_i v = v$ has no nontrivial solution with amplitude smaller than r. And hence, the nonexistence of nontrivial small solution to the boundary value problem Eqs. (2.4), (2.5) is established. This, in turn, leads to the nonexistence of small $2T$-periodic traveling wave solution $U(z)$ to the generalized Boussinesq equation satisfying the boundary conditions Eqs. (2.3), (2.4).

A consequence of Lemma 1 can be stated now.

LEMMA 2. Let v be an element of C_{2T}. If $v(z) = v(2T - z)$ for $z \in [0,2T]$, then $\mathcal{A}_i v(z) = \mathcal{A}_i v(2T - z)$, $i = 1,2$.

Let $r > 0$ and $B(0,r)$ be a bounded ball in C_{2T}, we then have the following theorem.

THEOREM 3. *$\mathcal{A}_i : C_{2T} \longrightarrow C_{2T}$, $i = 1,2$, is compact and $\|\mathcal{A}_i v\| < \|v\|$ for all nontrivial $v \in B(0,r)$ when T is small enough, $i = 1,2$.*

P r o o f. First we show $\mathcal{A}_i : C_{2T} \longrightarrow C_{2T}$, $i = 1,2$. Since it is obvious from Lemma 1 that $\mathcal{A}_i v(0) = \mathcal{A}_i v(2T)$ for each $v \in C_{2T}$, $i = 1,2$, it suffices to show that $\mathcal{A}_i v$, $i = 1,2$, is continuous on $[0, 2T]$.

Let v be an element in C_{2T}, we have

$$\frac{d\mathcal{A}_1 v(z)}{dz} = \frac{-1}{2\sinh \lambda_1 T} \int_0^z \sinh \lambda_1 (T - z + s) f(v(s))\, ds + \frac{1}{2\sinh \lambda_1 T} \int_z^{2T} \sinh \lambda_1 (T + z - s) f(v(s))\, ds, \tag{3.2}$$

$$\frac{d\mathcal{A}_2 v(z)}{dz} = \frac{1}{2\sin \lambda_2 T} \int_0^z \sin \lambda_2 (T - z + s) f(v(s))\, ds + \frac{-1}{2\sin \lambda_2 T} \int_z^{2T} \sin \lambda_2 (T + z - s) f(v(s))\, ds. \tag{3.3}$$

The existence of $d\mathcal{A}_1 v/dz$ and $d\mathcal{A}_2 v/dz$ implies that both $\mathcal{A}_1 v$ and $\mathcal{A}_2 v$ are continuous on $[0, 2T]$, and hence, we have proved $\mathcal{A}_i : C_{2T} \longrightarrow C_{2T}$, $i = 1,2$.

Let $\mathbf{S}$ be any bounded subset of C_{2T}, i.e., there exists an $L_0 > 0$ such that $\|v\| \le L_0$ for all $v \in \mathbf{S}$. Then since f is C^1 in its argument, there exists an $M_0 > 0$ such that

$$\|f(v)\| = \sup_{0 \le z \le 2T} |f(v(z))| \le \sup_{-L_0 \le w \le L_0} |f(w)| \le M_0, \qquad \forall v \in \mathbf{S}.$$

Since $\sin \lambda_2 T \neq 0$ and

$$\max_{0 \le z \le 2T} \int_0^{2T} |K_i(z,s)|\, ds \le 2/\lambda_i^2, \qquad i = 1,2,$$

we obtain from Eqs. (3.1) – (3.3)

$$\|\mathcal{A}_i v\| \le \frac{2M_0}{\lambda_i^2}, \qquad \forall v \in \mathbf{S}, \quad i = 1,2,$$

$$\|d\mathcal{A}_i v/dz\| \le \frac{TM_0}{\tau_i}, \qquad \forall v \in \mathbf{S}, \quad i = 1,2,$$

where $\tau_1 = 1$ and $\tau_2 = |\sin \lambda_2 T|$. Thus, $\mathcal{A}_i \mathbf{S}$, $i = 1, 2$, is uniformly bounded and equi-continuous, and by the Ascoli–Arzela Theorem both $\mathcal{A}_1$ and $\mathcal{A}_2$ are compact operators from C_{2T} into C_{2T}.

From the definition of K_i, Eqs. (2.8), (2.9), we see that for any fixed $z \in (0, 2T)$, the graph of $K_i(z, s)$, $i = 1, 2$, is just a translation of the graph of $K_i(0, s)$, $i = 1, 2$. Therefore, we have the following inequalities [5, 6]

$$\int_0^{2T} |K_1(z,s)|\, ds = \int_0^{2T} |K_1(0,s)|\, ds \le \frac{2}{\lambda_1^2}\left(1 - \frac{\lambda_1 T}{\sinh \lambda_1 T}\right), \tag{3.4}$$

$$\int_0^{2T} |K_2(z,s)|\, ds = \int_0^{2T} |K_2(0,s)|\, ds \le \frac{2}{\lambda_2^2}\left(\frac{\lambda_2 T}{\sin \lambda_2 T} - 1\right). \tag{3.5}$$

It should be noticed that T is small and the right-hand sides of the above two inequalities (3.4), (3.5) vanish when T goes to zero.

Let v be a nontrivial function in $B(0, r)$. We define

$$I = \{v(s) : \ v \in B(0,r), \ \ 0 \le s \le 2T\}.$$

It is obvious that $I \subseteq [-r, r]$ and $0 \in I$, since otherwise the equation $\mathcal{A}_i v = v$ has no solution in $B(0, r)$ because of the condition Eq. (2.4) and we are done. Using the Mean Value Theorem, we then have

$$f(v(s)) = f(0) + f'(c)v(s), \qquad \forall s \in [0, 2T],$$

where $c = c(s) \in I$. Hence, since f' is continuous in its argument, there exists an $N > 0$ such that

$$\|f'(c)\| \le \sup_{0 \le s \le 2T} |f'(v(s))| \le \sup_{-r \le w \le r} |f'(w)| \le N.$$

From the Lemma 1, we know

$$\int_0^{2T} K_i(z,s) f(0)\, ds = 0.$$

Therefore, we have

$$\begin{aligned} \|\mathcal{A}_1 v\| &= \sup_{0 \le z \le 2T} \left| \int_0^{2T} K_1(z,s) f(v(s))\, ds \right|, \\ &= \sup_{0 \le z \le 2T} \left| \int_0^{2T} K_1(z,s)[f(0) + f'(c)v(s)]\, ds \right|, \end{aligned}$$

$$
\begin{aligned}
&= \sup_{0\le z\le 2T}\left|\int_0^{2T} K_1(z,s)f'(c)v(s)ds\right|,\\
&\le \sup_{0\le z\le 2T}\int_0^{2T} |K_1(z,s)|\,\|f'(c)\|\,\|v(s)\|\,ds,\\
&\le N\|v\|\sup_{0\le z\le 2T}\int_0^{2T} |K_1(z,s)|\,ds,\\
&\le \frac{2N}{\lambda_1^2}\|v\|\left(1-\frac{\lambda_1 T}{\sinh\lambda_1 T}\right), \qquad \forall v\in B(0,r).
\end{aligned}
$$

It can be seen that when T is small enough we shall have

$$\frac{2N}{\lambda_1^2}\left(1-\frac{\lambda_1 T}{\sinh\lambda_1 T}\right)<1. \tag{3.6}$$

Therefore, we proved that when T is small enough, we shall have $\|\mathcal{A}_1 v\| < \|v\|$ for all nontrivial $v\in B(0,r)$. Similarly, we can also prove that when T is small enough,

$$\frac{2N}{\lambda_2^2}\left(\frac{\lambda_2 T}{\sin\lambda_2 T}-1\right)<1, \tag{3.7}$$

and hence, $\|\mathcal{A}_2 v\| < \|v\|$ for all nontrivial $v\in B(0,r)$.

□

By Theorem 3, we see that the equation $\mathcal{A}_i v = v$, $i=1,2$, has no nontrivial solution in $B(0,r)$ when the inequalities (3.6), (3.7) hold. This implies that Eq. (2.7) has no nontrivial solution in $B(0,r)$ when $C>0$ and

$$\frac{2N}{\lambda_1^2}\left(1-\frac{\lambda_1 T}{\sinh\lambda_1 T}\right)<1,$$

or when $C<0$ but $-C/(\alpha a^2)\neq (k\pi/T)^2$ with k being any integer and

$$\frac{2N}{\lambda_2^2}\left(\frac{\lambda_2 T}{\sin\lambda_2 T}-1\right)<1.$$

Therefore, we proved the following nonexistence theorem for small $2T$-periodic traveling wave solutions to the generalized Boussinesq equation.

THEOREM 4. *For any given small $T>0$, there exist an $r>0$ and $N>0$ such that $\|f'(v)\|\le N$ when $\|v\|\le r$. Thus to* Eq. (2.1) *with the boundary*

conditions Eqs. (2.3), (2.4), *there is no* $2T$*-periodic traveling wave solution* $U(z)$ *with amplitude less than* r *if (1)* $C > 0$ *and*

$$\frac{2N}{\lambda_1^2}\left(1 - \frac{\lambda_1 T}{\sinh \lambda_1 T}\right) < 1,$$

or (2) $C < 0$ *but* $-C/(\alpha a^2) \neq (k\pi/T)^2$ *with* k *being any integer, and*

$$\frac{2N}{\lambda_2^2}\left(\frac{\lambda_2 T}{\sin \lambda_2 T} - 1\right) < 1.$$

References

1. J. BOUSSINESQ, *Theorie de l'intumescence liquide appelee onde solitaire ou de translation se propageant dans un canal rectangulare*, Compte Rendus Acad. Sci., **72**, 755–759, 1871.
2. J. SCOTT RUSSELL, *Report on waves*, 14th Meeting of the British Association Report, York, 311–390, 1844.
3. J.L. BONA and R. SMITH, *A model for the two-way propagation of water waves in a channel*, Math. Proc. Camb. Phil. Soc., **79**, 167–182, 1976.
4. BAO-PING LIU and C.V. PAO, *On periodic traveling wave solutions of Boussinesq equation*, Quarterly of Appl. Math., **5**, 311–319, 1984.
5. E. SOEWONO, *A remark on a paper by Liu and Pao on the existence of periodic traveling wave solution to the KdV equation*, Appl. Anal., **25**, 293–299, 1987.
6. YUNKAI CHEN and XIAOGUI HE, *Nonexistence of small periodic traveling wave solutions to the power Kadomtsev–Petviashvili equation*, Differential Equations and Dynamical Systems [to appear].
7. G.B. WHITHAM, *Comments on periodic waves and solitons*, IMA J. Appl. Math., **32**, 353–366, 1984.
8. E. INFELD and G. ROWLANDS, *Nonlinear waves, solitons and chaos*, Cambridge University Press, 1992.
9. Y. CHEN, J. WU and S-L WEN, *An existence theorem of periodic traveling wave solutions to the power Kadomstev–Petviashvili equation*, Arch. Mech., **46**, 5, 797–804, 1994.
10. I. STAKGOLD, *Green's functions and boundary value problems*, John Wiley and Sons, New York 1979.

DEPARTMENT OF MATHEMATICS AND COMPUTER SCIENCE,
FAYETTEVILLE STATE UNIVERSITY, FAYETTEVILLE, NORTH CAROLINA, USA.

Received January 17, 1997.

Arch. Mech., 49, 4, pp. 705–736, Warszawa 1997

A Cosserat theory for elastoviscoplastic single crystals at finite deformation

S. FOREST, G. CAILLETAUD (PARIS) and R. SIEVERT (BERLIN)

IN THIS WORK, displacement and lattice rotation are regarded as independent degrees of freedom. They are connected only on the constitutive level and by the balance equations. The description of plastic deformation is based on the slip theory. Elastic lattice curvature and torsion are associated with couple-stresses. The continuum theory of dislocations has been revisited to derive the kinematics of plastic lattice torsion-curvature. Explicit constitutive equations and hardening rules are proposed to close the theory in the case of elastoviscoplasticity. The thermodynamical formulation of the model involves internal variables which are similar to the densities of statistically stored dislocations and the densities of geometrically necessary dislocations. Accordingly, the proposed Cosserat theory can be regarded, on the one hand, as the classical crystal plasticity theory complemented by lattice curvature and torsion variables and, on the other hand, as the continuum theory of dislocations closed by the missing hardening variables and constitutive equations within the appropriate micropolar framework. A generalization of Mandel's elastoviscoplastic decomposition of strain is used especially for the torsion-curvature measure at finite deformation.

1. Introduction

MANDEL [1] introduced the notion of oriented microelements characterized by some hidden directors into the theory of elastoviscoplasticity. The epoch-making expression "trièdre directeur" is directly taken from the Cosserat brothers' well-known work [2]. The relative rotation of neighbouring microelements may induce local couple stresses. To the first approximation Mandel neglects them and regards the single crystal and the polycrystal as a classical continuum. We propose here the strict treatment of the single crystal as a Cosserat continuum.

NYE [3] noticed that after bending or torsion, a crystal contains excess dislocations of a definite sign that give rise to lattice curvature. In a modelling of single crystals with more reference to dislocations, this additional deformation possibility should be taken into account. Furthermore KRÖNER [4] claimed that the macroscopic response of a medium to lattice curvature is the existence of actual Cosserat couple stresses. The couple-stresses may have the same order of magnitude as force-stresses under some circumstances [5, 6]. In these early works Kröner regards the dislocated crystal as a Cosserat medium. However, his theory deals with symmetric force-stresses and he suggests later that there may be fundamental differences between the dislocation theory and the Cosserat theory [7].

The reason for such a misunderstanding stems from the frequent use in literature of the Cosserat continuum as the medium in which single dislocations may be

embedded. KESSEL [8] computes the force and couple stress fields around screw and edge dislocations in a Cosserat continuum. In the present work we claim that the continuum containing a large number of dislocations in the sense of the continuum theory of dislocations [3], can be modelled as a Cosserat continuum. KRÖNER [9] argues that the rotation of the crystal lattice with dislocations is not the eigenrotation of physical particles but the rotation of a structure. This pleads against the constrained Cosserat theory that is usually used in the continuum theory of dislocations (see Sec. 3.4). As a result, in the Cosserat theory presented here, the rotational degrees of freedom are independent of the displacement field and are linked only on the constitutive level and by the balance equations. While the definition of the Cosserat directors involved in the continuum theory of dislocation is generally left unspecified, the "trièdre directeur" in this work is clearly made of three orthogonal lattice vectors attached to each volume element in a released state of the crystal element. As for them, CLAUS and ERINGEN [10] also erect a lattice triad at every point of the continuum. A most interesting point in their work is that they resort to a micromorphic continuum. They also propose a phenomenological treatment of micromorphic elastoplasticity but they do not derive the crystallographic expressions of plastic slip and curvature nor the necessary constitutive equations. WOŹNIAK [11, 12] devoted great attention to the structural interpretation of the additional degrees of freedom of the micromorphic continuum and considered also bodies with lattice structure. More recently, LE and STUMPF [13, 14] have reformulated the continuum theory of dislocations in the modern language of differential geometry and they also resort to an oriented continuum. In order to get a closed formulation of our model including constitutive equations, we will focus on the Cosserat continuum.

The characteristic size of the volume element must be large enough so that it contains a large number of dislocations and that a mean crystal orientation can be unambiguously defined at each time. It will finally depend on the structural application one aims at.

In Secs. 2.1 to 2.3, the main features of the Cosserat theory at finite deformation are recalled in order to introduce the subsequent developments in elastoviscoplasticity. The evolution rule for plastic curvature is derived from the continuum theory of dislocations in Sec. 3.3, after recalling the closure problem of the continuum theory of dislocations. Explicit constitutive equations are then proposed to solve this problem in Sec. 4. The notations and some classical results used throughout this article are explained in the Appendix.

2. A Cosserat theory for single crystals

2.1. Kinematics of the Cosserat continuum

A material point $M \in \mathcal{B}$ at time t_0 is described by its position $\underline{\mathbf{X}}$ and its inner state, for an arbitrary initial placement, chosen as the reference site. At time t, its position is $\underline{\mathbf{x}}(\underline{\mathbf{X}}, t)$ and its inner state $\underset{\sim}{\mathbf{R}}(\underline{\mathbf{X}}, t)$, in a given reference frame E. If

$(\underline{\mathbf{d}}_i)_{i=1,3}$ are three orthogonal lattice vectors in a released state at t and $(\underline{\mathbf{d}}_i^0)_{i=1,3}$ their initial placement in E, then the rotation $\underset{\sim}{\mathbf{R}}$ is defined through

$$\underline{\mathbf{d}}_i = \underset{\sim}{\mathbf{R}}\, \underline{\mathbf{d}}_i^0 \tag{2.1}$$

with

$$\underset{\sim}{\mathbf{R}}\, \underset{\sim}{\mathbf{R}}^T = \underset{\sim}{\mathbf{1}}, \qquad \underset{\sim}{\mathbf{R}}(\underline{\mathbf{X}}, t_0) = \underset{\sim}{\mathbf{1}} \qquad \text{and} \qquad \operatorname{Det} \underset{\sim}{\mathbf{R}} = 1. \tag{2.2}$$

A rotating frame $E^\sharp(M)$ is attached to the lattice structure at each point $M \in \mathcal{B}$ and each vector and tensor variable y considered with respect to $E^\sharp$ will be denoted by ${}^\sharp y$.

The rotation field $\underset{\sim}{\mathbf{R}}(\underline{\mathbf{X}}, t)$ can be replaced by the vector field $\underline{\mathbf{\Phi}}(\underline{\mathbf{X}}, t)$ given by Eq. (A.12) of the Appendix. The three components of $\underline{\mathbf{\Phi}}$ are three degrees of freedom of the continuum, in addition to the three components of the displacement field

$$\underline{\mathbf{u}}(\underline{\mathbf{X}}, t) = \underline{\mathbf{x}}(\underline{\mathbf{X}}, t) - \underline{\mathbf{X}}. \tag{2.3}$$

Here, $\underline{\mathbf{u}}$ and $\underline{\mathbf{\Phi}}$ are regarded as independent kinematic variables which can be connected on the balance or constitutive level or by some constraint.

The deformation gradient classically links the current infinitesimal material segment $d\underline{\mathbf{x}}$ with its initial position $d\underline{\mathbf{X}}$

$$d\underline{\mathbf{x}} = \underset{\sim}{\mathbf{F}}\, d\underline{\mathbf{X}} \tag{2.4}$$

so that

$$\underset{\sim}{\mathbf{F}} = \underline{\mathbf{u}} \otimes \underline{\nabla} = u_{i,j}\, \underline{\mathbf{e}}_i \otimes \underline{\mathbf{e}}_j \tag{2.5}$$

(in the absence of other indication, partial derivatives are taken with respect to the X_j).

Similarly, we compute the variation $d\underset{\sim}{\mathbf{R}}$ of microrotation along a material segment $d\underline{\mathbf{X}}$. Defining $\delta\, \underline{\mathbf{\Phi}}$ by

$$(d\underset{\sim}{\mathbf{R}})\, \underset{\sim}{\mathbf{R}}^T = \underset{\sim}{\mathbf{1}} \times \delta\underline{\mathbf{\Phi}} = \underset{\approx}{\epsilon}\, \delta\, \underline{\mathbf{\Phi}} \tag{2.6}$$

we derive

$$\delta\, \underline{\mathbf{\Phi}} = -\frac{1}{2}\, \underset{\approx}{\epsilon}\, (d\underset{\sim}{\mathbf{R}}\, \underset{\sim}{\mathbf{R}}^T) = \underset{\sim}{\mathbf{\Gamma}}\, d\underline{\mathbf{X}} \tag{2.7}$$

with

$$\underset{\sim}{\mathbf{\Gamma}} = \frac{1}{2}\, \underset{\approx}{\epsilon} : (\underset{\sim}{\mathbf{R}}\, (\underset{\sim}{\mathbf{R}}^T \otimes \underline{\nabla})). \tag{2.8}$$

The notation $\delta \underline{\Phi}$ means that $\delta \underline{\Phi}$ is not a total differential, as can be seen from (2.7). Contrary to $\underset{\sim}{\mathbf{F}}$, $\underset{\sim}{\Gamma}$ generally is not invertible. With respect to the local space frame $E^\sharp$,

$$(2.9) \qquad {}^\sharp d\underline{x} = {}^\sharp\underset{\sim}{\mathbf{F}}\, d\underline{X} \qquad \text{and} \qquad {}^\sharp\delta\underline{\Phi} = {}^\sharp\underset{\sim}{\Gamma}\, d\underline{X},$$

where ${}^\sharp d\underline{x} = \underset{\sim}{\mathbf{R}}^T\, d\underline{x}$ and ${}^\sharp\delta\underline{\Phi} = \underset{\sim}{\mathbf{R}}^T\, \delta\underline{\Phi}$, and

$$(2.10) \qquad {}^\sharp\underset{\sim}{\mathbf{F}} = \underset{\sim}{\mathbf{R}}^T\, \underset{\sim}{\mathbf{F}}, \qquad {}^\sharp\underset{\sim}{\Gamma} = \underset{\sim}{\mathbf{R}}^T\, \underset{\sim}{\Gamma}.$$

It can be seen that the relative measures ${}^\sharp\underset{\sim}{\mathbf{F}}$ and ${}^\sharp\underset{\sim}{\Gamma}$ are invariant under any Euclidean transformation [15]. Accordingly they are natural Cosserat strains for the development of constitutive equations. They are called respectively the Cosserat deformation tensor and the wryness (or bend-twist, or torsion-curvature) tensor. An alternative expression of the wryness tensor is then

$$(2.11) \qquad {}^\sharp\underset{\sim}{\Gamma} = -\frac{1}{2}\underline{\underline{\epsilon}} : (\underset{\sim}{\mathbf{R}}^T\, (\underset{\sim}{\mathbf{R}} \otimes \underline{\nabla})).$$

One defines next the velocity and the gyration tensor

$$(2.12) \qquad \underline{\mathbf{v}} = \dot{\underline{\mathbf{u}}} = \dot{u}_i\, \underline{\mathbf{e}}_i \qquad \text{and} \qquad \underset{\sim}{\boldsymbol{\upsilon}} = \dot{\underset{\sim}{\mathbf{R}}}\, \underset{\sim}{\mathbf{R}}^T$$

which can be replaced by the associated gyration vector

$$(2.13) \qquad \overset{\times}{\underline{\boldsymbol{\upsilon}}} = -\frac{1}{2}\underline{\underline{\epsilon}}\, \underset{\sim}{\boldsymbol{\upsilon}}$$

since it is skew-symmetric. The time derivative of the Cosserat strains can be related to the gradient of the latter quantities:

$$(2.14) \qquad {}^\sharp\dot{\underset{\sim}{\mathbf{F}}}\, {}^\sharp\underset{\sim}{\mathbf{F}}^{-1} = \underset{\sim}{\mathbf{R}}^T\, (\underline{\mathbf{v}} \otimes \underline{\nabla}^c - \underline{\mathbf{1}} \times \overset{\times}{\underline{\boldsymbol{\upsilon}}})\, \underset{\sim}{\mathbf{R}},$$

$$(2.15) \qquad {}^\sharp\dot{\underset{\sim}{\Gamma}}\, {}^\sharp\underset{\sim}{\mathbf{F}}^{-1} = \underset{\sim}{\mathbf{R}}^T\, \overset{\times}{\underline{\boldsymbol{\upsilon}}} \otimes \underline{\nabla}^c\, \underset{\sim}{\mathbf{R}},$$

where $\underline{\nabla}^c = \dfrac{\partial}{\partial x_i}\, \underline{\mathbf{e}}_i = \underset{\sim}{\mathbf{F}}^{-T}\, \underline{\nabla}$ (Euclidean representation, c stands for current).

$\underline{\mathbf{v}} \otimes \underline{\nabla}^c - \underset{\sim}{\boldsymbol{\upsilon}}$ is the relative velocity gradient and describes the local motion of the material element with respect to the microstructure.

2.2. Forces and stresses

In order to introduce forces and stresses and to deduce the equilibrium equations, we resort to the method of virtual power developed by GERMAIN [16] in the case of micromorphic media. The method is readily adapted to the case of a Cosserat continuum.

The virtual motions are the velocity $\underline{\mathbf{v}}$ and the gyration $\overset{\times}{\underline{\boldsymbol{\upsilon}}}$ (or microrotation rate vector). The next step is to choose the form of the virtual power of a system of forces. Within the framework of a first gradient theory, the virtual power of the internal forces is a linear form of the virtual motions and their gradients. The principle of material frame indifference requires that this linear form should be invariant under any Euclidean transformation. That is why we will work with the objective quantities $\underline{\mathbf{v}} \otimes \underline{\nabla}^c - \underset{\sim}{\upsilon}$ and $\overset{\times}{\underline{\boldsymbol{\upsilon}}} \otimes \underline{\nabla}^c$. The dual quantities involved in the linear form of the virtual power of the internal forces are denoted $\underset{\sim}{\boldsymbol{\sigma}}$ and $\underset{\sim}{\boldsymbol{\mu}}$ respectively, and are assumed to be objective tensors. For objectivity reasons the dual variable associated with $\underline{\mathbf{v}}$ is zero. For any subdomain $\mathcal{D} \subset \mathcal{B}$

$$\begin{aligned}
\mathcal{P}_{(i)} &= -\int_{\mathcal{D}} \left(\underset{\sim}{\boldsymbol{\sigma}} : (\underline{\mathbf{v}} \otimes \underline{\nabla}^c - \underset{\sim}{\upsilon}) + \underset{\sim}{\boldsymbol{\mu}} : (\overset{\times}{\underline{\boldsymbol{\upsilon}}} \otimes \underline{\nabla}^c) \right) dV \\
&= -\int_{\mathcal{D}} \left(\sigma_{ij}\, v_{i,j} + \mu_{ij}\, \overset{\times}{v}_{i,j} - \sigma_{ij}\, \upsilon_{ij} \right) dV \\
&= -\int_{\mathcal{D}} \left(\sigma_{ij}\, v_i + \mu_{ij}\, \overset{\times}{v}_i \right)_{,j} dV + \int_{\mathcal{D}} \left(\sigma_{ij,j}\, v_i + (\mu_{ij,j} - \epsilon_{ikl}\, \sigma_{kl}) \overset{\times}{v}_i \right) dV ,
\end{aligned}$$

that is

$$\mathcal{P}_{(i)} = -\int_{\partial\mathcal{D}} \left(\underline{\mathbf{v}} \cdot \underset{\sim}{\boldsymbol{\sigma}} + \overset{\times}{\underline{\boldsymbol{\upsilon}}} \cdot \underset{\sim}{\boldsymbol{\mu}} \right) \cdot \underline{\mathbf{n}}\, dS + \int_{\mathcal{D}} \left(\underline{\mathbf{v}} \cdot \underline{\operatorname{div}}\, \underset{\sim}{\boldsymbol{\sigma}} + \overset{\times}{\underline{\boldsymbol{\upsilon}}} \cdot (\underline{\operatorname{div}}\, \underset{\sim}{\boldsymbol{\mu}} + 2\, \overset{\times}{\underline{\boldsymbol{\sigma}}}) \right) dV \tag{2.16}$$

(in this subsection the partial derivatives are taken with respect to the current configuration). The virtual power of external forces reads

$$\mathcal{P}_{(e)} = \int_{\mathcal{D}} \left(\underline{\mathbf{f}} \cdot \underline{\mathbf{v}} + \underline{\mathbf{c}} \cdot \overset{\times}{\underline{\boldsymbol{\upsilon}}} \right) dS. \tag{2.17}$$

The virtual power of contact forces must then be defined

$$\mathcal{P}_{(c)} = \int_{\partial\mathcal{D}} \left(\underline{\mathbf{t}} \cdot \underline{\mathbf{v}} + \underline{\mathbf{m}} \cdot \overset{\times}{\underline{\boldsymbol{\upsilon}}} \right) dS. \tag{2.18}$$

The dual quantities of the velocity and microrotation rate in $\mathcal{P}_{(e)}$ and $\mathcal{P}_{(c)}$ have the dimensions of volume or surface force and moment, respectively. The principle of virtual power then states that

$$\forall\, \mathcal{D} \subset \mathcal{B}, \quad \forall\, (\underline{\mathbf{v}}, \overset{\times}{\underline{\boldsymbol{\upsilon}}}) \quad \mathcal{P}_{(i)} + \mathcal{P}_{(e)} + \mathcal{P}_{(c)} = 0.$$

In particular

$$\forall\, \mathcal{D} \subset \mathcal{B}, \quad \forall\, (\underline{\mathbf{v}}, \overset{\times}{\underline{\boldsymbol{\upsilon}}}) \,/\, \underline{\mathbf{v}} = \overset{\times}{\underline{\boldsymbol{\upsilon}}} = 0 \quad \text{on } \partial\mathcal{D},$$

$$\int_{\mathcal{D}} \left(\underline{\mathbf{v}} \cdot (\underline{\operatorname{div}}\, \underset{\sim}{\boldsymbol{\sigma}} + \underline{\mathbf{f}}) + \overset{\times}{\underline{\boldsymbol{\upsilon}}} \cdot (\underline{\operatorname{div}}\, \underset{\sim}{\boldsymbol{\mu}} + 2\, \overset{\times}{\underline{\boldsymbol{\sigma}}} + \underline{\mathbf{c}}) \right) dV = 0.$$

Assuming that the quantities are continuous on $\mathcal{B}$, the local equilibrium equations follow

$$\begin{aligned} \underline{\operatorname{div}}\, \underset{\sim}{\boldsymbol{\sigma}} + \underline{\mathbf{f}} &= 0\,, \\ \underline{\operatorname{div}}\, \underset{\sim}{\boldsymbol{\mu}} + 2\overset{\times}{\underset{\sim}{\boldsymbol{\sigma}}} + \underline{\mathbf{c}} &= 0. \end{aligned} \tag{2.19}$$

As a result, the principle of virtual power becomes

$$\forall\, \mathcal{D} \subset \mathcal{B}, \quad \forall\, (\underline{\mathbf{v}}, \overset{\times}{\underline{\boldsymbol{\upsilon}}}) \quad \int_{\partial \mathcal{D}} \left((\underset{\sim}{\boldsymbol{\sigma}}\, \underline{\mathbf{n}} - \underline{\mathbf{t}}) \,.\, \underline{\mathbf{v}} + (\underset{\sim}{\boldsymbol{\mu}}\, \underline{\mathbf{n}} - \underline{\mathbf{m}}) \,.\, \overset{\times}{\underline{\boldsymbol{\upsilon}}} \right) dV = 0,$$

from which the boundary conditions are deduced

$$\begin{aligned} \underset{\sim}{\boldsymbol{\sigma}}\, \underline{\mathbf{n}} &= \underline{\mathbf{t}}\,, \\ \underset{\sim}{\boldsymbol{\mu}}\, \underline{\mathbf{n}} &= \underline{\mathbf{m}}\,. \end{aligned} \tag{2.20}$$

$\underset{\sim}{\boldsymbol{\sigma}}$ is called the Cauchy force stress tensor and $\underset{\sim}{\boldsymbol{\mu}}$ the couple-stress tensor. They are generally not symmetric. A detailed account of Cosserat statics and dynamics can be found in [17].

2.3. Hyperelasticity

2.3.1. Energy balance. Let ε be the internal energy per unit mass, $\underline{\mathbf{q}}$ the heat flux vector, ϱ the current density. The energy balance equation reads then

$$\varrho\, \dot{\varepsilon} = \underset{\sim}{\boldsymbol{\sigma}} : (\underline{\mathbf{v}} \otimes \underline{\nabla}^c - \underset{\sim}{\boldsymbol{\upsilon}}) + \underset{\sim}{\boldsymbol{\mu}} : (\overset{\times}{\underline{\boldsymbol{\upsilon}}} \otimes \underline{\nabla}^c) - \operatorname{div}\, \underline{\mathbf{q}} \tag{2.21}$$

(any other inner heat supply is excluded for simplicity).

According to the thermodynamics of irreversible processes, the entropy principle is written

$$\varrho\, \dot{\eta} + \operatorname{div} \left(\frac{\underline{\mathbf{q}}}{T} \right) \geq 0, \tag{2.22}$$

where T denotes the temperature and η the entropy per unit mass.

Introducing the free energy $\psi = \varepsilon - \eta T$ and combining the energy and entropy equations, one derives the Clausius–Duhem inequality

$$-\varrho(\dot{\psi} + \eta T) + {}^{\sharp}\underset{\sim}{\boldsymbol{\sigma}} : ({}^{\sharp}\dot{\underset{\sim}{\mathbf{F}}}\, {}^{\sharp}\underset{\sim}{\mathbf{F}}^{-1}) + {}^{\sharp}\underset{\sim}{\boldsymbol{\mu}} : ({}^{\sharp}\dot{\underset{\sim}{\boldsymbol{\Gamma}}}\, {}^{\sharp}\underset{\sim}{\mathbf{F}}^{-1}) - \frac{1}{T}\, \underline{\mathbf{q}} \,.\, T\, \underline{\nabla}^c \geq 0, \tag{2.23}$$

where

$$\begin{aligned} {}^{\sharp}\underset{\sim}{\boldsymbol{\sigma}} &= \underset{\sim}{\mathbf{R}}^T\, \underset{\sim}{\boldsymbol{\sigma}}\, \underset{\sim}{\mathbf{R}}, \\ {}^{\sharp}\underset{\sim}{\boldsymbol{\mu}} &= \underset{\sim}{\mathbf{R}}^T\, \underset{\sim}{\boldsymbol{\mu}}\, \underset{\sim}{\mathbf{R}}, \end{aligned} \tag{2.24}$$

are rotated stress tensors with respect to the space frame $E^\sharp$ attached to the microstructure.

A material is said to be hyperelastic if its free energy and entropy are functions of ${}^\sharp\underset{\sim}{\mathbf{F}}$ and ${}^\sharp\underset{\sim}{\mathbf{\Gamma}}$ only. The Clausius–Duhem inequality (2.23) becomes

$$-\left(\varrho\frac{\partial\psi}{\partial\,{}^\sharp\underset{\sim}{\mathbf{F}}}-{}^\sharp\underset{\sim}{\boldsymbol{\sigma}}\,{}^\sharp\underset{\sim}{\mathbf{F}}^{-T}\right):{}^\sharp\dot{\underset{\sim}{\mathbf{F}}}-\left(\varrho\frac{\partial\psi}{\partial\,{}^\sharp\underset{\sim}{\mathbf{\Gamma}}}-{}^\sharp\underset{\sim}{\boldsymbol{\mu}}\,{}^\sharp\underset{\sim}{\mathbf{F}}^{-T}\right):{}^\sharp\dot{\underset{\sim}{\mathbf{\Gamma}}}$$
$$-\left(\varrho\,\eta+\varrho\frac{\partial\psi}{\partial T}\right)\dot{T}-\frac{1}{T}\underline{\mathbf{q}}.T\underline{\nabla}^c\geq 0.$$

Since this expression is linear in ${}^\sharp\dot{\underset{\sim}{\mathbf{F}}}$, ${}^\sharp\dot{\underset{\sim}{\mathbf{\Gamma}}}$ and $\dot{T}$, the last inequality implies

$$\eta=-\frac{\partial\psi}{\partial T} \tag{2.25}$$

and

$$\begin{aligned}{}^\sharp\underset{\sim}{\boldsymbol{\sigma}}&=\varrho\frac{\partial\psi}{\partial\,{}^\sharp\underset{\sim}{\mathbf{F}}}\,{}^\sharp\underset{\sim}{\mathbf{F}}^T,\\ {}^\sharp\underset{\sim}{\boldsymbol{\mu}}&=\varrho\frac{\partial\psi}{\partial\,{}^\sharp\underset{\sim}{\mathbf{\Gamma}}}\,{}^\sharp\underset{\sim}{\mathbf{F}}^T.\end{aligned} \tag{2.26}$$

2.3.2. Linear case; isotropic elasticity. Strain and torsion-curvature are small if $\|{}^\sharp\underset{\sim}{\mathbf{F}}-\underset{\sim}{\mathbf{1}}\|\ll 1$ and $\|{}^\sharp\underset{\sim}{\mathbf{\Gamma}}\|\,l\ll 1$, where l is a characteristic length. If, in addition, microrotations remain small, i.e. if $\|\underline{\mathbf{\Phi}}\|\ll 1$, then

$$\begin{aligned}\underset{\sim}{\mathbf{R}}&\simeq\underset{\sim}{\mathbf{1}}+\underset{\sim}{\mathbf{1}}\times\underline{\mathbf{\Phi}}=\underset{\sim}{\mathbf{1}}-\underset{\sim}{\epsilon}\,\underline{\mathbf{\Phi}},\\ {}^\sharp\underset{\sim}{\mathbf{F}}&\simeq\underset{\sim}{\mathbf{1}}+\underline{\mathbf{u}}\otimes\underline{\nabla}+\underset{\sim}{\epsilon}\,\underline{\mathbf{\Phi}}=\underset{\sim}{\mathbf{1}}+\underset{\sim}{\mathbf{e}},\\ {}^\sharp\underset{\sim}{\mathbf{\Gamma}}&\simeq\underline{\mathbf{\Phi}}\otimes\underline{\nabla}=\underset{\sim}{\boldsymbol{\kappa}}.\end{aligned} \tag{2.27}$$

Furthermore, ${}^\sharp\underset{\sim}{\boldsymbol{\sigma}}\simeq\underset{\sim}{\boldsymbol{\sigma}}$ and ${}^\sharp\underset{\sim}{\boldsymbol{\mu}}\simeq\underset{\sim}{\boldsymbol{\mu}}$. Accordingly, for linear elasticity, two four-rank elasticity tensors are introduced

$$\begin{aligned}\underset{\sim}{\boldsymbol{\sigma}}&=\underset{\approx}{\mathbf{E}}:\underset{\sim}{\mathbf{e}},\\ \underset{\sim}{\boldsymbol{\mu}}&=\underset{\approx}{\mathbf{C}}:\underset{\sim}{\boldsymbol{\kappa}}\end{aligned} \tag{2.28}$$

(no coupling between strain and torsion-curvature is possible as soon as point symmetry is assumed, even for the less symmetric solid [18]). Some symmetry properties of these tensors are derived from the hyperelasticity conditions (2.26)

$$E_{ijkl}=E_{klij}\qquad\text{and}\qquad C_{ijkl}=C_{klij}\,. \tag{2.29}$$

Further symmetry conditions can be obtained if material symmetries are taken into account. The form of the Cosserat elasticity tensors for all symmetry classes

has been established by KESSEL [18]. In the case of isotropic elasticity, the two classical Lamé constants λ, μ are complemented by 4 additional parameters [12]

$$\begin{aligned} \underset{\sim}{\sigma} &= \lambda \underset{\sim}{1} \operatorname{Tr} \underset{\sim}{e} + 2\mu \{\underset{\sim}{e}\} + 2\mu_c \}\underset{\sim}{e}\{ , \\ \underset{\sim}{\mu} &= \alpha \underset{\sim}{1} \operatorname{Tr} \underset{\sim}{\kappa} + 2\beta \{\underset{\sim}{\kappa}\} + 2\gamma \}\underset{\sim}{\kappa}\{ . \end{aligned} \tag{2.30}$$

2.4. Elastoplastic Cosserat single crystals

The works of SAWCZUK [19], LIPPMANN [20] and BESDO [21] are the first milestones in the plasticity theory of Cosserat continua at small strains. In the case of single crystals we resort to recent results in the Cosserat theory at large strains [22].

2.4.1. Strain decomposition. In single crystals, non-homogeneous plastic deformations may induce non-homogeneous permanent lattice rotations, which are associated with plastic lattice curvature. That is why elastic and plastic Cosserat deformations and curvatures are introduced : ${}^{\sharp}\underset{\sim}{\mathbf{F}}^e$, ${}^{\sharp}\underset{\sim}{\mathbf{F}}^p$, ${}^{\sharp}\underset{\sim}{\Gamma}^e$ and ${}^{\sharp}\underset{\sim}{\Gamma}^p$. By means of *elastic* strains, free energy can be stored *without* intrinsic dissipation, i.e. without dissipation of power of deformation. The plastic strain rates can occur only together with the intrinsic dissipation rate. Strain partition rules must then be proposed. The most general decomposition of the strains ${}^{\sharp}\underset{\sim}{\mathbf{F}}$ and ${}^{\sharp}\underset{\sim}{\Gamma}$ reads:

$${}^{\sharp}\underset{\sim}{\mathbf{F}} = {}^{\sharp}\hat{\underset{\sim}{\mathbf{F}}}({}^{\sharp}\underset{\sim}{\mathbf{F}}^e,\ {}^{\sharp}\underset{\sim}{\Gamma}^e,\ {}^{\sharp}\underset{\sim}{\mathbf{F}}^p,\ {}^{\sharp}\underset{\sim}{\Gamma}^p), \tag{2.31}$$

$${}^{\sharp}\underset{\sim}{\Gamma} = {}^{\sharp}\hat{\underset{\sim}{\Gamma}}({}^{\sharp}\underset{\sim}{\mathbf{F}}^e,\ {}^{\sharp}\underset{\sim}{\Gamma}^e,\ {}^{\sharp}\underset{\sim}{\mathbf{F}}^p,\ {}^{\sharp}\underset{\sim}{\Gamma}^p). \tag{2.32}$$

The multiplicative decomposition proposed in [23] is adopted for the partially pure elastic materials under consideration, but only for the Cosserat deformation:

$${}^{\sharp}\underset{\sim}{\mathbf{F}} = {}^{\sharp}\underset{\sim}{\mathbf{F}}^e\ {}^{\sharp}\underset{\sim}{\mathbf{F}}^p . \tag{2.33}$$

The expression

$${}^{\sharp}\dot{\underset{\sim}{\mathbf{F}}}\ {}^{\sharp}\underset{\sim}{\mathbf{F}}^{-1} = {}^{\sharp}\dot{\underset{\sim}{\mathbf{F}}}^e\ {}^{\sharp}\underset{\sim}{\mathbf{F}}^{e-1} + {}^{\sharp}\underset{\sim}{\mathbf{F}}^e\ {}^{\sharp}\dot{\underset{\sim}{\mathbf{F}}}^p\ {}^{\sharp}\underset{\sim}{\mathbf{F}}^{p-1}\ {}^{\sharp}\underset{\sim}{\mathbf{F}}^{e-1} \tag{2.34}$$

has to be substituted in the Clausius–Duhem inequality (2.23). This can be done also with the strain-functions (2.31) and (2.32) using the partial derivatives with respect to the elastic and plastic strain parts. At a dependence of the strain-functions ${}^{\sharp}\hat{\underset{\sim}{\mathbf{F}}}$ and ${}^{\sharp}\hat{\underset{\sim}{\Gamma}}$ only on the corresponding elastic parts (besides the plastic ones), substitution into the fundamental restriction (2.23) gives the hyperelastic constitutive equations in a general form [22]:

$$\begin{aligned} {}^{\sharp}\underset{\sim}{\sigma} &= \varrho \frac{\partial \psi}{\partial\, {}^{\sharp}\underset{\sim}{\mathbf{F}}^e} : \left(\frac{\partial\, {}^{\sharp}\hat{\underset{\sim}{\mathbf{F}}}}{\partial\, {}^{\sharp}\underset{\sim}{\mathbf{F}}^e} \right)^{-1} {}^{\sharp}\underset{\sim}{\mathbf{F}}^T , \\ {}^{\sharp}\underset{\sim}{\mu} &= \varrho \frac{\partial \psi}{\partial\, {}^{\sharp}\underset{\sim}{\Gamma}^e} : \left(\frac{\partial\, {}^{\sharp}\hat{\underset{\sim}{\Gamma}}}{\partial\, {}^{\sharp}\underset{\sim}{\Gamma}^e} \right)^{-1} {}^{\sharp}\underset{\sim}{\mathbf{F}}^T . \end{aligned} \tag{2.35}$$

Metals are materials which can behave in the current configuration purely elastically. Therefore the most natural assumption is that the elastic relations still have the form

$$
\begin{aligned}
{}^{\sharp}\underset{\sim}{\sigma} &= \varrho \frac{\partial \psi}{\partial\, {}^{\sharp}\underset{\sim}{F}^{e}}\, {}^{\sharp}\underset{\sim}{F}^{eT}, \\
{}^{\sharp}\underset{\sim}{\mu} &= \varrho \frac{\partial \psi}{\partial\, {}^{\sharp}\underset{\sim}{\Gamma}^{e}}\, {}^{\sharp}\underset{\sim}{F}^{eT},
\end{aligned}
\tag{2.36}
$$

as in the pure hyperelastic case, see (2.26). Then, setting the special constitutive relations (2.36) equal to the general hyperelastic forms (2.35), one obtains conditions for the strain-functions (2.31) and (2.32), from which the representation (2.33) and a decomposition of the entire wryness tensor can be derived [22]:

$$
{}^{\sharp}\underset{\sim}{\Gamma} = {}^{\sharp}\underset{\sim}{\Gamma}^{e}\, {}^{\sharp}\underset{\sim}{F}^{p} + {}^{\sharp}\underset{\sim}{\Gamma}^{p}. \tag{2.37}
$$

An elastic-plastic decomposition of the rotation $\underset{\sim}{R}$ [24], as of the displacement, is not recommendable, because these non-objective variables can not be connected with the quantities of energy and dissipation. Such a connection is possible only on the level of strains. The decomposition (2.37) has been assumed in [25]. Then the elastic constitutive equations (2.36) follow necessarily. The decompositions (2.33) and (2.37) enable one to define at each point the released state of the crystal for which stresses and couple stresses are removed and plastic deformation and curvature only remain. This is the reason why (2.37) is more suitable for crystals than a purely additional decomposition [26].

2.4.2. Kinematics of elastoplastic Cosserat single crystals. The plastic deformation of single crystals is the result of slip processes on slip systems. For each slip system s, we define

$$
\underline{m}^{s} = \underline{b}^{s} / \|\underline{b}^{s}\|, \tag{2.38}
$$

where $\underline{b}^{s}$ is the Burgers vector. $\underline{z}^{s}$ is the unit vector normal to the slip plane. As a result, the plastic strain rate takes the form

$$
{}^{\sharp}\dot{\underset{\sim}{F}}^{p}\, {}^{\sharp}\underset{\sim}{F}^{p-1} = \sum_{s \in S} \dot{\gamma}^{s}\, {}^{\sharp}\underset{\sim}{P}^{s}. \tag{2.39}
$$

γ^{s} is the amount of slip for the system s. ${}^{\sharp}\underset{\sim}{P}^{s}$ is given by the kinematics of slip

$$
{}^{\sharp}\underset{\sim}{P}^{s} = {}^{\sharp}\underline{m}^{s} \otimes {}^{\sharp}\underline{z}^{s}, \tag{2.40}
$$

where ${}^{\sharp}\underline{z}^{s} = \underset{\sim}{R}^{T}\, \underline{z}^{s}$. If we go back to the Eulerian representation

$$
\underline{v} \otimes \underline{\nabla}^{c} = \dot{\underset{\sim}{F}}\, \underset{\sim}{F}^{-1} = \dot{\underset{\sim}{R}}\, \underset{\sim}{R}^{T} + \underset{\sim}{R}\, {}^{\sharp}\dot{\underset{\sim}{F}}^{e}\, {}^{\sharp}\underset{\sim}{F}^{e-1}\, \underset{\sim}{R}^{T} + \underset{\sim}{R}\, {}^{\sharp}\underset{\sim}{F}^{e}\, {}^{\sharp}\dot{\underset{\sim}{F}}^{p}\, {}^{\sharp}\underset{\sim}{F}^{p-1}\, {}^{\sharp}\underset{\sim}{F}^{e-1}\, \underset{\sim}{R}^{T},
$$

we can split the last expression into its symmetric and skew-symmetric parts:

$$\{\underset{\sim}{\mathbf{v}} \otimes \nabla^c\} = \{\underset{\sim}{\mathbf{R}}\, {}^{\natural}\dot{\underset{\sim}{\mathbf{F}}}^{e}\, {}^{\natural}\underset{\sim}{\mathbf{F}}^{e-1}\, \underset{\sim}{\mathbf{R}}^{T}\} + \sum_{s\in S} \dot{\gamma}^s \{\, {}^{\star}\underline{\mathbf{m}}^s \otimes {}^{\star}\underline{\mathbf{z}}^s\} \tag{2.41}$$

and

$$\}\underset{\sim}{\mathbf{v}} \otimes \underset{\sim}{\nabla}^c\{ - \dot{\underset{\sim}{\mathbf{R}}}\, \underset{\sim}{\mathbf{R}}^{T} = \}\underset{\sim}{\mathbf{R}}\, {}^{\natural}\dot{\underset{\sim}{\mathbf{F}}}^{e}\, {}^{\natural}\underset{\sim}{\mathbf{F}}^{e-1}\, \underset{\sim}{\mathbf{R}}^{T}\{ + \sum_{s\in S} \dot{\gamma}^s \}\, {}^{\star}\underline{\mathbf{m}}^s \otimes {}^{\star}\underline{\mathbf{z}}^s\{\,, \tag{2.42}$$

where we have noted

$${}^{\star}\underline{\mathbf{m}}^s = \underset{\sim}{\mathbf{R}}\, {}^{\natural}\underset{\sim}{\mathbf{F}}^{e}\, {}^{\natural}\underline{\mathbf{m}}^s \qquad \text{and} \qquad {}^{\star}\underline{\mathbf{z}}^s = \underset{\sim}{\mathbf{R}}\, {}^{\natural}\underset{\sim}{\mathbf{F}}^{e-T}\, {}^{\natural}\underline{\mathbf{z}}^s\,. \tag{2.43}$$

Equation (2.42) clearly shows that the relative rotation rate of material lines with respect to the microstructure is due to the lattice rotation associated with slip processes, if elastic contributions are neglected.

We would like to compare the proposed formulation with Mandel's work. We are working with invariant tensors written in the microstructure space frame in order to get rid of undetermined rotations. An equivalent method is to deal with the so-called isoclinic configuration introduced by TEODOSIU [27] and MANDEL [23]. Their description reads

$$\underset{\sim}{\mathbf{F}} = \underset{\sim}{\mathbf{E}}\, \underset{\sim}{\mathbf{P}}\,, \tag{2.44}$$

where the rotation $\underset{\sim}{\mathbf{R}}^{\text{isoclinic}}$ appearing in the polar decomposition of $\underset{\sim}{\mathbf{E}}$ links the isoclinic reference frame to the working space frame. As a result, comparing (2.33) and (2.44) one can think of the equivalence

$$\underset{\sim}{\mathbf{E}} = \underset{\sim}{\mathbf{R}}\, {}^{\natural}\underset{\sim}{\mathbf{F}}^{e}\,. \tag{2.45}$$

However, considering the respective polar decompositions

$$\underset{\sim}{\mathbf{E}} = \underset{\sim}{\mathbf{R}}^{\text{isoclinic}}\, \underset{\sim}{\mathbf{U}}^{e} \qquad \text{and} \qquad {}^{\natural}\underset{\sim}{\mathbf{F}}^{e} = \underset{\sim}{\mathbf{R}}^{e}\, \underset{\sim}{\mathbf{U}}^{e}$$

we should have then

$$\underset{\sim}{\mathbf{R}}^{\text{isoclinic}} = \underset{\sim}{\mathbf{R}}\, \underset{\sim}{\mathbf{R}}^{e}\,. \tag{2.46}$$

Regarding the elastic behaviour in the classical case, lattice vectors are material vectors with respect to the intermediate released configuration. Within the proposed framework this is not exactly true any more. There is an additional rotation $\underset{\sim}{\mathbf{R}}^{e}$ of material fibres with respect to the microstructure, that could be attributed to the presence of heterogeneities. Nevertheless the constitutive theory must be such that $\underset{\sim}{\mathbf{R}}^{e}$ remains a corrective term.

The plastic lattice curvature and torsion are due to the presence of dislocations with a non-vanishing resulting Burgers vector (see Sec. 3). The curvature planes and torsion axes are therefore related to crystallographic directions. They can be represented by the effect of continuous edge and screw dislocations for each slip system. That is why we propose the following kinematics for the plastic wryness

$$\overset{\sharp}{\underset{\sim}{\Gamma}}{}^{p}\ \overset{\sharp}{\underset{\sim}{F}}{}^{p-1} = \sum_{s\in S} \frac{\dot{\theta}^s}{l}\ \overset{\sharp}{\underset{\sim}{Q}}{}^{s}. \tag{2.47}$$

The θ^s are angles that measure the plastic curvature and torsion over a characteristic length l. Explicit forms for $\overset{\sharp}{\underset{\sim}{Q}}{}^{s}$ are given in Sec. 4.1.

2.5. Dissipation

In the Clausius–Duhem inequality (2.23), a contribution to the overall entropy production is due to the development of rotation gradients. If no hardening variables are introduced, the intrinsic dissipation rate is

$$\begin{aligned}\dot{D} = {} & \underset{\sim}{\sigma} : \left(\underset{\sim}{R}\ \overset{\sharp}{\underset{\sim}{F}}{}^{e}\ \overset{\sharp}{\underset{\sim}{\dot{F}}}{}^{p}\ \overset{\sharp}{\underset{\sim}{F}}{}^{p-1}\ \overset{\sharp}{\underset{\sim}{F}}{}^{e-1}\ \underset{\sim}{R}^{T}\right) \\ & + \underset{\sim}{\mu} : \left(\underset{\sim}{R}\ \overset{\sharp}{\underset{\sim}{\Gamma}}{}^{e}\ \overset{\sharp}{\underset{\sim}{\dot{F}}}{}^{p}\ \overset{\sharp}{\underset{\sim}{F}}{}^{p-1}\ \overset{\sharp}{\underset{\sim}{F}}{}^{e-1}\ \underset{\sim}{R}^{T}\right) \\ & + \underset{\sim}{\mu} : \left(\underset{\sim}{R}\ \overset{\sharp}{\underset{\sim}{\dot{\Gamma}}}{}^{p}\ \overset{\sharp}{\underset{\sim}{F}}{}^{-1}\ \underset{\sim}{R}^{T}\right).\end{aligned}$$

Taking (2.39) and (2.47) into account,

$$\begin{aligned}\dot{D} = {} & \sum_{s\in S} \dot{\gamma}^s\, \underset{\sim}{\sigma} : {}^{\star}\underset{\sim}{P}^{s} \\ & + \sum_{s\in S} \dot{\theta}^s\, \underset{\sim}{\mu} : {}^{\star}\underset{\sim}{Q}^{s} \\ & + \underset{\sim}{\mu} : \left(\underset{\sim}{R}\ \overset{\sharp}{\underset{\sim}{\Gamma}}{}^{e}\ \overset{\sharp}{\underset{\sim}{\dot{F}}}{}^{p}\ \overset{\sharp}{\underset{\sim}{F}}{}^{p-1}\ \overset{\sharp}{\underset{\sim}{F}}{}^{e-1}\ \underset{\sim}{R}^{T}\right),\end{aligned} \tag{2.48}$$

where

$$\begin{aligned}{}^{\star}\underset{\sim}{P}^{s} &= \underset{\sim}{R}\ \overset{\sharp}{\underset{\sim}{F}}{}^{e}\ \overset{\sharp}{\underset{\sim}{P}}{}^{s}\ \overset{\sharp}{\underset{\sim}{F}}{}^{e-1}\ \underset{\sim}{R}^{T}, \\ {}^{\star}\underset{\sim}{Q}^{s} &= \underset{\sim}{R}\ \overset{\sharp}{\underset{\sim}{F}}{}^{e}\ \overset{\sharp}{\underset{\sim}{Q}}{}^{s}\ \overset{\sharp}{\underset{\sim}{F}}{}^{e-1}\ \underset{\sim}{R}^{T}.\end{aligned} \tag{2.49}$$

Three terms appear in the dissipation. The first one is the classical one: slip processes due to irreversible dislocation motion are dissipative. The second one is due to the evolution of plastic curvature and torsion. It is clear that homogeneous lattice rotation is definitely not a dissipative process, but plastic curvature due to non-homogeneous lattice rotation is related to the existence of

accommodation dislocations and therefore must be associated with dissipation. This will be investigated in Sec. 4.4. The last term reveals the independence of the elastic curvature-torsion measure from plastic changes of the material lines in the intermediate configuration. This is due to the lattice concept, which means that the elastic behaviour, given in (2.36), is primarily not influenced by plastic straining. Thus, the elastic strain measures are related to lattice line-elements and their reference to material lines produce an additional term in the plastic wryness rate. However, at small elastic strains, this term vanishes.

3. Closure of the continuum theory of dislocations

3.1. Closure problem of the continuum theory of dislocations

The origin of the continuum theory of dislocations goes back to Nye's epoch-making work on *"Some geometrical relations in dislocated crystals"* [3]. He introduced the dislocation density tensor $\underset{\sim}{\alpha}$ which will be presented in Sec. 3.2 and he established a link between $\underset{\sim}{\alpha}$ and lattice curvature. KRÖNER [28] proposed a general presentation of the theory and gave the set of partial differential equations to be solved in the linear static case for a given distribution of dislocations, and here for an infinite body

$$
\begin{aligned}
\underset{\sim}{\beta} &= \underset{\sim}{\beta}^{e} + \underset{\sim}{\beta}^{p}, \\
\underset{\sim}{\sigma} &= \underset{\approx}{\mathbf{E}}\,\{\underset{\sim}{\beta}^{e}\}, \\
\underline{\mathrm{div}}\,\underset{\sim}{\sigma} &= 0, \\
\underset{\sim}{\mathrm{curl}}\,\underset{\sim}{\beta}^{e} &= \underset{\sim}{\alpha},
\end{aligned}
\tag{3.1}
$$

where $\underset{\sim}{\beta} = \underline{\mathbf{u}} \otimes \underline{\nabla} = u_{i,j}\ \underline{\mathbf{e}}_i \otimes \underline{\mathbf{e}}_j$. In this part, we use Kröner's notations for historical reasons. It must be noted that, strictly speaking, the non-objective quantity $\underset{\sim}{\beta}$ cannot be decomposed entirely into an elastic and plastic part but the usual notations of the continuum theory of dislocations and of classical plasticity theory can be reconciled by the concept of isoclinic configuration as it was done in [29]. The continuum theory of dislocations is a way to think of dislocation theory as of a physical field theory. The system (3.1) enables us to find the stress-strain field around dislocations for some given arrangements. However such a theory cannot bridge the gap between the dislocation theory and plasticity theory since it does not predict the motion of dislocations. The dislocation distribution must be known at each step. In the dynamic theory of continuous distributions of dislocations, KRÖNER [28] and MURA [30, 31] introduce the dislocation flux tensor $\underset{\approx}{\mathbf{V}}$ which is related to the plastic deformation rate $\dot{\underset{\sim}{\beta}}^{p}$ by

$$
\dot{\underset{\sim}{\beta}}^{p} = -\left(\underset{\approx}{\epsilon} : \underset{\approx}{\mathbf{V}}\right)^{T} \tag{3.2}
$$

and we still have

$$\dot{\underset{\sim}{\alpha}} = -\operatorname{curl}\dot{\underset{\sim}{\beta}}^{p}. \tag{3.3}$$

For a single dislocation, the dislocation flux tensor reads

$$\underset{\equiv}{\mathbf{V}} = \underline{\mathbf{v}} \otimes \underline{\xi} \otimes \underline{\mathbf{b}}, \tag{3.4}$$

$\underline{\mathbf{v}}$ is the dislocation velocity vector, $\underline{\xi}$ is the dislocation line vector and $\underline{\mathbf{b}}$ the Burgers vector. In this case stress and strain can be obtained provided that $\underset{\sim}{\alpha}$ and $\underset{\equiv}{\mathbf{V}}$ are given at each time, which is of no help to derive a plasticity theory. For, the continuum theory of dislocations, even in more recent review articles like [33], does not provide constitutive equations. As pointed out by HAHN and JAUNZEMIS [34], in a complete theory of dislocations, the density and motion of dislocations should be derivable from the knowledge of initial conditions (and boundary conditions) only. This is what we call the closure problem of the continuum theory of dislocations.

Two attempts to derive the missing constitutive equations must be mentioned. On the one hand MURA [35] showed how the von Mises yield criterion and Prandtl–Reuss relations can be explained in terms of the dislocation velocity tensor and a so-called "gliding force". The underlying constitutive assumption is a linear relation between $\underset{\equiv}{\mathbf{V}}$ and the gliding force. According to [36] and [37], constitutive equations are also necessary to link plasticity and dislocation theories. On the other hand, HAHN and JAUNZEMIS [34] distinguish mobile dislocations (M) from immobile ones (I) with common line and Burgers vectors. $A^{ab} = A_I^{ab} + A_M^{ab}$ is the number of dislocations of Burgers vector $\underline{\mathbf{b}}^a$ and line vector $\underline{\xi}^b$. Using a large strain formulation, (3.1) combined with (3.4) yields

$$\dot{\underset{\sim}{\mathbf{F}}}^{p}\,\underset{\sim}{\mathbf{F}}^{p-1} = \sum_{a,b} \underline{\mathbf{b}}^a \otimes (\underline{\xi}^b \times \underline{\mathbf{v}}^{ab}) A_M^{ab} = \sum_a A^a V^a\, \underline{\mathbf{b}}^a \otimes \underline{\mathbf{z}}^a, \tag{3.5}$$

where

$$A^a V^a\, \underline{\mathbf{z}}^a = \sum_b A_M^{ab}\, \underline{\xi}^b \times \underline{\mathbf{v}}^{ab}$$

is normal to the slip plane. Evolution equations are proposed for A_I^a and A_M^a. Isotropic and kinematic hardening and a viscous stress are also introduced in the modelling. Climb mechanisms are not considered.

3.2. Statistical description of dislocation distribution

The dislocation network and dislocation sources distribution within a considered single crystal volume element often is or becomes so intricate that an exact description of all dislocation lines and Burgers vectors must be abandoned. Instead some overall and statistical information about the distribution may be

sufficient for the modelling of the plastic behaviour of the element. The only known attempts to develop a complete statistical theory of dislocations go back to ZORSKI [38] and KRÖNER [39]. The systematic approach comes up against tremendous difficulties which are still not overcome. This explains why the concepts reviewed in this section are only rudimentary tools which do not exhaust the complexity of dislocation structures.

3.2.1. Dislocation density tensor and the continuum theory of dislocations. Within the framework of the continuum theory of dislocations, the characteristic size l of the volume element is taken large enough for the effects of the dislocations within it to be averaged. The distribution of dislocations is made continuous by letting $b = \|\underline{\mathbf{b}}\|$ approach zero and increasing the number n of dislocations of each kind so as to keep nb constant [3]. The definition of the Burgers vector can be extended to continuous distributions of dislocations [27]. For that purpose one refers to the kinematic description proposed by MANDEL [23] making use of the isoclinic configuration and of the strain partition given by (2.44). In (2.44), $\underset{\sim}{\mathbf{E}}$ relates the infinitesimal vectors $d\underline{\zeta}$ and $d\underline{\mathbf{x}}$, where $d\underline{\zeta}$ results from the cutting and releasing operations of the infinitesimal current lattice vector $d\underline{\mathbf{x}}$

$$d\underline{\zeta} = \underset{\sim}{\mathbf{E}}^{-1}\, d\underline{\mathbf{x}}\,. \tag{3.6}$$

It can be seen that the decomposition (2.44) actually goes back to [40].

Accordingly, if S is a smooth surface containing $\underline{\mathbf{x}}$ in the current configuration and bounded by the closed line c, the true Burgers vector is defined as in [27]

$$\underline{\mathbf{b}} = \oint_c \underset{\sim}{\mathbf{E}}^{-1}\, d\underline{\mathbf{x}}\,. \tag{3.7}$$

The application of Stokes' formula (A.19) leads to the definition of the so-called true dislocation density tensor

$$\underset{\sim}{\boldsymbol{\alpha}} = -\mathrm{curl}^{\mathrm{c}}\, \underset{\sim}{\mathbf{E}}^{-1} = \underset{\sim}{\mathbf{E}}^{-1} \times \underline{\nabla}^{c} = -\epsilon_{jkl}\, E^{-1}_{ik,l}\, \underline{\mathbf{e}}_i \otimes \underline{\mathbf{e}}_j \tag{3.8}$$

such that

$$\underline{\mathbf{b}} = \int_S \underset{\sim}{\boldsymbol{\alpha}}\, \underline{\mathbf{n}}\, dS\,. \tag{3.9}$$

If the surface is infinitesimal of normal $\underline{\mathbf{n}}$, $d\underline{\mathbf{b}} = \underset{\sim}{\boldsymbol{\alpha}}\, \underline{\mathbf{n}}\, dS$ is the resulting true Burgers vector of dislocations crossing the surface dS. It is convenient to associate each component α_{ij} of the dislocation density tensor with a (super) dislocation characterized by its line vector $\underline{\mathbf{e}}_j$ and its Burgers vector $b_i\, \underline{\mathbf{e}}_i$ (no summation). As a result, the diagonal components of $\underset{\sim}{\boldsymbol{\alpha}}$ represent screw dislocations and the out-of-diagonal ones edge dislocations. For n dislocations per unit surface of Burgers vector $\underline{\mathbf{b}}$ and line vector $\underline{\xi}$, we have

$$\underset{\sim}{\boldsymbol{\alpha}} = n\, \underline{\mathbf{b}} \otimes \underline{\xi}\,. \tag{3.10}$$

3.2.2. Scalar dislocation densities and crystal plasticity. In the classical continuum theory of dislocations, the description of the dislocation distribution is restricted to the dislocation density tensor. It enables one to compute stress-strain fields for special distributions and even discrete dislocations for which $\underset{\sim}{\alpha}$ becomes the sum of Dirac's functions [28]. However the classical continuum theory of dislocations has failed to describe the elastoplastic behaviour of single crystals. The main reason is that the dislocation density tensor is not the relevant variable to explain the hardening processes. In [34], the kinematics of plastic deformation are derived from the dislocation velocity tensor and correspond exactly to the purely mechanical description of slip processes proposed by MANDEL [23]. The next step is the introduction of hardening variables as in the classical macroscopic plasticity theory. They are related to usual scalar dislocation densities that are commonly used by metal phycisists and which represent the total length of dislocation lines within a volume element. The multiplication and interaction of dislocations are responsible for the hardening of single crystals and the scalar densities are reliable measures for it. This type of description culminates with the work of MANDEL [23], ZARKA [41] and TEODOSIU and SIDOROFF [42]. In these theories the dislocation density tensor is not even mentioned since it is not the relevant quantity any more. Constitutive equations for hardening variables are proposed in a more or less phenomenological way and several elementary dislocation interaction processes are taken into account.

The main successes of these theories are the modelling of the tensile behaviour of single crystals, the lattice rotations [43] and the cyclic behaviour of single and polycrystals [44].

3.2.3. Proposed description. In this work we claim that both types of descriptions are required for the modelling of non-homogeneous deformation of single crystals. That is why the statistical description of dislocation distribution must contain at least:

- the dislocation density tensor $\underset{\sim}{\alpha}$ which accounts for the resulting Burgers vector across any infinitesimal surface,

and

- scalar dislocation densities ϱ^s or the associated hardening variables, for instance r^s and x^s already used in [45]. The kinematic hardening variables x^s are a measure for microscopically non-homogeneous spatial dislocation distributions that give rise to a vanishing resulting Burgers vector (dislocation cells...). Additional variables (densities of mobile and immobile dislocations...) may also be necessary.

It must be noted that the dislocation density tensor and the scalar dislocation densities are related, respectively, to the one-point and two-point dislocation correlations introduced by KRÖNER [39].

The scalar dislocation densities are necessary to account for the hardening or softening behaviour of the material whereas the dislocation density tensor may play a significant role when strong lattice incompatibilities are present.

3.3. Link between the dislocation density tensor and the lattice torsion-curvature tensor

3.3.1. Classical analysis at small strains and small rotations. NYE [3] introduces the rotation vector $\underline{\Phi}$ of the lattice and the curvature tensor $\underset{\sim}{\kappa} = \underline{\Phi} \otimes \underline{\nabla}$. At small strains and small rotations, the strain and rotation rate decomposition into elastic and plastic parts reads

$$\begin{aligned} \dot{\underset{\sim}{\beta}} &= \dot{\underset{\sim}{\beta}}^{e} + \dot{\underset{\sim}{\beta}}^{p} \\ &= \dot{\underset{\sim}{\varepsilon}} + \underset{\sim}{\omega} \\ &= \dot{\underset{\sim}{\varepsilon}}^{e} + \underset{\sim}{\omega}^{e} + \dot{\underset{\sim}{\varepsilon}}^{p} + \underset{\sim}{\omega}^{p} . \end{aligned} \tag{3.11}$$

$\underset{\sim}{\omega}^{p} = \underset{\sim}{\omega} - \underset{\sim}{\omega}^{e} = \underset{\sim}{\omega} - \underline{1} \times \dot{\underline{\Phi}}$ represents the relative rotation of material lines with respect to the lattice. As a result, relation (3.8) becomes

$$\dot{\underset{\sim}{\alpha}} = \operatorname{curl} \dot{\underset{\sim}{\beta}}^{e} = \operatorname{curl} \dot{\underset{\sim}{\varepsilon}}^{e} + \operatorname{curl} \underset{\sim}{\omega}^{e} . \tag{3.12}$$

In a way similar to KRÖNER [28], we derive

$$\begin{aligned} \operatorname{curl} \underset{\sim}{\omega}^{e} &= \epsilon_{jkl}\, \omega_{ik,l}\, \underline{e}_i \otimes \underline{e}_j \\ &= -\epsilon_{jkl}\, \epsilon_{ikm}\, \dot{\Phi}_{m,l}\, \underline{e}_i \otimes \underline{e}_j \\ &= -\epsilon_{klj}\, \epsilon_{kmi}\, \dot{\kappa}_{ml}\, \underline{e}_i \otimes \underline{e}_j \\ &= -(\delta_{ml}\, \delta_{ij} - \delta_{il}\, \delta_{mj})\, \dot{\kappa}_{ml}\, \underline{e}_i \otimes \underline{e}_j \\ &= \dot{\underset{\sim}{\kappa}}^{T} - (\operatorname{Tr} \dot{\underset{\sim}{\kappa}})\, \underline{1} . \end{aligned} \tag{3.13}$$

Neglecting the elastic strain, one obtains the expression proposed by NYE [3]

$$\underset{\sim}{\alpha} = \underset{\sim}{\kappa}^{T} - (\operatorname{Tr} \underset{\sim}{\kappa})\, \underline{1} \tag{3.14}$$

and its reverse form

$$\underset{\sim}{\kappa} = \underset{\sim}{\alpha}^{T} - \frac{1}{2} (\operatorname{Tr} \underset{\sim}{\alpha})\, \underline{1} . \tag{3.15}$$

Keeping the elastic term

$$\underset{\sim}{\alpha} = \operatorname{curl} \underset{\sim}{\varepsilon}^{e} + \underset{\sim}{\kappa}^{T} - (\operatorname{Tr} \underset{\sim}{\kappa})\, \underline{1} . \tag{3.16}$$

3.3.2. Analysis for the Cosserat theory. Within the framework of the Cosserat theory for single crystals presented in Part 2, we propose the following definition for the true dislocation density tensor

$$\underset{\sim}{\alpha} = -\operatorname{curl}^{c} ({}^{\sharp}\underset{\sim}{\mathbf{F}}^{e-1}\, \underset{\sim}{\mathbf{R}}^{T}) . \tag{3.17}$$

We try now to link the dislocation density tensor and the wryness tensor. Equation (3.17) becomes

$$\underset{\sim}{\boldsymbol{\alpha}} = -\left(\epsilon_{jkl}\,\frac{\partial\, {}^{\sharp}F^{e-1}_{im}}{\partial x_l}\,R_{km} + {}^{\sharp}F^{e-1}_{im}\,\epsilon_{jkl}\,R^{T}_{mk,L}\,F^{-1}_{Ll}\right)\underline{\mathbf{e}}_i \otimes \underline{\mathbf{e}}_j \tag{3.18}$$

(the comma denotes again a derivative with respect to the reference configuration). Note that,

$$\underset{\sim}{\boldsymbol{\Gamma}} = \frac{1}{2}\underset{\approx}{\epsilon} : (\underset{\sim}{\mathbf{R}}\,(\underset{\sim}{\mathbf{R}}^{T} \otimes \underline{\nabla})) \implies \underset{\sim}{\mathbf{R}}\,(\underset{\sim}{\mathbf{R}}^{T} \otimes \underline{\nabla}) = \underset{\approx}{\epsilon}\,\underset{\sim}{\boldsymbol{\Gamma}} \tag{3.19}$$

or, in components,

$$R^{T}_{mk,l} = -R^{T}_{mu}\,\epsilon_{ukv}\,\Gamma_{vl}\,.$$

As a result, (3.17) can now be written

$$\begin{aligned}\underset{\sim}{\boldsymbol{\alpha}} &= \underset{\sim}{\mathbf{A}}^{el} - {}^{\sharp}F^{e-1}_{im}\,R^{T}_{mu}\,\epsilon_{klj}\,\epsilon_{kvu}\,\Gamma_{vL}\,F^{-1}_{Ll}\,\underline{\mathbf{e}}_i \otimes \underline{\mathbf{e}}_j \\ &= \underset{\sim}{\mathbf{A}}^{el} + {}^{\sharp}\underset{\sim}{\mathbf{F}}^{e-1}\,\underset{\sim}{\mathbf{R}}^{T}\left((\underset{\sim}{\boldsymbol{\Gamma}}\,\underset{\sim}{\mathbf{F}}^{-1})^{T} - \mathrm{Tr}\,(\underset{\sim}{\boldsymbol{\Gamma}}\,\underset{\sim}{\mathbf{F}}^{-1})\underline{\mathbf{1}}\right) \\ &= \underset{\sim}{\mathbf{A}}^{el} + {}^{\sharp}\underset{\sim}{\mathbf{F}}^{e-1}\left(({}^{\sharp}\underset{\sim}{\boldsymbol{\Gamma}}\,{}^{\sharp}\underset{\sim}{\mathbf{F}}^{-1})^{T} - \mathrm{Tr}\,({}^{\sharp}\underset{\sim}{\boldsymbol{\Gamma}}\,{}^{\sharp}\underset{\sim}{\mathbf{F}}^{-1})\underline{\mathbf{1}}\right)\underset{\sim}{\mathbf{R}}^{T},\end{aligned} \tag{3.20}$$

where $\underset{\sim}{\mathbf{A}}^{el} = \epsilon_{jkl}\dfrac{\partial\, {}^{\sharp}F^{e-1}_{im}}{\partial x_l}\,R_{km}\,\underline{\mathbf{e}}_i \otimes \underline{\mathbf{e}}_j$. It can be checked that equation (3.16) is retrieved for small strains and rotations. We define

$${}^{\sharp}\underset{\sim}{\boldsymbol{\alpha}} = \underset{\sim}{\boldsymbol{\alpha}}\,\underset{\sim}{\mathbf{R}} \tag{3.21}$$

and $\underset{\sim}{\mathbf{R}}\,{}^{\sharp}\underset{\sim}{\mathbf{F}}^{e}\,\underset{\sim}{\boldsymbol{\alpha}}$ can be interpreted as the Cosserat counterpart of the local dislocation density tensor introduced in the classical continuum theory of dislocations.

Using the decomposition of the total wryness given by (2.37), the expression of the dislocation density tensor (3.20) becomes:

$$\begin{aligned}\underset{\sim}{\boldsymbol{\alpha}} = \underset{\sim}{\mathbf{A}}^{el} &+ {}^{\sharp}\underset{\sim}{\mathbf{F}}^{e-1}\left(({}^{\sharp}\underset{\sim}{\boldsymbol{\Gamma}}^{e}\,{}^{\sharp}\underset{\sim}{\mathbf{F}}^{e-1})^{T} - \mathrm{Tr}\,({}^{\sharp}\underset{\sim}{\boldsymbol{\Gamma}}^{e}\,{}^{\sharp}\underset{\sim}{\mathbf{F}}^{e-1})\underline{\mathbf{1}}\right)\underset{\sim}{\mathbf{R}}^{T} \\ &+ {}^{\sharp}\underset{\sim}{\mathbf{F}}^{e-1}\left(({}^{\sharp}\underset{\sim}{\boldsymbol{\Gamma}}^{p}\,{}^{\sharp}\underset{\sim}{\mathbf{F}}^{-1})^{T} - \mathrm{Tr}\,({}^{\sharp}\underset{\sim}{\boldsymbol{\Gamma}}^{p}\,{}^{\sharp}\underset{\sim}{\mathbf{F}}^{-1})\underline{\mathbf{1}}\right)\underset{\sim}{\mathbf{R}}^{T}.\end{aligned} \tag{3.22}$$

Considering now the released state for which force and couple stresses are removed, as defined at the end of Sec. 2.4.1., the remaining plastic curvature is related to the dislocation density tensor in the released state by:

$${}^{\sharp}\hat{\underset{\sim}{\boldsymbol{\alpha}}} = ({}^{\sharp}\underset{\sim}{\boldsymbol{\Gamma}}^{p}\,{}^{\sharp}\underset{\sim}{\mathbf{F}}^{p-1})^{T} - \mathrm{Tr}\,({}^{\sharp}\underset{\sim}{\boldsymbol{\Gamma}}^{p}\,{}^{\sharp}\underset{\sim}{\mathbf{F}}^{p-1})\underline{\mathbf{1}}\,. \tag{3.23}$$

In particular, $\hat{\underset{\sim}{\boldsymbol{\alpha}}}$ is known for a given distribution of edge and screw dislocations. This result motivates the definition of the kinematics of plastic curvature evolution in Sec. 4.1. Note that, starting from the same definition (3.17), DŁUŻEWSKI [46] considers elastic and plastic dislocation tensors which are related to the contributions of elastic and plastic curvatures in equation (3.22).

3.4. Constrained Cosserat theories

The work of the Cosserat brothers was almost forgotten until GÜNTHER rediscovered it in 1958 [47]. Furthermore Günther has revealed the close link between the Cosserat theory and the continuum theory of dislocations which has been thriving since the early fifties.

This explains why the continuum theory of dislocations has often been further developed within the framework of a Cosserat continuum, for instance in [48]. In [8] discrete screw and edge dislocations are embedded in the Cosserat continuum. However the physical meaning of the directors remains unclear in these works: are they independent lattice vectors or material vectors? How do they rotate? In many cases the resulting framework is that of a constrained Cosserat theory like in [19]. The rotation rate of the directors is then given by the skew-symmetric part of the overall deformation gradient

$$\dot{\underline{\Phi}} = -\frac{1}{2}\underline{\underline{\epsilon}}\,(\dot{\underline{u}} \otimes \underline{\nabla}). \tag{3.24}$$

The curvature tensor that we denote $\underset{\sim}{\chi}$ in the constrained case then becomes

$$\dot{\underset{\sim}{\chi}} = \dot{\underline{\Phi}} \otimes \underline{\nabla} = -\frac{1}{2}\,\epsilon_{imn}\,u_{m,nj}\,\underline{e}_i \otimes \underline{e}_j\,. \tag{3.25}$$

It is clear that because of this constraint the directors generally are not lattice vectors. Besides the microrotations are entirely determined by the displacement field, which is not the case in the theory presented in Sec. 1. Considering the decomposition of the deformation and bend-twist tensors into elastic and plastic parts, MURA [35] and many authors consider

$$\dot{\underset{\sim}{\beta}} = \dot{\underset{\sim}{\beta}}^{e} + \dot{\underset{\sim}{\beta}}^{p} \qquad \text{and} \qquad \dot{\underset{\sim}{\chi}} = \dot{\underset{\sim}{\chi}}^{e} + \dot{\underset{\sim}{\chi}}^{p} \tag{3.26}$$

with

$$\dot{\underset{\sim}{\chi}}^{e} = \dot{\underline{\Phi}}^{e} = -\frac{1}{2}\underline{\underline{\epsilon}}\,\dot{\underset{\sim}{\beta}}^{e} \qquad \text{and} \qquad \dot{\underset{\sim}{\chi}}^{p} = \dot{\underline{\Phi}}^{p} = -\frac{1}{2}\underline{\underline{\epsilon}}\,\dot{\underset{\sim}{\beta}}^{p}\,, \tag{3.27}$$

so that

$$\dot{\underline{\Phi}}^{e} \otimes \underline{\nabla} + \dot{\underline{\Phi}}^{p} \otimes \underline{\nabla} = \dot{\underset{\sim}{\chi}}\,, \tag{3.28}$$

which also implies the constraint (3.24). As for them, KOSSECKA and DE WIT [33] define

$$\begin{aligned} \underset{\sim}{\alpha}^{T} &= \epsilon_{pkm}\left(\beta^{p}_{lk,m} + \epsilon_{klq}\,\chi^{p}_{qm}\right)\underline{e}_p \otimes \underline{e}_l \\ &= \underset{\sim}{\mathrm{curl}}\,\{\underset{\sim}{\beta}^{p}\} + \underset{\sim}{\chi}^{pT} - \mathrm{Tr}\,\underset{\sim}{\chi}^{p}\,\underset{\sim}{1}\,. \end{aligned} \tag{3.29}$$

Finally they interpret $(\underset{\sim}{\mathrm{curl}}\,\underset{\sim}{\chi}^{p})^{T}$ as the disclination density tensor. However, these formula are not derived from a precise definition of the Burgers vector like in (3.7) or (3.17) and are therefore difficult to assess.

The main advantage of the previous restricted Cosserat theories is that no constitutive equations are required for the plastic curvature. But it must be noted that the expression of the dislocation density tensor (3.16) or (3.20) involves the total torsion-curvature tensor. As a result, nothing is known *a priori* about the elastic and plastic relative contributions, so that constitutive equations with a yield criterion for the plastic curvature may be necessary.

However, looking at Eq. (3.22) may lead one to propose the following relation:

$$(\overset{\sharp}{\underset{\sim}{\Gamma}}{}^{e}\ \overset{\sharp}{\underset{\sim}{F}}{}^{e-1})^{T} - \mathrm{Tr}\,(\overset{\sharp}{\underset{\sim}{\Gamma}}{}^{e}\ \overset{\sharp}{\underset{\sim}{F}}{}^{e-1})\,\underset{\sim}{1} = -\overset{\sharp}{\underset{\sim}{F}}{}^{e}\,\underset{\sim}{A}^{el}\,\underset{\sim}{R}\,, \tag{3.30}$$

which can be regarded as a definition for $\underset{\sim}{\Gamma}^{e}$. If we still accept the decomposition (2.37), $\underset{\sim}{\Gamma}^{p}$ can be deduced. In this case, there is no need for additional constitutive equations to close the problem. Nevertheless, it is not sure that Eq. (2.36) can be derived from this definition of the elastic wryness and, consequently, (2.37) does not necessarily hold. As a result, this definition is abandoned and Eq. (3.30) will not be used in the following. Instead we will stick to relations (2.33), (2.37), (2.39) and (2.47), and propose constitutive equations in Sec. 4. These constitutive equations will allow us to take the influence of plastic curvature on the hardening of the material into account.

3.5. Geometrically necessary dislocations and statistically stored dislocations

According to ASHBY [49], dislocations become stored in a plastically non-homogeneous solid for two reasons: dislocations are either required for the compatible deformation of various parts of the specimen or they accumulate by trapping each other in a random way. This gives rise on the one hand to the density ϱ_G of so-called geometrically necessary dislocations and on the other hand, to the density ϱ_S of statistically stored dislocations. The density ϱ_G can be computed approximately in some situations like plastic bending or punching. This variable comes directly from the continuum theory of dislocations and corresponds to the components of the dislocation density tensor $\underset{\sim}{\alpha}$. In Sec. 4 we will introduce additional inner variables which are directly related to the density ϱ_G of geometrically necessary dislocations for each slip system.

In contrast, the density ϱ_S belongs to the second group of variables that have been listed in Sec. 3.2, namely the hardening variables. However, as shown by Ashby in the case of two-phase alloys, geometrically necessary dislocations may lead to additional hardening. In Sec. 4 we will try to model this coupling effect between the two types of variables that describe the dislocation distribution.

The relative importance of ϱ_G and ϱ_S depends on the amount of overall plastic deformation, and on the type of solicitation. Clearly ϱ_G can dominate in the case of strong deformation gradients.

These considerations have led FLECK, MÜLLER, ASHBY and HUTCHINSON [50] to apply a so-called strain-gradient plasticity theory to the tension and torsion of copper wires with various diameters. The model is equivalent to a constrained Cosserat theory first proposed in [19]. The J_2-theory is extended to couple stresses in a way similar to [51]. However the modelling becomes questionable when applied to wires with diameters comparable to the grain size. In that case the constrained rotations of the model have nothing to do with local lattice rotations, as explained in Sec. 3.4, and the associated curvature is not a relevant variable.

4. Explicit constitutive equations

We propose a set of constitutive equations for the elastoviscoplastic deformation and intrinsic curvature of metal single crystals.

4.1. Kinematics of plastic deformation and curvature

The plastic flow due to slip on various slip systems has been studied in Sec. 2.4.2 (Eq. (2.39)). Similarly, an expression of the plastic curvature evolution has been proposed (Eq. (2.47)). An expression of ${}^\sharp\underset{\sim}{\mathbf{Q}}^s$ is now derived from the analysis of the dislocation density tensor in Sec. 3.3.2. The scalar γ^s represents the amount of slip due to the passage of dislocations of type s through the volume element, as for them the scalars θ^s represent the plastic curvature due to dislocations trapped in the volume element of characteristic length l. When stresses and couple stresses are released, the elastic contributions in Eq. (3.22) disappear so that a direct relation between residual plastic curvature and the dislocation density tensor is obtained (Eq. (3.23)). We consider then that $\underset{\sim}{\boldsymbol{\alpha}}$ can be decomposed into the contributions of edge and screw dislocations and we give in the following the curvature and torsion axes in the two cases. The amounts of curvature θ^s will be computed using constitutive equations proposed in the next section.

Curvature due to edge dislocations ($\perp$)

For edge dislocations, ${}^\sharp\underset{\sim}{\boldsymbol{\alpha}} = b\,{}^\sharp\underline{\mathbf{m}} \otimes {}^\sharp\underline{\xi}$.

$\underline{\xi}$ is the dislocation line vector and the normal to the glide plane is defined as

$$\underline{\mathbf{z}} = \underline{\mathbf{m}} \times \underline{\xi}. \tag{4.1}$$

The associated curvature is shown in Fig. 1, so that we take

$${}^\sharp\underset{\sim}{\mathbf{Q}}_\perp = {}^\sharp\underline{\xi} \otimes {}^\sharp\underline{\mathbf{m}}. \tag{4.2}$$

Arrays of edge dislocations of the same type give rise to lattice curvature in the plane $(\underline{\mathbf{m}}, \underline{\mathbf{b}})$. The rotation vector $\underline{\boldsymbol{\Phi}}$ has the same direction as the dislocation line vector.

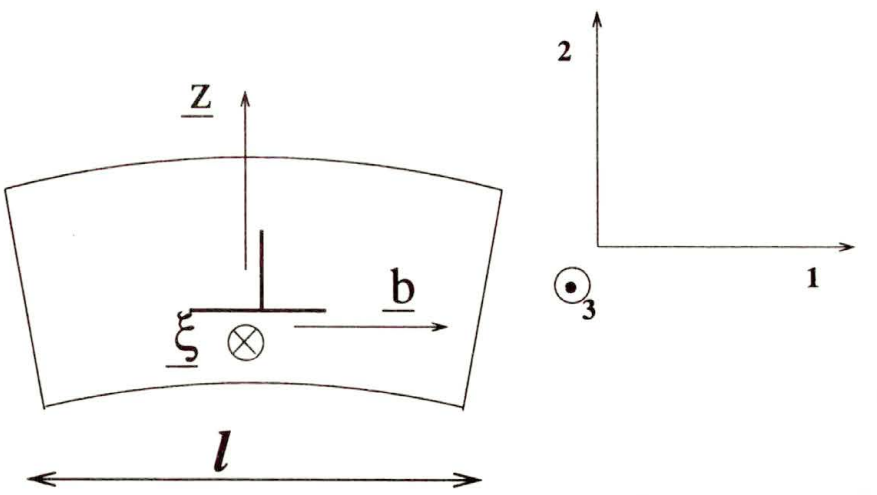

FIG. 1. Curvature due to edge dislocations.

Torsion due to screw dislocations ($\odot$)

For a screw dislocation, ${}^\sharp\underset{\sim}{\boldsymbol{\alpha}} = b\,{}^\sharp\underline{\mathbf{m}} \otimes {}^\sharp\underline{\mathbf{m}}$.

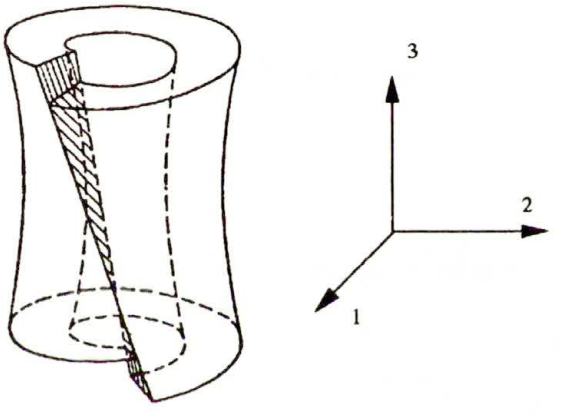

FIG. 2. Curvature due to a screw dislocations, after releasing the end couples (from [53]).

The associated curvature can be seen in Fig. 2, so that we take

$$ {}^\sharp\underset{\sim}{\mathbf{Q}}_\odot = \frac{1}{2}\underset{\sim}{\mathbf{1}} - {}^\sharp\underline{\mathbf{m}} \otimes {}^\sharp\underline{\mathbf{m}}. \tag{4.3}$$

The sign conventions for ${}^\sharp\underset{\sim}{\mathbf{Q}}_\perp$ and ${}^\sharp\underset{\sim}{\mathbf{Q}}_\odot$ are such that $\theta_\perp$ and $\theta_\odot$ are positive in Figs. 1 and 2. As a result, screw dislocations cause lattice torsion about the three reference axes. KRÖNER [28] noticed that a planar array of crossed screw dislocations with perpendicular Burgers vectors produces a twist of the lattice

about the third direction. This is equivalent to a grain boundary of the second kind. Grain boundaries of the first kind are generated by an array of edge dislocations with parallel Burgers and line vectors. Note that the result (4.3) is different from that proposed in [52], which gives no torsion with respect to the dislocation line axis. This seems to hold only when the couple that can be derived from the classical stress field around a screw dislocation is not released [53, 32]. Our expression (3.22) is derived from an extension of the definition of the Burgers vector for continuously distributed dislocations.

Lastly, we give the proposed kinematics of the plastic lattice torsion-curvature

$$(4.4) \qquad {}^{\natural}\dot{\underset{\sim}{\Gamma}}^{p}\ {}^{\natural}\underset{\sim}{\mathbf{F}}^{p-1} = \sum_{s\in S}\left(\frac{\dot{\theta}^s_{\perp}}{l}\ {}^{\natural}\underline{\xi}^s \otimes {}^{\natural}\underline{\mathbf{m}}^s + \frac{\dot{\theta}^s_{\odot}}{l}\left(\frac{1}{2}\underset{\sim}{1} - {}^{\natural}\underline{\mathbf{m}}^s \otimes {}^{\natural}\underline{\mathbf{m}}^s\right)\right).$$

4.2. Generalized Schmid's law

4.2.1. Peach and Koehler's force. KRÖNER [54] shows that Peach and Koehler's formula giving the force on a dislocation $(\underline{\mathbf{b}}, \underline{\boldsymbol{\xi}})$ due to a stress field $\underset{\sim}{\boldsymbol{\sigma}}$ applies also for a non-symmetric stress tensor. But it is important to derive again the formula taking care of any transposition. The force $\underline{\mathbf{f}}$ per unit length of dislocation is defined, for a unit length of dislocation, through

$$(4.5) \qquad \underline{\mathbf{f}} \,.\, d\underline{\mathbf{x}} = \underline{\mathbf{b}} \,.\, (\underset{\sim}{\boldsymbol{\sigma}}\,\underline{\mathbf{n}})\, dS = ((\underline{\mathbf{b}}\,\underset{\sim}{\boldsymbol{\sigma}}) \times \underline{\boldsymbol{\xi}}) \,.\, d\underline{\mathbf{x}},$$

where

$$(4.6) \qquad \underline{\mathbf{n}}\, dS = \underline{\boldsymbol{\xi}} \times d\underline{\mathbf{x}}.$$

The dislocation can move in its plane only if the component of the force in the glide plane

$$(4.7) \qquad b\tau = \underline{\mathbf{f}} \,.\, (\underline{\mathbf{n}} \times \underline{\boldsymbol{\xi}}) = \underset{\sim}{\boldsymbol{\sigma}} : (\underline{\mathbf{b}} \otimes \underline{\mathbf{n}})$$

reaches a threshold. This is the physical meaning of Schmid's criterion. We will use this criterion to compute the slip rate on slip system s

$$(4.8) \qquad \dot{\gamma}^s = \left(\frac{\mathrm{Max}\,(0,\ |\tau^s - x^s| - r^s)}{k^s}\right)^{n^s} \mathrm{sign}\,(\tau^s - x^s),$$

where $\tau^s = {}^{\natural}\underset{\sim}{\boldsymbol{\sigma}} : {}^{\natural}\underset{\sim}{\mathbf{P}}^s$ according to (4.7), and x^s and r^s are internal kinematic and isotropic hardening variables. x^s and r^s represent, respectively, the back-stress and the yield threshold, which are supposed to describe with sufficient accuracy the dislocation structure with a view to modelling the hardening behaviour. Parameters k^s and n^s account for viscosity properties.

4.2.2. Evolution law for the viscoplastic torsion-curvature variables. We consider an array of edge dislocations with $\underline{\mathbf{b}} = b\,\underline{\mathbf{e}}_1$, the normal to the glide plane $\underline{\mathbf{z}} = \underline{\mathbf{e}}_2$ and $\underline{\boldsymbol{\xi}} = -\underline{\mathbf{e}}_3$ (see Fig. 1). At small strains they produce a curvature

$$\underset{\sim}{\boldsymbol{\kappa}}^p = \frac{-nb}{l}\,\underline{\mathbf{e}}_3 \otimes \underline{\mathbf{e}}_1 = \kappa^p_{31}\,\underline{\mathbf{e}}_3 \otimes \underline{\mathbf{e}}_1 \,. \tag{4.9}$$

We will assume that such geometrically necessary dislocations are produced by local dislocation sources if the local moment $\underset{\sim}{\boldsymbol{\mu}} = m\,\underline{\mathbf{e}}_3 \otimes \underline{\mathbf{e}}_1$ ($m < 0$ here) is so high that the imposed curvature cannot be accommodated elastically any longer.

Generalizing the previous example, we propose the following expression of the viscoplastic curvature rate

$$\dot{\theta}^s = \left(\frac{\mathrm{Max}\,(0,\ |{}^\sharp\underset{\sim}{\boldsymbol{\mu}} : {}^\sharp\underset{\sim}{\mathbf{Q}}^s| - l\,r_c^s)}{l\,k_c^s} \right)^{n_c^s} \mathrm{sign}\,({}^\sharp\underset{\sim}{\boldsymbol{\mu}} : {}^\sharp\underset{\sim}{\mathbf{Q}}^s), \tag{4.10}$$

where r_c^s denotes the threshold and k_c^s and n_c^s are viscosity parameters. The formula is to be applied successively for edge and screw dislocations belonging to the same system. Equations (4.8) and (4.10) and the hardening rules of the next section close the theory based on multicriteria and associative flow rules. Accordingly, this theory is part of the associative generalized plasticity.

4.3. Expression of the free energy and hardening rules

The key-point of the thermodynamical analysis of a constitutive model for a dissipative system is the choice of the relevant internal variables on which the free energy may depend. We propose such a formulation of the previous model in the linear case for simplicity. In addition to the observable variables: deformation, curvature and temperature ($\underset{\sim}{\mathbf{e}}$, $\underset{\sim}{\boldsymbol{\kappa}}$, T) or equivalently ($\underset{\sim}{\mathbf{e}}^e$, $\underset{\sim}{\boldsymbol{\kappa}}^e$, T), the free energy is assumed to depend on the following internal variables:

- the variables ϱ_S^s, which are similar to the densities of statistically stored dislocations, and which are defined by

$$\dot{\varrho}_S^s = |\dot{\gamma}^s|; \tag{4.11}$$

- the variables ϱ_G^s, which are similar to the densities of geometrically necessary dislocations, and which are defined by

$$\varrho_G^s = \left| \frac{b\,\theta^s}{l} \right|; \tag{4.12}$$

- the kinematic hardening variables α^s.

We postulate then that the free energy is a quadratic form of these variables according to

$$
\begin{aligned}
(4.13)\qquad \varrho\psi(\underset{\sim}{\mathbf{e}}^e, \underset{\sim}{\boldsymbol{\kappa}}^e, T, \alpha^s, \varrho_S^s, \varrho_G^s) = {} & \frac{1}{2}\underset{\sim}{\mathbf{e}}^e : \underset{\approx}{\mathbf{E}} : \underset{\sim}{\mathbf{e}}^e + \frac{1}{2}\underset{\sim}{\boldsymbol{\kappa}}^e : \underset{\approx}{\mathbf{C}} : \underset{\sim}{\boldsymbol{\kappa}}^e + \frac{1}{2}\sum_{s\in S} c\,\alpha^{s2} \\
& + r_0 \sum_{s\in S} \varrho_S^s + \frac{1}{2}\sum_{r,s\in S} h^{sr}\,\varrho_S^s\,\varrho_S^r \\
& + r_{c0} \sum_{s\in S} \varrho_G^s + \frac{1}{2}\sum_{r,s\in S} h_c^{sr}\,\varrho_G^s\,\varrho_G^r \\
& + \sum_{r,s\in S} h_I^{sr}\,\varrho_S^s\,\varrho_G^r + f(T).
\end{aligned}
$$

Hardening matrices h^{rs} and h_c^{rs} have been introduced for each population of dislocations following [55], but a coupling term associated with the matrix h_I^{sr} must be added.

Assuming then that the thermodynamical forces corresponding to the variables ϱ_S^s, ϱ_G^s and α^s, respectively, are r^s, r_c^s and x^s, the following hardening rules are derived:

Isotropic hardening

$$
(4.14)\qquad r^s = \varrho\frac{\partial\psi}{\partial\varrho_S^s} = r_0 + \sum_{r\in S} h^{sr}\,\varrho_S^r + \sum_{r\in S} h_I^{sr}\,\varrho_G^r\,,
$$

$$
(4.15)\qquad r_c^s = \varrho\frac{\partial\psi}{\partial\varrho_G^s} = r_{c0} + \sum_{r\in S} h_c^{sr}\,\varrho_G^r + \sum_{r\in S} h_I^{sr}\,\varrho_S^r\,.
$$

Note that, for simplicity, we have omitted to split the terms $h_c^{sr}\,\varrho_G^r$ into $h_{c\perp}^{sr}\,\varrho_{G\perp}^r + h_{c\odot}^{sr}\,\varrho_{G\odot}^r$ in order to distinguish the contributions of edge and screw dislocations. The same holds for the terms involving matrix h_I^{sr}. Furthermore, a similar thermodynamical formulation can be worked out for nonlinear isotropic hardening [58]. It can be seen that a coupling between plastic deformation and curvature naturally arises from our choice of the free energy. The existence of additional hardening due to plastic curvature must be investigated experimentally.

Kinematic hardening

$$
(4.16)\qquad x^s = \varrho\frac{\partial\psi}{\partial\alpha^s} = c\,\alpha^s\,.
$$

We refer to [45] for the expression of the nonlinear evolution law for kinematic hardening:

$$
(4.17)\qquad \dot{\alpha}^s = \dot{\gamma}^s - d\,|\dot{\gamma}^s|\alpha^s\,.
$$

4.4. Dissipation

Introducing now the internal variables in the expression of the intrinsic dissipation rate derived in (2.5), one obtains

$$\dot{D} = \sum_{r\in S} \left(\tau^s \dot{\gamma}^s - x^s \dot{\alpha}^s - r^s \dot{\varrho}^s_S + \nu^s_\perp \dot{\theta}^s_\perp + \nu^s_\odot \dot{\theta}^s_\odot - r^s_{c\perp} \dot{\varrho}^s_{G\perp} - r^s_{c\odot} \dot{\varrho}^s_{G\odot} \right), \tag{4.18}$$

where

$$\nu^s_\perp = \frac{1}{l}\, {}^\sharp\underset{\sim}{\boldsymbol{\mu}} : {}^\sharp\underset{\sim}{\mathbf{Q}}^s_\perp \qquad \text{and} \qquad \nu^s_\odot = \frac{1}{l}\, {}^\sharp\underset{\sim}{\boldsymbol{\mu}} : {}^\sharp\underset{\sim}{\mathbf{Q}}^s_\odot. \tag{4.19}$$

The multiplication and motion of dislocations are dissipative processes. The three first terms in (4.18) account for dissipation due to slip activity whereas the remaining terms account for multiplication of geometrically necessary dislocations. In some cases the last terms can be neglected. But when strong lattice rotation gradients develop, they may well be the leading terms.

Some conditions on the material parameters can then be derived from the entropy principle. Taking the flow rules (4.8) and (4.10) and the definitions (4.11) and (4.12) into account, Eq. (4.18) can be rewritten in the form

$$\begin{aligned} \dot{D} = \sum_{r\in S} \Big[& (\tau^s - x^s)\, \mathrm{sign}\,(\dot{\gamma}^s) - r^s + c d \alpha^{s2} |\dot{\gamma}^s| \\ & + \dot{\theta}^s_\perp \left(\nu^s_\perp - r^s_{c\perp}\, \mathrm{sign}\,(\theta^s_\perp)\right) + \dot{\theta}^s_\odot (\nu^s_\odot - r^s_{c\odot}\, \mathrm{sign}\,(\theta^s_\odot)) \Big]. \end{aligned} \tag{4.20}$$

It can be checked in this formula that the positivity of the intrinsic dissipation rate is ensured if $c\,d > 0$ and if the marix $h^{rs}_{c\perp,\odot}$ is such that $r^s_{c\perp,\odot}$ is always positive.

5. Conclusions

Recent advances in the mechanics of generalized continua have been used to develop a Cosserat theory for single crystals at finite deformation and curvature. The decomposition of the relative deformation gradient into an elastic and plastic part is multiplicative as usual, whereas the wryness tensor admits a mixed additive-multiplicative decomposition. We have assumed that the plastic lattice curvature and torsion are accommodated, respectively, by edge and screw dislocations belonging to each slip system. The curvature and torsion angles over a characteristic length due to each type of dislocation are internal variables in addition to the cumulative amounts of slip for each slip system. Explicit constitutive equations have been proposed in the case of elastoviscoplasticity. An important consequence of the theory is that the plastic lattice curvature and torsion as well as the plastic spin are associated with dissipation. The production of geometrically necessary dislocations is clearly a dissipative process. There

is an overwhelming tendency to include these microstructural features of dislocated crystals into the framework of generalized continua. Since the pioneering work of GÜNTHER [47], CLAUS and ERINGEN [10] resorted to a micromorphic continuum. As for them, SMYSHLAYEV and FLECK [56] prefer to develop a strain gradient theory of slip. However they replace this plasticity problem by a problem of nonlinear elasticity at small strains. In contrast, our theory provides a set of kinematical and constitutive equations in elastoviscoplasticity at finite deformation on a physical and thermodynamical basis. Finally LACHNER *et al.* [57] have shown that polycrystals also can be regarded as Cosserat media. Homogenization techniques should enable one to derive a polycrystal model from the present theory.

Only a precise enough description of dislocation distribution within a volume element can enable one to model the plastic behaviour of single crystals. For that purpose, the continuum theory of dislocations resorts to the dislocation density tensor. In contrast, macroscopic elastoplasticity theory involves hardening variables which are related to scalar dislocation densities. In both theories, the expression "dislocation density" is seen to have a very different meaning. The dislocation density tensor and the scalar dislocation densities are independent measures of the dislocation distribution. The most important advantage of the proposed theory is to combine both descriptions within a single constitutive framework.

It must be noticed that only slip processes have been taken into account in the present work. Further developments are necessary to include climb processes, which may play a significant role during creep.

A coupling between plastic curvature and plastic deformation has been introduced on the level of the hardening rule to represent the influence of slip plane curvature on further dislocation motion. Experimental evidence of such hardening effects have been provided for instance in [59].

It is clear that the difference between the classical theory and the Cosserat theory can appear only if deformation and more precisely, lattice rotation is not homogeneous. The theory can therefore be applied to the prediction and the simulation of localized deformation modes like shear bands in single crystals. A theoretical analysis of such material instabilities is presented in [60], and ASARO and RICE [61] and DUSZEK-PERZYNA and PERZYNA [62] investigate the case of single crystals. An analysis and numerical simulations of localization phenomena in single crystals are presented in [63] for the classical theory. In [58] we have performed a bifurcation analysis for single crystals undergoing single slip using the Cosserat theory. Some crucial differences with respect to the classical case have been pointed out. For instance, according to the classical theory, slip bands and kink bands can occur for the same critical hardening modulus. This is no longer true for the Cosserat theory, which is strongly supported by experimental evidence.

Appendix

Notations

In this work, $\underline{\mathbf{a}}$ denotes a vector of the Euclidean space $\mathbf{E}$, $\underset{\sim}{\mathbf{A}}$ a second-rank Euclidean tensor, and $\underset{\approx}{\mathbf{A}}$ (resp. $\underset{\sim}{\underline{\mathbf{A}}}$) a third-rank tensor when operating on a vector (resp. a second-rank tensor). The same third-rank tensor is denoted by $\underline{\underline{\underline{\mathbf{A}}}}$ when regarded as a 3-linear form. The tensor product of two vectors $\underline{\mathbf{a}}$, $\underline{\mathbf{b}}$ is such that, for all $\underline{\mathbf{x}} \in \mathbf{E}$,

$$\begin{aligned} \underline{\mathbf{x}}\,(\underline{\mathbf{a}} \otimes \underline{\mathbf{b}}) &= \underline{\mathbf{x}} \,.\, \underline{\mathbf{a}}\,\underline{\mathbf{b}}\,, \\ (\underline{\mathbf{a}} \otimes \underline{\mathbf{b}})\,\underline{\mathbf{x}} &= \underline{\mathbf{b}} \,.\, \underline{\mathbf{x}}\,\underline{\mathbf{a}}\,, \end{aligned} \tag{A.1}$$

where the dot denotes the inner product on $\mathbf{E}$.

Let $(\underline{\mathbf{e}}_1, \underline{\mathbf{e}}_2, \underline{\mathbf{e}}_3)$ be a positive oriented orthonormal basis of oriented $\mathbf{E}$ with dimension 3. When written in components, the double contraction of second-rank tensors reads

$$\underset{\sim}{\mathbf{A}} \;:\; \underset{\sim}{\mathbf{B}} = A_{ij}\, B_{ij}\,. \tag{A.2}$$

We note $\underset{\approx}{\epsilon}$ the Levi-Civita tensor

$$\underset{\approx}{\epsilon} = \mathrm{Det}\,(\underline{\mathbf{e}}_j, \underline{\mathbf{e}}_k, \underline{\mathbf{e}}_l)\, \underline{\mathbf{e}}_j \otimes \underline{\mathbf{e}}_k \otimes \underline{\mathbf{e}}_l\,. \tag{A.3}$$

Notice the useful identity

$$\epsilon_{ijk}\, \epsilon_{ilm} = \delta_{jl}\, \delta_{km} - \delta_{jm}\, \delta_{kl}\,. \tag{A.4}$$

The following result concerning third-rank tensors have been used,

$$\begin{aligned} &\text{If} \qquad \underset{\sim}{\mathbf{B}} = \frac{1}{2}\, \underset{\approx}{\epsilon} \;:\; \underset{\sim}{\underline{\mathbf{A}}} = \frac{1}{2} \epsilon_{ikl}\, A_{klj}\, \underline{\mathbf{e}}_i \otimes \underline{\mathbf{e}}_j \\ &\text{and} \qquad A_{ijk} = -A_{jik}\,, \\ &\text{then} \qquad \underset{\approx}{\underline{\mathbf{A}}} = \underset{\approx}{\epsilon} \,.\, \underset{\sim}{\mathbf{B}} = \epsilon_{ijm}\, B_{mk}\, \underline{\mathbf{e}}_i \otimes \underline{\mathbf{e}}_j \otimes \underline{\mathbf{e}}_k\,. \end{aligned} \tag{A.5}$$

The cross product is defined by

$$\underline{\mathbf{a}} \times \underline{\mathbf{b}} = \underset{\approx}{\epsilon}\,(\underline{\mathbf{a}} \otimes \underline{\mathbf{b}}) = \epsilon_{ijk}\, a_j\, b_k\, \underline{\mathbf{e}}_i\,. \tag{A.6}$$

The symmetric and antisymmetric parts of tensor $\underset{\sim}{\mathbf{A}}$ are respectively denoted $\{\underset{\sim}{\mathbf{A}}\}$ and $\}\underset{\sim}{\mathbf{A}}\{$. There is then one and only one vector $\overset{\times}{\underline{\mathbf{A}}}$ such that, for all $\underline{\mathbf{x}}$,

$$\}\underset{\sim}{\mathbf{A}}\{\,\underline{\mathbf{x}} = \overset{\times}{\underline{\mathbf{A}}} \times \underline{\mathbf{x}} \tag{A.7}$$

and

$$\overset{\times}{\underline{\underline{\mathbf{A}}}} = -\frac{1}{2}\underline{\underline{\underline{\underline{\epsilon}}}}\,\underline{\underline{\mathbf{A}}} = -\frac{1}{2}\epsilon_{klm}\,A_{lm}\,\underline{\mathbf{e}}_k\,. \tag{A.8}$$

Following TROSTEL [60], we define a cross product between a second-rank tensor and a vector

$$\begin{aligned}(\underline{\mathbf{a}}\otimes\underline{\mathbf{b}})\times\underline{\mathbf{c}} &= \underline{\mathbf{a}}\otimes(\underline{\mathbf{b}}\times\underline{\mathbf{c}})\,,\\ \underline{\mathbf{a}}\times(\underline{\mathbf{b}}\otimes\underline{\mathbf{c}}) &= (\underline{\mathbf{a}}\times\underline{\mathbf{b}})\otimes\underline{\mathbf{c}}\,,\end{aligned} \tag{A.9}$$

so that

$$\underline{\underline{\mathbf{A}}}\times\underline{\mathbf{c}} = -(\underline{\mathbf{c}}\times\underline{\underline{\mathbf{A}}}^T)^T\,. \tag{A.10}$$

As a result

$$\}\underline{\underline{\mathbf{A}}}\{ = \underline{\underline{\underline{\underline{\mathbf{1}}}}}\times\overset{\times}{\underline{\underline{\mathbf{A}}}} = -\underline{\underline{\underline{\underline{\epsilon}}}}\,\overset{\times}{\underline{\underline{\mathbf{A}}}}\,. \tag{A.11}$$

Any element $\underline{\underline{\mathbf{R}}}$ of the orthogonal group can be represented by the element $\underline{\underline{\mathbf{\Phi}}}$ of the associated Lie group such that

$$\underline{\underline{\mathbf{R}}} = \exp(\underline{\underline{\underline{\underline{\mathbf{1}}}}}\times\underline{\underline{\mathbf{\Phi}}}) = \exp(-\underline{\underline{\underline{\underline{\epsilon}}}}\,\underline{\underline{\mathbf{\Phi}}})\,. \tag{A.12}$$

Concerning tensor analysis, our notations are:

Nabla operator

$$\underline{\nabla} = {}_{,i}\,\underline{\mathbf{e}}_i, \tag{A.13}$$

gradient operator

$$\underline{\mathrm{grad}}\,f = f\,\underline{\nabla} = f_{,i}\,\underline{\mathbf{e}}_i\,, \tag{A.14}$$

$$\underset{\sim}{\mathrm{grad}}\,\underline{\mathbf{u}} = \underline{\mathbf{u}}\otimes\underline{\nabla} = u_{i,j}\,\underline{\mathbf{e}}_i\otimes\underline{\mathbf{e}}_j\,, \tag{A.15}$$

curl operator

$$\underline{\mathrm{curl}}\,\underline{\mathbf{u}} = \underline{\mathbf{u}}\times\underline{\nabla} = \epsilon_{ijk}\,u_{j,k}\,\underline{\mathbf{e}}_i\,, \tag{A.16}$$

$$\underset{\sim}{\mathrm{curl}}\,\underline{\underline{\mathbf{A}}} = \underline{\underline{\mathbf{A}}}\times\underline{\nabla} = \epsilon_{hjk}\,A_{ij,k}\,\underline{\mathbf{e}}_i\otimes\underline{\mathbf{e}}_h\,. \tag{A.17}$$

Note that

$$\}\underline{\mathbf{u}}\otimes\underline{\nabla}\{ = \frac{1}{2}\underline{\underline{\underline{\underline{\epsilon}}}}(\underline{\mathrm{curl}}\,\underline{\mathbf{u}}). \tag{A.18}$$

We have made a wide use of theorem

$$\oint_L \underline{\underline{\mathbf{A}}}\,\underline{\mathbf{l}}\;dl = -\int_S (\underset{\sim}{\mathrm{curl}}\,\underline{\underline{\mathbf{A}}})\,\underline{\mathbf{n}}\;dS\,, \tag{A.19}$$

where the open surface S is bounded by the contour L.

References

1. J. MANDEL, *Equations constitutives et directeurs dans les milieux plastiques et viscoplastiques*, Int. J. Solids Structures, **9**, pp. 725–740, 1973.
2. E. COSSERAT and F. COSSERAT, *Théorie des corps déformables*, Hermann, Paris 1909.
3. J.F. NYE, *Some geometrical relations in dislocated crystals*, Acta Metall., **1**, pp. 153–162, 1953.
4. E. KRÖNER, *On the physical reality of torque stresses in continuum mechanics*, Int. J. Engng. Sci., **1**, pp. 261–278, 1963.
5. F. HEHL and E. KRÖNER, *Zum Materialgesetz eines elastischen Mediums mit Momentenspannungen*, Z. Naturforschg., **20 a**, pp. 336–350, 1965.
6. F.A. MCCLINTOCK, P.A. ANDRÉ, K.R. SCHWERDT and R.E. STOECKLY, *Interface couples in crystals*, Nature, No. 4636, pp. 652–653, 1958.
7. E. KRÖNER, *Mechanics of generalized continua*, Proc. of the IUTAM-Symposium on the Generalized Cosserat Continuum and the Continuum Theory of Dislocations with Applications, Freudenstadt, Springer-Verlag, Stuttgart 1967.
8. S. KESSEL, *Spannungsfelder einer Schraubenversetzung und einer Stufenversetzung im Cosseratschen Kontinuum*, ZAMM, **50**, 9, pp. 547–553, 1970.
9. E. KRÖNER, *A variational principle in nonlinear dislocation theory*, Proc. of the Second International Conference of Nonlinear Mechanics, pp. 59–64, Beijing 1993.
10. W.D. CLAUS and A.C. ERINGEN, *Three dislocation concepts and micromorphic mechanics*, Developments in Mechanics, Vol. 6, Proc. of the 12th Midwestern Mechanics Conference, 1971.
11. CZ. WOŹNIAK, *Thermoelasticity of bodies with micro-structure*, Arch. Mech. Stos., **19**, 3, pp. 335–365, 1966.
12. K. WILMAŃSKI and CZ. WOŹNIAK, *On geometry of continuous medium with micro-structure*, Arch. Mech. Stos., **19**, 5, pp. 715–723, 1967.
13. K.C. LE and H. STUMPF, *Finite elastoplasticity with microstructure*, Mitteilung aus dem Institut für Mechanik der Ruhr-Universität Bochum, No. 92, 1994.
14. K.C. LE and H. STUMPF, *Nonlinear continuum theory of dislocations*, Int. J. Engng. Sci., **34**, 3, pp. 339–358, 1996.
15. C.B. KAFADAR and A.C. ERINGEN, *Micropolar media: I the classical theory*, Int. J. Engng Sci., **9**, pp. 271–305, 1971.
16. P. GERMAIN, *The method of virtual power in continuum mechanics, Part 2: Microstructure*, SIAM, J. Appl. Math., **25**, 3, pp. 556–575, 1973.
17. W. NOWACKI, *Theory of asymmetric elasticity*, (Polish edition, 1977), Pergamon, 1986.
18. S. KESSEL, *Lineare Elastizitätstheorie des anisotropen Cosserat-Kontinuums*, Abhandlungen der Braunschweig. Wiss. Ges., Vol. 16, 1964.
19. A. SAWCZUK, *On yielding of Cosserat continua*, Arch. Mech. Stos., **19**, 3, pp. 471–480, 1967.
20. H. LIPPMANN, *Eine Cosserat-Theorie des plastischen Fließens*, Acta Mech., **8**, pp. 255–284, 1969.

21. D. BESDO, *Ein Beitrag zur nichtlinearen Theorie des Cosserat-Kontinuums*, Acta Mech., **20**, pp. 105–131, 1974.

22. R. SIEVERT, *Eine Systematik für elastisch-plastische Stoffgleichungen*, Dissertation, Schriftenreihe Phys. Ing.-Wiss., Band 23, TU Berlin 1992.

23. J. MANDEL, *Plasticité classique et viscoplasticité*, CISM, Udine, Springer Verlag, 1971.

24. P. STEINMANN, *A micropolar theory of finite deformation and finite rotation multiplicative elastoplasticity*, Int. J. Solids Struct., **31**, pp. 1063–1084, 1994.

25. P.H. DŁUŻEWSKI, *Finite deformations of polar media in angular coordinates*, Arch. Mech., **43**, 6, pp. 783–793, 1991.

26. C. SANSOUR and J. KECK, *Zum elasto-viskoplastischen Cosserat-Kontiuum*, Mitteilungen aus dem Institut für Mechanik der Ruhr-Universität Bochum, FRG, No. 93, pp. 38–41, 1994.

27. C. TEODOSIU, *A dynamic theory of dislocations and its applications to the theory of the elastic-plastic continuum*, [in:] Fundamental Aspects of Dislocation Theory, J.A. SIMMONS, R. DE WIT, R. BULLOUGH [Eds.], Nat. Bur. Stand. (U.S.), Spec. Pub., 317, Vol. II, 1970.

28. E. KRÖNER, *Kontinuumstheorie der Versetzungen und Eigenspannungen*, Ergebnisse der angewanden Mathematik, Vol. 5, Springer-Verlag, 1958.

29. E. KRÖNER and C. TEODOSIU, *Lattice defect approach to plasticity and viscoplasticity*, [in:] Problems of Plasticity, International Symposium on Foundations of Plasticity, Warsaw, A. SAWCZUK [Ed.], Noordhoff International Publishing, Leyden 1972.

30. T. MURA, *On dynamic problems of continuous distribution of dislocations*, Int. J. Engng. Sci., **1**, pp. 371–381, 1963.

31. T. MURA, *Continuous distribution of moving dislocations*, Philosophical Magazine, **8**, 89, pp. 843–857, 1963.

32. J.P. HIRTH and J. LOTHE, *Theory of dislocations*, Wiley-Interscience, 1982.

33. E. KOSSECKA and R. DE WIT, *Disclination kinematics*, Arch. Mech., **29**, 5, pp. 633–651, 1977.

34. H.T. HAHN and W. JAUNZEMIS, *A dislocation theory of plasticity*, Int. J. Engng. Sci., **11**, pp. 1065–1078, 1973.

35. T. MURA, *Continuous distribution of dislocations and the mathematical theory of plasticity*, Phys. Stat. Sol., **10**, pp. 447–453, 1965.

36. R.W. LARDNER, *Dislocation dynamics and the theory of the plasticity of single crystals*, ZAMP, **20**, pp. 514–529, 1969.

37. M. EISENBERG, *On the relation between continuum plasticity and dislocation theories*, Int. J. Engng. Sci., **8**, pp. 261–271, 1970.

38. H. ZORSKI, *Statistical theory of dislocations*, Int. J. Solids Structures, **4**, pp. 959–974, 1968.

39. E. KRÖNER, *Initial studies of a plasticity theory based upon statistical mechanics*, Inelastic Behaviour of Solids, M.F. KANNINEN, W.F. ADLER, A.R. ROSENFIELD, R.I. JAFFEE, McGraw-Hill, 1969.

40. B.A. BILBY, R. BULLOUGH, L.R.T. GARDNER and E. SMITH, *Continuous distributions of dislocations IV: Single glide and plane strain*, Proc. Roy. Soc., **A 236**, pp. 538–557, 1957.

41. J. ZARKA, *Généralisation de la théorie du potentiel plastique multiple en viscoplasticité*, J. Mech. Phys. Solids, **20**, 3, pp. 179–195, 1972.

42. C. TEODOSIU and F. SIDOROFF, *A theory of finite elastoviscoplasticity of single crystals*, Int. J. Engng. Sci., **14**, pp. 713–723, 1976.

43. R. FORTUNIER, *Contribution à l'étude de la déformation plastique des cristaux et des polycristaux*, thesis, Ecole des Mines de Saint-Etienne, 1987.

44. G. CAILLETAUD, *A micromechanical approach to inelastic behavior*, Int. J. Plasticity, **8**, pp. 55–73, 1992.

45. L. MÉRIC, P. POUBANNE and G. CAILLETAUD, *Single crystal modeling for structural calculations. Part 1. Model presentation*, J. Engng. Materials and Technology, **113**, pp. 162–170, 1991.

46. P. DŁUŻEWSKI, *On geometry and continuum thermodynamics of movement of structural defects*, Mech. of Materials, **22**, pp. 23–41, 1996.

47. W. GÜNTHER, *Zur Statik und Kinematik des Cosseratschen Kontinuums*, Abhandlungen der Braunschweig. Wiss. Ges., **10**, pp. 195–213, 1958.

48. H. SCHÄFER, *Das Cosserat-Kontinuum*, ZAMM, **47**, 8, pp. 485–498, 1967.

49. M.F. ASHBY, *The deformation of plastically non-homogeneous alloys*, [in:] Strengthening Methods in Crystals, A. KELLY and R.B. NICHOLSON [Eds.], Applied Science Publishers, London, pp. 137–192, 1971.

50. N.A. FLECK, G.M. MÜLLER, M.F. ASHBY and J.W. HUTCHINSON, *Strain gradient plasticity: theory and experiment*, Acta Metall. Mater., **42**, 2, pp. 475–487, 1994.

51. R. DE BORST, *A generalization of J_2-flow theory for polar continua*, Computer Methods in Appl. Mech. and Engng., **103**, pp. 347–362, 1993.

52. P.H. DŁUŻEWSKI, *Finite elastic-plastic deformations of oriented media*, MECAMAT'92, Int. Seminar on Multiaxial Plasticity, A. Benallal, R. Billardon, D. Marquis, Laboratoire de Mécanique et Technologie, Cachan, France, pp. 668–688, 1993.

53. J. FRIEDEL, *Dislocations*, Pergamon, 1964.

54. E. KRÖNER, *Die Versetzung als elementare Eigenspannungsquelle*, Z. Naturforschg., **11a**, pp. 969–985, 1956.

55. J. MANDEL, *Généralisation de la théorie de la plasticité de W.T. Koiter*, Int. J. Solids Structures, **1**, pp. 273–295, 1965.

56. V.P. SMYSHLYAEV and N.A. FLECK, *The role of strain gradients in the grain size effect for polycrystals*, J. Mech. Phys. Solids, pp. 465–495, 1996.

57. D. LACHNER, H. LIPPMANN and L.S. TÓTH, *On Cosserat plasticity and plastic spin for isotropic materials*, Arch. Mech., **46**, 4, pp. 534–539, 1994.

58. S. FOREST, *Mechanical modelling of non-homogeneous deformation of single crystals*, Doctoral Thesis, ENSMP, Paris 1996.

59. B. JAOUL, *Influence de la sous-structure de monocristaux d'aluminium sur la forme des courbes de déformation plastique*, C.R. Acad. Sci. Paris, Vol. 242, pp. 2372–2374, 1956.

60. H. PETRYK, *Material instability and strain-rate discontinuities in incrementally nonlinear continua*, J. Mech. Phys. Solids, **40**, 6, pp. 1227–1250, 1992.

61. R.J. ASARO and J.R. RICE, *Strain localization in ductile single crystals*, J. Mech. Phys. Solids, **25**, pp. 309–338, 1977.

62. M. DUSZEK-PERZYNA and P. PERZYNA, *Adiabatic shear band localization in elastic-plastic single crystals*, Int. J. Solids Structures, **30**, 1, pp. 61–89, 1993.

63. S. FOREST and G. CAILLETAUD, *Strain localization in single crystals: effect of boundaries and interfaces*, Eur. J. Mech., A/Solids, **14**, 5, pp. 747–771, 1995.

64. R. TROSTEL, *Vektor- und Tensor-Algebra*, Mathematische Grundlagen der technischen Mechanik I, Beiträge zur theoretische Mechanik, Vieweg, Wiesbaden 1993.

CENTRE DES MATÉRIAUX, CNRS
ECOLE DES MINES DE PARIS,
BP 87, 91003 Evry, France
e-mail: forest@mat.ensmp.fr
and
BUNDESANSTALT FÜR MATERIALFORSCHUNG UND -PRÜFUNG
Unter den Eichen 87, 12205 Berlin, Germany.

Received November 28, 1996; new version February 21, 1997.

Arch. Mech., 49, 4, pp. 737–766, Warszawa 1997

From material discrete memory patterns to the study of demagnetisation-like processes

A. TOURABI, P. GUELIN, D. FAVIER (GRENOBLE)
and W. K. NOWACKI (WARSZAWA)

Dedicated to the legacy of A.A.Ilyushin
as a token of scientific gratitude

THE PRESENT PAPER is an attempt to study the links between the constitutive pattern of the idealized behaviour of pure hysteresis and the general theory of demagnetisation-like processes of real materials. Modelling based on this discrete-memory pattern has been previously introduced, and used to describe rather successfully the puzzling properties of various deformable materials ranging from granular media to shape memory alloys and deformable ferromagnets or ferroelectrics. However, one of the five basic ingredients of the pattern has not been, up to now, studied extensively: it has been introduced rather as an assumption, namely that of the general possibility to obtain recurrent recovery of a unique thermomechanical initial neutral state. Therefore the aim of this paper is threefold: firstly, to give some tensorial mechanical examples suggesting that the fifth ingredient of the pattern is relevant with respect to the others; secondly, to suggest the importance of a general study of demagnetisation-like processes, purely mechanical or not; thirdly, to suggest that the fifth ingredient is not only relevant on the theoretical grounds and of importance at the level of physical principles, but may be also justified owing to data from now on available.

1. Introduction

i. RELIANCE on physical justifications of the material discrete-memory concept (1) is now rather soundly established in the field of nonlinear continuum mechanics: mainly based on results obtained from transmission electron microscopy, this reliance is fully compatible with the fact that the strain notion is essentially of discrete-memory form [1, 2]. The discrete-memory concept also proved to be rather effective regarding the modelling of the deformable media

(1) Owing to experimental evidences, this notion is frequently implemented in the numerical simulations performed in the field of multiaxial cyclic plasticity. The notion may be sketched through the path 01213 of Fig. 1: in order to describe this rate-independent behaviour with perfectly closed cycle, it is well known that it is necessary to take into account the following (discrete) sets of memorised states: state {0} along the path 01; states {0, 1} along the path 12; states {0, 1, 2} along 21; state {0} along 13.

which are, at the "micro"-scale, structured and with defects [3, 4, 5, 6]. However, such a pattern is still more like an incipient program rather than a theory already expanded for the benefit of engineers. This feature arises from the fact that two fundamental problems are still insufficiently clarified or entirely open, namely the demagnetisation-like problem and the preferred reference frame problem.

ii. Resolute endeavour is needed regarding the former, because it calls the whole pattern in question. In contrast, the choice among the possible solutions of the preferred reference frame problem is "only" decisive at the level of the definitions of the discrete-memory condition and of the thermomechanical rates, and also taking into account the material anisotropy or the case of large deformations and strains (obtained through monotonic loading or through cumulative second order effects of ratchet type). Moreover, regarding the second problem, the (unpublished) results obtained so far are not only encouraging but they are also an incentive to pursue in the direction already chosen [3], whereas no tensorial results were available, at the time, in the field of demagnetisation-like processes.

iii. Dilemma is therefore removed as to the hierarchy of research priorities, but the demagnetisation-like problem has many facets, the one-dimensional intuitions may act as ominous lures and any first approach, chosen tentatively, cannot rely on or refer to previous endeavours. To maintain the bearing of the results, the basic assumptions are chosen so as to focus the analysis on a special but not too restrictive case. Basically, the analysis is performed in the field of multiaxial plasticity ([2]): the aim is therefore to study the recovery of a relevant state under cyclic stress paths. The material under consideration is a rather idealised one: it does not undergo ageing, fatigue, damage, rate-independent hardening or viscous effects [5]. The main property of the material is that of elastic-plastic hysteresis regarding only the deviatoric part of the behaviour. Moreover, there are no coupling effects between deviatoric and isotropic part of the behaviour [6]. It must be also emphasised that there are no coupling effects between the mechanical behaviour and another behaviour such as that of ferrohysteresis: *the study may be considered as purely thermomechanical and the word demagnetization is not used in order to be reminiscent of coupling effects* ([3]). *In fact this word is convenient to suggest briefly the process of recovery which is studied here.* Moreover, this word is actually heuristic through a rule which is proved to be effective in order to perform some numerical simulations ("first loading in reverse" rule, introduced in § 3.3 point ii).

To simplify the formal features of the study, the material is supposed to be isotropic and its limit surface to be of Huber–von Mises type. The constitutive definition is given in the frame of the irrotational triaxial kinematics associ-

([2]) However, it is worth noting that, owing to the analysis of [3] resulting in (3.13) to (3.16), the mechanical case studied here may be considered as a special ferromagnetic case.

([3]) The same remark holds as to the heuristic terminology ("polarization") introduced by Hill in a purely elastic study [37].

ated with the extensions K_1, K_2, K_3 (the usual associated components of the strain rate tensor $\mathbf{D}$ being then: $\dot{K}_n/(1+K_n)$, $n=1,2,3$). Moreover, the stress paths are performed in the deviatoric plane, so that the vanishing of the first invariant I_σ of the Cauchy stress tensor $\boldsymbol{\sigma}$ (components σ_{11}, σ_{22}, σ_{33}) is always imposed. Consequently, the graphical sketches given for illustration are basically two-dimensional (in fact, the numerical simulations are obtained with a four-dimensional program, associated with the kinematics K_1, K_2, K_3, $2\tau_{23}$ and implemented by imposing the vanishing of I_σ and τ_{23}).

iv. As suggested by the abstract, the aim of the paper is threefold. Firstly, basic hints are introduced regarding the theoretical ground of the demagnetisation-like problem tackled with the help of the pure hysteresis pattern. Secondly, the study of a mechanical example is given for illustration: this study is an opportunity to suggest the interest of a general approach and to point out some puzzling features of the demagnetisation-like process. Thirdly, some remarks are introduced regarding the question of experimental evidence currently available in order to illuminate the enigma thereby appeared.

2. On the theoretical ground of the demagnetisation-like problem

2.1. Preliminaries on the fivefold structure of the pattern of pure hysteresis

i. Let us take as a starting-point the usual symbolic mechanical model consisting of an infinite number of springs and friction sliders [3, 4, 6]. More precisely, the model is an ordered infinite parallel succession of couples, each couple being defined by a spring and a friction slider associated in series. First of all, it is possible to perform, in the cyclic case, a careful analysis of this entirely well-defined model devoid of hidden variables (cf. [3], § 2.2.2 and 2.2.3, for example): the main result of this analysis is that the pattern is of discrete-memory form. Next, a thermodynamic analysis may be added (cf. [3], § 2.2.4, for example, or Appendix if necessary). Then, the analysis results in a radical departure from the classical point of view, because the reversible power Π is also of discrete-memory form. It is worth noting that accordingly, the associated intrinsic dissipation Φ and the disorder rate $\dot{I}$ are also of discrete memory form. Moreover the disorder rate plays, in a Gibbs-like balance equation, a role similar to that played by the entropy rate $T\dot{S}$ [7].

ii. The one-dimensional character of the model allows us to give easily a set of heuristic illustrations. Let t and t_R be the current time and the inversion time of reference because it is associated with the origin of the current branch of cycle. Then, along each current branch or arc of branch of cyclic evolution, the one-dimensional pattern is as follows:

1. Discrete memory existence expressed as the invariance of the current (dragged along from t_R to $t > t_R$) Almansi and Cauchy scalars (tensors) ${}^t_R\varepsilon$ and ${}^t_R\sigma$,

respectively:

$$\frac{\partial}{\partial t}\,{}^{t}_{R}\varepsilon \equiv \frac{\partial}{\partial t}\,{}^{t}_{R}\sigma \equiv 0. \tag{2.1}$$

2. Constitutive differential-difference equations of mechanical character (where the "Masing rule" is expressed through the piecewise constant similarity functional ω equal to 1 or 2), such as, for example:

$$\dot{\sigma} \equiv \frac{\partial}{\partial t}\Delta\,{}^{t}_{R}\sigma = G_0\left[1 - \left(\frac{\Delta\,{}^{t}_{R}\sigma}{\omega S_0}\right)^{c}\right]\frac{\partial \Delta\,{}^{t}_{R}\varepsilon}{\partial t}, \tag{2.2}_1$$

$$\Delta\,{}^{t}_{R}\varepsilon = \varepsilon - {}^{t}_{R}\varepsilon, \qquad \Delta\,{}^{t}_{R}\sigma = \sigma - {}^{t}_{R}\sigma,$$

the associated equations of thermodynamic character being:

$$\begin{aligned} \Pi &= -P_i - \Phi, & P_i &= -\sigma\dot{\Delta}^{t}_{R}\varepsilon, \\ \Phi &= \Delta\,{}^{t}_{R}\sigma\,\dot{\Delta}^{t}_{R}\varepsilon, & -\dot{Q}_{ii} &= \frac{\Phi - C}{\omega}, \\ C &= \dot{\Delta}^{t}_{R}\sigma\,\Delta\,{}^{t}_{R}\varepsilon, & \dot{I} &= \frac{(\omega-1)\Phi + C}{\omega}, \\ I(t_{R^+}) &= 0, & \dot{E} &= \frac{-P_i - \Phi + C}{\omega}, \end{aligned} \tag{2.2}_2$$

where the rates $\dot{E}$ and $-\dot{Q}_{ii}$ denote the current rates of internal energy (associated to the springs) and of internal intrinsic heat supply (due to the friction of the sliders), respectively (cf. Appendix, if necessary).

3. Inversion criterion giving the definition of the inversion time of reference t_R:

$$\text{if} \quad \delta W < 0 \quad \forall\, t \in]t, t+\delta t] \;\Rightarrow\; t = t_R, \quad \sigma(t) = {}^{t}_{R}\sigma, \quad W(t) = {}^{t}_{R}W \tag{2.3}$$

through the sign of a virtual variation (δW) because $(2.3)_1$ expresses the second principle of thermodynamics. In the form $(2.3)_1$ the criterion is expressed with the aid of the "help function" W:

$$W = \frac{2}{\omega^2}\int_{t_R}^{t} \Phi(t)\,dt, \qquad W(t_{R^+}) \equiv 0 \tag{2.4}$$

which is, here, of "ln cosh" form when $c = 2$. Other forms are introduced later (§ 3.3, point iii).

4. Algorithm A, also expressed with the aid of W, and giving ω, ${}^{t}_{R}\sigma$, and the set of still memorised variables $\{{}^{t}_{M}W\}$ and $\{{}^{t}_{M}\sigma\}$ (cf. [4] or [6], for example).

5. Existence of the *unique thermomechanical neutral* state defined by:

$$k = 1, \qquad \alpha = 1, \qquad n = 1,$$
$$_{M}W_1(0) = \infty, \qquad W(0_+) = 0, \qquad \omega(0) = 1, \qquad \Delta_0^{0+}\sigma = \Delta_0^{0+}\varepsilon = 0. \tag{2.5}$$

This basic state is restored by the rather well known "symmetrical" *slowly decreasing cyclic* path.

Under cyclic loading defined by a set of inversion times $\{t_I\}$ and by:

$$D^2 = 1, \qquad \Delta_R^t\varepsilon = \varepsilon(t) - {}_R^t\varepsilon = \varepsilon(t) - \varepsilon(t_R) = \pm(t - t_R),$$
$$t > t_R > 0, \qquad \Delta_0^t\varepsilon = \sum \Delta_R^t\varepsilon, \tag{2.6}$$

the one-dimensional behaviour of pure hysteresis is obtained (Fig. 1, obtained with $c = 0.8$, and suggesting the importance of the notion of sky-line, this curve being continuous only if symmetrical *slowly decreasing cyclic* paths are performed). Owing to the simple form of the stress rate definition, the useful integral forms are immediately obtained in the case $c = 2$:

$$(\sigma/S_0)^2 = 1 - \exp(-G_0W/S_0^2) \Leftrightarrow (\Delta\sigma/\omega S_0)^2 = 1 - \exp(-G_0W/S_0^2),$$
$$W = -(S_0^2/G_0)\ln\left[1 - (\sigma/S_0)^2\right] \Leftrightarrow W = -(S_0^2/G_0)\ln\left[1 - (\Delta\sigma/\omega S_0)^2\right], \tag{2.7}$$
$$W = (2S_0^2/G_0^2)\ln\cosh\left[G_0\varepsilon/S_0\right] \Leftrightarrow W = (2S_0^2/G_0^2)\ln\cosh\left[G_0\Delta\varepsilon/\omega S_0\right].$$

2.2. From the notions of state and of U.T.N. state to the role of the fifth ingredient

i. In the field of classical thermodynamics it is always admitted that the state of a physical system can be described using a Duhem set of "normal" variables: in short, if $D = 0$ and if the work of the external action vanishes during a temperature change, then the set is normal. The theory of linear infinitesimal thermoelasticity is a well known heuristic example of application ([4]). In this section, the attention is devoted to the symbolic model and the study is restricted to the case of a unique constant temperature, a choice which does not mean that the study of temperature-dependent symbolic models cannot bring heuristic hints ([8], § IV. 2.3). Therefore, one must pay attention to one of the assumptions generally not recalled, although always implied: in the classical definition of the state, there is no interference of the internal history of the system. By contrast with this usual assumption, the behaviour of the model suggests that the relevant set of state variables must include the history. In order to define a state in the sense both effective and deterministic in the large (cf. [9, 10] and point iii, below), it is indeed necessary to know not only the current strain, but also the current values of the piecewise constant functionals ω, ${}_R^t\varepsilon$, ${}_R^t\sigma$, and the current sets of

([4]) The aim of the section is neither to point out the special role of the temperature, nor to underline that the thermoelastic case is actually quite misleading, owing to the difficulties appearing in the thermohyperelastic case (cf. [8], § II.5).

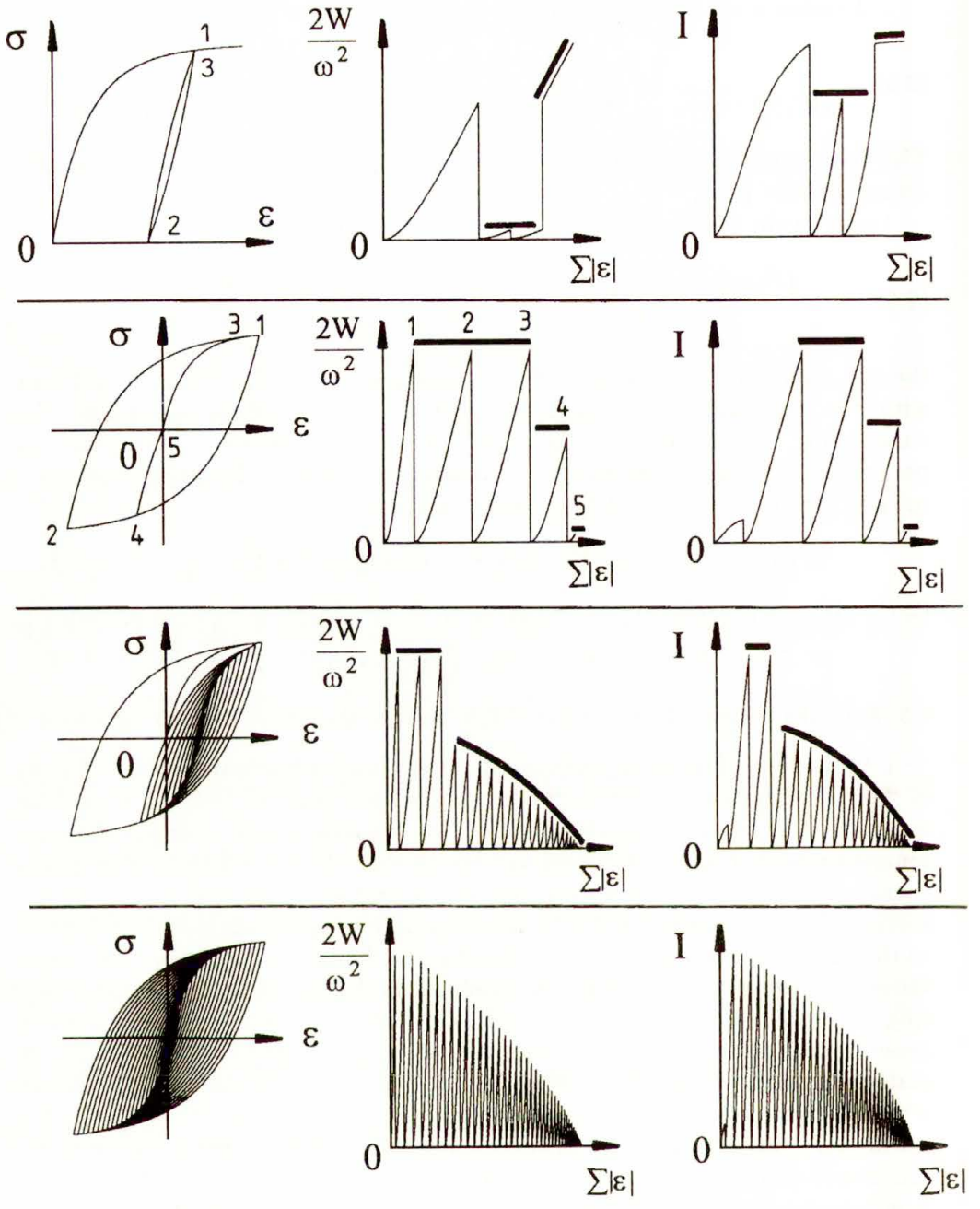

FIG. 1. Introduction of the sky-line notion through the one-dimensional form of the pattern.

the discrete and ordered series of the still memorised information $\{{}^{t}_{M}W\}$, $\{{}^{t}_{M}\sigma\}$. Taking as a starting point a well known, but often overlooked, graphical sketch, it is possible to stress the radical departure from the classical trend which is actually instilled by the discrete memory state notion.

ii. This well known graphical sketch gives the set of the individual states of spring strain of each couple for an imposed strain history (Fig. 2 a, where for sake of brevity S.S. is for *spring strain* reached at the current imposed strain; L.S. is for *limit strain* of a current couple of the model; S.E. is for *spring energy*; L.E. is for *limit energy*). Owing to (2.7), it is clear that, moreover, the strain variations $\Delta\,{}^{t}_{R}\varepsilon$ and the energy variations by intrinsic dissipation, W, are equivalent variables along each branch or arc of branch. Consequently, an equivalent graphical representation is possible if individual state of energy is associated with an imposed energy (Fig. 2 b, where the evolution of an ordered discrete set of *non-increasing* values of W may be conventionally displayed through the successive broken lines $\infty A0$, $\infty AB0$, $\infty ABC0$, ..., without introducing a physical definition of the $[0, \infty[$ axis of the integers). The specific "constitutive properties" (G_0, S_0, tanh function, ln cosh function) do not play any role, and the basic feature of the state appears: it is neither dimensional nor specific of a special reality (defined through parameters such as G_0 and functions such as tanh): it is basically generic and it involves an algorithm for the comparison of non-dimensional values.

The non-dimensional character is not restrictive, for it is sufficient in order to express the relative vicinity of the plastic limit of a couple, whatever may be the values of G_n and S_n: the interesting vicinity parameter of a given couple is the ratio S_n/G_n. The classical definition of the state is extensive-intensive in character ($S - T - \rho T dS$; $V - p - pdV/V$; $\varepsilon - \sigma - \sigma d\varepsilon$), and, in contrast, the new definition is basically topologic-algorithmic in character. In the pattern, this character is quite explicitly involved through (2.1), (2.3) and (2.4), but not clearly in (2.5). This point leads us to the question of the definition of the *unique thermomechanical neutral* state.

iii. Owing to the actual physical properties of the model, it is well known that after a fundamental *slowly decreasing cyclic* path, "symmetrical with respect to the origin", the demagnetized state is obtained: the graphical representation of this state is then close to the axis of abscissa (Figs. 2 c, 2 d, where for sake of brevity U.T.N. is for *unique thermomechanical neutral* state, I.H. is for *individual history*, F.L. is for *first loading*, E.L. is for *effective loading*, D.P. is for *demagnetisation process*, R.D.S. is for *remnant discrete set*). A similar state may be recurrently obtained, whatever may be the loading tentatively imposed in order to deviate from it (cf. [3], § 2.2.5). It cannot be identical with the axis itself, for the axis is the line of state for the incipient system, exclusively: this unique incipient state is always impossible to recover exactly, a property in accordance with the fact that the behaviour is always entirely irreversible. Returning

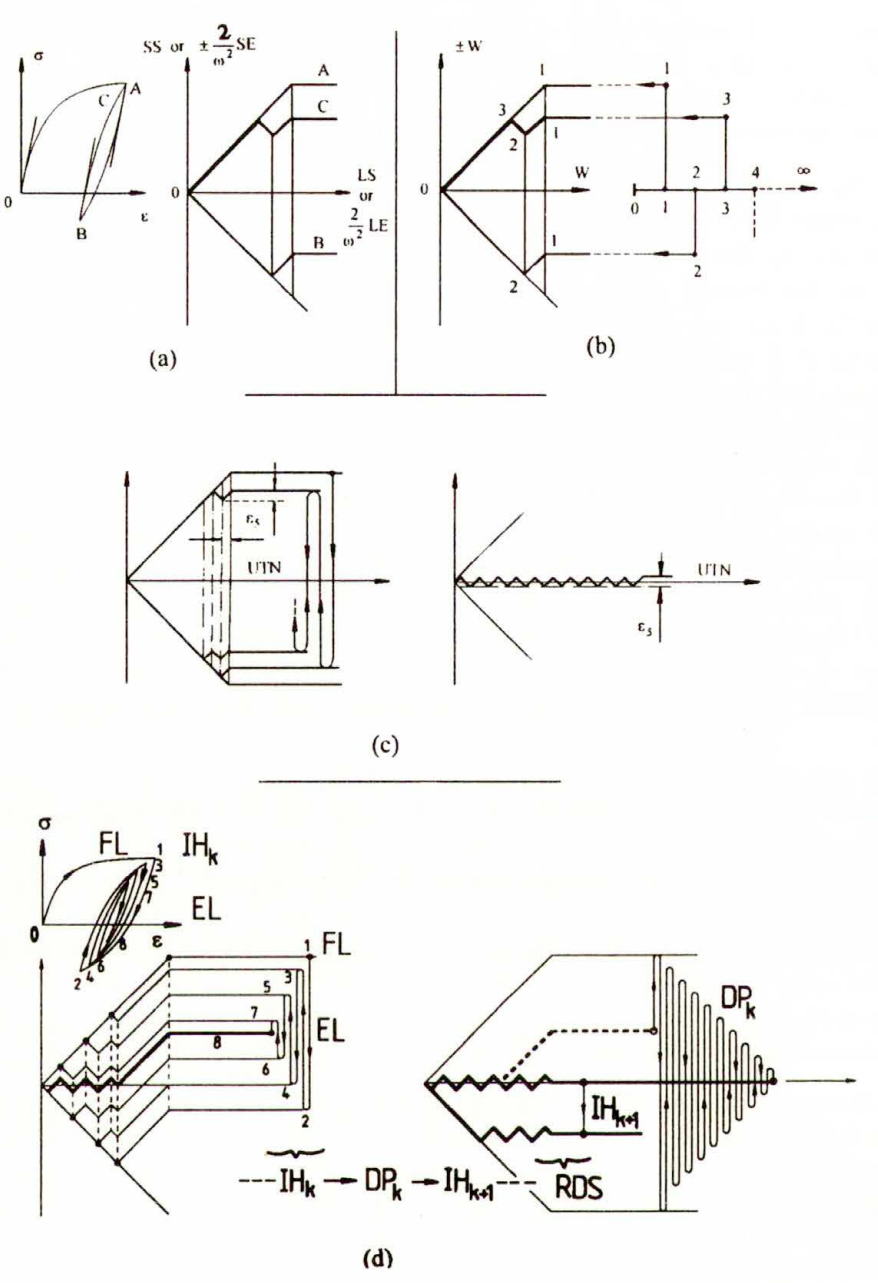

FIG. 2. Topological representation of the current states of the couples of the "springs-friction sliders" model or of the energetic state involved in the pattern.

to the physically relevant case, one notices that through a much more accurate demagnetisation-like process, the number of discrete information involved in the state is infinite: moreover, during any cyclic loading unable to fade the whole discrete set, the number of discrete information remains infinite (Fig. 2 d). Any sufficiently accurate demagnetisation-like process actually leads to a state which is so close to the (unique and unrecoverable) incipient state, that it is not necessary, practically, to discern between them. Hence, the set of all these states may be reduced to a unique state, recurrently recoverable. This *unique thermomechanical neutral* state may be defined with the aid of the unique approximation (2.5), provided that: 1) a sufficiently accurate demagnetised-like state exists, whatever the previous history may be; 2) a general strategy is defined in order to perform the indefinitely accurate demagnetisation. These conditions are fulfilled by the symbolic model and, obviously, by the one-dimensional pattern, built as close to the model as it is possible. In contrast, the fulfilment of these conditions is a puzzling problem in the three-dimensional, tensorial case. Consequently, the role of the fifth ingredient of the pattern is important at the level of physical principles [9, 10].

Indeed, it is well known that, when the principle of determinism is understood in the classical sense supported by Painlevé (1910), any pattern introducing the history to define the current state must be taken as a provisional pattern: anyway, it must be considered as devoid of sound significance in order to foster the improvement of knowledge, for: "La conception d'après laquelle, pour prdire l'avenir d'un système matériel, il faudrait connaître tout son passé, est la négation même de la science" [9]. In contrast, the principle of determinism was originally proposed with a more broad view, implying a continuous improvement of knowledge though involving possibly the history together with the causality principle [10]. In that spirit, the intrinsic properties of the symbolic model may, for example, suggest the following: if a system is restorable and if, for different times of recovery, the set of initial "generalised" causes of this isolated system are the same up to a space translation, the same phenomena occur in the system after these different times, up to this space translation. Restoration is not involved in the case introduced by Picard (1907). Following the fundamental analysis of Picard, where, for the first time, the distinction is introduced between the variables which are "visibles" and those which are "cachées", the general equations may be Galilean invariant "...mais il n'est pas possible néanmoins de remonter le cours du temps". Accordingly, "Il n'est donc pas impossible qu'un système irréversible puisse être conservatif et obéisse aux lois générales de la mécanique classique". Following Picard, the case where all the variables are "visibles" is fanciful, for it involves that the system is entirely reversible and that, consequently, it will be possible to stem the tide of time. The classical point of view is essentially an assumption ("une hypothése de non-hérédité"). The caution of Picard [5] may

[5] The caution of Picard echoes that exhibited by Gibbs to the point of the limit of validity of its fundamental equation.

be justified through the symbolic model. This model is indeed endowed with the following properties: 1) the behaviour is always entirely irreversible; 2) the definition of the state involves the past history since the last conventional U.T.N. state obtained with the aid of an accurate demagnetisation-like process; 3) the behaviour is not only nearly reversible "locally" (to the right of any inversion at time t_R) following the DE CARBON analysis [11], but also "globally reversible from one *unique thermomechanical neutral* state to the following one"; 4) from the very beginning of the first loading history, the exact incipient state is lost forever. Being restorable as accurately as required, the model is then in accordance with the determinism in the broad meaning of the term. In the sequel of this paper a fifth point is suggested: in the tensorial, three-dimensional case, it is possible to introduce a generalised pattern involving a theoretical property, especially interesting with respect to the Painlevé–Picard dilemma: if an appropriate set of variables is hidden on purpose, a basic classical feature of the behaviour (in short, an invariant form of the strain-stress behaviour) may appear as reversible in spite of the utter irreversibility. This puzzling behaviour happens during the generalised demagnetisation-like process necessarily associated with the pattern. Being entirely irreversible although apparently "reversible", the pattern is an example of theory where the history plays a basic role, "..., mais dans des conditions plus complexes encore", as anticipated by Picard.

2.3. From the multiaxial pattern to the study of the demagnetisation-like problem in general form

i. The sketch of the multiaxial pattern has been introduced previously (cf. [6] § 2.2 and 2.3 or [4] pp. 1186–1189, for example). Basically, the pattern is defined by introducing, in the stress space of Ilyushin type (cf. [38] or [3], § 3.5, for example), surfaces (or loops) along which the intrinsic dissipation rate Φ is annihilated and, therefore, W is constant [12, 6, 4]. Moreover, owing to (2.2), one considers the stress rate defined by the differential-difference equations:

$$\frac{\partial}{\partial t}\sigma_j^i = a_0\delta_j^i + a_1 D_j^i + a_2 \Delta_R^t \overline{\sigma}_j^i, \qquad \overline{\sigma}_j^i = \sigma_j^i - \frac{1}{3} I_\sigma \delta_j^i . \tag{2.8}$$

The definition in the preferred reference frame being not studied in the present paper, (2.8) is given in the frame of the irrotational kinematics under consideration. This constitutive form leads to a simple reversible isotropic part as soon as:

$$\begin{aligned} a_0 = \lambda I_D , \qquad a_1 = 2\mu, \qquad a_2 = \beta_4 \overline{M} , \\ \beta_4 = -\mu/(\omega S_0)^2, \qquad \overline{M} = \operatorname{tr}(\Delta_R^t \overline{\sigma}\, \overline{\mathbf{D}}) \qquad I_D = \operatorname{tr}(\mathbf{D}). \end{aligned} \tag{2.9}$$

The deviatoric part and its associated invariant scalar form (similar to $(2.2)_1$) are then:

$$\frac{\partial}{\partial t}\overline{\sigma_j^i} = a_1 \overline{D_j^i} + a_2 \Delta_R^t \overline{\sigma_j^i} , \tag{2.10}$$

$$\dot{\overline{\Pi}}_{\Delta\bar{\sigma}} = 2\mu\left(1 - \frac{2\overline{\Pi}_{\Delta\bar{\sigma}}}{(\omega S_0)^2}\right)\overline{M}, \qquad 2\overline{\Pi}_{\Delta\bar{\sigma}} = \mathrm{tr}\,(\Delta\bar{\sigma}\,\Delta\bar{\sigma}) = Q_\sigma^2\,. \tag{2.11}$$

If $Q_0 = \sqrt{2}S_0$ is the radius of the Huber–von Mises circle, the above invariant form yields:

$$\begin{aligned} Q_\Delta^2 &= (\omega Q_0)^2\left[1 - \exp(-\mu W/S_0^2)\right], \\ W &= -(S_0^2/\mu)\ln\left[1 - (Q_\Delta/\omega Q_0)^2\right]. \end{aligned} \tag{2.12}$$

These forms are similar to (2.7). The generalization of (2.9), (2.10) is obtained substituting to $\overline{M}$ the expression (3.6) and substituting to ωS_0 a scalar functional taking into account two requirements. The first one is that of "orientation" in the stress space of Ilyushin: the relative vicinity of asymptotic states must be defined for any current point of an unloading stress path [12, 6, 4]. The second requirement is that of "compatibility": during the first loading the neutral paths are circles centred at the origin, suggesting therefore the use of a general basic assumption consisting of the similarity of neutral paths with respect to the measured or *a priori* specified yield limit [12, 6, 4]. The formal consequences of this similarity hypothesis of the neutral loci is expressed through the identity between the mechanical definition and the thermodynamic definition of the neutral paths, whatever the W level may be. For the given (circular) shape of the (von Mises) yield limit, this simple identification allows, once for all, to obtain the scalar functional:

$$\gamma_4 = \frac{Q_{\Delta\bar{\sigma}}}{2\mu}A, \qquad A = 2\tan(\varphi_{\Delta\bar{\sigma}} - \varphi_R), \tag{2.13}$$

and the required tensorial generalisation of $(2.2)_1$, (2.9), (2.10) is:

$$\frac{\partial}{\partial t}\overline{\sigma_j^i} = 2\mu\overline{D_j^i} + \beta_4\left(\overline{M} + \gamma_4\dot{\varphi}_{\Delta\bar{\sigma}}\right)\Delta_R^t\overline{\sigma_j^i}\,. \tag{2.14}$$

A first consequence of this generalization is that the onset of the first unloading gives rise to a discontinuous process obtained through the sliding of a relevant set of neutral loci and giving, to the right of an inversion event, a family of loci without intersections (Fig. 3, where it is worth to note two points: firstly, the strains associated with R_1, IR and C are large with respect to S_0/μ; secondly, IR is an unfavourable initial state because the family of neutral loci has jumped). Secondly, it is useful to notice that the discrete memory process remains founded on information sets regarding the current and the previous reference states [12, 4]. As a consequence, the generalisation of the algorithm of the pattern may be easily obtained making use of the set $\{{}_M\varphi_R\}$ and of the associated "previous set":

$$\left\{{}_M\varphi_{\rho R}\right\}_n = \{0,\ \varphi(t_1),\ \ldots\}_n$$

and introducing the possibility of coincidence of the W levels without closing a cycle [12, 4].

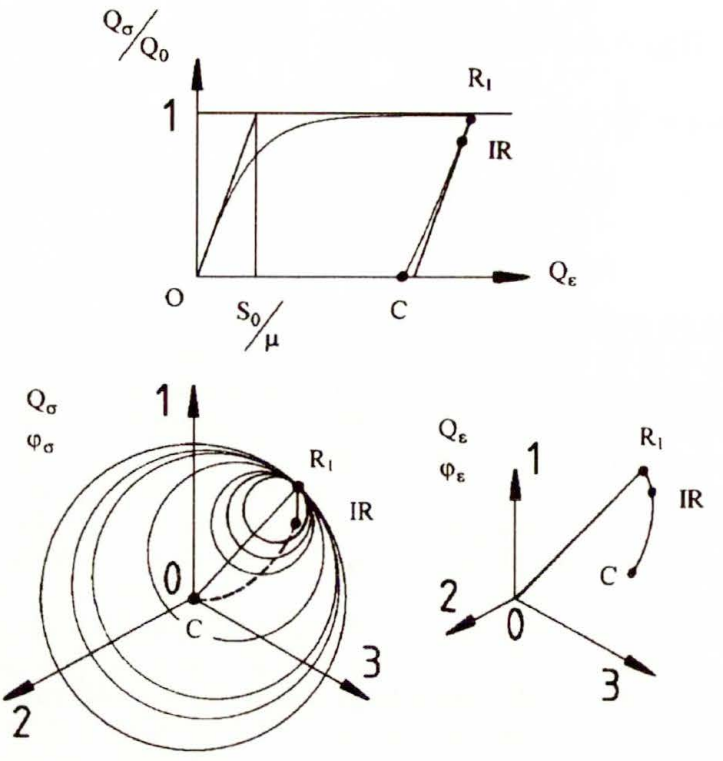

FIG. 3. Sketch suggesting the unfavourable initial residual states implemented in the study.

ii. The third consequence of the above process of generalisation is to give rise to a sophisticated feedback between the family of loci and the imposed cyclic loading. Accordingly, it becomes quite impossible to follow intuitively the global or local features of the functional correspondence between the stress and strain paths in the associated Ilyushin spaces (cf. Fig. 5 a, for example): neither the existence of the *unique thermomechanical neutral* state is *a priori* warranted, nor some intuitive set of strategies may be suggested (on the basis of some energetic or mathematical argument) as probably successful to recover it. The birth of the demagnetisation-like problem proceeds from this theoretical difficulty, necessarily involved in the definition of the pattern.

Moreover, it is now possible to give some hints regarding the notion of "unfavourable" remnant states. In short, such states are associated with strong irreversibility and weak symmetry of the family of iso-W loci. The first condition implies that large values of W are implemented. The second one implies that it is not necessary to start from a null field (stress) classical residual state: one may start the study of the demagnetisation-like process from the state IR (Fig. 3) close to R_1, the "historical field" (in the sense of CORB [13]).

3. A mechanical example suggesting the interest of a general study of the demagnetisation-like strategies

3.1. Towards a definition of the strategy

The main qualitative features of a strategy are, for example: the vicinity of the resulting demagnetised state to the idealised unique thermomechanical neutral state; the insensitivity or the weak dependence of this vicinity with respect to the loading; the question whether preliminary constitutive tests are required or not; the type of control. The main quantitative features are, basically, those associated with the accuracy of the recurrent recovery of a series of *unique thermomechanical neutral* states, lost as a result of successive loading paths which yield a series of successive associated residual states (Fig. 4, where the notations are those previously introduced in Fig. 2). If $\varepsilon_5 \ll 1$ denotes the vicinity parameter, the recovery of the idealised *unique thermomechanical neutral* state may be considered as obtained when

$$Q_\sigma/Q_0 < \varepsilon_5 \quad \text{or} \quad \min[W/(S_0^2/\mu)] < \varepsilon_5 \,. \tag{3.1}$$

If the insensitivity noticed above is warranted, a simple example is that of spiral-like type: the strategy is independent of preliminary constitutive tests, only stress-controlled, and the stress path is continuous up to any order. Then, the quantitative feature is the "pitch" of the spiral-like path; more precisely, the set of parameters involved in the definition of the family of paths. This case is

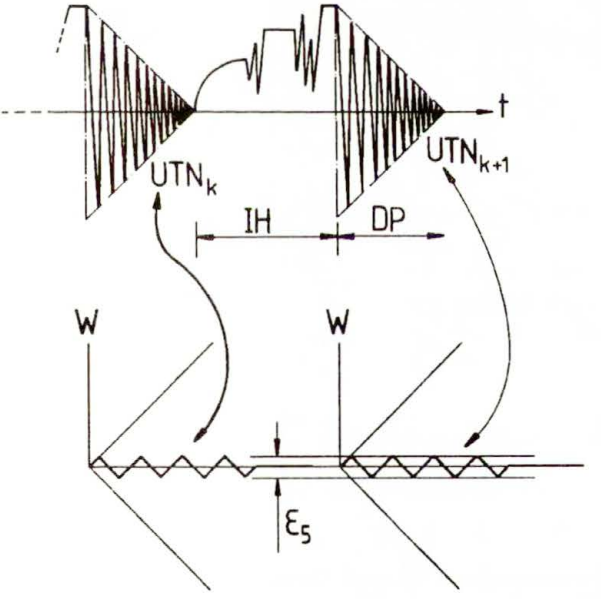

FIG. 4. Sketch suggesting the role of the fifth ingredient of the pattern.

studied below (§ 3.3). At this stage of the analysis one may limit oneself to a provisional definition which does not specify further the role of the variables of the state and of the constraints and costs: a strategy is then a family of stress paths allowing to obtain a series of accurate approximations of the idealised *unique thermomechanical neutral* state defined by the fifth ingredient of the pattern (Fig. 4). This vague definition will be commented upon later (§ 3.3, point viii).

3.2. Towards the choice of heuristic slowly decreasing cyclic stress paths

The aim of this paragraph is fourfold. Owing to the basic assumptions previously introduced (§ 1, point iii), the constitutive pattern may appear as rather theoretical and/or incomplete. It may be useful to counterbalance this (plausible) idea by showing that the model is nevertheless able to give results similar to those of the experiments. Secondly, it is useful to underline that intuitive strategies may prove to be immediately efficient as well as plainly false. Finally, it is useful to compare, even briefly, the piecewise continuous and the continuous slowly decreasing cyclic loading paths.

i. If one considers only simple classical mechanical paths (avoiding to implement neutral paths, for example), the properties of the pattern may appear as rather theoretical. However, if the first monotonous radial loading is followed by a constant pitch spiral first unloading path, then the properties of the pattern appear surprisingly unusual (Fig. 5 a, where Q denotes an invariant of the devia-

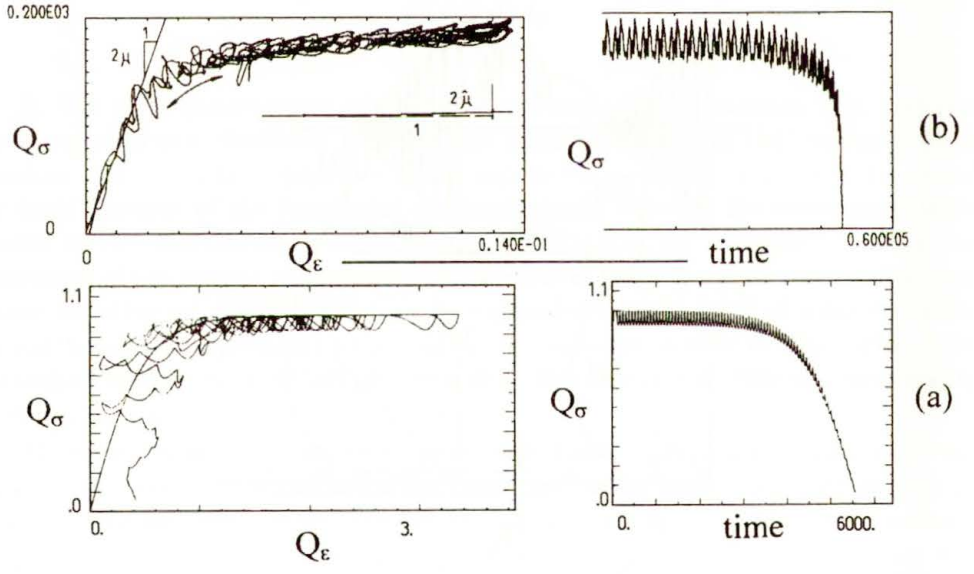

FIG. 5. Qualitative comparison between theoretical (a) and experimental (b) figures (stress-strain invariant diagrams are at left and stress second invariant – "time" diagrams are at right).

toric part of a tensor – cf. (2.11) for example) and the interesting point is that a similar figure is experimentally observed in the case of traction-torsion tests on thin tubes (Fig. 5 b, regarding the case of copper).

ii. It is easy to illustrate that intuitive simple strategies may yield rather encouraging results as well as grossly irrelevant ones. Typical examples of irrelevant strategies are obtained with the aid of unloading paths of one-dimensional type and of constant pitch spiral type: the trick consists of the neutral path which is included in the first loading process (Fig. 6, where the conventions of representation in the deviatoric planes of stress and strain are based on Cartesian axes XS and YS for the stress and XE and YE for the strain: these conventions allow to define the values of Q_σ/Q_0 and $Q_\varepsilon/S_0/\mu$).

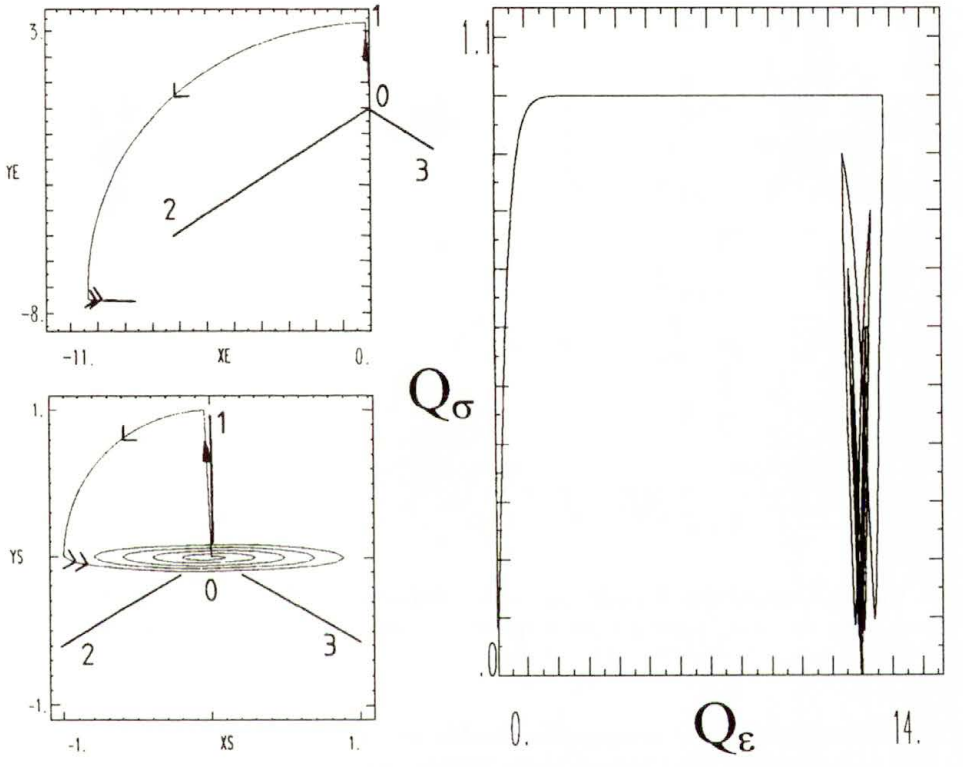

FIG. 6. An example of intuitive but unsuccessful continuous process of "demagnetisation".

iii. These examples are sufficient to suggest the interest of the simultaneous evolution of the intensity Q_σ and of the phase φ_σ of the stress deviator. Consequently, it is interesting to compare at least two types of S.D.C. stress paths, those which are piecewise radial and those which are continuous. The result may be summarised in mechanical form (Fig. 7, where the convention of the display is

that of Fig. 6). The interest of sophisticated paths is not obvious. The simplest type (the spiral-like one) of continuous path being actually cyclic, it must be, from now on, studied further.

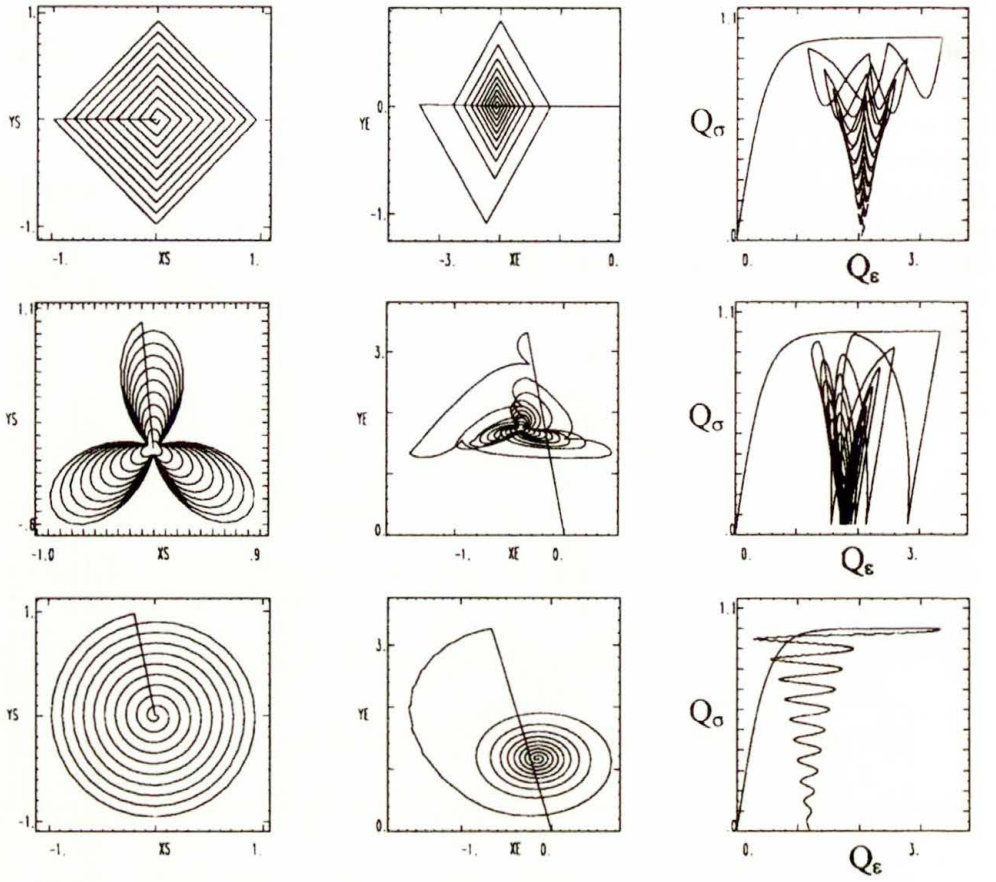

FIG. 7. Comparison between piecewise continuous and continuous processes: the 10 turns, constant pitch spiral-like case is relatively encouraging.

3.3. Towards the study of demagnetisation-like process in the special case of the spiral-like S.D.C. stress paths of slow-fast type

The numerical integrations are performed restricting to $n = 10$ the number of turns of the demagnetisation-like paths. Each turn of any spiral-like stress path is a 32-sides regular polyhedron, each side being described by 200 steps. From one point to the following one, the integration is obtained with the aid of a Runge–Kutta–Merson algorithm allowing an imposed accuracy provided that the number of subdivisions of a step remains smaller than 20. Owing to these numerical conditions, the integration can be performed "in a relevant way" even

when the state of stress is "very near" the Huber–von Mises limit surface, that is to say such as the difference $1 - Q_\sigma/Q_0$ is as small as 10^{-7}.

i. The parameter of the unfavourable residual state is defined as follows. Firstly, a radial first loading up to Q_σ sufficiently close to Q_0 to warrant a dissipated energy to be very much larger than S_0^2/μ ($W = nw \cdot S_0^2/\mu$, $nw \gg 1$), is performed. The parameter nw may be used to compare the subsequent numerical simulation imposing similar initial state of strain. Secondly, the radial first loading is followed by the small unloading of the first step of the integration, setting the iso-W circles in the most unfavourable non-symmetric state (point IR of Fig. 3).

ii. The simple strategy under consideration is spiral-like and of the slow-fast type to be understood as follows: the imposed variation of the deviatoric radius Q is defined by following the course of the first loading in reverse. The rate of the phase is defined by introducing a scalar parameter $n\varphi$. The associated formulas are given below (point iii).

iii. As suggested by (2.11) and $(2.2)_1$, the relative stress intensity and the reverse rule are obtained, with $\omega = 1$, starting from

$$
\begin{aligned}
Q_\Delta \, dQ_\Delta &= 2\mu \left(1 - \left(\frac{Q}{Q_0}\right)^c\right) \overline{M} \, dt, \\
\overline{M} \, dt &= Q_\Delta Q_D \, dt = Q_\Delta \, dQ_\varepsilon \,, \\
\omega &= 1, \qquad dW = \frac{2\overline{M}}{\omega^2} \,.
\end{aligned} \tag{3.2}
$$

Convenient values of c are 2/3, 1, 2. Owing to the reverse rule, the associated imposed S.D.C. stress paths are defined as follows. Let us introduce two parameters c_r and ξ, c_r playing the role of the constitutive parameter c and ξ being a "vicinity" parameter of the order of 10^{-7}. For $c_r = c_2$, and if HFR is for the historical field of Corb used as reference state, the associated relative stress x_R and the S.D.C. loading path definition are:

$$
\begin{aligned}
x_R &= \frac{Q_{\mathrm{HFR}}}{Q_0} = (1 - \xi)\left(1 - \exp\left(\frac{-\mu n w c_r}{Q_0^2}\right)\right)^{1/c_r}, \\
Q_{\mathrm{spiral}}(\varphi_\sigma) &= Q_0 \tanh(k_s(2\pi n - \varphi_\sigma)), \\
2\pi n k_s &= \frac{1}{2} \ln\left(\frac{1 + x_R}{1 - x_R}\right) = \tanh^{-1}(x_R)
\end{aligned} \tag{3.3}
$$

and for $c_r = c_1$ $(= 1)$, one obtains the same form regarding x_R, but the definition of Q_{spiral} is:

$$
Q_{\mathrm{spiral}}(\varphi_\sigma) = Q_0 \left(1 - \exp\left[k_s(2\pi n - \varphi_\sigma)\right]\right), \qquad 2\pi n k_s = \ln(1 - x_R). \tag{3.4}
$$

In the case of $c_r = c_0$ $(= 2/3)$, only an approximate definition of the S.D.C. stress path is available. It is obtained by neglecting the terms which are not of the $\ln(1 - Q/Q_0)$ form. For Q close to Q_0 this approximation results in the same form of the definition of x_R, because a factor $5 - 4(Q/Q_0)^{2/3}$ is close to 1. Hence:

$$x_R = (1 - \xi)\left(1 - \exp\left(\frac{-3nw\mu}{S_0^2}\right)^{3/2}\right).$$

A simple form may be used to define a function Q_{spiral} which is close to the exact solution of:

$$d\left(\frac{Q_\sigma}{Q_0}\right) \Big/ \left[1 - \left(\frac{Q_\sigma}{Q_0}\right)^{2/3}\right] = \left(\frac{2\mu}{Q_0}\right) dQ_\varepsilon$$

when Q_σ is close to Q_0. The form:

$$(3.5) \qquad Q_{\text{spiral}}(\varphi) = Q_0\left(1 - \exp\left((2\pi n - \varphi)k_s\right)^3\right), \qquad 2\pi n k_s = \ln(1 - x_R^{1/3}),$$

is simple and similar to that of the previous "exponential" case defined by (3.4).

iv. The numerical integration is performed with the following set of parameters: $S_0 = 200\,\text{MPa}$, $\mu = 75\,\text{GPa}$, $c = c_i$ $(i = 0, 1, 2,\ c_i = 2/3, 1, 2$ for example). A typical result is given under the usual mechanical form (Fig. 8, where the convention of the display is that of Fig. 6) and also under thermodynamic form (Fig. 9, where the discontinuities of the sky-lines are pointed out by the arrows, and where the strain measure $Q_\varepsilon^{\text{rad}}$ – cf. [4], equations (44) to (49) – is obtained by integration of a rate – Φ/Q_σ – which is of radial type in the Ilyushin space). One notices the following points: first, the number of inversion points is much greater than in the cases sketched in Fig. 7; secondly, the continuity and convexity of the W and I sky-lines are made conspicuous; thirdly, the spiral-like response in the strain space is of almost constant pitch type; fourthly, the unfavourable remnant state is not actually highly unfavourable, for the initial remnant strain (of the order of 510^{-3}) remains of the order of magnitude of $S_o/2\mu$.

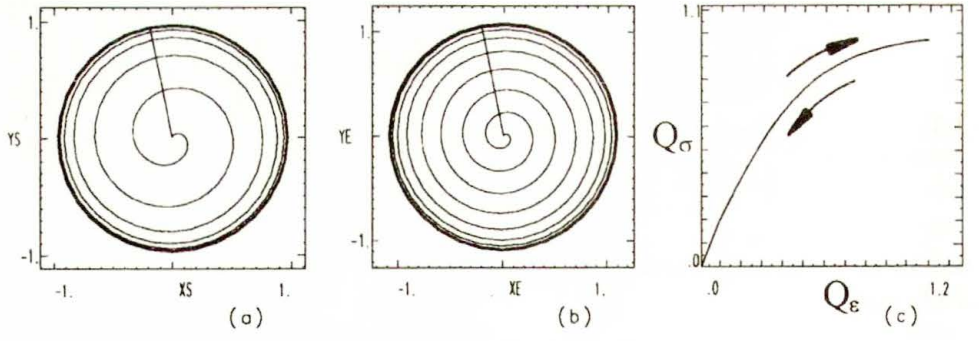

FIG. 8. An example of slow-fast spiral-like strategy.

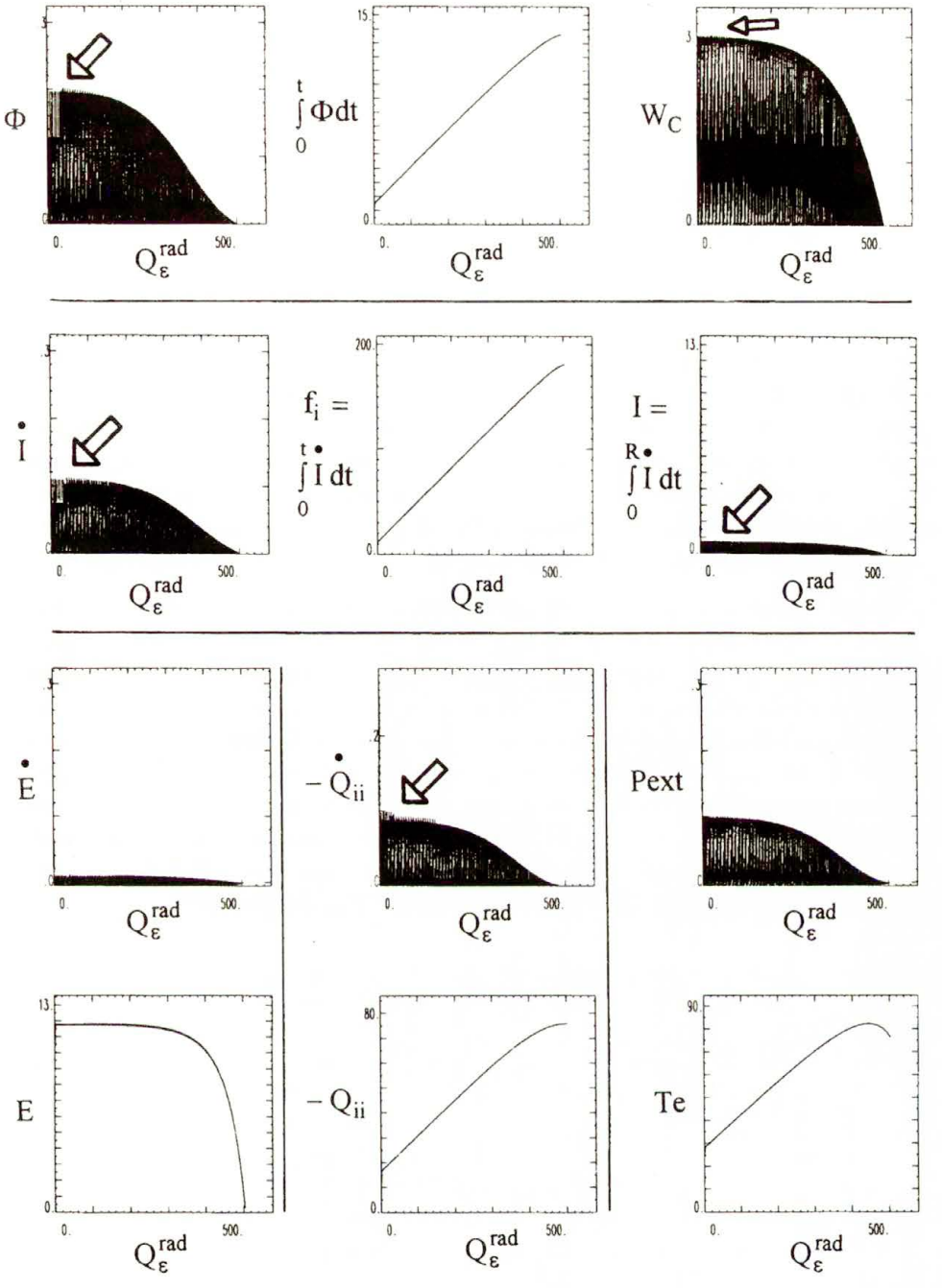

FIG. 9. Thermomechanics associated with the cyclic evolution introduced through Fig. 8.

v. A set of numerical simulations has been performed in order to study the role of increasingly large remnant strains with respect to the accuracy of the recovery of the U.T.N. state. The values of nw was: 8, 12, 16 for $c = c_2$; 12, 24, 32 for $c = c_1$; 24, 32, 48 for $c = c_0$. The last set is introduced (Fig. 10, where $Q\varepsilon/4$ is of the order of the elongation K in percent, and where it is possible to verify that the behaviour is similar to that of Fig. 5 a through the enlargement of the location pointed out by the symbol *). One notices the following points: firstly, the recovering of the remnant strain is more difficult to obtain for large c (convenient in the case of "hard" ferromagnetic materials) as well as for large residual strains; the strain response is coarsely similar to a constant pitch spiral when the demagnetisation-like process is not too bad, and the first turn is of importance for it is not well centred if the imposed stress state gets away too quickly from the limit Huber–von Mises circle; the W sky-line is strongly discontinuous when the recovery is only roughly performed; the lack of recovery is not associated with the breaking through the transition range; even when the relative recovery is very weak because the absolute recovery is constant, the final strain state remains on the first loading path obtained in the strain space.

vi. The purpose of the present paragraph is temporarily neglected in order to suggest without delay that the special results obtained above (as encouraging as they may be) do not necessarily warrant further success: the generalisation to the five (six)-dimensional case is still an open problem. Even if one relays on the previous analysis, it is indeed once more impossible to foresee the existence of the *unique thermomechanical neutral* state and the feature of a simple strategy: the origin of the difficulty is not associated with the appearance of a cumbersome formalism. Let σ_n $(n = 1, ..., 6)$ denote the components of the Cauchy stress tensor σ in the preferred reference frame. The associated Ilyushin deviatoric representation $(Q, \varphi^d, \theta_1, \theta_2, \theta_3)$ of the deviator $\overline{\sigma}$ is defined by:

$$Q^2 = q^2 + 2\sum_4^6 \sigma_n^2, \qquad q^2 = \sum_1^3 \overline{\sigma}_n^2,$$

$$\overline{\sigma}_1 = q\left(\frac{2}{3}\right)^{1/2} \cos\varphi^d, \qquad \overline{\sigma}_2 = q\left(\frac{2}{3}\right)^{1/2} \cos\left(\varphi^d - \frac{2\pi}{3}\right),$$

$$\overline{\sigma}_3 = q\left(\frac{2}{3}\right)^{1/2} \cos\left(\varphi^d + \frac{2\pi}{3}\right),$$

$$\sigma_{n+3} = \frac{Q}{\sqrt{2}} \cos\theta_n, \qquad n = 1, 2, 3.$$

Owing to the Huber–von Mises assumption, the yield surface is an hypersphere of the Ilyushin space and, by hypothesis, the neutral surfaces are also hyperspheres. This is the origin of the difficulty regarding the demagnetisation-like problem: the discontinuous feedback process between the "sliding of the neutral spheres"

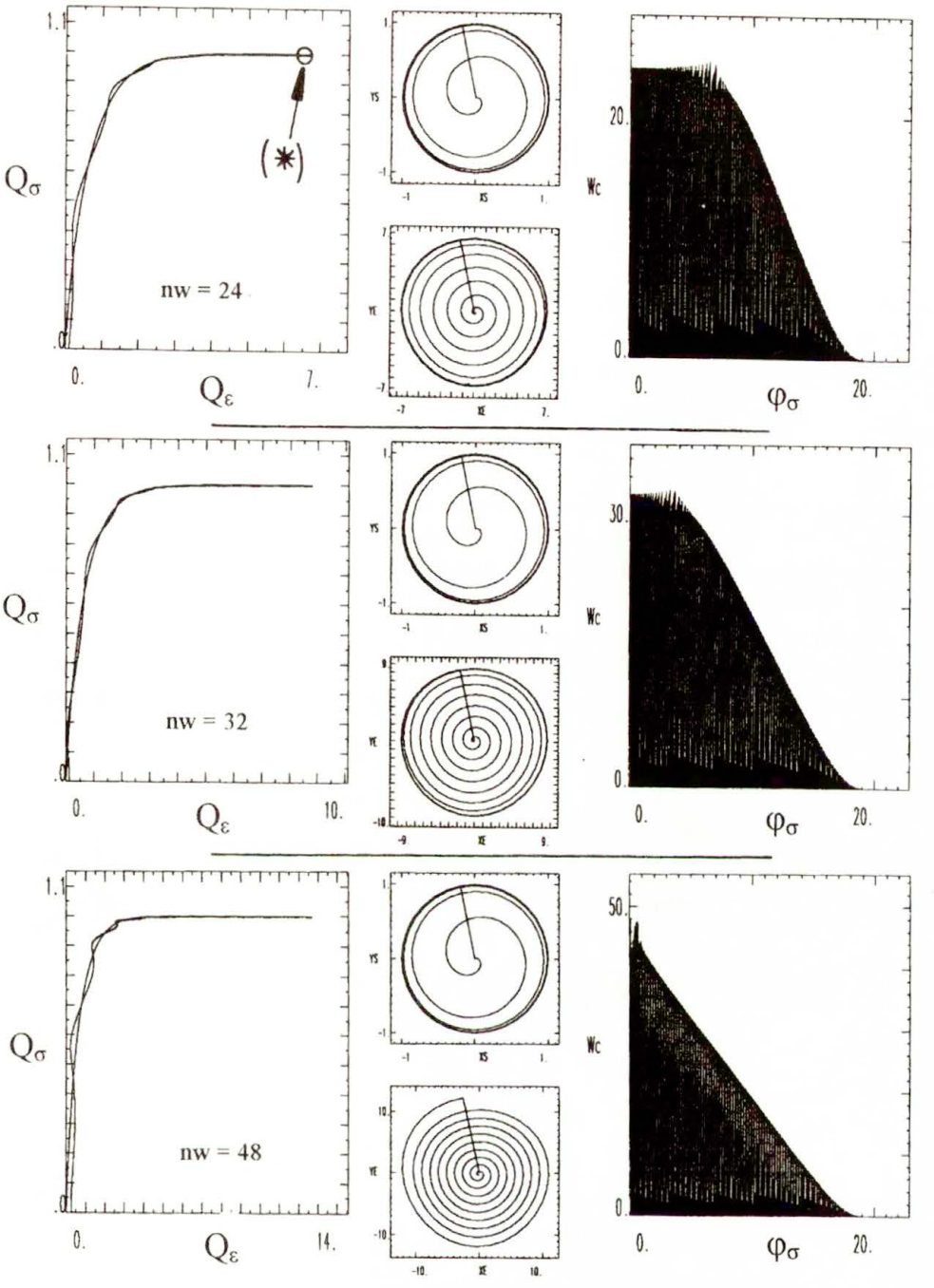

FIG. 10. Trying for demagnetisation of increasingly large residual strains ($c = c_0 = c_r$, $\xi = 10^{-7}$).

and the imposed cyclic loading may be, *a priori*, infinitely more sophisticated than in the simplest deviatoric situation studied above. In this simple situation, the ratio of the circumferencial path to the radial path was large in order to go along the yield circle "for a long time": the question is now to warrant that a four-dimensional path is able to go along "for a long 4-time" and in a relevant way. The point is more puzzling than the cumbersome character of the formal features, already briefly suggested elsewhere [3].

It is worth noting that one of the main interests of the present digression is also to point out the puzzling problem of the physical interpretation of the Cauchy stress tensor, a problem which is made conspicuous through the intrinsic dissipation form:

$$\overline{\Phi} = \Gamma \dot{p} + \left[(\overline{M} + \gamma_4 \dot{\varphi}^d)_{\text{spiral}} + (\delta_{41}\dot{\theta}_1 + \delta_{42}\dot{\theta}_2 + \delta_{43}\dot{\theta}_3)_{\text{cyclic}} \right] \tag{3.6}$$

of discrete memory type through the scalar functionals Γ, γ_4, δ_{4n} $(n = 1, 2, 3)$. The first term of the right-hand is related to the possible isotropic-deviatoric coupling effects, and the bracket suggests the distinction "$(Q, \varphi)_{\text{spiral}}$" versus "$(\theta)_{\text{cyclic}}$", and the special interest of shear tests and of approaches similar to that introduced by LODGE regarding shear flows [39]. Consequently, a strategy *a priori* interesting is that of (θ-cyclic)-(φ-spiral-like) wrapping type (Fig. 11 a, where the deviatoric plane of Ilyushin is equatorial and where the initial point 0 plays a role

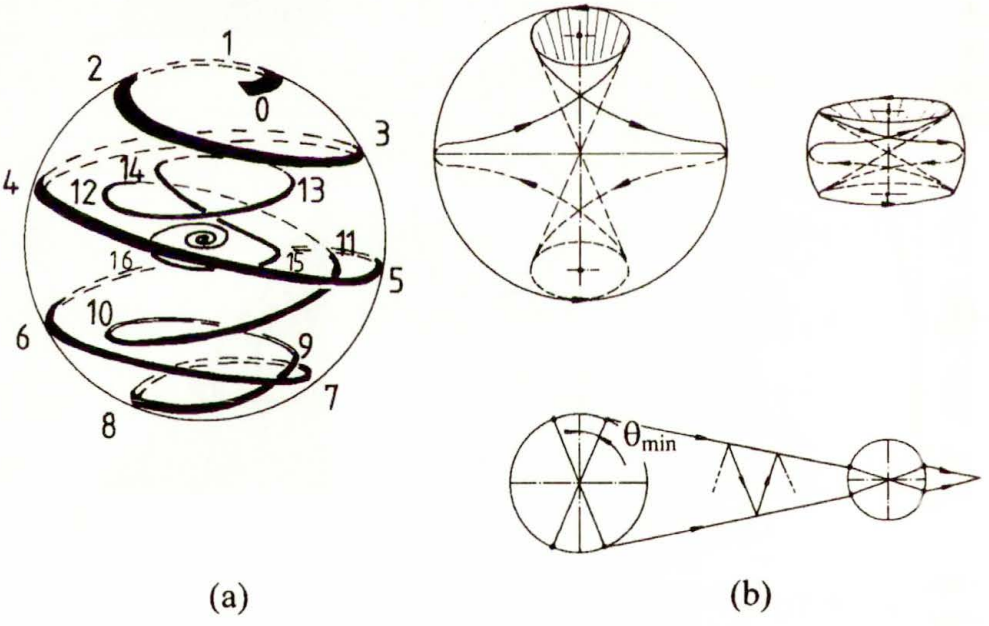

FIG. 11. Sketch of the multiaxial demagnetisation through the $(\theta_{\text{cyclic}} - \varphi_{\text{spiral}})$ wrapping.

similar to that of IR in Fig. 3). It can be generalized under the "3-wrapping" form (curves of the five-dimensional Ilyushin space yielded through three simultaneous wrappings of symmetric *slowly decreasing cyclic* type, as sketched in Fig. 11 b). This strategy is interesting as soon as the preferred reference frame problem is considered because a cyclic process must be imposed on the shear stress components through a symmetric *slowly decreasing cyclic* path starting from the interval $[\theta_{\min},\ \pi - \theta_{\min}]$ and leading to the $\pi/2$ value, so as to recover this frame [3].

vii. Let us now return to the problem of the Unique Thermomechanical Neutral state, underlining the relationship between the state of disorder and the state of dissipated energy.

The effective *evolution* $E(S_0, \mu, c)$ is to be understood as a series of couples of individual history (demagnetisation-like) processes through a relevant *slowly decreasing cyclic* paths. Each individual history is a sequence of two paths, the first loading and the effective loading path, and each demagnetisation leads to an approximate *unique thermomechanical neutral* state (Fig. 4). In the simple tensorial case studied above, the situation is not so clear as in the one-dimensional case. When σ tends towards zero, each successive disorder-order outburst tends also towards zero by definition of the pattern, and the external control does not introduce variations of disorder during the evolution from one individual history to the next one. In spite of the fact that no mathematical proof has been provided, the result obtained above leads to the conclusion that a necessary condition to recover a fading strain $\Delta_R^t\varepsilon$ is the continuity of the W sky-line during a demagnetisation-like process. However, the *unique thermomechanical neutral* state is no more defined through the simple scalar form of differences $W_k - W_{k+1}$: the evolution of the centres of the iso-W circles (Fig. 3) is now associated with the W sky-line continuity. For very large W never reached, the location of the centers is the axis. For the largest values actually reached and involved at the beginning of the demagnetisation-like process, the jumps of the centers are small and the short shaking leads quickly to the final positions of the centres: by contrast, the jumps of the centers are large and the required shaking lengthened for the small values of W leading also, but with "delay" (not viscous delay), to the final positions of the associated centres. The approximate *unique thermomechanical neutral* state is associated with the set of the final positions of the centres of iso-W circles. The geometry of this set is not studied. Even in the spiral-like simple case, the numerical investigation is cumbersome: to study, for example, a conjecture of helix-like geometry with envelope of fading radius, it must involve a very large number of inversion points.

viii. Among the results obtained through numerical evidences it is worth to note the following points: the approximate *unique thermomechanical neutral* state may be obtained through a spiral-like *slowly decreasing cyclic* loading path in the stress (field) Ilyushin space (reduced to a plane in the case under consider-

ation) and the pattern is therefore deterministic in the broad sense of the term; during a *slowly decreasing cyclic* loading path of demagnetisation, the behaviour exhibits a mechanical feature which looks like that of the reversible type in spite of the fact that the process is entirely irreversible (cf. point v); the first loading behaviour and the feature of the demagnetisation-like process are associated (cf. point v) in a way which is a generalisation of the one-dimensional property, namely: the apexes of the symmetric cycles are on the first loading curve; the first loading appears as the generic form of the basic demagnetisation-like feature (cf. point ii) which is necessary in order to obtain the recurrent recovery of the line of the *evolution* $E(S_0, \mu, c)$: in short, ontogenesis recurs philogenesis; regarding the dissipated energy, the main part of an evolution consists of the demagnetisation-like processes. By contrast, regarding the total variation of internal energy, the main part of the evolution consists of the individual histories. Moreover, cyclic disorder-order outbursts are permanent.

4. Remarks on experimental evidence supporting the notion of idealised systems entirely irreversible although rejuvenating

4.1. Plastic hysteresis and the mesoscale problem

i. Both at the elementary microscale (dislocation pinning effect, Frank – Read source effect) and at the usual macroscale (push-pull, traction-torsion and shear tests at constant temperature and low "constant" strain rate) it is now clear that the behaviour of polycrystal-like materials is of pure hysteresis type when the rates of all "hardening" or "softening" effects simultaneously fade temporarily or finally [14, 15, 16]. It is also worth noting that the genuine nature of granular media behaviour is directly taken into account with the aid of the pattern of pure hysteresis extended to the case of isotropic and deviatoric coupling effects [6].

ii. However, the situation may appear as quite puzzling at the scale of the mesoscale substructures of the material point (walls, veins and microbands of various types, and labyrinths). This scale is that of the "natural intermediate level of milli-structure" introduced by KRUMHANSL [40]. For nearly 30 years it has been possible to observe such mesostructures, especially in the case of fatigue tests [17, 18, 19, 20]. The microanalysis has been generally performed in the null stress, residual strain state. Accordingly, given the current stage of results, to introduce a basic assumption of pure hysteresis type, namely the actual possibility of cyclic steady annihilation and creation of the mesostructures periodically converted one into another, is neither intuitive nor evident, in spite of the impressive number of available references [21]. Moreover, the consequences of a demagnetisation-like process have never been studied, involving possibly a basic gap in the experimental approach.

iii. The question of mesoscale structures may be provisionally revisited bringing together, from now on, the fields of plastic hysteresis and the field of ferrohysteresis. Such an attempt follows the analysis given by Friedel in his preface to the summer school at YRAVALS [22]: "Si ces dislocations sont retenues dans les cristaux, c'est par une friction solide qui les y bloque et qu'il faut surmonter pour les propager et les multiplier: sauf dans le cas extrême du fluage de Nabarro pur, la plasticité des cristaux a nécessairement ce caractère hystérétique violent qui la rapproche des phénomènes d'aimantation des corps ferromagntiques; tout indique qu'il en est de même de la plasticité à froid des amorphes."

4.2. Ferrohysteresis as the current genuine heuristic case

i. It is well known that, at macroscale, the behaviour of ferromagnets is compatible with the pure hysteresis pattern and that the accuracy and the repeatability of the demagnetisation-like process is of basic technological importance [23]: a similar situation exists regarding micro-devices implying high information densities [24].

ii. It is also possible to underline a rather relevant compatibility at the microscale level (cf. for example, [3, 25, 26, 24]). However, a comprehensive study is both out of the range of this paper and beyond the competence of the authors. The aim is "only" to underline an important experimental result, extremely difficult to obtain in the arena of mechanical tests: during a cyclic loading of fatigue type, field-controlled on the interval $[0, H]$, the microstructural pattern is cyclic, periodically restored [25, 26], as recalled by the sketch (Fig. 12, where the interpretation of the imperfect recovery attracts our attention to the analysis of RAYLEIGH [27]).

iii. However, the afore-mentioned restoration is not perfect. In spite of the "structural stability" of the sample (thin layer of a single crystal endowed with an initial lattice of bubbles), a "loss of memory" [25] is observed when many field cycles are applied. One notices also that no demagnetisation-like process is implemented in order to study the possible restoration of the initial lattice of bubbles. Moreover, the result is obtained by implementing a process which is basically one-dimensional and infinitely more simple than the processes which may be involved in three-dimensional mechanical samples submitted to multiaxial loading. One may also add that the coupled fields effects are not encompassed in the investigation [28, 29, 30]. Nevertheless, the special result under consideration may be remembered as sufficient in order to clarify the enigma of "restoration at all relevant scales" and associated appearance of reversibility yielded by an entirely irreversible system. Invariant material defect allows material discrete memory, Néel relationship between reversibility and irreversibility, and exchange of various forms of energy, including, at the ordinary point of a branch of cycle, that associated with disorder.

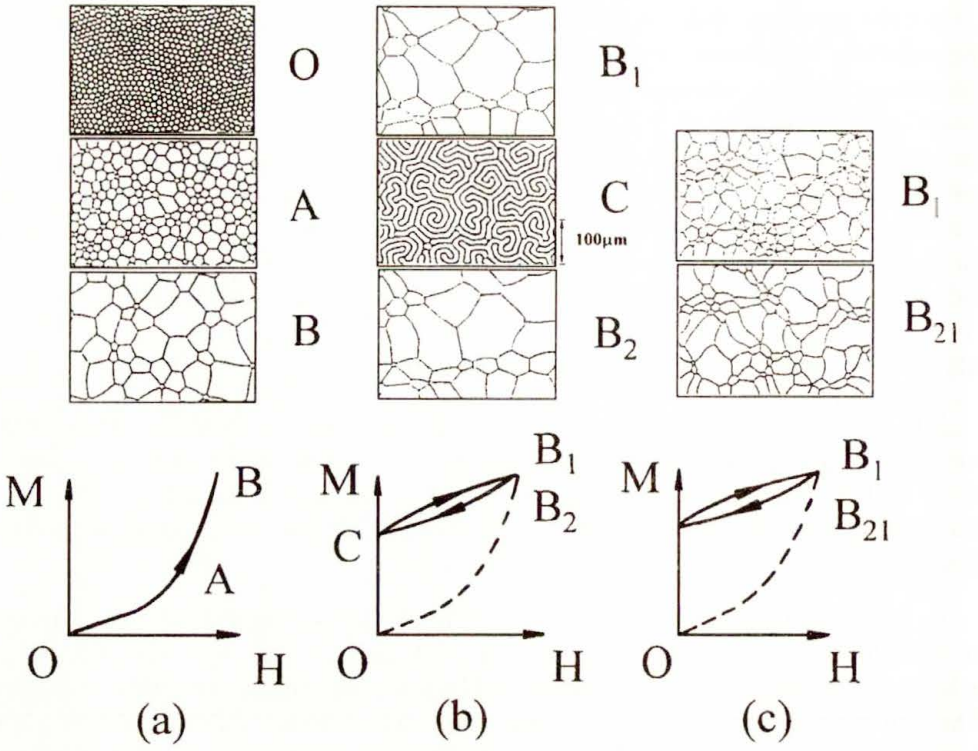

FIG. 12. Evolution of a bubble lattice (from Figs. 1, 2 and 3 of [26]): a) first loading; b) fatigue-like effective loading with almost recovered labyrinth and cellular patterns associated with null field and maximum field, respectively; c) however, the cellular pattern is not perfectly recoverable whatever may be the number of cycles.

5. Concluding remarks

i. One encouraging result has been obtained (§ 3.3 point v), suggesting what may be, perhaps, the simplest strategy available to tackle the demagnetisation-like problem. However, neither the isotropic six-dimensional "general" case, nor the role of the preferred reference frame, nor even the problem of the anisotropic cases have been studied comprehensively enough. Neither were they exemplified through any special results: the general pattern of pure hysteresis remains insufficiently investigated regarding these basic theoretical features. Accordingly, the study of the features which are of outstanding interest for engineers, such as hardening, "viscous" effects [32] or coupled fields effects, is still rather untimely. But it is worth noting that the implementation of the current pure hysteresis pattern in finite element approaches is from now on, relevant in order to prepare for the numerical simulation of the six-dimensional pattern and of the general kinematics in the coming years [33, 34, 35].

ii. In its current state, the pattern of pure hysteresis is, from now on, heuristic when some particular insight is needed at the level of fundamental microscopic processes involving the notion of dislocation [3, 14, 15, 16]. Accordingly, if a general phenomenological theory may be introduced under the five (or six)-dimensional form (§ 3.3, point vi), most likely it will not be entirely incomplete in the sense of BUNGE [31], especially regarding the problem of the (basically three-dimensional) second order effects, of the generalised ratchet type.

iii. The present provisional study of demagnetisation-like mechanical processes may be transposed to the case of ferrohysteresis (cf. Footnote 2). It is worth noting that the discrete memory pattern is then useful in order to avoid, from time to time, the drawbacks initiated through the implementation of basic classical concepts. For example, the "anomalous" effect introduced in [36] may be immediately recognised as normal in the frame of the discrete memory pattern: the increase of magnetisation along the path going from H_1 to H_2 (Fig. 1 of [36] is indeed a standard hysteresis behaviour [3].

Appendix. Two basic rates – those of internal energy and of internal intrinsic heat supply-involved by the symbolic model

i. If $g''(e)\,de$ denotes the rigidity coefficient for the couples having their limit strain values between e and $e+de$, and if ε is the current external strain imposed during the first monotonic loading, then the resulting stress for the couples whose limit value is not reached is:

$$\sigma_1 = \int_{\varepsilon}^{\infty} \varepsilon g''(e)\,de.$$

For the other couples for which the friction slider move, the resulting stress is:

$$\sigma_2 = \int_{\varepsilon}^{\infty} e g''(e)\,de.$$

The total stress is:

$$\sigma = G_0\varepsilon - g(\varepsilon) = S(\varepsilon), \qquad G_0 = \int_0^{\infty} g''(e)\,de = g'(\infty), \qquad g'' = -\sigma'' \geq 0.$$

The internal power is then:

$$P_i = -\sigma_1\dot{\varepsilon} - \sigma_2\dot{\varepsilon} = -\sigma\dot{\varepsilon} = -(G_0\varepsilon - g(\varepsilon))\dot{\varepsilon} = -S(\varepsilon)\dot{\varepsilon}\,.$$

The mechanical behaviour is described in terms of the function $g(e)$ such as:

$$g(0) = 0, \qquad g'(0) = g'(\infty) - G_0 = 0, \qquad g''(0) = g''(\infty) = 0.$$

The curvature rule is: g'' is not negative on R^+, the interval of definition of g.

ii. By definition of s_1 and s_2, the basic rates are:

$$\dot{E} = \varepsilon\dot{\sigma}(\varepsilon) = \sigma\dot{\varepsilon} - (\sigma\dot{\varepsilon} - \varepsilon\dot{\sigma}) = -P_i + \dot{Q}_{ii}\,,$$
$$-\dot{Q}_{ii}(\varepsilon) \equiv \sigma_2\dot{\varepsilon} = \sigma(\varepsilon)\dot{\varepsilon} - \varepsilon\dot{\sigma}(\varepsilon)$$

in the first loading case and, in the cyclic case:

$$\Delta\,{}^{t}_{R}\sigma = \int_{\Delta\varepsilon/2}^{\infty} \Delta\varepsilon g''(e)\,de + \int_{0}^{\Delta\varepsilon/2} 2eg''(e)\,de$$
$$= 2\left[G_0\frac{\Delta\varepsilon}{2} - g\left(\frac{\Delta\varepsilon}{2}\right)\right] = 2S\left(\frac{\Delta\varepsilon}{2}\right),$$
$$-2\dot{Q}_{ii}(\Delta\,{}^{t}_{R}\varepsilon) = \Delta\,{}^{t}_{R}\sigma\frac{\partial}{\partial t}\Delta\,{}^{t}_{R}\varepsilon - \Delta\,{}^{t}_{R}\varepsilon\frac{\partial}{\partial t}\Delta\,{}^{t}_{R}\sigma\,,$$
$$2\dot{E}(\Delta\,{}^{t}_{R}\varepsilon) = (\sigma + {}^{t}_{R}\sigma)\frac{\partial}{\partial t}\Delta\,{}^{t}_{R}\varepsilon + \Delta\,{}^{t}_{R}\varepsilon\frac{\partial}{\partial t}\Delta\,{}^{t}_{R}\sigma\,.$$

The generic description of the cyclic properties is then $(2.2)_2$.

References

1. P. GUELIN, W.K. NOWACKI and P. PEGON, *Etude des schémas thermomécaniques à mémoire discrete: bases physiques et formalisme du schéma d'hystérésis pure*, Arch. Mech., **37**, 4-5, pp. 343–363, 1985.
2. P. PEGON and P. GUELIN, *Etude des schémas thermomécaniques à mémoire discrete: problèmes aux limites en grandes déformations élastoplastiques*, ibid, pp. 465–483.
3. A. TOURABI, P. GUELIN and D. FAVIER, *Towards the modelling of deformable ferromagnets and ferroelectrics*, Arch. Mech., **47**, 3, pp. 437–483, 1995.
4. A. TOURABI, P. GUELIN, B. WACK, P. PEGON, D. FAVIER and W.K. NOWACKI, *Useful scalar parameters for multiaxial fatigue studies*, Fatigue Fract. Engng. Mater. Struct., **19**, 10, pp. 1181–1195, 1996.
5. D. FAVIER, P. GUELIN, A. TOURABI, B. WACK and P. PEGON, *Ecrouissages schémas thermomécaniques et à variables internes: Méthode de définition utilisant le concept d'Hystérésis pure*, Arch. Mech., **40**, 5-6, pp. 611–640, 1988.
6. P. PEGON, P. GUELIN, D. FAVIER, B. WACK and W.K. NOWACKI, *Constitutive scheme of discrete memory form for granular materials*, Arch. Mech., **43**, 1, pp. 3–27, 1991.
7. P. GUELIN, *Remarques sur l'hysteresis mécanique*, J. de Meca., **19**, 2, pp. 217–247, 1980.
8. D. FAVIER, *Contribution à l'étude théorique de l'élastohystérésis à température variable-application aux propriétés de mémoire de forme*, Thesis, Univ. of Grenoble, 1988.
9. T. VOGEL, *Théorie des systèmes évolutifs*, Chap. II, Gauthier-Villars, Paris 1965.
10. T. VOGEL, *Pour une théorie mécanique renouvelée*, Chap. 6, Gauthier-Villars, Paris 1973.
11. C. DE CARBON, *Déformation des solides*, C.R. Acad. Sc. Paris, 215, pp. 241–244, 1942.
12. P. PEGON, *Contribution à l'étude de l'hystérésis élastoplastique*, Thesis, Univ. of Grenoble, 1988.

13. B.W. CORB, *Effects of magnetic history on the domain structure of small NiFe shapes*, J. Appl. Phys., **63**, 8, pp. 2941–2943, 1988.

14. A. TOURABI, *Contribution à l'étude de l'hystérésis élastoplastique et de l'écrouissage de métaux et alliages réels*, Thesis, Univ. of Grenoble, 1988.

15. D. FAVIER, P. GUELIN, F. LOUCHET, P. PEGON, A. TOURABI and B. WACK, *Microstructural origin of hysteresis and application to continuum modelling of solid behaviour*, [in:] Continuum Models and Discrete Systems, G.A. MAUGIN [Ed.], Longman Scientific & Technical, Harlow (G.B.), 2, pp. 110–119, 1990.

16. B. WACK and A. TOURABI, *Some remarks on macroscopic observations and related microscopic phenomena of the mechanical behaviour of metallic materials*, Arch. Mech., **44**, 5, pp. 621–662, 1992.

17. T. MAGNIN, J. DRIVER, J. LEPINOUX and L.P. KUBIN, *Aspects microstucturaux de la déformation cyclique dans les métaux et alliages C.C. et C.F.C.: Saturation cyclique et localisation*, Revue Phys. Appl., **19**, pp. 483–502, 1984.

18. H.J. ROVEN and E. NES, *The cyclic stress-strain response of a low alloyed steel-plateau in the cyclic stress-strain curve*, Scripta Metallurgica, **21**, pp. 1727–1732, 1987.

19. K.V. RASMUSSEN and O.B. PEDERSEN, *Fatigue of copper polycrystals at low plastic strain amplitudes*, Acta Metallurgica, **28**, pp. 1467–1478, 1980.

20. A.T. WINTER, O.B. PEDERSEN and K.V. RASMUSSEN, *Dislocation microstructures in fatigued copper polycrystals*, Acta Metallurgica, **29**, pp. 735–748, 1981.

21. A. LUFT, *Microstructural processes of plastic instabilities in strengthened metals*, Progress in Materials Science, **35**, pp. 97–204, 1991.

22. P. GROH, L.P. KUBIN and J-L. MARTIN, *Dislocations et deformation plastique*, Editions de Physique, Proc. Summ. Sch. Phys. Metal., Yravals 1979.

23. A. SHAHVAROOGHI and A.J. MOSES, *High-speed computerised dc magnetisation and demagnetisation of mild steel*, J. Magn. Magn. Mat., **133**, pp. 386–389, 1994.

24. C. COQUAZ, D. CHALLETON, J.L. PORTESEIL and Y. SOUCHE, *Memory effects and nucleation of domain structures in small Permalloy shapes*, J. Magn. Magn. Mat., **124**, pp. 206–212, 1993.

25. M. PORTES DE ALBUQUERQUE and P. MOLHO, *Memory effect in a labyrinth domain structure in bubble materials*, J. Magn. Magn. Mat., **113**, pp. 132–136, 1992.

26. M. PORTES DE ALBUQUERQUE and P. MOLHO, *Evolution of a magnetic cellular pattern under field cycles*, J. Magn. Magn. Mat., **140–144**, pp. 1869–1870, 1995.

27. J.J. STOKER, *Nonlinear vibrations in mechanical and electrical systems*, Wiley, 1950.

28. M.J. SABLIK, H. KWUN and G.L. BURKHARDT, *Model for the effect of tensile and compressive stress on ferromagnetic hysteresis*, J. Appl. Phys., **61**, 8, pp. 3799–3801, 1987.

29. H. IKUTA, N. HIROTA, Y. NAKAYAMA, K. KISHIO and K. KITAZAWA, *Giant magnetostriction in* $Bi_2\ Sr_2CaCu_2O_8$ *single crystal in the superconducting state and its mechanism*, Phys. Rev. Letters, **70**, 14, pp. 2166–2169, 1993.

30. A. HERPIN, *Théorie du magnétisme* (p. 795), P.U.F., Paris 1969.

31. M. BUNGE, *Foundations of physics*, Chap. 3, Vol. 10 of Springer Tracts in Natural Philosophy, 1967.

32. Y. YESHURUN, A.P. MALOZEMOFF and A. SHAULOV, *Magnetic relaxation in high temperature superconductors*, Rev. Modern Phys., **68**, 3, pp. 911–949, 1996.

33. G. RIO, P.Y. MANACH and D. FAVIER, *Finite element simulation of shell and 3D mechanical behaviour of NiTi shape memory alloys*, Arch. Mech., **47**, 3, pp. 537–556, 1995.

34. G. RIO, D. FAVIER and H. DEPLATS, *Finite elements simulation of mechanical behaviour of shape memory alloys coupled with a non-stationary thermal field*, J. de Physique, C8, **5**, pp. 215–220, 1995.

35. P.Y. MANACH, D. FAVIER and G. RIO, *Finite element simulations of internal stresses generated during the pseudoelastic deformation of NiTi bodies*, J. de Physique, C1, **6**, pp. 235–244, 1996.

36. K. O'GRADY and S.J. GREAVES, *Anomalous effects in minor hysteresis loops*, IEEE Trans. Mag., **31**, 6, pp. 2794–2796, 1995.

37. R. HILL, *New derivations of some elastic extremum principles*, Progress in Applied Mechanics, the Prager anniversary volume, The Macmillan Company, New York, pp. 99–106, 1963.

38. A.A. ILYUSHIN, *Plasticity. Foundations of general mathematical theory, First part: Geometrical representation of the loading processes* [in Russian], Akad. Nauk S.S.S.R., Moscow 1963.

39. A.S. LODGE, *Body tensor fields in continuum mechanics, with applications to polymer rheology*, Academic Press, New York 1974.

40. J.A. KRUMHANSL, *Some considerations of the relations between solid state physics and generalized continuum mechanics*, Proceeding of the IUTAM-Symposium of Freudenstadt and Stuttgart, 1967: Mechanics of Generalized Continua, editor E. Kröner, pp. 298–311, Springer-Verlag, 1968.

UNIVERSITE JOSEPH FOURIER, GRENOBLE, FRANCE

e-mail: Ali.Tourabi@img.fr

and

POLISH ACADEMY OF SCIENCES
INSTITUTE OF FUNDAMENTAL TECHNOLOGICAL RESEARCH

e-mail: wnowacki@ippt.gov.pl

Received January 28, 1997; new version June 2, 1997.

Arch. Mech., **49**, 4, pp. 767–790, Warszawa 1997

The shock wave structure by model equations of capillarity

K. PIECHÓR (WARSZAWA)

IN THIS PAPER we investigate the influence of the capillarity terms on the shock wave structure. To this end we compare the shock structures derived from the viscosity-capillarity model and from the Navier–Stokes equations, i.e. the viscosity model. Let A and ε characterize the values of the capillarity and viscosity effects, respectively. First, we prove that if the ratio $A/\varepsilon^2 \ll 1$ then the viscosity-capillarity and viscosity shock structures differs but only a little. Secondly, if $A/\varepsilon^2 \gg 1$ then the viscosity-capillarity shock waves are oscillatory, whereas the viscosity waves are never such. Thirdly, to investigate the intermediate case of $A/\varepsilon^2 \approx 1$ we study numerically so-called impending shock splitting. This effect consists in that the shock profile has two inflection points, under suitably chosen data, instead of one, what is usual. Our calculations show that the capillarity, if strong enough, kills this effect totally.

1. Introduction

AS IT IS WELL KNOWN, the Navier–Stokes equations with the van der Waals equation of state rule out certain experimentally observed phase boundaries. To circumvent this difficulty, SLEMROD [1] for van der Waals fluids and TRUSKINOVSKY [2] for elastic bars introduced higher order gradients to the dispersive equations basing on the Korteweg's theory of capillarity. Consequently, the viscosity-capillarity equations were used mainly to study various problems concerning phase transitions.

The aim of this paper is an investigation of the influence of the capillarity effects on the shock wave structure. To our knowledge this topic is almost untouched. Exceptions are the papers by AFFOUF and CAFLISCH [3], and by ABEYARATNE and KNOWLES [4] where some results concerning our problem can be found.

We start with the capillarity equations deduced from a kinetic four-velocity model of the Enskog–Vlasov equation [5], and look for solutions in the form of travelling waves.

We define the shock wave as a plane travelling wave which is supersonic with respect to the sound speed in the equilibrium state ahead of it and subsonic with respect to that behind it.

We distinguish between viscosity and viscosity-capillarity shock waves. The shock wave is, by definition, a viscosity wave if its structure is described by the Navier–Stokes equations, and it is a viscosity-capillarity one if its structure is described by the capillarity equations, i.e. the Navier–Stokes equations with additional terms representing capillarity forces.

In Sec. 2 we present equations which we use to describe shock wave structures, and show that the viscosity-capillarity shocks can be oscillatory, provided that the capillarity coefficient is sufficiently large, whereas the viscosity shocks have monotone profiles.

In Sec. 3 we discuss the problem of so-called impending shock splitting. Roughly speaking, the question is that within the Navier–Stokes equations with a non-convex equation of state like the van der Waals one, one can choose such state after the wave and its speed that the shock profile has two inflection points instead of one, what is usual [7]. In this section we reconsider this problem, but within the framework of the capillarity equations. Numerically we show that if the capillarity coefficient is very small, then the viscosity-capillarity shock wave profiles differ but a little from the corresponding viscosity ones. However, our calculations show that the increase of the capillarity coefficient kills the effect of the impending shock splitting, so it should be treated as an artefact introduced by the Navier–Stokes equations.

In Sec. 4 we show how to extend these results to other scalar equations of travelling waves.

We complete the paper with Sec. 5, where we prove rigorously that if the capillarity coefficient is small enough, then the viscosity and capillarity shock wave profiles differ by a little only.

2. The model equations of capillarity and the travelling waves

The model equations of capillarity we consider in this paper consist of the following system of two partial differential equations [5]

$$\frac{\partial}{\partial t}w - \frac{\partial}{\partial x}u = 0, \tag{2.1}$$

$$\frac{\partial}{\partial t}u + \frac{\partial}{\partial x}p(w,u) = \varepsilon\frac{\partial}{\partial x}\left(\mu\frac{\partial}{\partial x}u\right) + A\frac{\partial}{\partial x}\left[\frac{5}{w^6}\left(\frac{\partial}{\partial x}w\right)^2 - \frac{2}{w^5}\frac{\partial^2}{\partial x^2}w\right]. \tag{2.2}$$

In (2.1), (2.2), $t > 0$ is the time, $x \in \mathbb{R}$ is the Lagrangian mass coordinate, u is the velocity, w is the specific volume, p is the pressure, and $\varepsilon\mu$ is the coefficient of viscosity.

The pressure formula reads

$$p = p(w,u) = \frac{1-u^2}{2(w-b)} - \frac{a}{w^2}, \tag{2.3}$$

where a and b are positive constants; a is the ratio of the mean value of the potential of the attractive intermolecular forces to the mean kinetic energy of molecules, and b can be taken to be equal to unity.

Next, $\varepsilon > 0$ is a parameter, and $\mu = \mu(w, u)$ is given by

$$\mu(w,u) = \frac{1 - u^2 + 2b^2 w^2 \varrho^2(w)}{8w^2 \varrho(w)}, \qquad \varrho(w) = \frac{w}{w-b}. \tag{2.4}$$

Finally, $A > 0$ is another parameter, the term proportional to it represents the capillarity forces. Therefore A is called the capillarity coefficient.

We consider Eqs. (2.1), (2.2) in the domain $\mathcal{D}$ defined by [6]

$$\mathcal{D} = \left\{(w,u) \ : \ w > b, \quad u^2 < 1 - \frac{a}{2b}, \quad \frac{a}{2b} < 1\right\}. \tag{2.5}$$

For $(w, u) \in \mathcal{D}$, the mass density $1/w$ does not exceed the close-packing density $1/b$, and the pressure p is positive (also the viscosity μ is strictly positive).

Two simplified versions of our equations, namely the first one with $\varepsilon = 0$, $A = 0$, and the second one with $\varepsilon > 0$ but $A = 0$, are called the Euler and Navier–Stokes model equations of hydrodynamics, respectively. They were analyzed in [6].

A travelling wave solution to (2.1), (2.2) is a solution of the form

$$(w,u)(x,t) = (w,u)(z), \qquad z = \frac{x - st}{\varepsilon} \in \mathbb{R}, \tag{2.6}$$

where $s = \text{const}$ is the wave-speed, such that

$$\lim_{z \to -\infty} (w,u)(z) = (w_l, u_l), \tag{2.7}$$

$$\lim_{z \to \infty} (w,u)(z) = (w_r, u_r), \tag{2.8}$$

$$\lim_{z \to \pm\infty} (w',u')(z) = (0,0), \tag{2.9}$$

$$\lim_{z \to \pm\infty} (w'',u'')(z) = (0,0), \tag{2.10}$$

where the dash $'$ denotes differentiation with respect to z.

Usually, the left-hand equilibrium state (w_l, u_l) is treated as given, and the right-hand state (w_r, u_r) has to be determined. However, we proceed in a different way. Namely, we introduce the notions of the states before and after the wave:

the state before the wave is defined by

$$(w_b, u_b) = \begin{cases} (w_r, u_r) & \text{for} \quad s > 0, \\ (w_l, u_l) & \text{for} \quad s < 0, \end{cases} \tag{2.11}$$

and the state after the wave is by definition

$$(w_a, u_a) = \begin{cases} (w_l, u_l) & \text{for} \quad s > 0, \\ (w, u) & \text{for} \quad s < 0. \end{cases} \tag{2.12}$$

The case of $s = 0$ is not considered in this paper.

We take the state after the wave as given.

Now, we act in a very standard way. Namely, we substitute (2.6) into Eqs. (2.1), (2.2), perform one integration with respect to z, and use the limit conditions (2.7) – (2.10). Having done that we find that the states before and after the wave are related algebraically

$$\begin{aligned} sw_b + u_b &= sw_a + u_a\,, \\ -su_b + p(w_b, u_b) &= -su_a + p(w_a, u_a). \end{aligned} \tag{2.13}$$

These relations are called the Rankine – Hugoniot conditions and were in detail analyzed in [6].

Next, we find the velocity u. It is given by

$$u = u_a - s(w - w_a), \tag{2.14}$$

where w is a solution of the following limit value problem

$$\alpha^2 \left[\frac{2}{w^5} w'' - \frac{5}{w^6} w'^2\right] + s\mu(w)w' + f(w) = 0, \tag{2.15}$$

where $\alpha = A/\varepsilon^2$, and

$$\mu = \mu(w) = \mu(w) = \mu\left(w, u_a - s(w - w_a)\right) > 0, \tag{2.16}$$

$$f(w) = s^2(w - w_a) + p(w, u_a - s(w - w_a)) - p(w_a, u_a), \tag{2.17}$$

subject to the conditions

$$\lim_{z \to -\infty} w(z) = \begin{cases} w_a & \text{for} \quad s > 0, \\ w_b & \text{for} \quad s < 0, \end{cases} \tag{2.18}$$

$$\lim_{z \to \infty} w(z) = \begin{cases} w_b & \text{for} \quad s > 0, \\ w_a & \text{for} \quad s < 0, \end{cases} \tag{2.19}$$

$$\lim_{z \to \pm\infty} w'(z) = 0, \qquad \lim_{z \to \pm\infty} w''(z) = 0. \tag{2.20}$$

These conditions must be supplemented by Eqs. (2.13), which we write in the form

$$f(w_a) = 0, \qquad f(w_b) = 0. \tag{2.21}$$

We take the following two assumptions:

A1. The equation $f(w) = 0$ has no solutions between w_a and w_b.

A2. The following inequalities hold true

$$f'(w_a) < 0, \tag{2.22}$$

$$f'(w_b) > 0. \tag{2.23}$$

Explicitly (2.22) and (2.23) are equivalent to

$$s^2 - sp'_u(w_a, u_a) + p'_w(w_a, u_a) < 0, \tag{2.24}$$

and

$$s^2 - sp'_u(w_b, u_b) + p'_w(w_b, u_b) > 0, \tag{2.25}$$

respectively.

The characteristic speeds (sound speeds) $c_\pm(w, u)$ are defined as the real solutions of (cf. [6])

$$c^2 - sp'_u(w, u) + p'_w(w, u) = 0. \tag{2.26}$$

Hence, (2.24) is equivalent to

$$c_-(w_a, u_a) < s < c_+(w_a, u_a), \tag{2.27}$$

what means that the wave is subsonic with respect to the state after it.

Next, we notice that (2.25) is equivalent to

$$s < c_-(w_b, u_b) \qquad \text{or} \qquad s > c_+(w_b, u_b), \tag{2.28}$$

i.e. the wave is supersonic with respect to the state ahead of it.

The solution of (2.15) – (2.21) with $f(w)$ satisfying A1 and A2 is called the viscosity-capillarity shock wave, and the graph of the solution is called the shock wave structure or profile.

The aim of this paper is to compare the viscosity-capillarity shock waves to the viscosity ones, which are solutions of

$$s\mu(w)w' + f(w) = 0, \tag{2.29}$$

with $\mu(w)$ and $f(w)$ given by (2.16), (2.17), respectively, and satisfying the limit conditions (2.18), (2.19), and $(2.20)_1$. We assume also that Eqs. (2.21) and A1, A2 hold true.

The first observations concerning the differences between the two descriptions can be derived from *the analysis of the points of equilibrium*. This is a standard procedure. We linearize equations (2.15) or (2.29) around, say, $w = w_a$, and find that the characteristic exponents satisfy

$$\alpha\frac{2}{w_a^5}\lambda_a^2 + s\mu(w_a)\lambda_a + f'(w_a) = 0, \tag{2.30}$$

if Eq. (2.15) is concerned, or

$$s\mu(w_a)\lambda_a + f'(w_a) = 0, \tag{2.31}$$

for the case of Eq. (2.29).

Thanks to (2.22), Eq. (2.30) has two real solutions $\lambda_a^- < 0 < \lambda_a^+$. Of course, the solution to (2.31) is always real.

If we perform the linearization around $w = w_b$, then the characteristic exponents, this time labelled with the subscript b, will satisfy an equation similar to (2.30) (respectively (2.31)). But this time, owing to (2.23) the characteristic exponents in the viscosity-capillarity case can be complex if α is sufficiently large. The characteristic exponent in the viscosity case is always real.

Thus we obtain

OBSERVATION 1.

If α is sufficiently large, then the viscosity-capillarity shock wave structure is oscillatory in the downstream part of its profile. The viscosity shock wave structure is always monotonic.

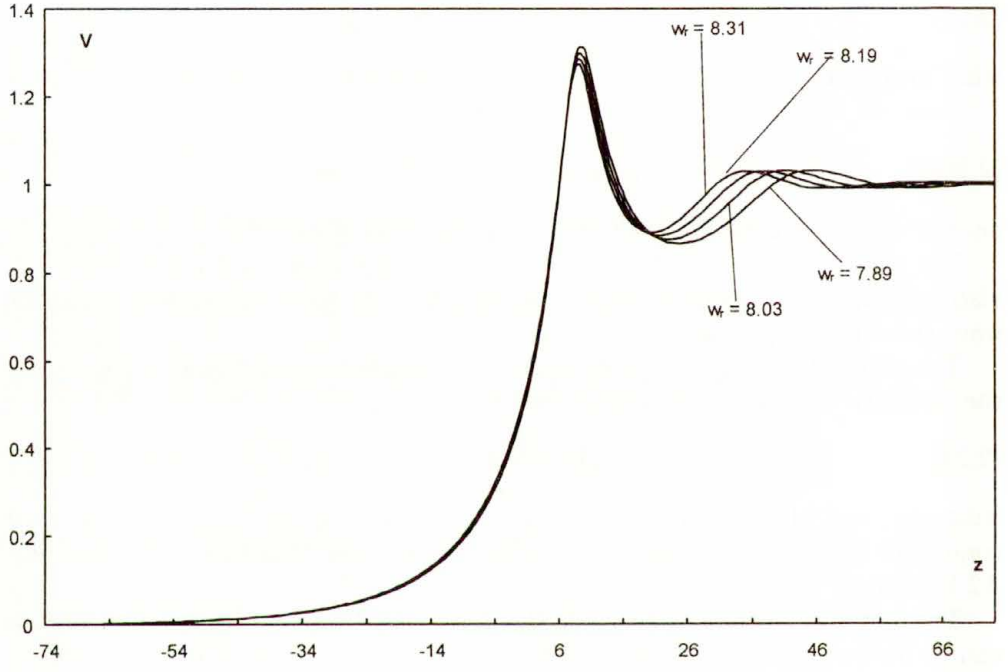

FIG. 1. Normalized oscillating shock structures, $\alpha = 100$.

The graphs of oscillatory shock waves are presented in Fig. 1 (see also [3]). Experimentally, oscillatory shock waves were observed in [11].

3. The impending shock splitting

The notion of impending shock splitting was introduced by CRAMER and CRICKENBERGER [7] to denote such shock structures which are monotone, but

have two inflection points instead of one, what is usual. If the impending shock wave occurs then, roughly speaking, the shock profile consists of two domains where rapid, shock-like changes take place, separated by a region in which the profile is quite flat.

Cramer and Crickenberger used the nonisothermal Navier–Stokes equations with a realistic equation of state, but they ignored capillarity forces. The profiles with an impending shock splitting are presented in Fig. 10 of their paper [7].

Later, using our model equations of van der Waals fluids with capillarity effects neglected we obtained quite similar results [6].

For the sake of completeness of our arguments we give a series of shock profiles exhibiting the impending shock wave splitting (see Fig. 2). Of course, they resemble the quoted results of [6] and [7].

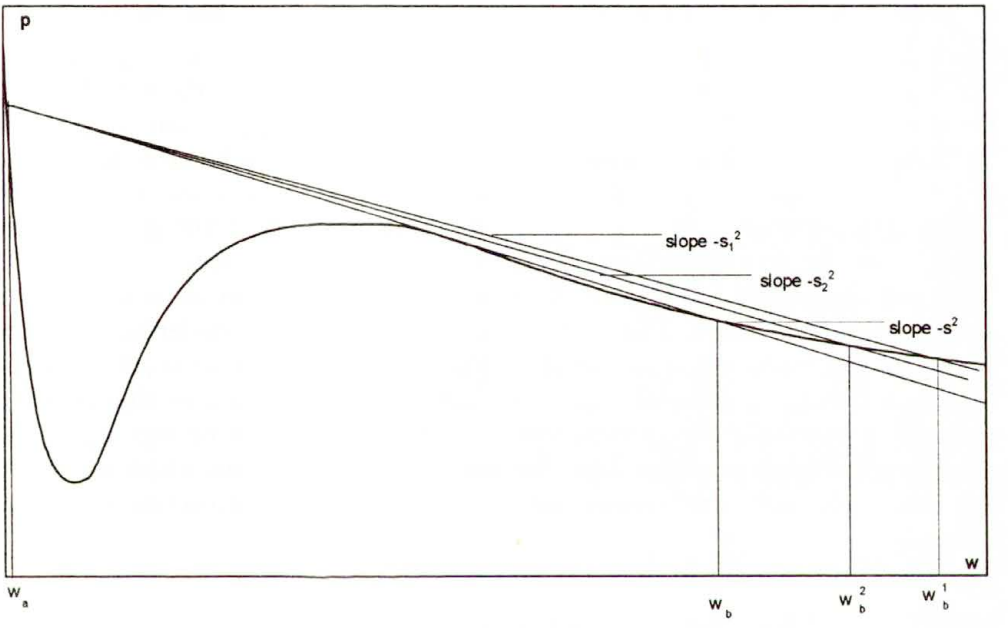

FIG. 2. Schematic diagram of the pressure and the Rayleigh radii.

We explain briefly how to obtain such results (see also [7]). First, we ignore the capillarity terms, i.e. we set $\alpha = 0$ in Eq. (2.15). Consequently, we consider the problem consisting of Eq. (2.29) subject to (2.18), (2.19), and $(2.20)_1$. We start from the simpler case of isothermal gas with the pressure p given by

$$p(w) = \frac{T}{w-b} - \frac{a}{w^2}, \tag{3.1}$$

where $T = \text{const}$ is the dimensionless temperature.

If T is such that

$$\frac{1}{4}\frac{a}{b} < T < \frac{81}{256}\frac{a}{b}, \tag{3.2}$$

then the pressure is positive for $w > b$, but the graph of $p(w)$ in the $w-p$ plane is a concave or even nonmonotonic curve. Under (3.2), the curve $p = p(w)$ has two points of inflection, say, at $w = w^*$ and at $w = w^{**}$, such that $b < w^* < w^{**}$.

Let us take the the state after the wave w_a such that $b < w_a < w^*$, and let $\overline{s} > 0$ be such that the Rayleigh radius $r(w) = -s^2(w - w_a) + p(w_a)$ is tangent to $p = p(w)$ at $w = \overline{w}$, $w^* < \overline{w} < w^{**}$. Now, we take a sequence $\{s_n\}$ of speeds such that $s_{n+1} > s_n > 0$, $n = 1, 2, ...$, and $\lim_{n\to\infty} s_n = \overline{s}$ (see Fig. 2). Then the Rayleigh radii $r_n = -s_n^2(w - w_a) + p(w_a)$ lie above the graph of $p = p(w)$ for w between $w = w_a$ and $w = w_b^{(n)}$, where $w = w_b^{(n)}$ is the w-coordinate of the other point of intersection of $p = p(w)$ with $p = r_n(w)$. This guarantees that, for any n, the functions $f_n(w) = p(w) - r_n(w)$ are negative for w between w_a and $w_b^{(n)}$. Hence, our limit value problems have unique solutions. However, for sufficiently large n, the Rayleigh radii are almost tangent to the graph of $p = p(w)$, but lying above it. Therefore, for sufficiently large n, the function $f_n(w)$ can be arbitrarily close to zero in a vicinity of $w = \overline{w}$. Consequently, in this vicinity the derivative of $w = w(z)$ with respect to z is close to zero. This means that the graphs of the solutions in the $z-p$ plane become flatter and flatter, as n tends to infinity.

In our case, when the pressure depends not only on w but on u as well, the situation is more difficult. This is due to the fact that, when considering the shock wave problem, we have to consider $p(w, u)$ along the Hugoniot locus (cf. [6]) what results in that the profiles of $p(w, u)$ depend on s as well. So they change when changing s, but the Rayleigh radii remain unchanged. Luckily, by regrouping the parameters present in our problem we can reduce it to a form which resembles the isothermal case, and consequently we can use the construction described above.

Indeed, as it follows from (2.14) we can write

$$u = \widetilde{u}_a - s(w - b), \tag{3.3}$$

where

$$\widetilde{u}_a = u_a + s(w_a - b) = \text{const}. \tag{3.4}$$

Next, (2.3), (2.17) and the above yield

$$f(w) = \widetilde{p}(w) - \widetilde{p}(w_a) + \widetilde{s}^2(w - w_a), \tag{3.5}$$

where

$$\widetilde{p}(w) = \frac{T_a}{w - b} - \frac{a}{w^2}, \tag{3.6}$$

with

$$T_a = \frac{1 - \tilde{u}_a^2}{2} = \text{const}, \tag{3.7}$$

and

$$\tilde{s} = s/\sqrt{2}. \tag{3.8}$$

Formula (3.6) resembles (3.1) if we identify T_a with T.

When preparing the graphs presented in Figs. 1 and 3–7, we kept w_a and T_a fixed and changed s. Consequently we changed u_a, i.e. we took $u_a = u_a(s)$, in agreement with (3.4) and (3.7).

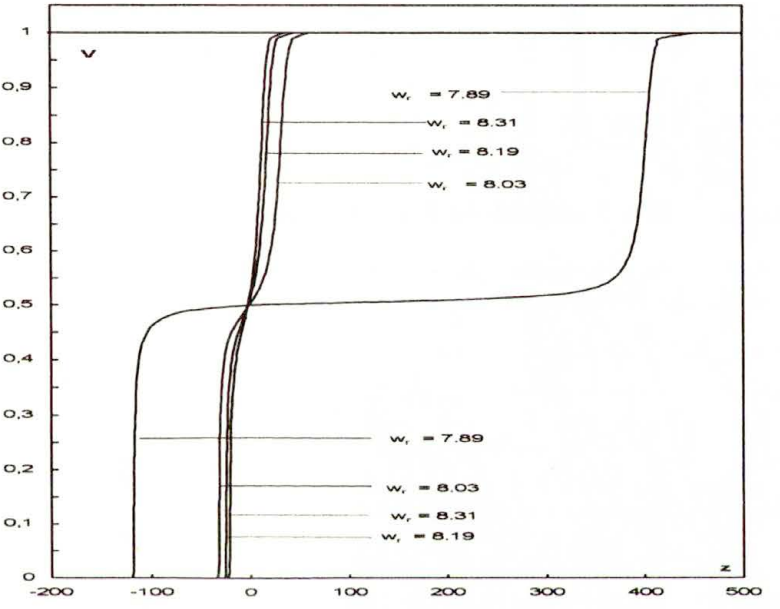

FIG. 3. Normalized shock structures for $\alpha = 0$.

Next, we reconsidered the shock wave structure problem using Eq. (2.15) and the same values of T_a, w_a, and s_n. Let us notice that the Rankine–Hugoniot conditions (2.13) are the same in the viscosity and in the capillarity-viscosity case.

In Figs. 1 and 3–7 the normalized specific volume V defined by

$$V = (w - w_l)/(w_r - w_l)$$

is shown for $\alpha = 100$, 0, 0.5, 1.0, 5.0, and 10.0.

Now, let us take a greater value of α, i.e. $\alpha = 1$ (Fig. 5). We see that the impending shock splitting is still observable, but the overall shock thickness has decreased by the factor of 4.

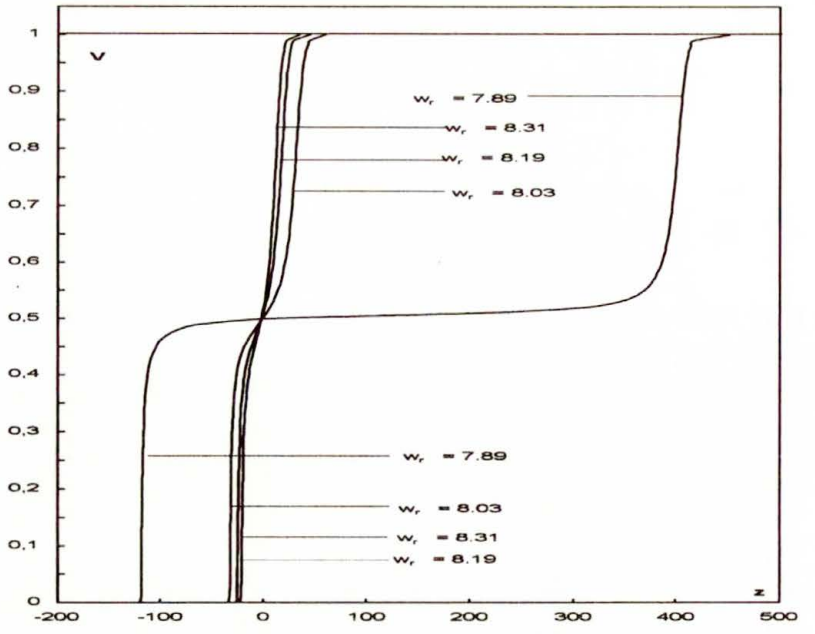

FIG. 4. Normalized shock structures for $\alpha = 0.5$.

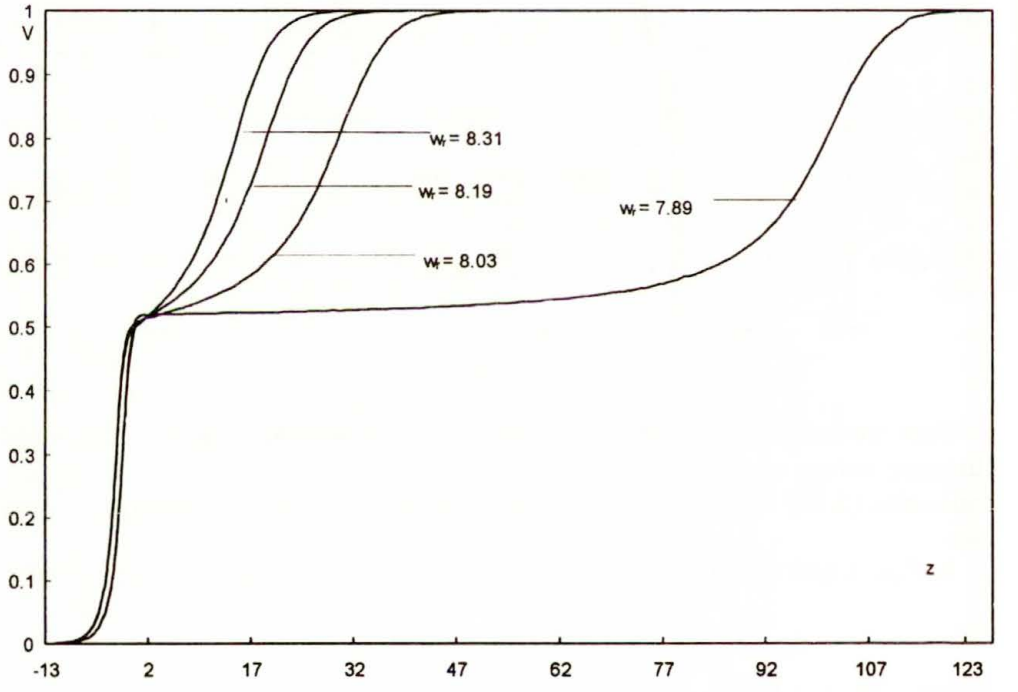

FIG. 5. Normalized shock structures for $\alpha = 1$.

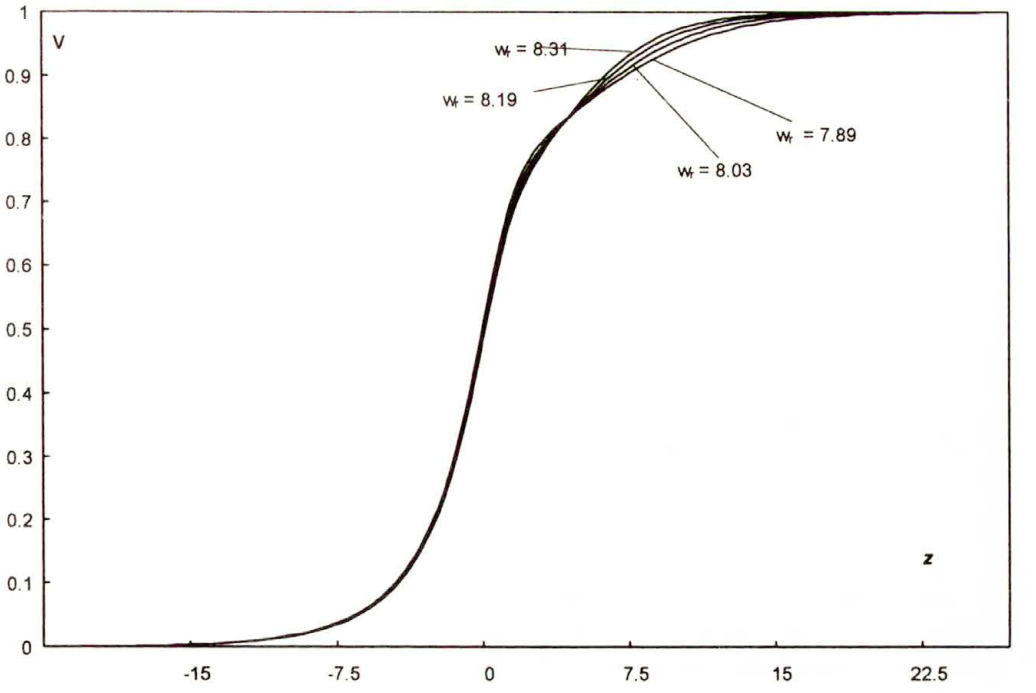

FIG. 6. Normalized shock structures for $\alpha = 5$.

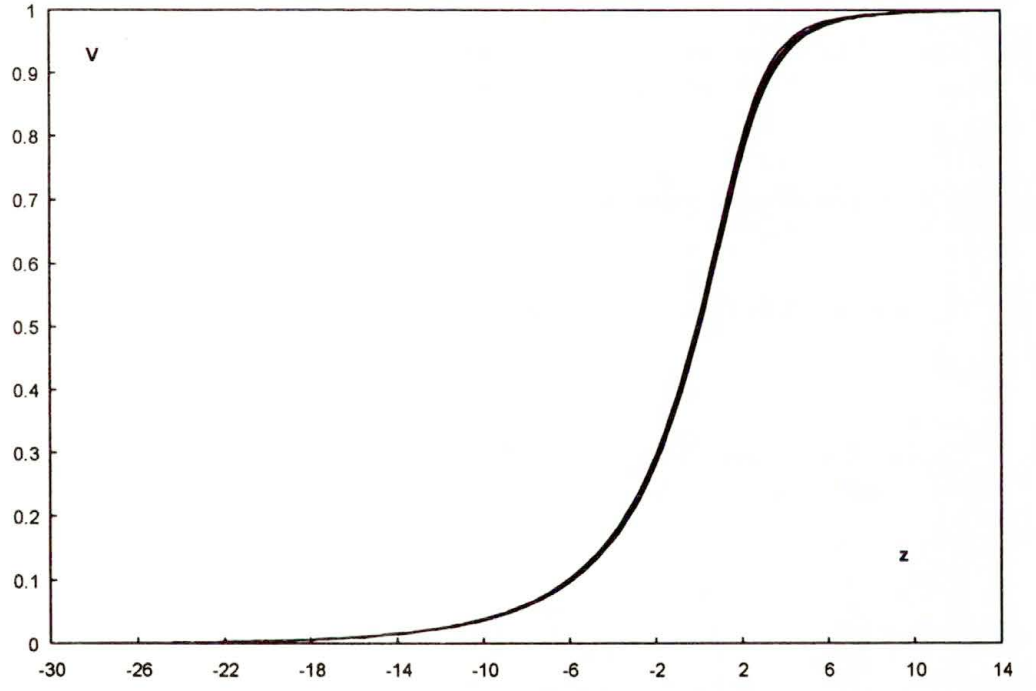

FIG. 7. Normalized shock structures for $\alpha = 10$.

If we increase the value of α even more to, $\alpha = 5$ and $\alpha = 10$ like in Figs. 6 and 7, respectively, then it turns out that the splitting disappears. If we continue to increase the value of the capillarity coefficient, then the shock wave can become oscillatory without any splitting (cf. the previous section and Fig. 1).

4. Generalization of these results

We show below that our equation (2.15) for plane travelling waves can be put into a more general and standard scheme, and simplified at the same time. We have not done this up to now because we used Eq. (2.15) for our calculations described in the previous section.

We consider a more general problem than that of (2.15) – (2.20), namely we take

$$\alpha\left[A(w)w'' + B(w)w'^2\right] + s\mu(w; w_a, s)w' + f(w; w_a, s) = 0, \tag{4.1}$$

subject to the limit conditions (2.18) – (2.20).

Here, $\alpha > 0$ is a parameter, $A(w)$ and $B(w)$ are given continuous functions of $w > b$, where b can be such as previously or any other fixed real number; s is the wave speed, and $w_a > b$ is a fixed quantity. Next, the source function $f(w; w_a, s)$ and the viscosity coefficient $\mu(w; w_a, s)$ are given smooth functions of their arguments such that

i) $\mu(w; w_a, s)$ is strictly positive, i.e. there is a positive constant μ_0 such that for any w, $w_a > 0$ and any admissible value of s

$$\mu(w; w_a, s) \geq \mu_0 > 0; \tag{4.2}$$

ii) for any admissible value of s

$$f(w_a; w_a, s) = 0; \tag{4.3}$$

iii) there exists $w_b > b$, $w_b \neq w_a$ such that

$$f(w_b; w_a, s) = 0, \tag{4.4}$$

i.e. $w_b = w_b(w_a, s)$.

Finally, $A(w)$ is assumed to be strictly positive as well, that is there exists a positive constant, say A_0, such that

$$A(w) \geq A_0 > 0, \tag{4.5}$$

for $w > b$.

Let

$$D(w) = \exp\left[\int_{w_a}^{w} \frac{B(\zeta)}{A(\zeta)} d\zeta\right], \tag{4.6}$$

and let us define the transformation

$$w \longrightarrow U(w) = \frac{\int_{w_a}^{w} D(\zeta)\, d\zeta}{\int_{w_a}^{w_b} D(\zeta)\, d\zeta}. \tag{4.7}$$

Since $D > 0$, then $U'_w > 0$ and this transformation is invertible; i.e. there is a twice differentiable function $U \to w(U)$ such that

$$w(0) = w_a \qquad \text{and} \qquad w(1) = w_b\,. \tag{4.8}$$

By applying the transformation (4.7) to Eq. (4.1), the latter reduces to

$$\alpha U'' + sM(U)\,U' + F(U) = 0, \tag{4.9}$$

where

$$M(U) = \frac{\mu(w(U); w_a, s)}{A(w(U))}\,, \tag{4.10}$$

and

$$F(U) = F(U; w_a, s) = \frac{D(w(U))}{A(w(U)) \int_{w_a}^{w_b} D(\zeta)\, d\zeta} f(w(U); w_a, s). \tag{4.11}$$

The limit conditions (2.18) – (2.20) become

$$\lim_{z \to -\infty} U(z) = \begin{cases} 0 & \text{for} \quad s > 0, \\ 1 & \text{for} \quad s < 0, \end{cases} \tag{4.12}$$

$$\lim_{z \to \infty} U(z) = \begin{cases} 1 & \text{for} \quad s > 0, \\ 0 & \text{for} \quad s < 0, \end{cases} \tag{4.13}$$

$$\lim_{z \to \pm\infty} U'(z) = 0, \qquad \lim_{z \to \pm\infty} U''(z) = 0. \tag{4.14}$$

Equations (4.2), (4.3) take the form:

for any $w_a > b$, $w_b > b$, and s

$$F(0; w_a, w_b, s) = 0, \tag{4.15}$$

there is $w_b = w_b(w_a, s) > b$ such that

$$F(1; w_a, w_b, s) = 0. \tag{4.16}$$

The limit value problem of the type (4.9), (4.12)–(4.14) along with (4.15), (4.16) was considered in many papers on the isothermal travelling waves solutions to conservation principles (an extensive list of references is given in [6]). Also, a similar problem arises in the analysis of travelling waves in reaction-diffusion systems. The difference between the conservation principles and the reaction-diffusion ones is that the source term $F(U)$ in the latter case does not depend on the wave speed s and that (4.16) holds for any w_a, w_b and/or eventually other parameters. So, in this case there is nothing like the Rankine–Hugoniot conditions (see [8] and the references therein).

In the case of our original equation (2.15)

$$A(w) = 2/w^5, \qquad B(w) = 5/w^6 = \frac{1}{2}A'_w(w).$$

Hence, as the function $D(w)$ we take $D(w) = w^{-5/2}$. Therefore

$$U(w) = \frac{w^{-3/2} - w_a^{-3/2}}{w_b^{-3/2} - w_a^{-3/2}}. \tag{4.17}$$

The inverse to it $w = w(U)$ is then

$$w(U) = \left[w_a^{-3/2} + U\left(w_b^{-3/2} - w_a^{-3/2}\right)\right]^{-2/3}. \tag{4.18}$$

Now, we establish the equivalence between the limit value problems (4.1)–(4.3) subject to conditions (2.18)–(2.20) and that of (4.9), (4.12)–(4.16).

First, due to (4.5)–(4.7) and (4.10), (4.11) we have immediately

PROPOSITION 1.

i) $M(U) > 0$ if and only if $\mu(w) > 0$;
ii) $F(U) > 0$ (< 0) if and only if $(w_b - w_a)f(w) > 0$ (< 0);
iii) $F(U_0) = 0$ if and only if $f(w_0) = 0$, where $U_0 = U(w_0)$.

We have also

PROPOSITION 2.

The singular point $(\overline{w}, 0)$ of Eq. (4.1) in the plane of (w, w') is of the same type as the singular point $(\overline{U}, 0)$ of Eq. (4.9) in the (U, U')-plane.

P r o o f. To perform the classification of a singular point of a dynamic system we consider the asymptotic behaviour of its solutions as $z \to -\infty$ or, respectively, $z \to \infty$.

To this end we linearize, first, Eq. (4.1) around $(\overline{w}, 0)$ and obtain a linear, second order differential equation whose characteristic equation reads

$$\alpha A(\overline{w})\lambda^2 + s\mu(\overline{w})\lambda + f'(\overline{w}) = 0. \tag{4.19}$$

The similar procedure yields in the case of Eq. (4.9)

$$\alpha\Lambda^2 + sM(\overline{U})\Lambda + F'_U(\overline{U}) = 0. \tag{4.20}$$

But from (4.6), (4.11) we have

$$F'_U(U) = \frac{D(w(U))}{A^2(w(U)) \int\limits_{w_a}^{w_b} D(\zeta)\,d\zeta} \left[B(w(U)) - A'_w(w(U))\right] f(w(U)) \frac{dw}{dU} + \frac{D(w(U))}{A(w(U)) \int\limits_{w_a}^{w_b} D(\zeta)\,d\zeta} f'_w(w(U)) \frac{dw}{dU}.$$

But, as it follows from (4.7)

$$\frac{D(w(U))}{\int\limits_{w_a}^{w_b} D(\zeta)\,d\zeta} \frac{dw}{dU} = 1.$$

Therefore

$$F'_U(U) = \frac{B(w(U)) - A'_w(w(U))}{A^2(w(U))} f(w(U)) + \frac{f'_w(w(U))}{A(w(U))}. \tag{4.21}$$

Consequently

$$F'_U(\overline{U}) = \frac{f'_w(\overline{w})}{A(\overline{w})}. \tag{4.22}$$

Using (4.10) and (4.22) in Eq. (4.20) we see immediately that it coincides with Eq. (4.19). The proof is complete.

As we assume that neither $A(w)$ nor $B(w)$ depend on α, we can apply transformation (4.6), (4.7) to the viscosity shock wave problem (2.29), (2.18), (2.19), and $(2.20)_1$. This problem changes to

$$sM(U; w_a, w_b, s)U' + F(U; w_a, w_b, s) = 0, \tag{4.23}$$

and the limit conditions (4.12), (4.13), and $(4.14)_1$. Here M and F are the same as previously. Also, we assume that (4.15) and (4.16) hold.

Finally, (2.22) and (2.23) take the form

$$F'_U(U_a) < 0, \qquad F'_U(U_b) > 0, \tag{4.24}$$

where $U_a = U(w_a)$, $U_b = U(w_b)$.

We transfer to here the terminology of the previous section, and the waves described by Eq. (4.9) are called the viscosity-capillarity waves, whereas those described by Eq. (4.23) are called the viscosity waves.

i) *The oscillating viscosity-capillarity waves*

Setting in Eq. (4.20), $\overline{U} = U_a$ and using (4.24) we see that the point $(U_a, 0)$ is the saddle in the (U, U')-plane. The similar analysis for $\overline{U} = U_b$ shows that the characteristic exponents at this state of equilibrium can have nonzero imaginary parts, so the waves can be oscillatory downstream. Similarly as previously, the viscosity shock waves are never oscillatory, what follows from Eq. (4.23) and assumption (4.24).

ii) *The impending shock splitting*

Let there exist $w_a = \overline{w}_a$, $w_b = \overline{w}_b$, $s = \overline{s}$ such that

$$F(1; \overline{w}_a, \overline{w}_b, \overline{s}) = 0,$$

and let there be $\overline{U}$ that $0 < \overline{U} < 1$, and

$$F(\overline{U}; \overline{w}_a, \overline{w}_b, \overline{s}) = 0.$$

We take sequences $w_a^{(n)} \to \overline{w}_a$, $w_b^{(n)} \to \overline{w}_a$, $s^{(n)} \to \overline{s}$ as $n \to \infty$, such that

$$F(1; w_a^{(n)}, w_b^{(n)}, s^{(n)}) = 0, \qquad F(U; w_a^{(n)}, w_b^{(n)}, s^{(n)}) \neq 0 \quad \text{for} \quad 0 < U < 1.$$

The shock profiles obtained from Eq. (4.9) for such values of the parameters and sufficiently large n will exhibit the impending shock splitting (cf. Proposition 1).

4.1. The numerical procedure

In order to solve numerically the limit value problem of the type (2.15) and (2.18) – (2.20) we reduce first Eq. (2.15) to the form (4.9) by means of the transformation (4.17), (4.18). We have to distinguish two cases: the first one concerns large values of α, whereas the second – the small ones. In the first case, the classical fourth-order Runge–Kutta method works well. In the second case, α is a small singular parameter since it multiplies the highest derivative of the equation. Owing to that, the problem becomes numerically stiff and an implicit scheme has to be used. In the case of Eq. (4.9) the problem is relatively simple. Namely, with the substitution

$$U' = V(U) \tag{4.25}$$

we reduce our problem to

$$\frac{dV}{dU} = -\frac{F(U)}{\alpha V} - \frac{s}{\alpha} M(U), \tag{4.26}$$

with the boundary conditions

$$V(U=0)=0, \qquad V(U=1)=0. \tag{4.27}$$

We decided upon the so-called trapezoidal rule [10], which consists in the following. Let us consider the generic initial value problem

$$y' = \phi(x,y),$$

subject to the initial condition

$$y(0) = x_0\,.$$

The numerical scheme is

$$y_{n+1} - y_n = \frac{1}{2}h\left[\phi(x_n,y_n) + \phi(x_{n+1},y_{n+1})\right], \tag{4.28}$$

where h is the step.

In our case $x = U$, $y = V$, and ϕ is the right-hand side of Eq. (4.26). The numerical scheme yields, in our case, an algebraic quadratic equation for V_{n+1} whose solution provides a recursive relation between this quantity and U_n, U_{n+1}, and V_n.

We start the iteration process from a point (U_0, V_0) close to (0,0) (the latter is a saddle in the (U,V)-plane) and continue the calculations until we reach a small vicinity of the point (1,0) (which is the stable node in the same plane). In this way we obtain the function $V(U)$, i.e. the right-hand side of Eq. (4.25). Integrating it in the standard way we find $U = U(z)$. Finally we use (4.18) and obtain $w = w(z)$.

5. The case of small α

In this section we prove that the viscosity-capillarity and viscosity shock profiles do not differ much, provided that α is sufficiently small.

We assume in this section that w_a, w_b, and s are such that Eq. (4.16) is satisfied. First, we take the following

DEFINITION

For $i = 0,1,2,3$

$$\|y\|_i = \sup_{z\in\mathbb{R}} \left(|y(z)| + |y'(z)| + \ldots + |y^{(i)}(z)|\right),$$

and

$$\mathcal{B}_i = \left\{y \in C^i(\mathbb{R}) \;:\; \|y\|_i < \infty, \quad y'(z),\ldots,y^{(i)}(z) \to 0 \quad as \quad |z| \to \infty\right\}.$$

Also let for $i = 0, 1$

$$\mathcal{B}_i^0 = \left\{ y \in \mathcal{B}_i \ : \ y(z) \to 0 \quad as \quad |z| \to \infty \right\}$$

and

$$\mathcal{B}_2^0 = \left\{ y \in \mathcal{B}_2 \ : \ y(0) = 0 \quad and \quad y(z) \to 0 \quad as \quad |z| \to \infty \right\}.$$

THEOREM.

α) *Let the function* $M(U)$ *satisfy*

i) $M(U) \in C^2((-\delta, 1+\delta))$ *for some positive* δ,

ii) $M(U) \geq M_0 > 0$ *for* $U \in (-\delta, 1+\delta)$,

where M_0 *is a constant.*

β) *Let the function* $F(U)$ *satisfy*

i) $F(U) \in C^2((-\delta, 1+\delta))$ *for the same* δ *as previously,*

ii) $F(0) = 0, \quad F(1) = 0,$

iii) $F(U) < 0$ *for* $U \in (0, 1)$,

iv) $F'_U(0) < 0, \quad F'_U(1) > 0.$

Then

1. *Equation* (4.21) *has a unique solution* $U_0(z) \in \mathcal{B}_1$ *satisfying the limit conditions* (4.12), (4.13) *and the initial condition* $U_0(0) = 1/2$;

2. *Equation* (4.9) *has a unique solution* $U(z) \in \mathcal{B}_2$ *satisfying the same limit conditions and the initial condition* $U(0) = 1/2$, *provided that* α *is sufficiently small;*

3. *There is a constant* $C > 0$, *independent of* α, *such that*

$$\|U(z) - U_0(z)\|_1 < \alpha C, \tag{5.1}$$

for α *sufficiently small.*

Only Part 3 of the assertions of the Theorem needs a proof; Parts 1 and 2 are presented for sake of completeness of the theses and can be easily proved by the phase plane analysis, even without the assumption that α is small (see [8] for the case of reaction-diffusion systems, and [9] for the case of conservation laws).

The following observation collects some properties of $U_0(z)$ which will be used in the proof of Part 3 of the Theorem.

OBSERVATION 2. Under the assumptions on $M(U)$ and $F(U)$ taken in the Theorem,

$$sU'(z) > 0 \qquad \text{for} \quad z \in \mathbb{R}, \tag{5.2}$$

$$\frac{U_0''(z)}{U_0'(z)} \in \mathcal{B}_1\,, \tag{5.3}$$

and

$$U_0'(z),\ U_0''(z) = \begin{cases} O(e^{\kappa_- z}) & \text{as} \quad z \to -\infty, \\ O(e^{\kappa_+ z}) & \text{as} \quad z \to \infty, \end{cases} \tag{5.4}$$

where

$$\kappa_- = \begin{cases} -\dfrac{F_U'(0)}{sM(0)} & \text{for} \quad s > 0, \\ -\dfrac{F_U'(1)}{sM(1)} & \text{for} \quad s < 0, \end{cases}$$

$$\kappa_+ = \begin{cases} -\dfrac{F_U'(1)}{sM(1)} & \text{for} \quad s > 0, \\ -\dfrac{F_U'(0)}{sM(0)} & \text{for} \quad s < 0. \end{cases} \tag{5.5}$$

The proof is immediate, hence it is omitted.

Now, we make the substitution in Eq. (4.9)

$$U = U_0 + h. \tag{5.6}$$

To prove Parts 2 and 3 of the Theorem it is sufficient to show that the equation for h resulting from Eq. (4.9) has a solution in $\mathcal{B}_2^0$, and that

$$\|h\|_1 < \alpha C \tag{5.7}$$

for some positive constant C independent of α, the latter being sufficiently small.

To this end we write the equation for h in the form

$$\alpha h'' + sM(U_0)h' - sM(U_0)\frac{U_0''}{U_0'}h = -\alpha U_0'' - G(h), \tag{5.8}$$

where $G:\ \mathcal{B}_i^0 \to \mathcal{B}_{i-1},\ i = 1, 2$, is a nonlinear differential operator defined by

$$G(h) = s\left[M(U_0 + h) - M(U_0)\right]h' + s\left[M(U_0 + h) - M(U_0) - M_U'(U_0)h\right]U_0' + \left[F(U_0 + h) - F(U_0) - F_U'(U_0)h\right].$$

The linear differential operator generated by the left-hand side of Eq. (5.8) we denote by L_α, i.e.

$$L_\alpha h = \alpha h'' + sM(U_0)h' - sM(U_0)\frac{U_0''}{U_0'}h. \tag{5.9}$$

$L_\alpha h : \mathcal{B}_2^0 \to \mathcal{B}_0^0$.

Hence, according to this scheme we have to show first, that L_α has the inverse $L_\alpha^{-1} : \mathcal{B}_0^0 \to \mathcal{B}_2^0$.

LEMMA. For sufficiently small positive α, the linear operator L_α has the inverse $L_\alpha^{-1} : \mathcal{B}_0^0 \to \mathcal{B}_2^0$ and, when treated as an operator from $\mathcal{B}_0^0$ into $\mathcal{B}_1^0$, is bounded, i.e. for every $g \in \mathcal{B}_0^0$ there is a positive constant, say C, such that

$$\|L_\alpha^{-1} g\|_1 \leq C\|g\|_0 . \tag{5.10}$$

P r o o f. We rewrite the equation $L_\alpha h = g$ in the form

$$\alpha h'' + \left[sM(U_0) - \alpha\frac{U_0''}{U_0'}\right] h' - \left[sM(U_0)\frac{U_0''}{U_0'} + \alpha\left(\frac{U_0''}{U_0'}\right)'\right] h = g - \left(\frac{U_0''}{U_0'}h\right)' \equiv \tilde{g} \tag{5.11}$$

or

$$\alpha\left[h' - \frac{U_0''}{U_0'}h\right]' + sM(U_0)\left[h' - \frac{U_0''}{U_0'}h\right] = \tilde{g}.$$

Integrating this linear equation we get

$$h' - \frac{U_0''}{U_0'}h = V\tilde{g}, \tag{5.12}$$

where V is a linear integral operator $V : \mathcal{B}_0^0 \to \mathcal{B}_1^0$ defined by

$$V\tilde{g} = \begin{cases} \dfrac{1}{\alpha q(z)} \displaystyle\int_{-\infty}^{z} q(\zeta)\tilde{g}(\zeta)\,d\zeta, & \text{if} \quad s > 0, \\ -\dfrac{1}{\alpha q(z)} \displaystyle\int_{z}^{-\infty} q(\zeta)\tilde{g}(\zeta)\,d\zeta, & \text{if} \quad s < 0, \end{cases} \tag{5.13}$$

and

$$q(z) = \exp\left[\frac{s}{\alpha}\int_0^z M(U_0(\zeta))\,d\zeta\right]. \tag{5.14}$$

The operator $V : \mathcal{B}_0^0 \to \mathcal{B}_1^0$ is bounded. First, let us notice that if $\lim\limits_{|z|\to\infty} \tilde{g}(z) = 0$, then $\lim\limits_{|z|\to\infty} (V\tilde{g})(z) = 0$. To prove this use the de l'Hospital rule.

Secondly, there is a constant $C > 0$, independent of α, such that

$$\|V\tilde{g}\|_0 \leq C\|\tilde{g}\|_0 . \tag{5.15}$$

Indeed, let $s > 0$. We have obviously

$$|V\tilde{g}| \leq \frac{\|\tilde{g}\|_0}{\alpha} \int_{-\infty}^{z} \exp\left[-\frac{s}{\alpha}\int_{\zeta}^{z} M(U_0(\tau))\,d\tau\right] d\zeta.$$

Now, making use of Assumption (α)(ii) of the Theorem we obtain

$$\int_{-\infty}^{z} \exp\left[-\frac{s}{\alpha}\int_{\zeta}^{z} M(U_0(\tau))\,d\tau\right] d\zeta \leq \int_{-\infty}^{z} \exp\left[-\frac{sM_0}{\alpha}(z-\zeta)\right] dz = \frac{\alpha}{sM_0}.$$

Hence, (5.15) is proved. The case of $s < 0$ is treated in a similar way. Now we proceed to Eq. (5.12). Its solution is

$$h(z) = U_0'(z)\int_0^z \frac{(V\tilde{g})(\zeta)}{U_0'(\zeta)}d\zeta. \tag{5.16}$$

Of course, $h(0) = 0$. Next, making use of Observation 2 we check easily that $h(\pm\infty) = 0$. So, $h(z)$ as given by (5.16) is an element of $\mathcal{B}_2^0$, indeed.

From (5.16) the estimate follows

$$|h(z)| \leq \|V\tilde{g}\|_0 \left|U_0'(z)\int_0^z \frac{d\zeta}{U_o'(\zeta)}\right|.$$

It follows from Observation 2 that there is a constant, say $C_1 > 0$, such that

$$\left|U_0'(z)\int_0^z \frac{d\zeta}{U_0'(\zeta)}\right| \leq C_1.$$

Of course, C_1 does not depend on α, because $U_0(z)$ is independent of α.

Hence, the following estimate holds true

$$\|h(z)\| \leq C_1\|V\tilde{g}\|_0. \tag{5.17}$$

Next, making use of Eq. (5.12), Observation 2, and (5.17) we conclude that there is a constant C_2, independent of α such that

$$\|h'(z)\|_0 \leq C_2\|V\tilde{g}\|_0.$$

Therefore, there is a constant $C_3 > 0$, independent of α, such that

$$\|h(z)\|_1 \leq C_3\|V\tilde{g}\|_0. \tag{5.18}$$

Equation (5.16) is an integro-differential equation equivalent to (5.12), and thus to $L_\alpha h = g$. Explicitly, this equation is of the form

$$h(z) = U_0'(z) \int_0^z \frac{(Vg)(\zeta)}{U_0'(\zeta)} d\zeta - \alpha U_0'(z) \int_0^z \frac{\left[V\left(\frac{U_0''}{U_0'}h\right)'(\zeta)\right]}{U_0'(\zeta)} d\zeta \equiv T(h). \tag{5.19}$$

To solve this equation we apply the method of successive approximations setting

$$\begin{aligned} h_0 &= T(0), \\ h_{k+1} &= T(h_k), \qquad k = 0,\ 1,\ 2, \dots . \end{aligned} \tag{5.20}$$

By induction we show that, for sufficiently small α, there is a constant $C > 0$, independent of α, such that

$$\|h_k\|_1 \leq C\|g\|_0\,, \qquad k = 0, 1, 2, \dots . \tag{5.21}$$

Next, we check easily that for small α the following is true:

$$\|T(h_1) - T(h_2)\|_1 \leq \alpha C \|h_1 - h_2\|_1\,,$$

i.e. for small α, $T(h)$ is a contraction mapping from $\mathcal{B}_1^0$ into itself. Thus, the sequence defined by (5.20) is convergent in $\mathcal{B}_1^0$, its limit, as k tends to ∞, $h(z)$ satisfies Eq. (5.19), and it is the unique solution. But, any solution of Eq. (5.19) in $\mathcal{B}_1^0$ is also its solution in $\mathcal{B}_2^0$. Hence, the limit function $h(z)$ is also the unique solution of this equation in $\mathcal{B}_2^0$. Consequently, it is the unique solution to the equation $L_\alpha h = g$. Moreover, since (5.21) holds for every k, it holds also for the limit of the sequence. It means that $h(z)$ satisfies

$$\|h\|_1 \leq C\|g\|_0\,,$$

and this is (5.10). The proof is complete.

P r o o f of the Theorem. Solving Eq. (5.8) in $\mathcal{B}_2^0$ we get

$$h_{k+1} = -\alpha L_\alpha^{-1} U_0'' - L_\alpha^{-1} G(h_k), \qquad k = 0, 1, 2, \dots \tag{5.22}$$

with $h_0 = 0$.

The operator $G(h)$ has the following two properties:

i) $G(0) = 0$,

ii) for every $\varepsilon > 0$, there is $\delta(\varepsilon) > 0$ such that, if $\|h_1\|_1 \leq \delta(\varepsilon)$, $\|h_2\| \leq \delta(\varepsilon)$, then $\|G(h_1) - G(h_2)\|_1 \leq \varepsilon \|h_1 - h_2\|_1$.

Using them and the Lemma we show easily that there is a constant $C > 0$, independent of α, such that

$$\|h_k\|_1 \leq \alpha C, \qquad k = 0, 1, 2, ..., \tag{5.23}$$

and that the sequence $\{h_k\}$ is convergent as $k \to \infty$, to the limit $h(z) \in \mathcal{B}_1^0$. This limit function is the unique solution of Eq. (5.8) in $\mathcal{B}_1^0$, so it is its unique solution in $\mathcal{B}_2^0$. Additionally, the limit $h(z)$ satisfies $\|h\|_1 \leq \alpha C$, with the constant C being the same as in (5.23), provided that α is sufficiently small. The proof of the Theorem is complete.

Acknowledgment

The author thanks Professor T. PŁATKOWSKI whose comments were very helpful in avoiding serious mistakes.

References

1. M. SLEMROD, *Admissibility criteria for propagating boundaries in a van der Waals fluid*, Arch. Rational Mech. and Anal., **81**, 301–315, 1983.
2. L. TRUSKINOVSKY, *Equilibrium interphase boundaries*, Sov. Phys. Doklady, **27**, 551–553, 1982 [Dokl. Akad. Nauk SSSR, **265**, 306–311, 1982].
3. M. AFFOUF and R.E. CAFLISCH, *A numerical study of Riemann problem solutions and stability for a system of viscous conservation laws of mixed type*, SIAM J. Appl. Math., **51**, 3, 605–634, 1991.
4. R. ABEYARATNE and J.K. KNOWLES, *Implications of viscosity and strain-gradient effects for the kinetics of propagating phase boundaries in solids*, SIAM J. Appl. Math., **51**, 5, 1205–1211, 1991.
5. K. PIECHÓR, *A four-velocity model for van der Waals fluids*, Arch. Mech., **47**, 6, 1089–1111, 1995.
6. K. PIECHÓR, *Travelling wave solutions to model equations of van der Waals fluids*, Arch. Mech., **48**, 4, 675–709, 1996.
7. M.S. CRAMER and A.B. CRICKENBERGER, *The dissipative structure of shock waves in dense gases*, J. Fluid Mech., **223**, 325–355, 1991.
8. A.I. VOLPERT, V.A. VOLPERT and V.A. VOLPERT, *Travelling wave solutions of parabolic systems*, Translations of Mathematical Monographs, Vol. **140**, American Mathematical Society, Providence 1994.
9. R. HAGAN and M. SLEMROD, *The viscosity-capillarity admissibility criterion for shocks and phase transitions*, Arch. Rational Mech. and Anal., **83**, 333–361, 1983.

10. J.D. LAMBERT, *Computational methods in ordinary differential equations*, John Wiley and Sons, London 1973.

11. A.A. BORISOV, AL.A. BORISOV, S.S. KUTELADZE and V.E. NAKORYAKOV, *Rarefaction shock wave near the critical liquid-vapour point*, J. Fluid Mech., **126**, 59–73, 1983.

POLISH ACADEMY OF SCIENCES
INSTITUTE OF FUNDAMENTAL TECHNOLOGICAL RESEARCH
e-mail: kpiechor@ippt.gov.pl

Received December 16, 1996.

Arch. Mech., 49, 4, pp. 791–804, Warszawa 1997

Dynamic response of a fluid-saturated elastic porous solid

S. BREUER (ESSEN)

IN THIS PAPER, the field equations governing the dynamic response of a fluid-saturated elastic porous media are analyzed and built up for the study of the consolidation problem and the one-dimensional wave propagation. The two constituents are assumed to be incompressible. A one-dimensional numerical solution is derived by means of the standard Galerkin procedure and the finite element method. As a result of the incompressibility, there is only one independent dilatational wave propagating in the solid and the fluid phase. This work can provide further understanding of the wave propagation in porous materials, not only in view of the propagation speed, but also with respect to the development of the amplitudes.

1. Introduction

A FLUID-SATURATED POROUS MEDIUM is a portion of space occupied partly by a solid phase (solid skeleton) and partly by a void space filled with fluid, e.g. water. The mechanical behaviour of such a medium is governed mainly by the interaction of the solid skeleton with the fluid. This interaction occurs in quasi-static problems, like foundations, but is particularly strong in dynamic problems, for example earthquakes. In contrast to wave propagation in one-component bodies, the wave propagation in a porous medium has special characteristics. As usual, we have two different kinds of waves, the compression (longitudinal) wave and the shear (transversal) wave. But in a porous medium with compressible constituents, the compression wave has two different velocities, a fast P1 wave and a slow P2 wave. In this contribution, however, the constituents are assumed to be incompressible and as a result of this assumption, the P1 velocity is infinite.

The two-phase behaviour of a fluid-saturated porous medium can only be predicted quantitatively by elaborate numerical computation, which fortunately is possible today due to the development of powerful computers.

Many computations done in the field of dynamics of porous media have made use of BIOT'S theory [1], because Biot's theory leads to quite good results for linear elastic problems. But as this theory has not been developed from the basic equations of mechanics, its further development causes many problems.

In this investigation, the calculation of the dynamic response of a fluid-saturated elastic porous solid is based upon the macroscopic porous media theory

(TPM – Theory of Porous Media), which is defined as the mixture theory restricted by the volume fraction concept. Readers interested in details of this theory are referred to the papers of de BOER [8], BLUHM [2], BLUHM and DE BOER [3], EHLERS [10] and BOWEN [4, 5]. In order to simplify the problem, thermal effects and exchanges of mass between the constituents are excluded, and single constituents are treated as incompressible.

In Sec. 2 the governing equations of the above mentioned theory are discussed and the field equations and constitutive relations are taken into account. In the third section these equations are built up for the numerical computation. The finite element method is used for the discretisation of the basic equations and the time integration is done by the Newmark method. In Sec. 4 the dynamic consolidation problem of a one-dimensional elastic porous body and the wave propagation in this medium is investigated. Solutions obtained by the finite element method are compared with the existing analytical solutions based on the same theory. This paper ends with some concluding remarks in Sec. 5.

2. Governing equations

2.1. Kinematics and the concept of volume fraction

Considering the kinematics of the fluid-saturated porous medium, which is an immiscible mixture of the constituents φ^α with particles X^α ($\alpha = S$: solid phase, $\alpha = F$: fluid phase), it is assumed that at any time t each spatial point is simultaneously occupied by the particles X^S and X^F. These particles X^α proceed from different reference positions $\mathbf{X}_\alpha$ at time $t = t_0$. Thus, each constituent is assigned its own independent motion function $\boldsymbol{\chi}_\alpha$, from which the velocity $\mathbf{x}'_\alpha$, the acceleration $\mathbf{x}''_\alpha$ and the deformation gradient $\mathbf{F}_\alpha$ can be calculated:

$$\mathbf{x} = \boldsymbol{\chi}_\alpha(\mathbf{X}_\alpha, t), \qquad \mathbf{x}'_\alpha = \mathbf{x}'_\alpha(\mathbf{X}_\alpha, t), \qquad \mathbf{x}''_\alpha = \mathbf{x}''_\alpha(\mathbf{X}_\alpha, t), \qquad \mathbf{F}_\alpha = \mathrm{Grad}_\alpha\, \boldsymbol{\chi}_\alpha\,,$$

where Grad_α means the derivative with respect to $\mathbf{X}_\alpha$. The volume fractions

$$n^\alpha = n^\alpha(\mathbf{x}, t)$$

are defined as the local ratios of the constituent volumes v^α with respect to the bulk volume v of the control space B_S, which is shaped by the solid skeleton

$$dv^\alpha = n^\alpha\, dv, \qquad v^\alpha = \int_{B_S} n^\alpha\, dv.$$

With the aid of the volume fractions

$$v = \int_{B_S} dv = \sum_{\alpha=1}^{\kappa} v^\alpha = \int_{B_S} \sum_{\alpha=1}^{\kappa} dv^\alpha = \int_{B_S} \sum_{\alpha=1}^{\kappa} n^\alpha\, dv,$$

we get the volume fraction condition

$$\sum_{\alpha=1}^{\kappa} n^{\alpha} = 1. \tag{2.1}$$

The volume fraction condition (2.1) plays an important role as a constraint in the constitutive theory of porous media, see DE BOER [8] or BLUHM and DE BOER [3].

Each of the constituents φ^{α} has a real density $\varrho^{\alpha R}$, which is defined as the mass of φ^{α} per unit of v^{α}. With the aid of the volume fraction concept, these properties can be "smeared" over the control space and we obtain the partial density

$$\varrho^{\alpha} = n^{\alpha}\, \varrho^{\alpha R}.$$

2.2. Field equations

Excluding mass exchanges and thermal effects, the mechanical behavior of a fluid-saturated porous solid is described in BLUHM [2] and EHLERS [10] by the balance equation of mass for each single constituent

$$(\varrho^{\alpha})'_{\alpha} + \varrho^{\alpha} \operatorname{div} \mathbf{x}'_{\alpha} = 0, \tag{2.2}$$

the balance equation of momentum

$$\operatorname{div} \mathbf{T}^{\alpha} + \varrho^{\alpha}(\mathbf{b} - \mathbf{x}''_{\alpha}) + \mathbf{s}^{\alpha} = \mathbf{0}, \tag{2.3}$$

and the volume fraction condition that changes for a binary mixture into the saturation condition

$$n^{S} + n^{F} = 1. \tag{2.4}$$

In these equations $\mathbf{T}^{\alpha}$ is the partial Cauchy stress tensor, $\mathbf{b}$ the external acceleration, and $\mathbf{s}^{\alpha}$ the interaction force of the constituents. In addition, "div" is the divergence operator and the symbol $(...)'_{\alpha}$ denotes the material time derivative with respect to the trajectory of φ^{α}.

As the sum of the interaction forces must vanish, we obtain for a binary mixture

$$\mathbf{s}^{F} + \mathbf{s}^{S} = \mathbf{0}.$$

The balance equation of moment of momentum leads, excluding any moment of momentum supply, to a symmetric stress tensor

$$\mathbf{T}^{\alpha} = \mathbf{T}^{\alpha T}.$$

2.3. Constitutive relations

Since the number of unknown fields $(\mathbf{T}^\alpha, \boldsymbol{\chi}^\alpha, \mathbf{s}^\alpha)$ is larger than the number of field equations, we have to introduce constitutive relations for $\mathbf{T}^\alpha$, $\mathbf{s}^\alpha$ and the density $\varrho^{\alpha R}$. As both constituents are incompressible, we have

$$\varrho^{\alpha R} = \text{constant}.$$

With this assumption, the volume fractions can be calculated from the balance equations of mass (2.2) and with the aid of the deformation gradient, one obtains

$$n^\alpha = n^{\alpha 0} (\det \mathbf{F}_\alpha)^{-1},$$

where $n^{\alpha 0}$ describes the initial porosity of φ^α.

The constitutive relations for the solid and fluid stress tensor $\mathbf{T}^\alpha$ and for the interaction force $\mathbf{s}^\alpha$ $(\alpha = S, F)$ consist of two terms, where the former, as a result of the saturation condition, is proportional to the pore pressure p, while the latter represents the extra quantities, index $(...)_E$, determined by the deformation:

$$\begin{aligned} \mathbf{T}^\alpha &= -n^\alpha p \mathbf{I} + \mathbf{T}^\alpha_E, \\ \mathbf{s}^F &= p \operatorname{grad} n^F + \mathbf{s}^F_E. \end{aligned}$$

The partial effective stress tensor of the fluid can be neglected:

$$\mathbf{T}^F_E \approx \mathbf{0},$$

and the partial effective stress tensor of the solid can be expressed by the law of SIMO and PISTER [12]:

$$\mathbf{T}^S_E = \frac{1}{\det \mathbf{F}_S} \left(\mu^S \mathbf{B}_S + \left[\lambda^S \ln(\det \mathbf{F}_S) - \mu^S \right] \mathbf{I} \right),$$

where λ^S and μ^S are the Lamé constants of the solid material and $\mathbf{B}_S = \mathbf{F}_S \mathbf{F}_S^T$ is the left Cauchy-Green tensor.

The interaction between the fluid and solid constituents, caused by the motions, can be described by the extra supply term of momentum

$$\mathbf{s}^F_E = -\frac{(n^F)^2 \gamma^{FR}}{k^F} \mathbf{w}_F,$$

with $\mathbf{w}_F = (\mathbf{x}'_F - \mathbf{x}'_S)$ being the seepage velocity, γ^{FR} the real specific weight of the fluid and k^F the Darcy permeability parameter.

3. Numerical solution concept

3.1. Solution strategy

An effective way to solve the system of equations and to match the problem to the boundary and initial conditions consists in combining the balance equations of momentum (2.3) of both constituents

$$\begin{aligned}(3.1)\qquad &\operatorname{div}(\mathbf{T}^S + \mathbf{T}^F) + (\varrho^S + \varrho^F)\mathbf{b} - \varrho^S \mathbf{x}_S'' \\ &\qquad - \varrho^F \left[(\mathbf{w}_F + \mathbf{x}_S')_S' + \operatorname{grad}(\mathbf{w}_F + \mathbf{x}_S')\,\mathbf{w}_F\right] = \mathbf{0}\end{aligned}$$

as well as the balance equation of momentum of the fluid,

$$\begin{aligned}(3.2)\qquad &\operatorname{div}\mathbf{T}^F + \varrho^F\left(\mathbf{b} - \left[(\mathbf{w}_F + \mathbf{x}_S')_S' + \operatorname{grad}(\mathbf{w}_F + \mathbf{x}_S')\mathbf{w}_F\right]\right) \\ &\qquad - \frac{\gamma^{FR}(n^F)^2}{k^f}\,\mathbf{w}_F = \mathbf{0}.\end{aligned}$$

The remaining equations and unknowns can be substituted by a combination of the balance equations of mass (2.2) together with the saturation condition (2.4). Considering the incompressibility of both constituents, we get:

$$(3.3)\qquad \operatorname{div}(n^F \mathbf{w}_F + \mathbf{x}_S') = 0.$$

In these equations the fluid velocity $\mathbf{x}_F'$ is replaced by $\mathbf{x}_F' = \mathbf{w}_F + \mathbf{x}_S'$, for a better fit to the boundary conditions. For example, at an undrained boundary it causes less problems to prescribe $\mathbf{w}_F = 0$, i.e., $\mathbf{x}_S' = \mathbf{x}_F'$.

3.2. Weak formulation

For numerical computations, a standard Galerkin procedure was chosen. Therefore, each of the basic equations (3.1), (3.2), (3.3) has to be multiplied by a weighting function. For Eq. (3.1), a virtual solid displacement $\bar{\mathbf{u}}_S$ is chosen. The volume integral of a divergence can be transformed, see DE BOER [7], into a surface integral

$$\begin{aligned}\int_B \Big\{&(\mathbf{T}_E^S - p\,\mathbf{I})\cdot\operatorname{grad}\bar{\mathbf{u}}_S + \varrho^S\,\mathbf{x}_S''\cdot\bar{\mathbf{u}}_S \\ &+ \varrho^F\left[(\mathbf{w}_F + \mathbf{x}_S')_S' + \operatorname{grad}(\mathbf{w}_F + \mathbf{x}_S')\mathbf{w}_F\right]\cdot\bar{\mathbf{u}}_S\Big\}\,dv \\ &= \int_A \mathbf{t}\cdot\bar{\mathbf{u}}_S\,da + \int_B (\varrho^S + \varrho^F)\mathbf{b}\cdot\bar{\mathbf{u}}_S\,dv,\end{aligned}$$

where $\mathbf{t}$ is the stress vector on the surface of the mixture, including the stress on the solid and the stress on the fluid.

For Eq. (3.2), a virtual seepage velocity $\bar{\mathbf{w}}_F$ was taken into account and the volume integral was transformed into a surface integral

$$\int_B \Big\{(-p \operatorname{div} \bar{\mathbf{w}}_F) + \frac{\gamma^{FR} n^F}{k^f} \mathbf{w}_F \cdot \bar{\mathbf{w}}_F + \varrho^{FR} \Big[(\mathbf{w}_F + \mathbf{x}'_S)'_S + \operatorname{grad} (\mathbf{w}_F + \mathbf{x}'_S) \mathbf{w}_F \Big] \cdot \bar{\mathbf{w}}_F \Big\} dv = - \int_A p \, \bar{\mathbf{w}}_F \cdot \mathbf{n} \, da + \int_B \varrho^{FR} \mathbf{b} \cdot \bar{\mathbf{w}}_F \, dv.$$

Equation (3.3) represents the saturation condition together with the mass balance equations, and it has been multiplied by a virtual pressure $\bar{p}$

$$\int_B \operatorname{div} \left(n^F \, \mathbf{w}_F + \mathbf{x}'_S \right) \bar{p} \, dv = 0.$$

3.3. Solution algorithm

From the weak formulation, one gets 3 scalar equations with the unknown functions $(\mathbf{u}_S, \mathbf{w}_F, p)$. For the discretisation of the problem, the unknown functions $(\mathbf{u}_S, \mathbf{w}_F, p)$, as well as their time derivatives and the corresponding weighting functions $(\bar{\mathbf{u}}_S, \bar{\mathbf{w}}_F, \bar{p})$ are approximated by linear shape functions. Since the values of the weight functions are not specified, the coefficient multiplied by the value of the weight function must vanish. Now, the 3 scalar equations of the weak formulation are split into n equations, where n is the number of unknowns at each node, multiplied by the number of nodes per element. Thus, the discretisation of the problem leads to a system of n equations with the unknowns $(\mathbf{u}_S, \mathbf{u}'_S, \mathbf{u}''_S, \mathbf{w}_F, \mathbf{w}'_F, p)$. The matrix of the coefficients multiplied by the value of the discrete unknowns are denoted by **M**, **D**, **K**. **M** means the mass matrix and is connected with the second time derivative of the unknowns. **D** represents the damping matrix and is coupled with the first time derivative of the unknowns, and at last **K** denotes the stiffness matrix and is connected with the unknowns. The index M, F or K in Eq. (3.4) means, that these coefficients come from the balance equation of mixture (M), the balance equation of fluid (F) or from the saturation condition (K). The second index represents the kind of unknowns, 1 stands for the motion of solid, 2 for the motion of fluid and 3 for the pressure. **F** determines the load vector of the mixture (M) and of the fluid (F). Equation (3.4) shows the problem after the discretisation in the form of a matrix equation.

$$\begin{pmatrix} \mathbf{M}_{M1} & 0 & 0 \\ \mathbf{M}_{F1} & 0 & 0 \\ 0 & 0 & 0 \end{pmatrix} \begin{pmatrix} \mathbf{u}''_S \\ 0 \\ 0 \end{pmatrix} + \begin{pmatrix} \mathbf{D}_{M1} & \mathbf{D}_{M2} & 0 \\ \mathbf{D}_{F1} & \mathbf{D}_{F2} & 0 \\ \mathbf{D}_{K1} & 0 & 0 \end{pmatrix} \begin{pmatrix} \mathbf{u}'_S \\ \mathbf{w}'_F \\ 0 \end{pmatrix} + \begin{pmatrix} \mathbf{K}_{M1} & \mathbf{K}_{M2} & \mathbf{K}_{M3} \\ 0 & \mathbf{K}_{F2} & \mathbf{K}_{F3} \\ 0 & \mathbf{K}_{K2} & 0 \end{pmatrix} \begin{pmatrix} \mathbf{u}_S \\ \mathbf{w}_F \\ p \end{pmatrix} = \begin{pmatrix} \mathbf{F}^M \\ \mathbf{F}^F \\ 0 \end{pmatrix}. \tag{3.4}$$

The Newmark method was chosen for the time integration and with the help of the result of the last time step, the problem can be converted into a $n \times n$ matrix with an update of the load vector.

4. Examples

4.1. Consolidation problem

Taking the linear theory into account, DE BOER *et al.* [9] presented an analytical solution for an infinite halfspace using the Laplace transformation. Thus there is an excellent example for the comparison of the analytical and the numerical solution. In order to model the half-space via the finite element method, a column of 10 m depth and 2 m^2 surface was taken into account. The solution was calculated for a very short time, so that no signal of the rigid boundary in 10 m depth could influence the solution. The upper boundary of the column is perfectly drained and loaded in the first case by a sine load (q):

$$q_1(t) = 3\sin(\omega t) \quad \left[\frac{\text{kN}}{\text{m}^2}\right], \qquad \omega = 75\ \text{s}^{-1},$$

and in another case by a step load (q):

$$q_2(t) = 3 \quad \left[\frac{\text{kN}}{\text{m}^2}\right].$$

The other boundaries are undrained and rigid, see Fig. 1. The material parameters are taken from [9] as:

$$\begin{aligned} \mu^S &= 5583\ \text{kN/m}^2, & \lambda^S &= 8375\ \text{kN/m}^2, \\ \varrho^{SR} &= 2000\ \text{kg/m}^3, & \varrho^{FR} &= 1000\ \text{kg/m}^3, \\ n_{0S}^S &= 0.67, & k^f &= 0.01\ \text{m/s}. \end{aligned}$$

As expected, the displacement-time behaviour starts with a large time-gradient, which decreases with passing time. We can compare this behaviour with a strong damped vibration-system, which has in fact the same structure after the dicretisation.

Figure 2 shows the surface displacement under both the loads. It shows a good agreement between the analytical and the numerical solution. In the case of the sine load, there is no visible difference between both the solutions.

In the example mentioned above, the external acceleration was neglected. Thus the calculation has started when the settlement under its own weight is finished. An interesting point is to show the settlement under its own weight, without an external load. This result is to be seen in Fig. 3.

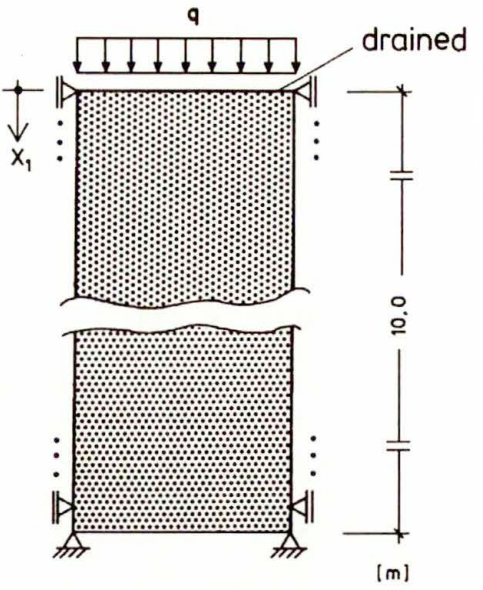

FIG. 1. Example.

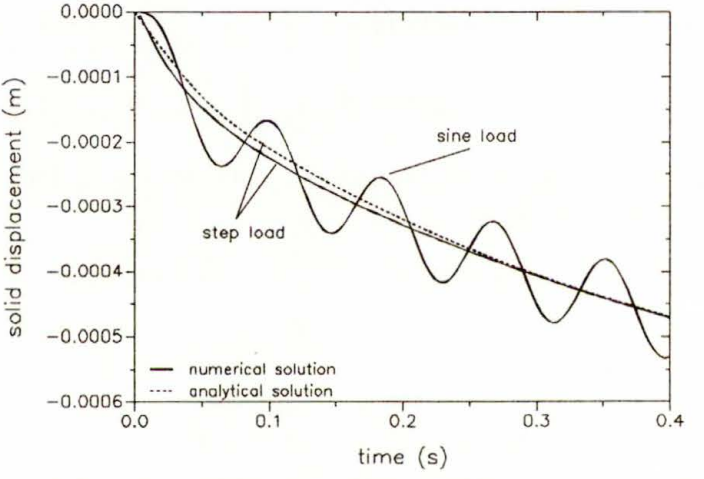

FIG. 2. Comparison between an analytical and a numerical solution.

We can see that at the begining, the weight of the whole column:

$$\int_V (\varrho^S + \varrho^F)\,\mathbf{b}\,dv = 167\,\mathrm{kN}\ [\mathbf{e}_1],$$

is causing the pore pressure. With the passage of time, the effective stress in the solid increases to $-\,67\,\mathrm{kN/m^2}$, and the pore pressure it decreases to $100\,\mathrm{kN/m^2}$,

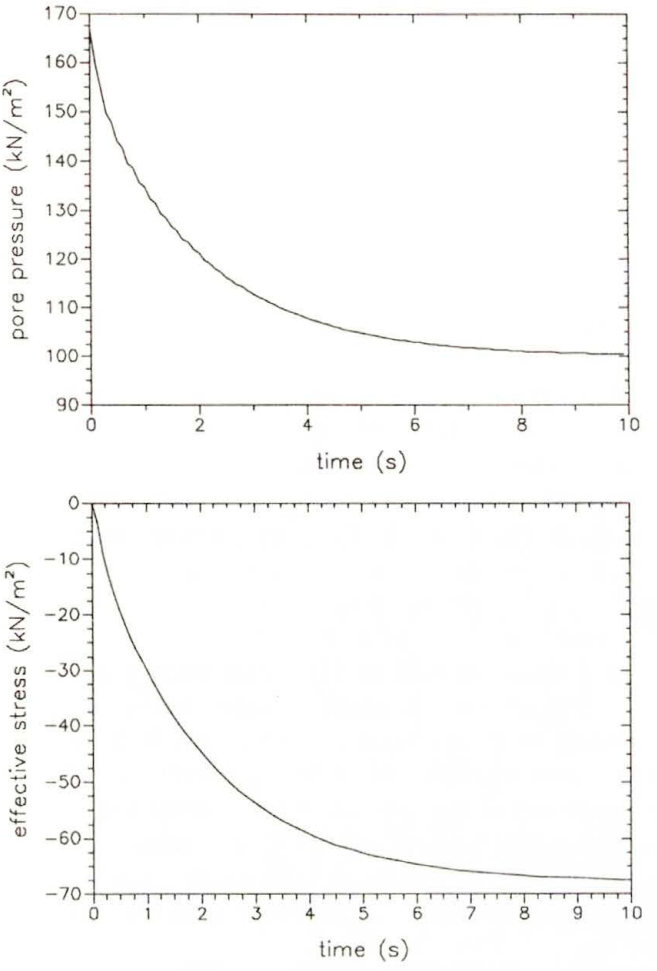

FIG. 3. Pore pressure and effective stress under its own weight.

which is the exact pore pressure of a water column of 10 m depth,

$$\int_0^{10} \varrho^{FR} \mathbf{b}\, dx = 100\,\mathrm{kN/m^2}.$$

The part of the weight entering the solid is exactly the weight of the solid minus the uplift:

$$\int_V n^S(\varrho^{SR} - \varrho^{FR})\, \mathbf{b}\, dv = 67\,\mathrm{kN}.$$

In the case of a linear theory we can neglect the external acceleration; only in the case, when we are intrested in the absolute value of the pore pressure, displacement or stress, we have to add the initial values.

4.2. One-dimensional wave propagation

The second example is the one-dimensional wave propagation in the same structure as shown in the first example, where only the Darcy parameter has changed: $k^f = 10\,\mathrm{m/s}$.

4.2.1. Step load. In the first case the column was once again loaded with the Heaviside function, but with a different amplitude: $q_3(t) = 100\,\mathrm{kN}$ (see Fig. 1).

According to BIOT'S theory [1], with two compressible constituents there are two longitudinal waves in a porous medium. One wave is transmitted through the fluid (P1-wave) and the other is transmitted through the elastic structure of the solid skeleton (P2-wave), see [11]. These two waves are coupled through the coupling effect produced by motions of the solid and fluid. In this article both constituents are incompressible, thus the speed of the wave transmitted through the fluid (P1-wave) is infinite.

This is illustrated by Fig. 4, where the pore pressure versus time is shown. The pore pressure at the bottom of the column changes directly from the static value of $100\,\mathrm{kN/m^2}$ up to the static value plus the external load per $\mathrm{m^2}$. This is according to the statement of TERZAGHI [13], where he found out that the whole external load is firstly carried by the water body and then, while water is flowing out, the solid skeleton is going to take the external load. In Fig. 4 there are some oscillations in the pressure, which result from the big jump in the pressure. Furthermore, the diagram shows when the disturbance is reflected from the bottom or the top of the column. If we observe Fig. 4 in detail, we can see that the pressure at the bottom is $100\,\mathrm{kN/m^2}$ (static value) + $100\,\mathrm{kN/m^2}$ (external load) = $200\,\mathrm{kN/m^2}$. In 2 m depth (this point in the Fig. 4 is called top), the value is $20\,\mathrm{kN/m^2}$ (static value) + $100\,\mathrm{kN/m^2}$ (external load) = $120\,\mathrm{kN/m^2}$.

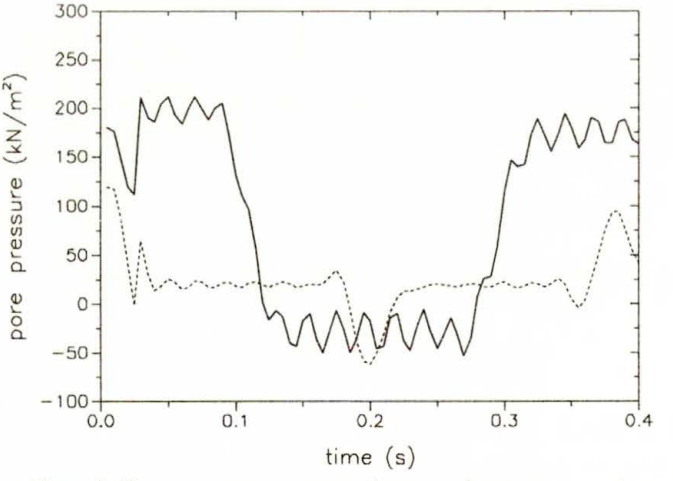

FIG. 4. Pore pressure versus time. — bottom, - - - top.

We see, that the information about the external load is transmitted with an infinite velocity through the incompressible fluid. The pore pressure at the top soon decreases to the static value of $20\,\mathrm{kN/m^2}$ as the solid skeleton takes up the external load. But it takes time till the disturbance travelling in the solid skeleton reaches the bottom of the column. This happens at $t = 0.1\,\mathrm{s}$, when the pore pressure decreases to the static value ($100\,\mathrm{kN/m^2}$).

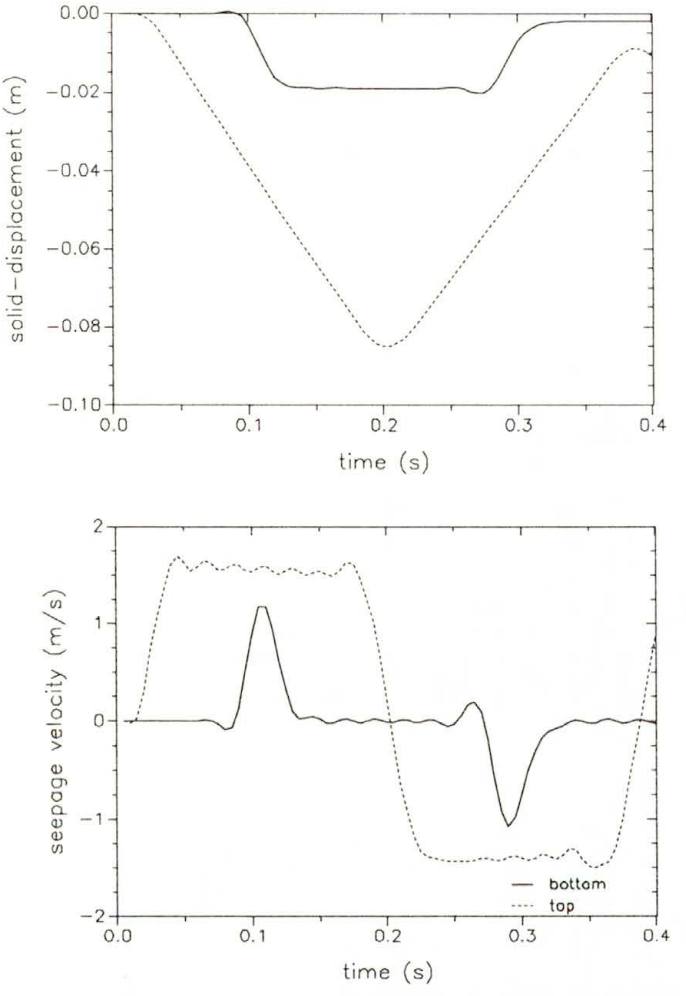

FIG. 5. Solid displacement and seepage velocity versus time.

In comparison with Fig. 5, where the solid displacement and the seepage velocity are shown, it can be observed that at time 0.1 s the P2-wave (transmitted by the elastic structure) hits the rigid bottom of the column and is reflected. This is coupled with a change in the pore pressure and the seepage velocity. At the time-instant 0.2 s, the P2-wave reaches the unfixed top of the column and the

sign of the disturbance changes, see [6, 14]. At the time-instant 0.3 s the P2-wave hits the rigid bottom again, and at time 0.4 s one period of this procedure is closed.

4.2.2. Impulse load. Another good example to show the coupling between solid displacement and pore pressure is to load the column with an impulse load:

$$f_4(t) = \begin{cases} 100\sin(314.16/\mathrm{s}\,t)\,\mathrm{kN} & \text{for } 0 < t < 0.01\,\mathrm{s}, \\ 0 & \text{for } t > 0.01\,\mathrm{s}. \end{cases}$$

The dynamic response at time 0.02 s of the column, as described above, is shown in the Fig. 6, where the solid strain and the pore pressure are exhibited versus the length of the column. The top is at $x = 10\,\mathrm{m}$ and the bottom at $x = 0\,\mathrm{m}$.

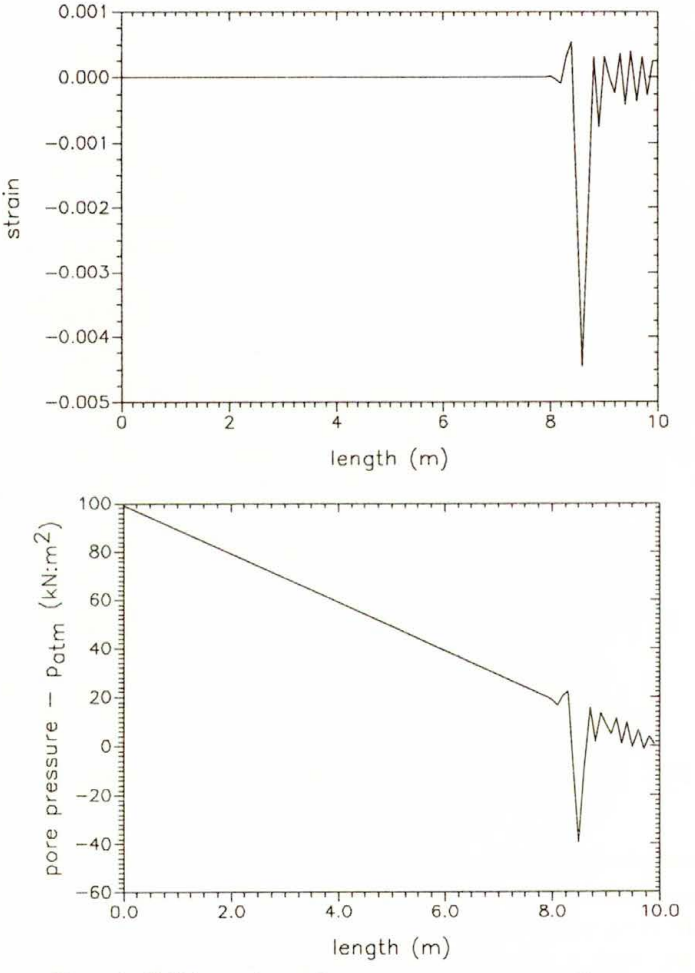

FIG. 6. Solid strain and pore pressure versus time.

The line in the pore pressure diagram from 100 to $0\,[\mathrm{kN/m^2}]$ is the static solution for the pore pressure under its own weight. We can see a disturbance travelling with the speed of the P2 wave in the pore pressure as well as in the solid strain.

5. Concluding remarks

The dynamic response of an incompressible fluid-saturated porous media is studied. The calculation via the finite element method is based upon the incompressible porous media model of DE BOER [8] and BLUHM [2]. The first application of this theory in this paper is the numerical solution of the consolidation problem. This numerical solution in comparison with the existing analytical solution shows a good agreement. In the second application the propagation of longitudinal waves is studied. According to Biot's theory (Biot treated compressible constituents), there are two longitudinal waves: a P1 wave transmitted by the pore fluid and a P2 wave transmitted by the elastic structure. This paper shows that the speed of the P1 wave, transmitted in the incompressible pore fluid, is infinite and only the P2 wave, transmitted by the elastic structure, can be observed in porous media with incompressible constituents.

Acknowledgments

The author is grateful to Prof. Dr.-Ing. R. DE BOER and Priv.-Doz. Dr.-Ing. J. BLUHM for their critical comments offered during the preparation of this paper. This work has been supported by the Deutsche Forschungsgemeinschaft (Germany).

References

1. M.A. BIOT, *Theory of propagation of elastic waves in fluid-saturated porous solid. 1. Lower-frequency range*, J. Acoust. Soc. Am., **28**, 168–178, 1956.
2. J. BLUHM, *A consistent model for saturated porous media*, Habilitation Thesis, University of Essen, 1996.
3. J. BLUHM and R. DE BOER, *The volume fraction concept in the porous media theory*, Report MECH 94/5, FB 10/Mechanik, Universität-GH Essen, to appear in: Zeitschrift für Angewandte Mathematik und Mechanik (ZAMM), 1994.
4. R.M. Bowen, *Incompressible porous media models by use of the theory of mixtures*, Int. J. Engng. Sci., **18**, 1129–1148, 1980.
5. R.M. Bowen, *Compressible porous media models by use of the theory of mixtures*, Int. J. Engng. Sci., **20**, 697–735, 1982.
6. S. BREUER, *Numerische Berechnung der Ausbreitung und Reflexion von longitudinal Wellen in linear elastischen Stäben*, pp. 51–66, [in:] Beiträge zur Mechanik, Festschrift zum 60. Geburtstag von Prof. Dr.-Ing. Reint de Boer, Forschungsbericht aus dem Fachbereich Bauwesen, **66**, Universität Essen, 1995.

7. R. DE BOER, *Vektor- und Tensorrechnung für Ingenieure*, Springer-Verlag, Berlin 1982.
8. R. DE BOER, *Highlights in the historical development of the porous media theory: Toward a consistent macroscopic theory*, Applied Mech. Reviews, **49**, 201–262, 1996.
9. R. DE BOER, W EHLERS and Z. LIU, *One-dimensional transient wave propagation in fluid-saturated incompressible porous media*, Arch. Appl. Mech., **63**, 59–72, 1993.
10. W. EHLERS, *Poröse Medien – ein kontinuumsmechanisches Modell auf der Basis der Mischungstheorie*, Forschungsbericht aus dem Fachbereich Bauwesen, **49**, 1989.
11. F.E. RICHART, J.R. HALL and R.D. WOODS, *Vibrations of soils and foundations*, Prentice-Hall, New Jersey 1970.
12. J.C. SIMO and K.S. PISTER, *Remarks on constitutive equations for the finite deformation problems: Computational implications*, Comp. Meth. Appl. Mech. Engng., **46**, 201–215, 1984.
13. K. VON TERZAGHI and R.B. PECK, *Soil mechanics in engineering practice*, Wiley, New York 1948.
14. F. ZIEGLER, *Technische Mechanik der festen und flüssigen Körper*, Springer Verlag, Wien 1985.

INSTITUTE OF MECHANICS, FB 10, UNIVERSITY OF ESSEN,
45117 ESSEN, GERMANY.
e-mail: breuer@mechanik.bauwesen.uni-essen.de

Received December 30, 1996; new version May 5, 1997.